TRIBO-PERFORMANCE OF MULTILAYER SURFACE COATING ON GRANITE DUST FILLED METAL ALLOY COMPOSITES

PhD Thesis

VIKASH GAUTAM

(2012RME9546)

DEPARTMENT OF MECHANICAL ENGINEERING
MALAVIYA NATIONAL INSTITUTE OF TECHNOLOGY, JAIPUR
JLN MARG, JAIPUR-302017, India
JUNE, 2016

TRIBO-PERFORMANCE OF MULTILAYER SURFACE COATING ON GRANITE DUST FILLED METAL ALLOY COMPOSITES

VIKASH GAUTAM

(2012RME9546)

Thesis submitted
as a partial fulfillment of the requirements of the degree of
Doctor of Philosophy
to the

Department Of Mechanical Engineering
Malaviya National Institute of Technology,
Jaipur-302017, India
June, 2016

Dedicated to

My Parents & Brother

Malaviya National Institute of Technology, Jaipur

Mechanical Engineering Department

CERTIFICATE

This is to certify that the thesis entitled "**Tribo-performance of Multilayer Surface Coating on Granite Dust Filled Metal Alloy Composites**", submitted by **Mr. Vikash Gautam** (ID No: 2012RME9546) in partial fulfilment of the requirements for the award of **Doctor of Philosophy** in Mechanical Engineering Department to the Malaviya National Institute of Technology, Jaipur is an authentic record of research work carried out by him under my supervision and guidance. To the best of our knowledge, the work incorporated in this thesis has not been submitted elsewhere for the award of any degree.

(Vikash Gautam)
Date: ID No: 2012RME9546

This is to certify that the above statement made by the candidate is correct to the best of my knowledge and belief.

Dr. Amar Patnaik
Supervisor
Assistant Professor,
Mechanical Engineering Department
MNIT Jaipur

Prof. I.K. Bhat
Supervisor
Director
MNIT Jaipur

ACKNOWLEDGEMENT

Before anything, thanks to God Almighty for the blessings and giving me the health and strength to complete my thesis successfully. Hopefully, God will always help and blessing me in the future.

I would like to extend my sincere thanks to my supervisor **Dr. Amar Patnaik & Prof. I. K. Bhat** for his valuable guidance and constant support throughout the research work, without his guidance patience and constant encouragement, completion of the thesis would not have been possible the same as presented here.

I am also grateful to Professor **G. S. Dangayach** Head of the Mechanical Engineering Department for his help and cooperation. I appreciate the encouragement from faculty members of the Mechanical Engineering Department, Malaviya National Institute of Technology Jaipur.

I would also like to extend my appreciation to my PhD committee members, **Prof. G. S. Dangayach**, Dr. **Amar Patnaik** and **Dr. Harlal Singh Mali** for giving me valuable suggestion time-by-time and serving on my committee. My special thanks to **Mr. Mukesh Kumar** who offered a lot of help during my PhD study.

My special thanks to my fellow research scholar Manoj Pawar, Shiv Ranjan, Ashiwani Kumar, Vikas Kukshal and who offered a lot of help during my PhD study. I also thank to all technical staffs Krishan kant Shankla, Ram Singh Bairwa, Lakshman singh Rathore that helped me directly and indirectly in my thesis work.

Finally, I wish also to express my love and gratitude to my mother Smt. Urmila Devi, father Shri Virendra Singh and brother Jai Prakash Gautam for their emotional support and encouragement through the duration of my study.

Date

MNIT Jaipur **(VIKASH GAUTAM)**

ABSTRACT

Slurry erosive wear causes degradation of parts of hydraulic turbine like blades, casing etc. by repetitive impact of hard abrasive particles with water (known as slit). Composites are widely used as structural components in such environments. Composites not only serve specific purposes but also exhibit desirable properties at macroscopic or microscopic scale. From the data on the service life of composite structures available in the literature, it can be said that they are durable, maintain dimensional integrity, resist fatigue loading and are easily maintainable and repairable. Due to this composite materials are continuously used in new structural applications in aircrafts, aerospace, marine, civil construction, automotive industries etc.

In this thesis, granite particulate filled (0-6 wt.%) aluminum alloyed composites system and their coating variants are designed and fabricated successfully. AA1050 and AA 5083 aluminum alloy as matrix material is taken, granite power as reinforcement and for coating CrN and CrN + SiN are used. Mechanical stir casting fabrication technique is adopted followed by physical vapor deposition technique for getting coating over the samples. The composite-systems undergo investigations like physical, mechanical, thermo-mechanical, and fracture analysis. Further, slurry erosive wear behavior is successfully investigated using Taugchi DOE technique.

The experimental results lead to flowing observations. The granite particulate reinforcement in varying content leads to increase in void content. This observed to decline as the coating is made on the alloyed composite. Thus single/multi layer coating of CrN and CrN + SiN proves to be beneficial in reducing the content of voids. The flexural strength observed to decline from 375.13 MPa to 315.93 MPa i.e. by 16% as the granite content increases from 0 wt.% to 6 wt.% in AA5083 alloyed composites. The flexural strength decline from 395.29 MPa to 339.9 MPa i.e. by 14% as the granite content increases from 0 wt.% to 6 wt.% in case of single coated AA5083 alloyed composites. Further, the flexural strength decline from 411.13 MPa to 369.19 MPa i.e. by 10.2% as the granite content increases from 0 wt.% to 6 wt.% in case of multilayered coated AA5083 alloyed composites. Similarly The flexural strength observed to decline from 327.3 MPa to 211.8 MPa i.e. by 35.2% as the granite content increases from 0 wt.% to 6 wt.% in AA105050 alloyed composites. After deposition of CrN coating the flexural strength decline from 355.29 MPa to 242.19 MPa i.e. by 29% as the granite content increases from 0 wt.% to 6 wt.% in case of single coated AA10550 alloyed composites. Further, the

flexural strength decline from 395.13 MPa to 253.16 MPa i.e. by 25.82% as the granite content increases from 0 wt.% to 6 wt.% in case of single coated AA10550 alloyed composites. The hardness increases from 68 Hv to 107 Hv by inclusion of granite powder 0-6 wt.% in 5083 aluminum alloy composites, similarly after deposition of single layer coating of chromium nitride on the above set of composite; hardness magnitude increases from 193 Hv to 259 Hv. Further, deposition of coating of silicon nitride on the single layer coated composites hardness improves from 213 Hv to 279 Hv respectively. However, in case of granite powder filled 1050 aluminum alloy composites the hardness increases from 32 Hv to 61.2 Hv with filler content in the alloyed composite. Whereas, with coating of CrN on the granite powder filled 1050 aluminum alloy the hardness of the composites further increases from xx to 123 Hv. Again, on increase in coating thickness i.e. for multilayer coating on the granite powder filled alloy composites the hardness improves in comparison to single layer and uncoated particulate filled aluminum alloy composites. The impact strength of 5083 & 1050 aluminum alloy improves after addition of granite powder and it further improved by deposition of Chromium nitride (CrN) coating or Silicon nitride/Chromium nitride (SiN/CrN) coating on granite powder filled composites. The magnitude of stress intensity factor increases in both the formulations and with increment in the crack length. The minimum stress intensity factor (0.159) is observed at crack length of 1 mm for 0 wt.% granite powder filled 1050 aluminum alloy composites and maximum stress intensity factor (1.169) is observed at crack length 4 mm for multilayer coated 6 wt.% granite powder filled 5083 aluminum alloy composites. The thermo-mechanical properties such as storage modulus (E'), loss modulus (E'') and loss tangent factor (Tan δ) are investigated for series of composites in three point bending mode. Both, coated and uncoated granite powder reinforced aluminum alloy composites are subjected to temperature range from 29-250ºC using dynamic mechanical analyzer. The presence of granite powder as reinforcement in both alloy composites improved their slurry erosion wear resistance. However, single layer and multilayer coating has significant effect on slurry erosion characteristics of granite powder reinforced 5083 & 1050 aluminum alloy composites. The slurry erosion characteristics of these composites have been successfully analyzed using Taguchi experimental design and the significant control factors such as impact velocity, impingement angle and slurry concentration influencing the slurry erosion rate have been identified through successful implementation of analysis of variance

(ANOVA). The corrosion rate decreases with time and corrosion rate increases with pH value of the solution for both coated and uncoated granite powder reinforced alloy composites.

Finally, the ranking order of the formulations is computed using ENTROPY-VIKOR approach. This technique make use of the results of mechanical, physical, fracture, corrosion wear and slurry erosion wear behavior of the investigated composites. The analysis shows the following ranking order of the composites: B-12 (Rank-1) > B-11 (Rank-2) > B-10 (Rank-3) > B-9 (Rank-4) > B-8 (Rank-5) > B-7 (Rank-6) > A-12 (Rank-7) > A-11 (Rank-8) > A-10 (Rank-9) > A-9 (Rank-10) > B-6 (Rank-11) > B-5 (Rank-12) > A-8 (Rank-13) > A-7 (Rank-14) > A-6 (Rank-15) > A-5 (Rank-16) > A-4 (Rank-17) > B-4 (Rank-18) > A-3 (Rank-19) > B-3 (Rank-20) > A-2 (Rank-21) > B-2 (Rank-22) > B-1 (Rank-23) > A-1 (Rank-24). Thus, B-12 specimen (multi-layered; 6 wt.% granite content; AA 5083 alloy) system proves to have optimal performance among other set of composites.

Table of Contents

******

LIST OF FIGURES

****

LIST OF TABLES

****

Chapter 1

INTRODUCTION

1.1 Background and Motivation

Mankind since industrial revolution develops many appliances, gadgets, equipments, machineries etc. with objective to make the human life easy, comfortable and efficient. The desire to make such appliances more technological advanced with energy-efficiency is the keen motto of our scientist/scholars and all such appliances generally consume electric-power. The sources of power may be classified into conventional (viz. fire-wood, coal, petroleum, natural gas, hydel-power etc.) and non-conventional (energy sources like solar, wind, nuclear, geothermal, tidal etc.) as shown in Figure 1.1. The overall contribution of hydro-power is around 26% in developing economy like India [1].

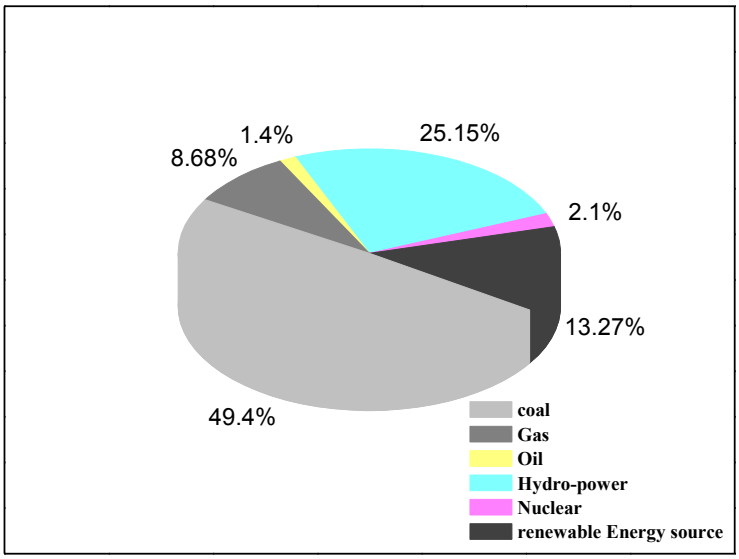

Figure 1.1 Sources of electricity in India by Installed Capacity as of 2013 [1]

Recently the Government of various states across the world shows keen interest in improving the efficiency of their hydro-power plant projects so that electricity production could be enhanced, in-order-to meet the increasing demand. Hydro-power plant comprises of dam built across the river so as to create large reservoir of water to certain height. Then the water is allowed to flow through channels (Figure 1.2) so that it strikes the turbine blades with greater force that rotates the turbine shaft, those in-turns coupled with generator to produce electricity.

The flowing water comprises of sand abrasive particles (called as slit) that have an impact on turbine blades, causing their erosion. This is a typical case of slurry erosion that caused rapid wearing, fracturing and corroding of the turbine blade material consequently maintenance cost manifolds, blade life decreases and plant has to shut-down temporary. The erosion accelerates in rainy season as sand abrasive content in slit manifolds. Such situations could be avoided and only by have a blade materials that have strong resistance to slurry erosive wear henceforth longer life. Conventionally, material used for turbine blades are metals/alloys like various grades of steel. At present, the materials scholars are experimenting with different alloyed composites (neat/coated) so as to enhance the blade life under such slurry erosive environment.

Research scholar's world-wide reported such research work like Ramesh et al. [2] reported slurry erosive behavior of aluminum alloy composite reinforced with silicon nitride (SiN) particulate. Likewise reinforcement of Silica, SiC, flyash in aluminum alloy are available in various literatures [4-6]. Conventionally, steel (304 steel, 410 steel, mild steel, CF8M steel), aluminum (1050, 2024, 5083, 6061, 7075), titanium (Ti6Al4V, Ti-8AL-1MO-1V, Ti-5AL-2SN) are reported in literatures [6-8, 9-11, 12-14].

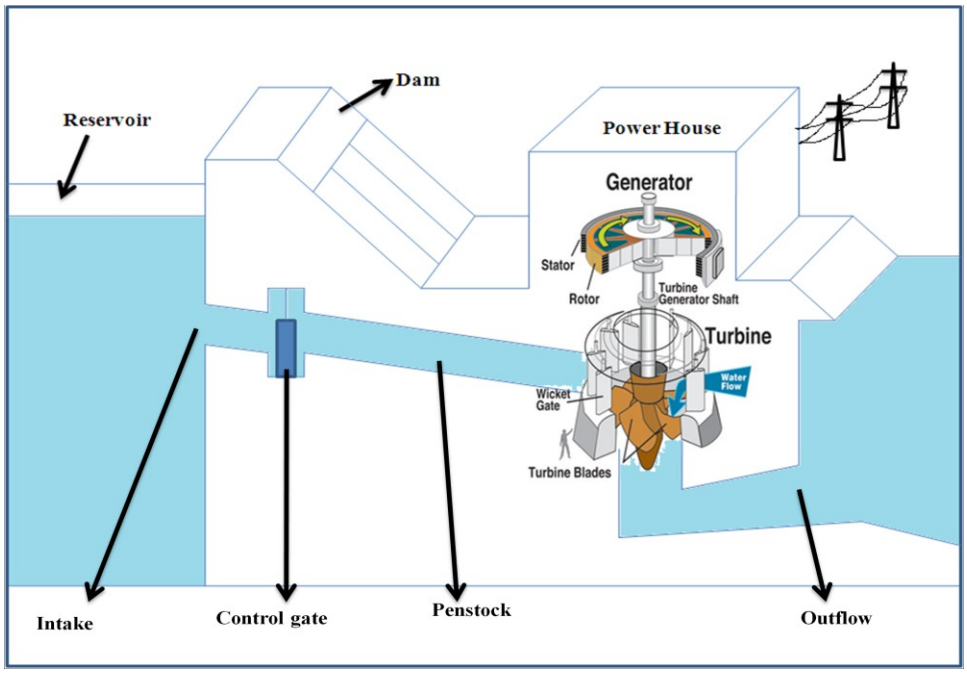

Figure 1.2 A inside view of hydro power plant [3]

Slurry erosion wear of material are controlled by factors like material factors (like hardness, toughness, microstructure, chemical composition, surface properties etc.), process

parameters (like impact pressure, impact velocity of slurry, slurry concentration, sand particle size etc.), and environmental conditions (temperature, pH, etc.).

Composite materials are designed/tailored materials having combination of two or more physically/chemically distinct phases insoluble into each other and have adhesion at inter-phase level [15]. Composites comprises of two phases, matrix and reinforcement. On the basis of matrix phases there are Organic matrix composites (OMCs) (like polymer matrix composites, carbon-carbon composites etc.), Ceramic matrix composites (CMCs) (like GF-SiC, CF-Al_2O_3 etc.), Metal matrix composites (like SiC-Al, Al_2O_3-Al, TiO_2-Al) respectively. Similarly, on basis of reinforcement phase there are fiber reinforced composites like (CFRP, GFRP etc.) and particulates reinforced composites like SiC-Al, Al_2O_3-Al, TiO_2-Al etc. [226, 227]. Composites are one of the most widely used materials because of their adaptability to sustain in different conditions. Composites not only serve specific purposes but also exhibit desirable properties at macroscopic or microscopic scale [15]. From the data on the service life of composite structures available in the literature, it can be said that they are durable, maintain dimensional integrity, resist fatigue loading and are easily maintainable and repairable. Due to this composite materials are continuously used in new structural applications [16, 17] in aircrafts, aerospace, marine, civil construction, automotive industries etc.

The material used for turbine blades are metals/alloys like various grades of steel that reported to damage badly in slurry erosive conditions. This problem forced the material scientist to come-up with new engineered/designed material that can perform well in such conditions. This scope could be achieved with the use of MMCs. There are two ways of having MMCs, one is having metal materials and another is to have alloyed metals as matrix. This matrix can be reinforced with particulates (having shape spherical, cubic, tetragonal, other irregular or regular shape) like ceramics that enable enhancement of its toughness so-as-to withstand slurry erosive environment. Such kind of research is going on over three decades. It is reported in various literatures [4-8] that ceramic reinforcement into metal-matrix or alloyed-metal- matrix offer unique characteristics that make them prominent candidate for such applications. Among them ceramic-alloy-metal-matrix composite offers better characteristics over others. The scholars like Hemanth et al. [4] studied the slurry erosion performance of chilled aluminum alloy reinforced with fused silica and observed that the wear resistance of the MMCs was increased till 9 wt.% of dispersoid content. The copper chill shows major effect on wear resistance because of its high

VHC. Effect of flyash reinforcement on slurry erosive wear of aluminum matrix composite was investigated by Ramachandra et al. [6] and made this observation that slurry erosive wear resistance increased with increase in flyash content. The slurry erosive wear of specimens was decreased due to formation of passive layer on the surface. Wear loss forming a protective layer against impact of slurry resistance of reinforced samples has decreased with increase in flyash content. Erosive wear of aluminum alloy composites was evaluated experimentally by Das et al. [7] and made this observation that composites exhibited better wear resistance than the matrix alloy. The wear resistance is increased with increment of SiC content in alloy matrix. Composites exhibited better wear resistance in acidic media than NaCl media. Materials exhibited more wear rates in acidic media than NaCl media at lower sand concentrations and at higher sand concentrations the wear is higher in NaCl media compared to acidic media. Influence of experimental parameters on the erosive-corrosive wear of Al-SiC particle composite was studied by Das et al. [8]. They observed that the wear rate of Al-SiC composite was found to be a strong function of sand concentration, angle of impingement and the radial distance. The wear rate of the composite was increased with increasing angle of impingement, radial distance and sand concentration. Erosion rate decreases with decrement in erodent particle size.

Material scholars also have tested alloyed composites with different ceramic coatings with the objective of increasing material life and superior properties under slurry erosive conditions. Scholars like Grewal et al. [9] carried out work on slurry-erosion performance of hydro-turbine steels coated through detonation gun spray technique. The result shows that coated samples exhibit better slurry wear behavior as compared to bared samples. Slurry erosive behavior of High Velocity Oxygen Fuel (HVOF)-Spray Cr_2O_3 coated turbine steels was studied by Goyal et al. [10]. They concluded that HVOF-sprayed Cr_2O_3 coating enhanced the slurry erosion resistance of the steels and rotational speed was found to be the most dominating factor for slurry erosive wear in all cases. Slurry erosion behavior of Al_2O_3 and Al_2O_3-$13TiO_2$ coated CF8M steel by detonation gun spray technique under hydro accelerated conditions was conducted by Bhandari et al. [12]. In their result, the mass loss of the eroded specimens confirmed that D-gun spray Al_2O_3-$13TiO_2$ coated steel resists slurry erosion much better than the Al_2O_3-coated steel. During the slurry erosion of Al_2O_3-coated steels, slurry concentration and average particle size were found as dominating factors in comparison of rotational speed. On the other hand, in the case of Al_2O_3-$13TiO_2$-coated steel, rotational speed was found dominating in

comparison of slurry concentration and average particle size. In another work in same year [13] slurry erosion performance of WC-10Co-4Cr coatings on CF8M steel using detonation gun-sprayed was investigated. They found that D-gun-sprayed WC-10Co-4Cr coatings shows reduction in the erosion rates of the CF8M steel. During the slurry erosion test of CF8M steel, slurry concentration and rotational speed were found more dominant factors in comparison of average particle size. In the case of D-gun-sprayed WC-10Co-4Cr coatings, average particle size was found more dominant factor in comparison of slurry concentration and rotational speed.

The literature reports [13, 14] of various scholars world-wide found that the performance reliability of the components in an assembly could easily be enhanced by surface modifications methods like plating, surface hardening, diffusion, thin film deposition, thermal spray etc.. Such components observed to maintain their functionality even in harsh operating conditions like high temperatures, pH-environments, corrosive-conditions etc.

The surface modification method is a science of developing a thin layer or coating of materials (that may be a pure metal, alloy metal, ceramics, polymers, composites etc.) on bulk substrate such that together coating-substrate system imparts better surface finish, performance, or functionality than the individual materials [18]. Thereby protecting the substrate materials from any kind of damage during the service life and hence able to modify most of the properties manifold like tribological, mechanical, thermo-mechanical, electro-chemical, optical, electrical, electronic, magnetic/acoustic, biocompatible etc. [9,10].

Over the decade or so, the material scientists are trying to develop cost-effective technology of surface modification for exploiting at commercial level [9,10]. During the course, numerous techniques were developed and most frequently techniques are discussed in Figure 1.3. The different surface modification techniques may be classified as plating, diffusion process, surface hardening, thin film coating and thermal spraying. The details of these techniques are:

1.2 Plating or Electro-plating: The variant of plating method are electro-deposition, electroless deposition, electro-chemical conversion coating and electro-forming. In this process substrate (necessarily conducting) forms a cathode electrode, coating material is anode electrode and both is in an appropriate electrolyte [19]. As the current passes through the electrolytic solution, ions from the coating material electrode pass through the electrolyte and get deposited on the substrate cathode electrode, in this way thin layer of coating get deposited over the substrate. In electro-less plating process deposition occurs by catalytic reduction of the solute present in the

plating bath. In electrochemical conversion coating method, the electrolyte itself consists of coating material and a thin coating layer gets deposited over the substrate electrode as a result of reaction between the electrolyte-substrate [20]. Electroforming was the process of electro-depositing a material on a removable mandrel to make a part and modified its physical, mechanical or corrosion properties [21].

1.3 Diffusion Processes or case hardening: In diffusion process, an element like boron, carbon, nitrogen, aluminum, chromium, silicon, boron etc. is made to diffuse into the surface of the substrate at higher temperature. The higher temperature reported to accelerate the diffusion phenomena [**22**]. Depending upon the element to diffuse, its variant is named accordingly like boronising, carbonizing, nitriding, carbonitriding, chromising, siliconising, etc. [23-25].

1.4 Surface hardening: In this method, the temperature of the material is raised around and below its melting point, then holding it for some-time and then quenching it in different medium like oil, water, air etc. depending upon its TTT curve. This results in desired micro-structure and hence alters its overall properties [26, 27].

1.5 Thin Film Coating: In this process a thin layer of a pure element or a compound can be deposited on the substrate [28]. It has two variant viz. (a) Physical Vapour Deposition (PVD) and (b) Chemical Vapour Deposition (CVD).

1.5.1 Physical Vapour Deposition (PVD): The physical vapour deposition technique comprises of (i) thermal vapour deposition (ii) Magnetron-sputter coating (iii) ion-plating coating. In thermal vapour deposition method, both substrate and coating material are kept facing towards each other in an evacuated chamber. The coating material evaporates directly from solid state by the application of heat/pressure and gets deposited over the substrate in the form of uniform thin-coating [29]. In magnetron sputter coating method [30] both substrate and coating materials are connected across two electrodes (viz. anode and cathode) with a suitable power supply having inert gas environment in a vacuum chamber. The inert gas gets ionized under the influence of electric-filed. The positive ions move towards the cathode (i.e. the coating material) and dislocate ions from it. These ions rush toward the anode and deposit on the substrate surface. The ion plating method is a combination of above methods where the coating material (cathode electrode) is heated and at the same time inert-gas plasma is introduced in the vacuum chamber [31]. The ions of coated materials thereby gets deposited over the substrate inform of uniform thin layer. With this method coating of pure elements/compounds could be deposited.

1.5.2 Chemical Vapour Deposition (CVD):

In this methods substrate and coating material is kept in evacuated chamber with a provision of heating to required temperature (700°C or above). Thereafter, appropriate gas is introduced in chamber for chemical reaction, due to which a thing coating layer gets deposited over the substrate surface [32]. Hence, the rate of deposition in CVD is higher than PVD.

1.6 Thermal Spraying: In this method [33, 34], finely divided molten coating material (like metallic, ceramic or polymeric substances) is sprayed onto the substrate kept in front of the impinging jet. Here, rate of deposition is higher than all deposition techniques. The adhesion strength of thermal spray coating is superior among all coating methods.

Various statistical tools such as (Taguchi, ANNOVA, ANN, Surface response method etc.) have been utilized for analysis, prediction and/or optimization of a number of engineering processes. These methods facilitate the user to investigate the significance of each factors involved in an experiment on the output response. Slurry erosion wear is a complex wear phenomenon involving various control factors that affect the performance output (i.e. the slurry erosion rate) and implementation of appropriate statistical techniques for process optimization. But unfortunately, such studies have not been satisfactorily reported so far. In present research Taguchi experimental design statistical approach is adopted. This technique provides a simple, systematic and efficient methodology for the analysis of the control factors. Based on the above discussion and literature survey, the present research work aims to apply thermal vapor coating technique on granite powder reinforced aluminum alloy metal matrix composites and investigate their physical, thermo-mechanical, fracture behavior and corrosion, slurry erosion wear analysis of particulate filled metal alloy composites.

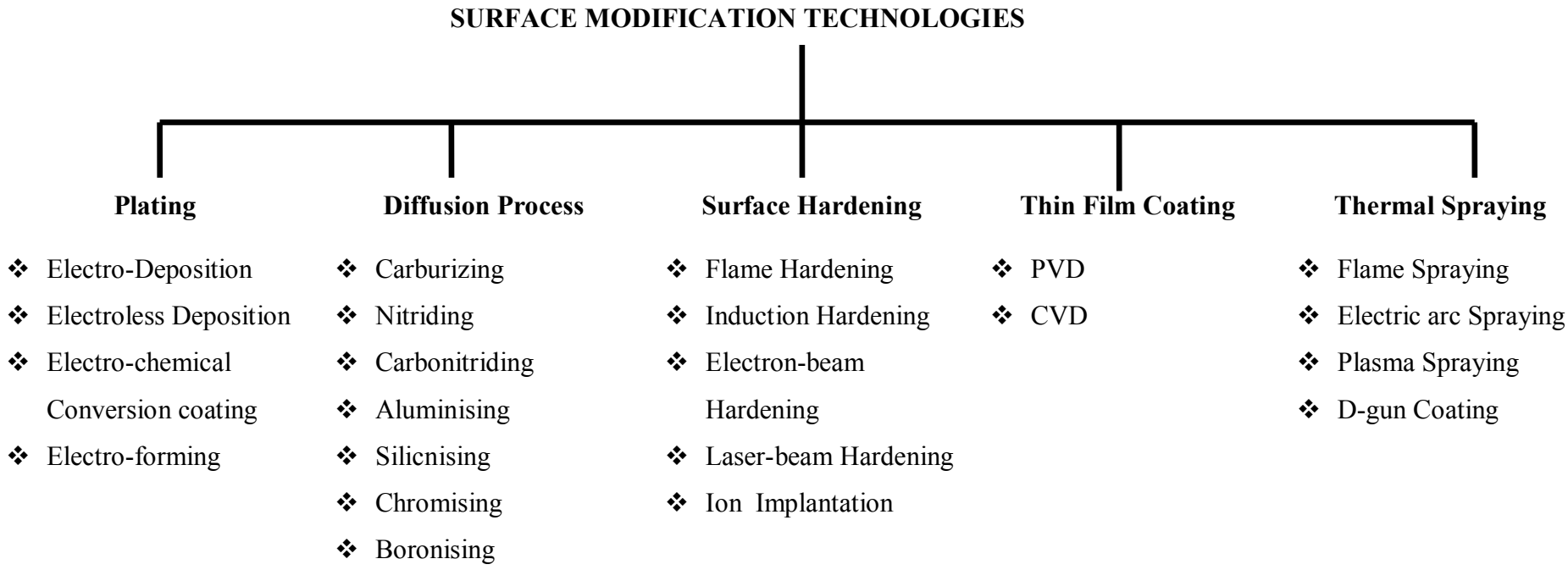

Figure 1.3 Various forms of surface modification technologies [7]

1.7 Outline of the thesis manuscript

The subsequent chapters of the thesis are organized as below:

Chapter 2: This chapter presents literature review on various themes of coated and uncoated metal matrix composites like physical properties, mechanical properties, fracture properties, thermo-mechanical properties, corrosive properties, and slurry erosive wear behavior. It also has literatures on implementation of Design of Experiments (DOE) and optimization techniques often used by various researchers for process parameter optimization. At the end research summery, research gaps and objective of the present research is presented.

Chapter 3: This chapter discusses details of (i) materials (i.e. matrix, reinforcement, and coating), (ii) the formulations, (iii) the fabrication technique of alloyed composites, (iv) the coating method employed for preparation of the specimen. It also discuss characterization methodology like physical, mechanical, fracture, thermo-mechanical, corrosive, slurry-erosive etc. It also presents Taguchi DOE methods and VIKOR multi-criteria-decision-making approach for formulation ranking.

Chapter 4: This chapter presents discussion on results of physical and mechanical characteristics of the alloyed composites under investigation.

Chapter 5: This chapter presents discussion on results of fracture and thermo-mechanical characteristics of the alloyed composites under investigation

Chapter 6: This chapter presents results on corrosive and slurry erosive wear properties of the alloyed composites under investigation. The results analysis using surface wear morphology using SEM and AFM is also reported.

Chapter 7: This chapter presents ranking of the formulations under investigation using multi-criteria-decision making techniques tool like ENTROPY-VIKOR.

Chapter 8: This chapter summarizes (i) findings of the investigation, (ii) conclusions drawn from the research work, (iii) scope for future work.

******

Chapter 2

LITERATURE REVIEW

This chapter presents the review of work done by material scholars world-wide over the last three decades reported in various literatures. It embraced literatures on particulate filled metal matrix composites (MMCs) and coating variations of the same under slurry erosive wear environment. Thus, review is organized so as to understand the subject completely. It has details of work done as reported in literatures on the following themes:

- ✓ Physical & Mechanical characterization of MMCs
- ✓ Fracture characterization and its mechanism in MMCs
- ✓ Thermo-mechanical characterization of MMCs
- ✓ Corrosion behavior and its mechanism in MMCs
- ✓ Slurry erosive wear behavior and its mechanism in MMCs
- ✓ Techniques of Design of Experiments (DOE), its implementation and other optimization techniques like Taugchi Optimization methods etc.
- ✓ Multi-criteria decision making methods for analyzing results

2.1. On Physical and Mechanical characterization of MMCs (coated/uncoated)

The physical and mechanical characterizations of MMCs (coated/uncoated) become significant in order to understand their functional aspects under mechanical loading. Such characterization reports of successful MMCs, developed by various material scholars are presented in this section. In general it is observed that such properties are dependent upon particulate type reinforcement, matrix material, coating material, thickness and deposition methods etc. For example, mechanical properties of 50 wt.% SiC/Al5210 MMCs was reported by Xiao-dong et al. [35]. According to them bending strength of the composites increases, while the fracture toughness of the composites decreases with the increase in reinforcement. Similarly, Milan et al. [36] evaluated the effects of particle size, particle volume fraction, and matrix strength on mechanical properties of two different Al alloys, reinforced with silicon carbide particles (SiC) and found that with increase in particle volume fraction; the tensile strength increases, ductility decreases and toughness reduced. Mechanical behavior of AlSiCuMgNi alloys reinforced with TiB_2 particles was discussed by Zhao et al. [37] and reported that the ultimate tensile strength (UTS) of the composites increases with increment in percentage of TiB_2 reinforcement in the

matrix. Tong et al. [38] reported the mechanical properties of SiC-particulate filled titanium composites and found increase in the tensile strength and ductility of SiC-particulate filled titanium composites by shock wave method. Effect of the porosity on the mechanical of properties of particulate filled composites was reported by Aqida et al. [39]. According to them, almost all mechanical properties of cast-composites decrease. The failures of such composites initiated from the pores within the matrix material and reinforcement-matrix interface; may attribute to voids coalescence. Wang et al. [40] evaluate the mechanical properties of a novel ZnO/Cu composite and reported that increase of ZnO content exhibits a relative good interfacial bonding and leads to decreased density but increases hardness. Mechanical properties of TiN reinforced aluminum MMCs by microwave sintering was studied by Venkateswarlu et al. [41]. They found that increasing TiN from 10 to 30 wt.% showed superior hardness as compared to Al-TiN composites prepared by hot pressing. Singla et al.[42] evaluated the mechanical properties of SiC filled Al matrix composites and reported that increase in proportion of SiC in Al matrix improved the hardness and impact strength. Mechanical properties of graphite particles reinforced aluminum alloy matrix was reported by Barekar et al. [43]. They found that a uniform distribution of graphite particles within an aluminum alloy matrix was achieved by stir casting fabrication technique and addition of graphite particles within an aluminum alloy matrix of improved the tensile strength (UTS) and tensile elongation of the composites. Poddar et al. [44] synthesized AZ91D composites reinforced with silicon carbide (SiC) particulates and evaluate its mechanical properties and found that the presence of SiC particulate shows significant improvement in hardness, elastic modulus and yield strength. The effect of manganese on mechanical properties of Zn–Al based ZA-8 alloy fabricated through gravity casting was investigated by Turk et al. [45]. They found that the variation of hardness, 0.2% yield strength, UTS, impact strength and the creep strength of ZA-8 alloy increased with the addition of manganese content. Sharma et al. [46] investigated the mechanical properties of composites consisting of ZA-27 alloy reinforced with Zircon particles. In this regard they reported that ultimate tensile strength, yield strength, simultaneously hardness, and Young's modulus of the composites enhanced, but ductility and impact strength decreased with increase of zircon content in base alloy. Effect of the hot forging process on the microstructure and mechanical properties of aluminum alloys AA2618 reinforced with 20 vol.% of alumina particles (Al_2O_3) was examined by Ceschini et al. [47]. They reported that induced a slight increase in hardness, tensile

strength, elastic modulus and an evident increase in tensile elongation. Daoud et al. [48] studied tensile properties of rolled Al5Mg-Al_2O_3MMCs and found that the addition of Al_2O_3 increased the 0.2% proof stress and reduced both the tensile strength and ductility, compared with the monolithic alloy. Seah et al. [49] evaluated the mechanical properties of aluminum/quartz particulate composites cast using metallic and non-metallic chills. They found that in the Al/quartz composites tested, UTS of the chilled composites were found to increase as the content of quartz particulates was increased up to approximately 6% by weight fraction. Effect of adding Mg and Si to aluminum matrix on the thermo-mechanical properties was investigated by Ren et al. [50] and reported that with increment of Si content in the aluminum enhance the elastic modulus. However, excessive Si beyond 12 wt% reduced the bending strength of the composites. An optimum content of Mg addition to aluminum was found to be 4–8 wt%, at which the composites exhibited good mechanical properties. Geng et al. [51] evaluated the tensile properties of in situ synthesized titanium matrix composites reinforced by TiB and Nd_2O_3 at elevated temperature and found that the ductility of the composites improves with the content of neodymium and the test temperatures. Mechanical characterization of Al–4.5% Cu alloy with fly ash metal matrix was evaluated by Mahendra and Radhakrishna [52]. The results show an increase in hardness, tensile strength, compression strength, and impact strength with increasing the fly ash content. The density decreases with increasing fly ash content. Zhang et al. [53] investigated mechanical properties of pressureless infiltrated SiC/Cu composites. They were reported that elastic modulus was insensitive to alloying elements, while bending strength decreased dramatically when excessive alloying elements dissolved in the matrix. Fluidity and tensile Properties of Aluminum/Hematite particulate composites was studied by Sharma et al. [54]. The results shows that the ultimate tensile strength and Young's modulus of the composite increased while the liquid fluidity and solid ductility decreased with the increase in hematite content in the composite specimens. Hyo et al. [55] examined the mechanical properties of SiC/Al-Si metal matrix composites and conclude that tensile strength, hardness increased with increase the SiC particle. Chua et al. [56] influenced of SiC particles on mechanical properties of Mg based composite. Yield and ultimate tensile stresses show a decrease with the increase in the particle size and volume fraction of SiC particulates. Influence of reinforcing phase such as shape, size, volume fraction and distribution on mechanical properties of particulate reinforced metal matrix composites studied by Lim and Dunne [57]. They concluded that the strengthening

offered by the particulate reinforcement occurs only over a small range of plastic strain from the onset of composite yielding. The hardening saturates at a particular volume fraction, but for higher volume fraction of reinforcement, eventually drops below that of the unreinforced matrix material at higher plastic strain. Breval [58] in his review on synthesis routes to metal matrix composites with specific properties found that the hardness, modulus of elasticity and electrical resistivity do not change significantly below - 25 wt.% of reinforcement. Micro-structural and mechanical characteristics of in situ metal matrix composites discussed by Tjong and Ma [59] and reported that the reinforcements were formed in situ by exothermal reactions between elements or between elements and compounds exhibit excellent mechanical properties. Xian-dong et al. [60] evaluated different properties of particle reinforced cast ZL-109 alloy and ZA-27 alloy MMCs with SiC, Si_3N_4, B4C, Al_2O_3 and the graphite flakes as reinforcement and found that the tensile strength of the composites reinforced by ceramic particles was slightly decreased as compared to that of the matrix alloys, still remained at a relatively high level for a particular value of particle fraction, the hardness markedly increasing with the addition of ceramic particles, amongst which B_4C particle has the strongest effect and the ductility of the tensile sample was significantly reduced, as compared to that of the unreinforced material. Tensile behavior of pure aluminum reinforced with ≥ 40 vol.% alumina particles studied by Kouzeli et al. [61]. They observed that the initial stiffness of infiltrated Al_2O_3–Al composites was controlled by the volume fraction of reinforcement, while the yield stress was a function primarily of particle size. Neither of these properties was significantly influenced by the shape of the reinforcement. Chawla and Shen [62-63] reviewed the mechanical behavior of wrought particle reinforced light alloy metal matrix composites with a particular emphasis on tensile, creep, and fatigue behavior and observed that with increase in volume fraction, more load was transferred to the reinforcement which also results in a higher ultimate tensile strength and the work hardening rate was increased with increasing volume fraction of reinforcement (and decreasing matrix volume). In an another finding, they correlated hardness and tensile strength in particle reinforced metal matrix composites and found that a unique relationship between hardness and tensile strength does not exist, especially in cases where the matrix strength was relatively low. The reinforcement fraction so appear plays an important role in affecting the hardness strength relation.

Kaataih et al. [64] revealed that the addition of TiO_2 particles has significant effect on mechanical properties of the MMCs because with increase in reinforcement content the ultimate tensile strength, yield strength and hardness of the composite increase while the ductility of the composite decreases. Increase in hardness was due to the TiO_2 particles acting as barriers to the movement of dislocation and contribute positively to the hardness of the composites. Effect of zircon content on mechanical properties was studied by Abdizadeh et al. [65]. It was found that with increase in zircon content increases the hardness of the metal matrix composite increases due to random distribution of zircon particles. zircon particles were agglomerate in a region and would not change during sintering with increase in zircon content and the direct contact between these regions causes weak binding between the boundaries and thus reduces the strength of the composites. Kok [66] reported that the mechanical properties such as tensile strength, hardness increase and elongation decreases with decreasing size of the particle and increasing the volume fraction and also the density of the composites increased with increasing weight percentage and size of the particle where as the porosity of the composites increased with decreasing size and increasing weight percentage of particles. The addition of quartz particles had positive effect on lead alloy mechanical properties studied by Sharma et al. [67] and found that the addition of quartz particles had positive effect on lead alloy as it increases the hardness, ultimate tensile strength, impact strength and hardness. Increment in mechanical properties was due to the quartz particle act as barriers for the movement of dislocations or to the presence of hard particle which impart strength to soft matrix. NiZ et al. [68] studied the effect of TiC addition on mechanical properties of steel and concluded that TiC addition to austenitic stainless steels on both mechanical properties and oxidation resistance at ambient and elevated temperature, tensile strengths of austenitic stainless containing 5% TiC were notably higher than those of the matrix without TiC addition, Besides tensile strengths, creep resistance of austenitic stainless steels was also significantly increased by TiC addition at elevated temperature of 923 K. Li et al. [69] carried out work on mechanical behaviors of in situ TiC particulates reinforced Ni matrix composites and find that The in situ TiC reinforced Ni matrix composite exhibits relative high hardness, moderate yield strength, good ultimate tensile strength and transverse flexural strength. Mechanical properties of novel magnesium/ nickel composite studied by Hassan et al. [70] and concluded that presence of nickel in inter-metallic compound improve hardness, stiffness and ultimate tensile strength of magnesium but it adversely affect ductility of magnesium matrix.

Mechanical properties of nickel-coated titanium carbide particulates reinforced iron matrix composites investigated by Yi et al. [71] and concluded that the addition TiC particles improves tensile strength, hardness and elongation but coating of Ni on TiC further improves mechanical properties duet to proper interface bonding between Ni coated TiC particles and Iron matrix. Ramesh et al. [72] reported that addition of silicon nitride particles in matrix alloy has resulted in higher hardness and ultimate tensile strength of the composites. Micro hardness varies with increase in percentage weight of Ni-P coated silicon nitride particles in Al6061 alloy. Velasco et al. [73] studied the mechanical properties of TiCN reinforced high speed steel and concluded that addition of TiCN particles into matrix improve hardness and its interfacial strength due to proper adhesion between matrix and reinforcement.

Effect of TiO_2 coating on mechanical properties was reported by Li et al. [74]. It was concluded that TiO_2 coating can improved the interfacial bonding strength between the matrix and $Mg_2B_2O_5W$, which lead to a higher efficiency of load transfer from the matrix to $Mg_2B_2O_5W$ and then higher mechanical properties of $Mg_2B_2O_5W$ /TiO_2/AZ91D composite. TiO_2 coating results in the improvements in the flexural strength and flexural modulus by addition of $Mg_2B_2O_5W$. Investigation of mechanical properties of borided Nickel 201 alloy was carried out by Gunes et al. [75]. It was obtained that boried layer improved hardness of composites as compared to untreated Nickel 201 alloy. Fellner et al. [76] reported that electroless nickel co-deposition on boron and silicon improves microhardness of composites. Mechanical behavior of α-Al_2O_3-coated SiC particle reinforced nickel matrix composites was studied by Wu et al. [77]. It was observed that α-Al_2O_3-coated SiC particles act as effective reinforcements in nickel matrix composites and enhance its strength and hardness. Wu et al. [78] reported that with the addition of the EN interlayer, the composite hardness of the duplex coating assembly CrNrENrMS was improved more than three times as compared to the single coating CrNrMS, SiO_2 particles significantly. Lin et al. [79] studied the hardness of TiN/Zr/ZrN multilayer coatings deposited on titanium alloys by vacuum cathodic arc ion plating method and found that samples with 24 periods have higher hardness than those with 3 and 12 periods. Influences of parameters on mechanical properties of $Cr_{13}Ni_5Si_2$ based composite coating by laser-induction hybrid cladding was studied by Wang et al. [80] and concluded that the hardness (H) and elastic modulus (E) of the coatings were proportional to the volume fraction of the $Cr_{13}Ni_5Si_2$. Xiong et al. [81] examined the effect of cold sprayed aluminum alloy coating on mechanical properties. It was

reported that shear adhesive bond strength or tensile adhesive bond strength reduced with increase in coating thickness. Chen et al. [82] discussed the effect of cu content on mechanical properties of Cr–Cu composite coatings fabricated via mechanical alloying method. They observed that the coating prepared in the powder of 35 wt.% Cu shows the best surface roughness, coating adhesion and mechanical properties among all set of composition coating. Mechanical properties of Al_2O_3/Al bi-layer coated AZ91 magnesium alloy was evaluated experimentally by Xin et al. [83]. The results shows that Al inter-layer enhance the hardness and adhesion strength between the coating and substrate. Ou et al. [84] investigated the mechanical properties of CrN/TiN superlattice coatings deposited by high-power pulsed magnetron sputtering technique. They observed that high-power pulsed magnetron sputtering technique Λ was increased from 5.7 to 10.2 nm, improvement in mechanical properties. Effects of thickness, processing technique, and cooling rate on the flexural strength was studied by Lima et al. [85] and found that the thickness of the veneer ceramic coating influenced the flexural strength of the all-ceramic bi-layer system, synthesis through all processing technique and cooling protocol. Sharma and Gupta [86] investigated the flexural properties of metal-matrix composite cladding on austenitic stainless steel substrate and concluded that clad significantly improved hardness and flexural strength. Mechanical properties of diamond coating was investigated by Bouzakis et al. [87] and concluded that diamond coating improves hardness and impact strength of composites. Shan et al. [88] evaluated the bonding strength of SiC coating by chemical vapor deposition method and results shows that the transition layer plays a positive role in improving the bonding situation between SiC coating and C/C substrate and restraining the cracking of the coating. Mechanical analysis of titanium multiphase coating produced by plasma nitriding on aluminum alloy was investigated by Zhang and Yan [89] and concluded that micro-hardness improved by nitriding process due to formation of TiN0.3 phase or nitriding process improves adhesion properties of composites. Yang et al. [90] examined the effect of Nb addition on mechanical properties of FeAl coating and concluded that Nb atom implantation in coating improves hardness, adhesion strength or strength of coating. The combined effects of Cu and Ag addition on mechanical properties of CrCuAgN PVD coatings were discussed by Liu et al. [91]. It was found that the combined Cu+Ag concentration influence the hardness of PVD coating. Bouzakis et al. [92] studied the adhesion and impact properties of diamond like coating deposited on steel substrate by physical vapor deposition technique. They observed that diamond

like coating exhibited good adhesion and impact strength. Mechanical properties of CrN/TiN multilayer coatings deposited by pulsed dc magnetron sputtering method were studied by Ou et al. [93]. They observed that the coatings exhibited high toughness, hardness and cohesion/adhesion strength with high HF levels and Lc. Cheng et al. [94] evaluated the mechanical properties of TiC–TiB2/CoCrCuFeNi high entropy alloy coatings deposited steel samples and concluded that TiB2 and TiC reinforced HEA coatings improves hardness and other mechanical properties of composites. Mechanical properties of pulsed DC magnetron sputtered TiN-WSx/TiN bilayer coating was studied by Banerjee and Chattopadhyay [95] and results shows that addition of 6.2 wt.% of WSx increased the nano-hardness of the composite coating as compared to pure TiN, however, further addition led to a progressive fall in nano-hardness. The adhesion strength also improved with the WSx content in pure TiN coating. Li et al. [96] investigated the influence of TiO_2 content on mechanical properties of a Cr_2O_3–TiO_2 composite coating deposited by plasma spraying technology method. They observed that TiO_2 content increased the porosity of coating and due to formation of $(Cr0.88Ti0.12)_2O_3$ phase hardness improved. Adhesion strength of nano-structured 5La3TiYSZ, 8LaYSZ and 8CeYSZ coatings prepared by atmospheric plasma spraying was studied by Jin et al. [97]. They observed that adhesion strength of as sprayed nano-structured 5La3TiYSZ, 8LaYSZ and 8CeYSZ magnitude 52.24, 49.91 and 50.81 MPa, respectively. Hamzah et al. [98] investigated the mechanical properties of plasma sprayed NiCrAlY/nano-YSZ duplex coating on Mg–1.2Ca–3Zn alloy and concluded that NiCrAlY/nano-YSZ dual layer coating enhance hardness or bond strength of composites. Mechanical properties of plasma electrolytic oxide coatings on AZ31 Mg alloy produced by twin roll casting was studied by Aktug et al. [99] and results shows that the micro hardness or surface roughness of the coatings were increased with increasing concentration of Na_2SiO_3 electrolyte solution but adhesion strength shows no change. Hamzah et al. [100] investigated the mechanical properties of plasma sprayed NiCrAlY/nano-YSZ duplex coating on Mg–1.2Ca–3Zn alloy and concluded that NiCrAlY/nano-YSZ dual layer coating enhance hardness or bond strength of composites.

From the above literatures it could be understood that particulate filled MMCs may results in increase in the mechanical properties except hardness. Hardness magnitude increases slightly, that could future be improved by applying coatings over MMCs.

2.2. On fracture characterization of MMCs (coated/uncoated)

The fracture characterization of MMCs (coated/uncoated) becomes significant as it indicates toughness of a material or energy absorbed by material before it fractures. Material having good fracture strength can withstand longer under slurry erosive environment. Applying coating over them further manifolds its fracture strength. Fracture property of MMCs are dependent upon Volume of fraction of reinforcement, Coating thickness, Inter-particle spacing and strength of the particles, Spatial particles distribution of particle (i.e., particle clustering), Microstructure of matrix, interfacing, and loading velocity. Such characterization reports of successful MMCs, developed by various material scholars are presented in this section. For example, romanova et al. [101] reported *n*umerical analysis of the reinforcing particle shape and interface strength effects on the deformation and fracture behavior of an Al/Al_2O_3 composite. The found that fracture properties are strongly affected by the reinforcing particle size, shape, volume fraction, and spatial distribution. Similarly, fracture toughness of TiC and AlN particles reinforced Al matrix composites investigated by Cui et al. [102]. They were conclude that the fracture toughness of TiCp and AlNp/Al composite was a function of reinforcement volume fraction and size. Again, Park et al. [103] investigated the fracture toughness of 6061 aluminum-magnesium-silicon alloy reinforced with 20 vol.% Al_2O_3-based polycrystalline composites. They observed that the fracture toughness decreased progressively with increasing particle volume fraction, the effect becoming less pronounced as the volume fraction increased. Effect of particle size, particle volume fraction and matrix strength on fracture toughness properties of SiC Reinforced Al Alloys was studied by Milan et al. [36]. They observed that in fracture toughness tests, an increase in particle volume fraction reduced the fracture toughness of the composites. The presence of porosity affect the fracture properties of SiC/Al matrix composites was studied by Aqida et al. [39] and found that increasing ceramic particles content in MMC will drop the fracture toughness as the formation and merge of voids within the matrix tend to cause fracture in MMC. Oh et al. [104] studied the effects of short-fiber/particle hybrid reinforcement on fracture toughness and fatigue crack growth in metal matrix composites. The fracture toughness (*KIC*) increases with increasing of particle contents and particles effectively reduced the void formation and coalescence. Fracture behavior of SiC/AZ91 magnesium matrix composite fabricated by stir casting was investigated by Wang et al. [105]. The fracture mechanism of SiC/AZ91 composite was controlled by particle/matrix interface obtained by stir casting

fabrication technique. Mochida et al. [106] observed fracture toughness of Al_2O_3 particles reinforced Al alloys metal matrix composite by In-Situ tensile testing under plastic straining. The results shows that the Young's modulus decreases with plastic strain and fracture toughness depend on the particle size. Joel Hemanth [107] studied the fracture toughness of Al-boron particulate composites cast in sand moulds containing metallic (copper, steel and cast iron) and non-metallic (silicon carbide). They observed that fracture toughness of the Al-boron composites increase as the content of boron particulates increased up to approximately by 6% weight fraction. Stress intensity factor for a single edge notched specimen with clamped ends of SCS-6/Ti-24Al-11Nb composite were evaluated by Blatt et al. [108]. The investigation was indicated that the Single Edge (T) geometry with clamped ends can be successfully used for fracture and fatigue crack growth testing of monolithic and composite specimens. Seah et al. [49] studied the fracture toughness of aluminum/quartz particulate composites cast using metallic and non-metallic chills. They found that in the tested Al/quartz composites, fracture toughness of the chilled composites were increased as the content of quartz particulates increased up to approximately 6% by weight fraction. The effect of the hot forging process on fracture properties of aluminum alloys AA2618 reinforced with 20 vol.% of alumina particles (Al_2O_3) at room and high temperature was studied by Ceschini et al. [47]. They observed that fracture surfaces, both at room and high temperature, are characterized by particle reinforcement debonding, due to a weak interface, and ductile failure of the matrix. Similarly Kruzic et al. [109] reported the effect of ambient and elevated temperature of alumina boned with Copperr/Niobium/Copper inter layers on fracture toughness values. They observed that fracture toughness is decreases ~50% for temperature range 25°C to 1000 °C and decrement was attributed to reduction in toughening contribution from the plastic work associated with deforming the copper phase at temperatures near its melting point.

Agrawal and Sun [110] studied the fracture mechanisms of two metal–ceramic composites, Cu/Al_2O_3 and Al/Al_2O_3 and concluded that the crack propagated inside the metallic phase and at the interface for the Cu/Al_2O_3 composite was due to a high level of tensile thermal stresses inside the metallic phase, as well as due to low contiguity of ceramic phase. Fracture characteristics of the 2009/SiC aluminium alloy composite discussed by Srivatsan et al. [111]. From the results they concluded that the intrinsic brittleness of the reinforcing SiC particulates coupled with the propensity for it to fracture due to localized in homogeneous deformation and

local stress concentration results in particulate cracking and interfacial failure through debonding being the dominant damage modes. Gupta et al. [112] focused on interfacial behavior in a SiC reinforced 6061 Al alloy and from its fractographic analysis indicated a strong correlation between the failure modes operative under tensile loading and the type of heat treatment. The effect of volume fraction of reinforcement on fracture toughness was discussed by Wang et al. [113]. They were observed that when the volume fraction was <6%, the composite had improved fracture toughness but with the increases of volume fraction of reinforcement (>6%), the fracture toughness decreases slowly at the initial stages and then decreases rapidly towards the end. The reason for the above mentioned behavior was given as the fracture failure mechanisms consist of crack nucleation, growth, coalescence and crack propagation. Chichili and Ramesh [114] discussed the dynamic failure of an alumina particle reinforced 6061-T6 aluminum alloy composite and found ductile failure through void nucleation, growth and coalescence and substantial void sheet formation. Fracture toughness of Al 356-SiCp aluminum matrix composite was investigated through an experiment by Ranjbaran et al. [115]. They observed that the low-toughness fracture was an inherent property of this composite due to the difference between the elastic and thermal properties of the two ingredients. The degradation in fracture toughness is due to the strain hardening capacity and by stress intensification introduced by the SiC particle geometry. Simultaneously the high localized damage leading to premature fracture at near of matrix interface. Velasco et al. [116] studied the influence of Ni3Al inter-metallic particles on the fracture behavior of aluminum matrix (2014) composite materials and found that the addition of inter-metallic does not modify the fracture behavior of the matrix.

The effect of metal particles on the fracture toughness of ceramic matrix composites was investigated experimentally and through mathematical model by Konopka et al. [117]. They found that found that the metal particle distribution in the matrix will influence the crack propagation. Given a defined volume fraction of metal particles in the matrix and size of these particles, a different level of uniformity of their distribution will result in a different number of metal particles encountered by the propagating crack. Similarly Ergun et al. [118] developed a numerical model to study the effect of crack position on stress intensity factor in particle-reinforced metal-matrix composites. They observed that the loading condition does not have much effect on mode I (K1) stress intensity factor but significant effect on mixed mode (K2). In general, K1 and K2 values increases as absolute values depending on increasing crack length.

Again a microstructure based model on elastic–plastic finite element analysis and observed that the clustering nature of particles in the matrix dominates the failure mode of particle reinforced metal matrix composites (PRMMCs) was developed by Sozhamannan et al. [119]. The plastic constrain was increased with an increase in the volume of the particle. Particle fracture, interface decohesion, volume fraction and size of particle dominates the failure of PRMMCs. Heo et al. [120] used Virtual crack closure technique to calculate the stress intensity factor of an elliptical arc and concluded that the mode I stress intensity factors for elliptical arc through cracks in mechanical joints in the cases of clearance are larger than those of no clearance, but the amount of clearance has little effects on the stress intensity factors.

Guluzade et al. [121] reported that the fracture toughness of composites changed little with increasing notch depths for AISI 1040 steel and 314 steel. Fracture properties of an infiltrated TiC-1080 steel studied by Rittel et al. [122] and concluded that fracture toughness increase with the loading rate was related to energy dissipation through TiC micro cracking in the damage zone; Dynamic loading induces a significantly higher level of localized damage around the crack-tip, as opposed to quasi-static loading. Zhang et al. [123] has been investigated the fatigue fracture behavior of tungsten monofilament-reinforced composites. The fatigue behavior of the composite was superior to that of the base metal even under strain control. This superiority was attributed to the following two factors: (1) Delay in the formation of a fatal crack because of the uniform distribution of the PSBs; (2) Maintenance of the crack growth in stage I for most of the fatigue life of the composite by the reinforcement keeping the matrix stress low. Bacon et al. [124] discuss the effect of volume fraction titanium diboride reinforcement on MMC showed a faster growth rate compared to other metallic materials, with a gradient m of the faster growth rate in the MMC was due to the particle cracking ahead of the crack tip within the process zone. Final fracture occurred at a lower value, consistent with the lower fracture toughness value as static failure modes dominate crack propagation. This can be explained by the fact that at relatively low DK the lower stresses at the crack tip will predispose large particles to fracture, as the large particles were more likely to contain flaws. There was a process zone of damage that develops ahead of the crack tip in which particle fracture occurs. Increment in particle volume fraction increase fracture causes a progressive increase in the ductile rupture of the matrix, as greater stress was placed upon the matrix with increasing reinforcement particle fracture. Effect of cyclic straining at elevated-temperature on fracture behavior of nickel-based

superalloy studied by Ye et al. [125] and find that with increasing number of pre-straining cycles, the tensioned fracture presents the transition features from ductile-to-brittle mode, which was associated with the depletion of the ductility (or toughness) inherent in the material and in agreement with the reduction in macro-plastic property parameters (4f, d and n) during high temperature fatigue failure process. The reduction of the static toughness during fatigue represents the exhaustion of the ability to absorb specific energy up to fracture in the alloy, which was essentially associated with the irreversible dissipation of the cyclic plastic strain energy in the course of fatigue failure. Schlenther et al. [126] observed that crack nucleation in the brittle phases, followed by plastic tearing of the ligaments in the crack wake until final rupture occurs in the matrix. The closure forces exerted by the ductile ligaments lead to the failure-tolerant behavior. Strong segregation and formation of brittle inclusions lead to crack nucleation not only in the ceramic but also in the metallic phase. The use of high strength steels increases the onset of crack nucleation and propagation. The fracture behavior of two metal matrix composites (MMCs) at different aging conditions Investigated by Sabirov et al. [127] and the result of the analysis suggested that the maximum principle stresses in the particles at the moment of void initiation are not constant, but exhibit a dependency on the composite yield strength. Fracture behavior of steel based metal matrix composites studied by Srivastan et al. [128] and concluded that with an increase in TiC reinforcement in matrix phase fracture was dominated due to cracking of particles and decohesion at matrix-particle interphase. Final failure occur by fast fracture in composite matrix thorough the formation, limited growth and coalescence of voids.

Wang et al. [129] examined the fatigue failure of Ti and TiN coated stainless steel and revealed that the Ti coating have significant effect on fatigue failure as compared to TiN coating. Tin coating failure occurred due to the shear stress that arose from the plastic strain of the substrate in the intermediate and central zones. Fatigue behavior of SAE 1045 steel coated with Colmonoy 88 alloy investigated by Cabrera et al. [130] and find that the cracks formed at the free surface of the coating can traverse the entire coating thickness and bifurcate along the interface, leading to the delamination of the coating from the substrate. Such cracks can also activate sharp notches on the interface and continue their propagation into the substrate. Fadhli et al. [131] observed that fracture surfaces shows cracks were formed at both the interface between coating and substrate, and in the coating itself due to availability of nonmelted particles and

voids in the coating, presence of alumina particles in the coating substrate interface, significantly contributed to crack initiation in the coating and the coating–substrate interface. Fatigue properties and crack propagation behavior of stainless caststeel for turbine runner of hydraulic power generation studied by Natsume et al. [132] and observed that a linear relationship between the fatigue crack growth rate and the stress intensity range K, effective stress intensity range K_{eff} in the case of long fatigue crack. However, crack growth rate of small crack observed in plane bending fatigue tests has widely scattered. The fracture behavior of 304 stainless steel coatings deposited on low carbon steel substrate by cold gas dynamic spray (CGDS) was studied by Xian-ming et al. [133]. They observed that the initial crack generated at the surface of the coating and propagated from the surface to the interface along the weakly bonded interfaces between the particles. When the rolling reduction was large enough, the secondary crack would generate at the interface between the coating and substrate and then propagated along the bonded interface leading to the coating separating from the substrate. Faisal et al. [134] proposed a model provides a way forward for determining the fracture toughness (K1c) of brittle materials where no radial cracks were developed. The proposed model using the total surface crack and total surface crack length excluding total surface radial cracks (e.g. edge cracks) can provide a way forward for determining the Vickers indentation fracture toughness of brittle materials, where crack other than Palmqvist or half-penny/radial median cracks were developed. Li et al. [135] discussed the thickness-dependent fracture characteristics of ceramic coatings bonded on the alloy substrates and found that when the thickness of the coatings was smaller than about 200 μm, the multiple transverse cracks occur in the coatings and propagate into the substrates with increasing deformation. When the thickness of the coatings was larger than about 300 μm, the interface crack between the coatings and the substrates was the main fracture mode. Effect of heat treatment on fracture toughness properties of monolayer (TiAlN), multilayer (AlTiN/TiN) coated tool steel observed by Podgornik et al. [136] and found that deep cryogenic treatment increases fracture toughness of cold-work tools steel while maintaining or only marginally reducing core hardness. Huang et al. [137] discussed the tensile fracture behavior of Ni- and Cr-C/Ni-coated high-carbon tool steel and found that the fracture feature with a cup-and-cone appearance was observed for the uncoated and Ni-coated steel specimens and cracking plateau feature was observed for the fractured Cr-C/Ni-coated steel specimen. Cracking in the Cr-C/Ni-coated steel specimen initiated from the outer Cr-C coating and propagated through the Ni

coating and then into the steel substrate, forming an obvious cracking plateau. Under tensile stress application, branch cracking occurred in the Cr-C/Ni-coated steel specimen during crack propagation to form a fracture appearance with some cracking facets and cracks. Tensile fracture behavior of thermal barrier coatings on superalloy observed by Chen et al. [138] for the A/A TBC, the crack initiates at the top coating, then passes through the top coating and the bond coating, at last deflects at the interface between the bond coat and the substrate; while for the A/H TBC, the crack also develops at the top coating, then transits the top coating, finally kinks and propagates along the interface between the top coat and the bond coating. At high temperature, few cracks can be detected in the coating and only a small area of spallation occurs. The fracture position was located within the top coating near the interface between the top coating and the bond coating. Fracture toughness of nano-structured alumina-13% titania coatings was examined by Rico et al. [139] and found that fracture toughness magnitude was increased due to its hierarchical microstructure and to the role played by the partially melted particles. These particles operate as obstacles to the crack propagation. Movahedi [140] discussed the fracture toughness behavior of NiAl-based nano-composite HVOF coatings and observed that Fracture toughness value evidently indicates that the NiAl-15 wt% (Al_2O_3-13% TiO2) nano-composite coating was tougher (7.12 MPa m1/2) than the NiAl inter-metallic coating (4.28 MPa-$m^{1/2}$) and that the brittle mechanism dominates in the NiAl inter-metallic coating. Evaluation of fracture toughness of ZrN hard coatings by internal energy induced cracking method was investigated by Huang et al. [141]. They found that fracture toughness of ZrN coatings was related to both residual stress and preferred orientation, which were controlled by deposition parameters. Cho et al. [142] studied the fracture strength of Mg-C refractory material and observed that the fracture strength of the MgO–C was successfully increased by using the Al-coated graphite, even when the antioxidant content was reduced to 50% of the standard composition. Opening-mode fractures of a brittle coating bonded to an elasto-plastic substrate discussed by Chen et al. [143] and found that the theoretical prediction was able to effectively capture the varying trend of the crack spacing with respect to the coating thickness. As the coating layer was much thinner and more brittle than the substrate, a plane strain formulation was used to analyze the elastic field in the coating. Wen et al. [144] investigated the fracture behavior of TiN/SiN*x* nano-multilayer coatings on Si(1,1,1) substrates and found that the interfacial fracture toughness for the multilayer coatings was associated with the preferred

orientation for the TiN layer and the interfaces between TiN and SiNx layers in the multilayer stack. The TiN/SiNx multilayer coating on Si(1,1,1) with a TiN(1,1,1) preferred orientation exhibits a higher interfacial fracture toughness. Effects of structure and interfaces on fracture toughness of CrN/AlN multilayer coatings was studied by Schlogl et al. [145] and observed that the CrN/w-AlN multilayer coating pillar instantly fails without pre-damage at a maximum load than the CrN coating and SEM investigations of the fracture pattern of a broken pillar fragment suggest that the crack initiation takes place at the interface between the c-CrN and w-AlN layers. Kumar et al. [146] evaluated the fracture Toughness Properties of nickel coated T-6 7075 aluminum alloy and found that the increase in thickness of the EN coating fracture toughness properties of Al 7075-T6 alloy increases and it was observed that the nature of the crack deviates from the nature of the pre-crack i.e., unstable crack growth due to the strong adhesion between the EN coating and the Aluminum alloy

From the literature it is understand that particle addition improve the fracture toughness and it further improve by coating deposition on MMCs. Particle volume fraction, particle shape, size and coating thickness significantly affect fracture properties of MMCs.

2.3. On thermo-mechanical properties of MMCs (coated/uncoated)

The behavior of thermo-mechanical properties or dynamic mechanical properties with respect to temperature (proportional to heat input) becomes significant factor to understand material behaviors across the working temperature range under dynamic loading. It is observed that material undergoes changes under such conditions and may attributed to oxidation and degradation, and/or physical changes, the glass transition in polymers, conversions/inversions in ceramics and phase changes in metals etc. Such characterization reports of successful MMCs, developed by various material scholars are presented in this section. For example, Sastry et al. [147] studied damping behavior of aluminite particles which reinforced ZA-27 alloy metal matrix composites. They reported that the value of damping capacity increases with respect to increasing temperature whereas the value of dynamic modulus decreased. The damping property depends on weight percentage of the reinforcement and increases with increase in weight percentage of reinforcement, due to dislocation generation and motion as a result of plastic deformation at metal/reinforcement interface. Girish et al. [148] discussed the damping behavior of graphite filled ZA-27 alloy composites fabricate through compo casting method. They report the damping capacity of composite increases with increasing volume fraction of graphite

particulates or with respect to increasing temperature. Similarly, the effect of Si and Mg addition on damping behaviour was studied by Ren et al. [50] and reported that addition of Si and Mg leads towards higher porosity in the composites due to poor wettability between Al and Si composites which affects thermo-physical properties. Dynamic mechanical response of alloy composites was studied by Lu et al. [149] and found that the damping capacities of the composites were dependent on volume fraction and interfacial bond between particulate and matrix. Zhang et al. [150] investigated the damping behavior of SiC reinforced with 1040 aluminum alloy composites and found that thermal cycling was responsible for increasing damping capacity, which was generated by internal friction of Al/SiC MMCs. The damping capacities of graphite particles reinforced magnesium matrix composites fabricated by stir casting method was investigated by Wu et al. [151].The results show that damping increased for volume fraction 0-10wt.-% of graphite beyond 10 wt.-% damping almost keep constant. Di-qing et al. [152] examined the damping properties of Mg-Cu based alloy and reported that Mg-Cu alloys shows good damping capacities, but as Cu content increased it decreases the damping capacities. Damping capacity of TiC reinforced magnesium matrix composites was evaluated by Cao et al. [153] and observed that the damping capacity increases with the increase in reinforcement volume percentage which was due to dislocation damping at room temperature and at higher temperature due to interface damping. Effect of SiC and Graphite particles on the damping behaviour of 6061Al metal matrix composites fabricated by Spray deposition method was evaluated by Zhang et al. [154]. They foundthat the damping capacity of 6061 Al can be improved significantly by the addition of either SiC or graphite particles. In another work in year [155] they reported the damping behaviour of Al_2O_3, SiC and graphite particulate reinforced 2519Al metal matrix composites fabricated by Spray deposition method. They observed that Spray deposition process significantly improve damping properties. Wu et al. [156] evaluated the damping properties of fly-ash reinforced aluminum alloy composites and reported that addition of fly-ash into bse matrix improved the damping capacity. Effect of Ti and Mg on the damping behavior of in situ aluminum composites was studied by Zhang et al. [157] and reported that Ti and Mg can affect the damping capacity of Al/5 wt.% TiB_2 composite due to their interface change between TiB_2 reinforcement and Al matrix. Pabst et al. [158] examined the damping behavior of alumina–zirconia composites at room temperature and reported that the damping of dense alumina-zirconia composites increases with increasing zirconia content. Deng et al.[159]

investigated the damping behavior of micron and submicron SiC particulate reinforced magnesium matrix composites at higher temperature. They found that composite exhibits the best damping capacity at high temperature; the reasons can be attributed to the fine grain size, high dislocation density, abundant interfaces and interfacial slipping. Effect of interphase on the damping capacity of Particulate reinforced metal matrix composites investigated by Gu et al. [160] and reported that change in interphase thickness improves the damping of composite. In another work [161] they studied the effect of surface coating of particulate on the overall damping of particulate-reinforced metal matrix composites and found that coating thickness improves the damping of composite. Hu et al. [162] discussed the damping behavior of SnO_2 & Bi_2O_3 coated $Al_{18}B_4O_{33}$ whiskers reinforced aluminum composites and found that SnO_2 & Bi_2O_3 coating strongly affects the damping capacities of the coated composites. The damping capacities decrease and the damping peak shifts towards higher temperatures with the increasing frequency. Damping behavior of barium titanate ceramic filled aluminum composites was investigated by Gen-lian et al. [163] and concluded that $BaTiO_3$ceramic with large grain size exhibits high damping capacity below the Curie temperature. Prasad and Shoba [164] experimentally evaluated the damping behavior of SiC and rice husk ash reinforced hybrid aluminum composites. The results shows that the addition of micro sized particulates increases the damping capacity of the A356.2 alloy and damping capacity increases with the increase in the percentage of the reinforcement.

Liu et al. [165] investigated the damping behavior of Bi_2O_3 coated and uncoated alumina borate whisker reinforced aluminum composites. It was revealed that the addition of uncoated alumina borate whisker increased the damping properties but after Bi_2O_3 coating on alumina borate whisker damping peaks shift toward the 300^0C. In another work [166] they examined the damping behavior of Bi_2O_3 coated and SnO_2-coated Alumina borate whiskers reinforced aluminum alloy composites. They were concluded that the damping behavior of the ABOw/Al composite does not change before and after undergoing the thermal cycling and SnBi/Al composite shows changes before and after undergoing the thermal cycling. Effect of electro-ceramic particles on damping behaviour of aluminum hybrid composites fabricated by ultrasonic cavitation and mechanical stirring methods was examined by Montalba et al. [167]. They concluded that ultrasonic cavitation treatment (UST) assisted by mechanical stirring (MS), improved wettability between the aluminum alloy matrix and the reinforcement and improved

the damping capability of the HMMCs. Similar work done by Gu et al. [168] for cu coated and uncoated SiC particulates reinforced magnesium matrix composites and observed that dynamic modulus of the coated SiC particulate reinforced composite was improved strongly compared with that of the uncoated. Again SnO_2-coated and uncoated alumina borate whiskers reinforced aluminum matrix composites damping behavior was studied by Hu et al. [169] and found that damping capacity of the coated composites was higher than that of non-coated one and this improvement was attributed to the contribution of SnO_2-coating. In another work [170] they were studied the damping behavior SnO_2-coated and uncoated alumina borate whiskers reinforced aluminum matrix composites and concluded that the damping behavior of the coated composites strongly depend on the strain amplitude at higher strain amplitudes.

The damping properties of the CIIR/PMMA multilayered damping composites were investigated by Zhang et al. [171] and concluded that with increasing the layer number, the loss peak of CIIR/PMMA multilayered composite moves to high temperature or with decreasing the CIIR layer thickness, the height of loss peak decreases and the position of loss peak moves to room temperature. Chia et al. [172] studied the visco-elastic properties of plasma sprayed NiCoCrAlY coatings and found that at the low frequency region (0.01–0.1 Hz), the coating exhibited visco-elastic behavior, and at higher frequencies (1-100 Hz), an elastic behavior. Effect of interface between coating and substrate on damping capacity of coating systems was investigated by Wang et al. [173] and found that interface between coating and substrate had a significant effect on the damping. Thin interface shows greater damping capacity as compared to thick interface. Emadoddin et al. [174] experimentally evaluated the damping behavior of Al/SiC multilayer composite fabricated by roll bonding method. The results shows that by increasing the percentage of reinforcing particles, the natural frequency and damping capacity increases or by increasing the number of layers in constant thickness the damping capacity increases. Effect of SiC coating on damping behavior of C/SiC composites was investigated by Zhang et al. [175] and found that SiC coating shows no influence on damping behavior of C/SiC composites. Prasad et al. [176] observed the effect of white layer formed during wire cut EDM process and the milling process on damping capacity of rice husk ash reinforced A356.2 alloy composites. It was revealed that damping capacity of the composite increased due to the increment in the dislocation density and plastic zone with the percentage increase in the reinforcement. The specimen prepared through wire cut EDM machined exhibits low damping values. The reduction

in damping can be attributed to the formation of white layer which acts like a protective layer to dissipate elastic strain energy which results in reduction of damping values. In another work [177] they were studied the effect of heat treatment of white layer formed during wire cut EDM process and the milling process on damping capacity of rice husk ash reinforced A356.2 alloy composites. It was revealed that heat treated samples exhibit higher damping values due to decrement in white layer formed during wire cut EDM process and the milling process and this white layer act as a protective layer to dissipate heat energy to the surroundings. Khor et al. [178] studied the dynamic mechanical properties of plasma sprayed Ni-based alloys and reported that NiAl coating shows the good damping characteristics but it reduced by addition of chromium (NiCrAlY) in coating material and it further improved by addition of cobalt (NiCoCrAlY) in existing coating material. In another work [179] they examined the mechanical behavior of ZrO2/NiCoCrAlY coating and found that graded ZrO_2/NiCoCrAlY coating shows better dynamic storage modulus as compared to 100% ZrO_2 and NiCoCrAlY coating. The effect of interface MCrAlY coating through air plasma spraying (APS) and electron beam physical vapor deposition (EB-PVD) and substrate on damping property was evaluated by Fu et al. [180] and concluded that the damping of "vertical" interface structure was slightly higher than the damping of "horizontal" interface structure in the same bending mode. The damping capacity of yttria-stablized zirconia, deposited by air plasma spraying (APS) or electron-beam physical-vapor-deposition (EB-PVD) was investigated by Patsias et al. [181] and concluded that electron-beam physical-vapor-deposition (EB-PVD) coating method shows better damping capacity as compared to air plasma spraying (APS) coating.

From the literatures it is understood that particles (Particle volume fraction, particle shape, size), coating material and its thickness significantly affect thermo-mechanical properties of MMCs.

2.4. On corrosion behavior of MMCs (coated/uncoated)

Corrosion is well known phenomena of gradual destruction of materials by chemical reaction with its environment. Principally it involves electrochemical oxidation of metals in presence of oxidant like oxygen e.g. rusting of iron i.e. formation of iron oxides is well-known example of electrochemical corrosion. Hence corrosion produces oxide(s) or salt(s) of the original metal. As a consequence of corrosion, the materials properties start to loosen out e.g. strength, appearance and permeability to liquids and gases etc. Various material scholars reported their research work

on corrosion behavior and mechanism in MMCs like Wu et al. [182] studied the corrosion behavior of TiC particle-reinforced stainless steel and concluded that the addition of TiC particles to 304SS resulted in no rapid pit propagation but maintained a high corrosion rate in the whole immersion time. Similarly, Corrosion behavior of gold-imitation copper alloy in saltspray environment was studied by Xiao et al. [183] and concluded that gold-imitation increased the corrosion resistance of alloy due to formation of multi-layer film on the surface of the alloy aftera period of time in salt spray environment. Pardo et al. [184] investigated the effect of silicon carbide particle addition on corrosion properties of magnesium alloy fabricated through powder metallurgy process. It was revealed that the addition of SiCp increased the degree of corrosion and promoted cracking and spalling of the corrosion layer for increasing exposure times. Corrosion behavior of magnesium alloys was examined in salt spry environment by Zhao et al.[185] and they were observed that corrosion behavior controlled by the following factors (i) the composition of the alpha-Mg matrix, (ii) the volume fraction of second phase and (iii) the electrochemical properties of the second phase. Martin et al. [186] investigated the corrosion behavior of extruded AZ61 magnesium alloy in salt spray environment and concluded that the corrosion rate was higher for the immersion surfaces as compared to the salt spray surfaces, based on both thickness loss and weight loss. Corrosion mechanism of extruded AZ61 magnesium alloy in salt spray and immersion environment was studied by Walton et al. [187] and made this conclusion that the distance of pits was higher for the salt spray environment than the immersion environment. The intergranular corrosion area fraction was initially higher for the immersion environment than the salt spray environment, but around 48 h and on, the salt spray intergranular corrosion area fraction was higher. Song et al. [188] studied the corrosion behavior of extruded AM30 magnesium alloy in salt spray and immersion environment. The results show that the distance of pits was higher for the salt spray environment than the immersion environment. The intergranular corrosion area fraction was initially higher for the immersion environment than the salt spray environment, but around 48 h and on, the salt spray intergranular corrosion area fraction was higher. Effect of Cu addition on corrosion behavior ofZn-30Al alloy synthesis through spray atomization and deposition technique was investigated by Wang et al. [189]. It was revealed that the addition of 1% Cu improves its corrosion behavior significantly or 2% and 4% Cu additions reduce the corrosion resistance. Seetharaman et al. [190] discussed the corrosion performance of 2024 aluminium alloy under salt fog conditions and reported that the

corrosion rate decreases with the increase of pH value from acidic to neutral or corrosion rate decreases with the increase of spraying time. As chloride ion concentration was increased corrosion rate increases in the salt spray corrosion test condition. Effect of cerium addition on corrosion behavior of AZ61+ XCe alloy under salt spray test was evaluated by Manivannan et al. [191] and concluded that the cerium addition improved the corrosion resistance of AZ61 alloy due to formation of Al-Cephase which refines the α grain size and retards the growth of β phase. In another work [192] they studied the corrosion performance of cast Mg-6Al-1Zn+XCa alloy under salt spray test and found that the calcium addition upto1.5 wt.% decreases the corrosion rate and increases further with above addition.

Arrabal et al. [193] examined the corrosion behavior of a magnesium matrix composite with a silicate plasma electrolytic oxidation coating and found that the addition of SiC to the AZ92 magnesium matrix slightly increased the corrosion degradation in 3.5% NaCl solution and salt fog. Lopez et al. [18] studied the corrosion behavior of TiN coated Steel in aqueous slurries and find that Adherence between the TiN coating and the steel substrate strongly affected the generalized corrosion resistance of steel. Sun et al. [194] investigated corrosion characteristics of 304 stainless steel laser-alloyed with Cr–CrB_2 and concluded that intergranular corrosion, pitting and non-uniform corrosion co-exist on the alloyed specimens. Corrosion resistance of each microstructure and corresponding chemical composition play an important role in determining the corrosion resistance of laser treated specimens. Laser surface alloying 304 Stainless Steel with Cr–CrB_2can improve corrosion resistance of it with proper processing parameters (laser power 2.5 kW, scanning speed in the range of 10–20 mm/s). Work on Electrochemical evaluation of the corrosion behavior of steel coated with titanium-based ceramic layers done by Alkhateeb et al. [195] and observed that different titanium-based CVD coatings like TiN, TiB_2 and TiBN with a thickness of about 2 μm enhance the corrosion resistance, the TiB_2 coated steel shows a relatively compact layer with a fine grain size, which act as an efficient barrier against steel corrosion. Also the TiBN coating shows promising low-defect morphology and results in enhancement of the corrosion resistance. By increasing the boron content, the preferred orientation of the titanium nitride coated steel changed from {111} and {311} to {200}, {220} and {222}. This leads to a decrease in the number of micro-cracks in the TiN layer resulting in an enhanced corrosion resistance of the coated steel. Schlenther et al. [126] find that corrosion resistance was strongly affected by the melt processing, ceramic particulates or of titanium does

not lead to a further decrease of the corrosion resistance. Corrosion behavior of microwave-sintered austenitic stainless steel composites studied by Padmavathi et al. [196] and concluded that microwave sintering results in higher densification and a relatively refined microstructure in both pure 316L and 316L–YAG composites which leads to achieve a good corrosion resistance. Role of $Al_{18}B_4O_{33}$ Whisker in Micro-arc Oxidation Process of Mg Matrix Composite and Protective Properties of the Oxidation Coating investigated by Wang et al. [197] and concluded that the microarc oxidation coating can provide effective corrosion protection for $Al_{18}B_4O_{33}$/AZ91 composite by greatly restraining both cathodic reaction and anodic reaction. Work on improvement of the corrosion resistance of Cr–N coated aluminum matrix composite by magnetron sputter done by Hu J et al. [198] and observed that the sputtered coating includes metallic Cr, CrN and Cr_2N, among which CrN was dominant. The CrN coated composite presents significantly decreased the susceptibility of the coated composite to pitting corrosion. Effect of changing the silica coating pH on the corrosion characteristics of A6092/SiC aluminum metal matrix composite in chloride media studied by Hamdy et al. [199] and observations are concluded that Silica conversion coating on AMMC surface, and a primer and a final topcoat will be crucial to reach adequate anti-corrosion properties. The optimum pH was determined to be ~12.9 which was the neutral silica solution pH. This pH value was critical where increasing or decreasing it has a negative effect on the corrosion resistance. Anti-corrosion micro-arc oxidation coatings on SiCP/ AZ31 magnesium matrix composite studied by Xue et al. [200] and made conclusion that after micro-arc surface treatment, the corrosion current density decreases almost three orders of magnitude, and the corrosion resistance of the SiC/AZ31 composite was significantly improved. However, its corrosion resistance also depends on the coating thickness. Hu et al. [201] carried out research about corrosion resistance of cerium-based conversion coatings on alumina borate whisker reinforced AA6061 composite and concluded that cerium-based chemical conversion coating was an effective method to improve the resistance to localized corrosion of the composite and concentration of $CeCl_3$ significantly influences on the corrosion behavior. Effect of phytic acid on the corrosion inhibition of composite film coated on Mg-Gd-Y alloy investigated by Guo et al. [202] and made conclusion that SANP-P layer provided good corrosion protection by a protective film made of PSPF composite film containing phytic acid as the principal component for corrosion inhibition in a neutral salt environment. The SANP-P layer played a key role in the improved adhesion and barrier property of the PSPF

composite film coated on the Mg-Gd-Y alloy substrate in a corrosive environment. Wang et al. [203] carried work on microarc oxidation coating formed on SiC/AZ91 magnesium matrix composite and its corrosion resistance and made observation that the corrosion resistance of SiC/AZ91 composite was improved greatly by MAO coating. Influence of chloride ion concentration on corrosion behavior of plasma sprayed alumina coatings on AZ31B magnesium alloy studied by Thirumalaikumarasamy et al. [204] and concluded that the corrosion rates of the uncoated magnesium and alumina coatings were increased with increasing chloride ion concentration. Jegadeeswaran et al. [205] discussed the corrosion performance of HVOF Sprayed Al2O3+CoCrAlTaY on Ti-31 Alloy in Salt Environment and reported that the HVOF sprayed coatings and it reduces corrosion rate by more than 5 times compared to uncoated Ti-31 alloy. Corrosion properties of aluminized layer formed on the surface of AZ91D magnesium alloy was studied by Niu et al.[206] and found that the passivated films of aluminum coatings reduce the porosity of coatings and have good corrosion resistance. Richard et al.[207] evaluated the corrosion behavior of thermally sprayed nano ceramic coatings and concluded that the Al_2O_3-13 wt.% TiO_2 coatings improved corrosion resistance. Gurr et al. [208] investigated the corrosion behavior of NiVAl multilayer coatings and concluded that the NiVAl multilayer coatings improved corrosion resistance. Corrosion properties of PVD coating deposited on magnesium alloys was studied by Hoche et al. [209] and reported that the TiMgGdN-HiPIMS coating shows superior corrosion resistance and withstands the salt spray test as long as 360 h. Damato et al. [210] conduct corrosion study of Laser surface alloying of an A356 aluminium alloy using nickel and Ni-Ti-C and concluded that the all alloyed surfaces resulted poor corrosion resistance compared to the untreated material. Corrosion behavior of aluminum-alloyed coating on AZ91D magnesium alloy was studied by Zhong et al. [211] and concluded that the aluminum-alloyed coating can efficiently improve the corrosion resistance of the AZ91D magnesium alloys compared with the bared magnesium alloys. Magnani et al. [212] discussed the corrosion properties of WC-Co coatings sprayed on AA7050 and reported that the different spray parameters strongly affected the corrosion resistance of coating. Corrosion performance of magnetron sputtered TiN coatings deposited on aluminium alloys was experimentally evaluated by Diesselberg et al. [213] and results shows that coatings act as an effective corrosion barrier in the salt spray environment. Dejun and Jinchun [214] discussed the corrosion properties of anodic oxide film on 7475 aluminum alloy in salt spray environment and found that the protective layer

of Al2O3 in aluminum alloy improve the corrosion resistance. Corrosion resistant performance of thermal sprayed aluminum was investigated by Chang et al. [215] and concluded that the thermal-sprayed aluminum layer enhance corrosion resistance of alloy. Natishan et al. [216] compare the carrion properties of thermal spray coatings and electrodeposited hard chromium in slat fog environment and concluded that the EHC and WCr-Co coating exhibits same corrosion resistance. Corrosion performance of zirconium based conversion coating on the aluminum alloy 1050 was investigated by Golru et al. [217] and reported that the Zr conversion layer improved the corrosion resistance of alloy.

It is understood form above present literature that addition of particulate improves corrosion resistance for a range of time as time increase corrosion resistance start to decrease. Deposition of coating significantly improved the corrosion resistance of MMCs.

2.5. On slurry erosive wear behavior of MMCs (coated/uncoated)

The slurry erosive wear behavior of MMCs (coated/uncoated) becomes significant to understand wear and its mechanism in material. This determines the maintenance frequency or servicing life of turbine directly and indirectly the cost associated with it. This future could be enhanced by provide good material coating over such MMCs. There are various literatures highlighting such research, e.g. Effect of particle size on slurry erosion wear aluminum alloy (AA6063) was studied by Desale et al. [218] and found that particle size in power law relationship with slurry erosion wear changes at the critical particle size depending on its kinetic energy. In another work [219] they studied slurry erosion wear of ductile materials under normal impact condition was ratio of erodent hardness to target material hardness. Slurry erosion wear was strong affected by velocity and particle size but less affected by solid concentration. Jha et al. [220] discussed the Effect of impinging angle and rotating speed on erosion behavior of aluminum alloy (AA1900) and reported that slurry erosive wear of the aluminum increases with increment in impingement angle and rotation speed of specimen. Influence of alloy composition, nature of the slurry and traversal distance on slurry erosion wear of zinc based alloy was investigated by Prasad et al. [221] and found that slurry erosion wear loss increased with traversal distance on other hand slurry concentration reduced the slurry erosion resistance of zinc based alloy. In another work [222] it was revealed that the presence of sand particles in the liquid reduced the wear rate of the samples. Lynn et al. [223] examined the effect of particle size on the slurry erosion and concluded that the mass loss increase with impact velocity of particles and decreased with

decrement in particle size under conditions of erosion testing. The mass loss rate was proportional to the amount of kinetic energy dissipate by particles impact. Prasad et al. [224] exhibits Slurry wear characteristics of a zinc-based alloy and concluded that wear rate increases with increase in particle concentration in slurry with in a limit after that it decrease and it also increases with distance. In another work in the year 2004 [225] they concluded that addition of silicon improved the slurry erosive characteristic of zinc-based alloy and concluded that wear rate increased with distance and then decreased again at longer traversal distances, high traversal speed caused reduction in the wear rate and wear rate increases with increases the pH of the medium.

Influence of heat treatment on slurry erosive wear performance of Al6061 alloy studied by Ramesh et al. [226] and concluded that increment in sand concentration or speed of slurry rotation has resulted increased in slurry erosive wear. Ice quenched specimens' shows better slurry erosive wear resistance compared with air and water quenched specimens. Operating time also has shown influence on slurry erosive wear resistance. Aging duration increment resulted increase in slurry erosive wear resistance for all the quenching media. Gupta et al. [227] shows the effect of heat treatment on erosive-corrosive wear properties of eutectic Al-Si alloy and found that erosion resistance of the as-cast Al-Si alloy was observed to be superior to that of the conventional Al samples. On other hand heat treatment deteriorated the wear resistance of the Al-Si alloy. Erosion wear of high-carbon steel in coal and bottom-ash slurries was investigated by Modi et al. [228] and concluded that the wear loss of the specimens increased with traversal distance in all cases. The steel in the annealed condition revealed nearly ten times more material loss than the steel subjected to the hardening treatment in both slurry environments. Higher material loss was observed in steel samples in the bottom-ash slurry than in the coal slurry due to the high hardness and less fracturing tendency of the mineral constituents. Suchanek et al. [229] investigated the influence of microstructure on erosion resistance of steels and observed that quenched, low tempered carbon and high-alloy steels exhibits maximum erosive wear at impact angles of 30-45.As the carbon content increased the erosion resistance of quenched carbon and low-alloy steels grows linearly. Presence of type M_7C_3 and$M_{23}C_6$ complex carbides in the microstructure of quenched high-alloy steels was helps in enhancement their erosion resistance. The erosion resistance of hardened high-speed steel was lower than hardened chromium steels. Increment in quenching temperature was enhancing the erosion resistance of HS11-0-4 high-speed steel due to increment

of carbon and carbide-forming elements in martensite phase. The share of retained austenite grows relatively slightly.

Zhang et al. [230] studied the slurry erosive wear of yttrium reinforced 304 stainless steel and found that yttrium addition improved the erosion resistance of 304 stainless steel. Slurry erosion performance of chilled aluminum alloy reinforced with fused silica was carried out by Hemanth et al. [4] and observed that the wear resistance of the MMCs was increased till 9 wt.% of dispersoid content. The copper chill shows major effect on wear resistance because of its high VHC. Fang et al. [5] evaluate the erosion resistance of SiC reinforced Ti-based metal matrix composites experimentally in SiC water slurry. They were observed that SiC ceramic had a maximum erosion rate at a normal impact angle 90^0, Ti matrix showed maximum erosion at about 158, while the erosion rate for the Ti-6Al-4VrSiC composite appeared a maximum at about 458, after then it remained nearly constant. Effect of flyash reinforcement on slurry erosive wear of aluminum matrix composite was investigated by Ramachandra et al. [6] and made this observation that slurry erosive wear resistance increased with increase in flyash content. The slurry erosive wear of specimens was decreased due to formation of passive layer on the surface. Wear loss forming a protective layer against impact of slurry resistance of reinforced samples has decreased with increase in flyash content. Erosive wear of aluminum alloy composites was evaluated experimentally by Das S et al. [7] and made this observation that composites exhibited better wear resistance than the matrix alloy. The wear resistance was increased with increment of SiC content in alloy matrix. Composites exhibited better wear resistance in acidic media than NaCl media. Materials exhibited more wear rates in acidic media than NaCl media at lower sand concentrations and at higher sand concentrations the wear was higher in NaCl media compared to acidic media. Influence of experimental parameters on the erosive–corrosive wear of Al-SiC particle composite studied by Das et al. [8] and find that The wear rate of Al-SiC composite was found to be a strong function of sand concentration, angle of impingement and the radial distance. The wear rate of the composite was increased with increasing angle of impingement, radial distance and sand concentration. Erosion rate decreases with decrement in erodent particle size. Abnormal erosion–slurry velocity relationship of high chromium cast iron with high carbon concentrations investigated by Chung et al. [231] and observed that the erosion loss was higher at low slurry velocities. As the slurry velocity was raised, the erosion loss first decreased and then increased for hypereutectic HCCIs due to high carbon concentrations. Wang et al. [232]

studied the slurry erosive characteristics of mild and stainless steels in alkaline slurries containing alumina particles and observed that in alkaline slurry wear resistance in an ascending order was mild steel, BS6323, the AISI 410 stainless steel, and the AISI 304 stainless steel. Study of the parametric dependence of erosion wear for the parallel flow of solid–liquid mixtures was studied by Gandhi BK et al. [233] and find that erosion was strong influenced by velocity and less influence by concentration and particle size. In another work [234] they studied the effect of multi-sized particulate slurries on erosion wear and concluded that aaddition of finer particles than 75 μm in slurries reduces the erosion wear. Erosion wear was increased with addition of coarse size particles into fine particles slurry.Erosion behaviour of WC-based MMCs in liquid–solid slurries investigated by Neville et al. [235] and observed that erodent size was strongly affect the relative performance of different materials. Study erosive-corrosive wear characteristics of aluminum alloy composites through factorial design of experiments studied by Mondel et al. [236] find that Radial distance was the most dominating factor to control wear of composites. However effect of impingement angle in the direction of slurry was taken in consideration also. Material removal mechanism of Al-SiC particle composite during erosion was investigated by Das et al. [237] and find that at higher speed and higher impingement angle, the overall material loss was higher. The wear rate of composite at a speed of 900 rpm was almost 5-10 times more than that at 600 rpm. The wear rate at 90º angle of impingement was about four times more than that at 0° impingement angle. The reduction in wear rate was observed after a critical sliding distance and finally reaches to saturation. The reduction in wear rate was due to work hardening of the surface, blunting of the edges of the erodant in corrosive media.

Slurry erosive behavior of HVOF-spray Cr_2O_3 coated turbine steels studied by Goyal et al. [9] and concluded that HVOF-sprayed Cr_2O_3 coating enhance the slurry erosion resistance of the steels and rotational speed was found to be the most dominating factor for slurry erosive wear in all cases. Grewal et al. [10] carried out work on slurry-erosion performance of hydro-turbine steels coated through detonation gun spray technique. The results shows that coated samples shows better slurry wear behavior as compared to bared samples. Slurry erosion characteristics and erosive wear mechanisms of laser surface alloying Co-based and Ni-based coatings was investigated by Shivamurthy et al. [11] and observed that for a particular erodent size at different angle of impingement erosion performance in this order LSA steel <Stellite 6 LSA

steel<substrate 13Cr-4Ni steel. LSA coating based samples shows better erosion resistance than other coating. Slurry erosive wear of physically vapor deposited TiN and CrN coated composites studied by Wang et al. [238] they found that TiN or CrN coated milled steel samples shows better resistance in slurry of alumina particles containing sodium carbonate and hydrogen carbonate. Slurry erosion behavior of Al_2O_3 and Al_2O_3–$13TiO_2$ coated CF8M steel by detonation gun spray technique under hydro accelerated conditions conduct by Bhandari et al. [12]. They were concluded that mass loss of the eroded specimens confirm that D-gun spray Al_2O_3-$13TiO_2$ coated steel resists slurry erosion much better than the Al_2O_3-coated steel. During the slurry erosion of Al_2O_3-coated steels, slurry concentration and average particle size were found dominating factors in comparison of rotational speed. On the other hand, in the case of Al_2O_3–$13TiO_2$-coated steel, rotational speed was found dominating in comparison of slurry concentration and average particle size. In another work in same year [13] slurry erosion performance of wc-10co-4cr coatings on cf8m steel using detonation gun-sprayed was investigated and found that D-gun-sprayed WC-10Co-4Cr coatings shows reduction in the erosion rates of the CF8M steel. During the slurry erosion test of CF8M steel, slurry concentration and rotational speed were found more dominant factors in comparison of average particle size. In the case of D-gun-sprayed WC-10Co-4Cr coatings, average particle size was found more dominant factor in comparison of slurry concentration and rotational speed. Manisekaran et al. [14] carried out a research about slurry erosion studiesof surface modified 13cr-4ni steels and also studied the effect of angle of impingement and particle size. They were concluded that Laser hardening of 13Cr-4Ni steels shows better erosion resistance at all angles of impingement than pulse plasma nitriding. Ramesh et al. [2] reported the effect of coating on slurry erosive wear performance of Al6061 alloy and observed that material removable rate was steeply increases with increase in slurry concentration on other hand it decrease with increased coating thickness for all slurry concentration. The effect of TiN coating on erosion resistance of a-Ti alloy in saline slurry studied by Tu et al. [239] and concluded that TiN coated a-Ti specimens showed an increment in volume loss with the slurry velocity. At low slurry velocities TiN coating deposited samples presented better slurry erosion corrosion resistance. Under the saline slurry impact conditions, the material removal of the TiN coating was dominant at low and intermediate slurry velocities. For the a-Ti substrate, the results showed erosion corrosion process was dominant in the slurry velocity range. Caicedo et al. [240] investigated the erosive-

corrosive behavior of CrN/AlN coated AISI D3 steel, 304 stainless steel samples and observed that CrN/AlN coated samples shows less mass loss as compared to bared AISI D3 steel, 304 stainless steel. The reduction in mass loss was around 39% after deposition of CrN/ AlN multilayers for the highest impact angle of 90º. When the steel D3 was coated with CrN/AlN multilayer this new system improves corrosion erosion resistance of 304 stainless steel, however, when the impact angle was modified the impact energy of the particles was automatically increased, therefore, under high impact angles 90º the corrosive-erosive effect was greater for all three systems treated in this study, although the corrosive-erosive effect was less prominent in the CrN/AlN coated steel. Coatings offer protection to the industrial steel surface. Work on the erosive-corrosive wear performance of laser-clad Ni-Cr_3C_2 composite coating and its microstructure was done by Zhang et al. [241] and made this conclusion that coating erosion resistance was increased by increasing addition amounts of carbide in the coating within considered range. Coating reduced the erosive-corrosive wear rate upto 50% as compared to that of stainless steel in acid slurry. The enhancement in erosive-corrosive resistance was due to formation of ductile austenite structure and observation of M7C3 hard compound in coating. Lopez et al. [18] studied the erosion-corrosion behavior of TiN-coated stainless steels in aqueous slurries and find that with increment in impact velocity of erosive reduced, which revealed the effect of TiN coating on erosion performance. Slurry erosive wear resistance of TiN coatings using slurry jet impact test was studied by Iwai et al. [242] and find that TiN coating improves erosion resistance of alloy samples. Among all sets the TiN coating deposited under the highest substrate temperature shows highest wear resistance. Sandwich structured WC-Co-Cr thermally sprayed coatings of different intermediate layers wear performance was investigated by Hadad et al. [243]. It was revealed that Cermet, combinations with Ni-Cr and Ni-plating coating shows high adhesive strength. The interface of Ni-plating-X shows fewer enhancements in adhesion strength and wear performance. Combination of Co-Cr does not show only low adhesive strength value and cohesive but cermet and combination with interlayer Ni-Cr 80–20 showed high wear and adhesion performance. Shivamurthy et al. [244] study the slurry erosive wear characteristics of laser surface alloyed 13Cr-4Ni steel and found that 13Cr-4Ni or colmonoy 88 coating exhibited the power law characteristics i.e. slurry erosive wear rate $\propto$ Slurry velocity. 13Cr-4Ni steel shows neither ductile nor brittle mode of erosion behaviour on other hand colmonoy 88 and stellite 6 coating show brittle mode of erosion under silica sand particles of 100 µm and at slurry

velocity of 12 m/s condition. Slurry erosion behavior of plasma sprayed Cr_2O_3-3%TiO_2 coatings was investigated by Singh et al. [245] find that both the coatings exhibited enhancement in material loss with increment in slurry concentration. NC_3T coating shows better slurry erosion performance as compared to CC_3T coating.Slurry erosion resistance of thermally sprayed oxide coatings studied by Knuuttila et al. [246] and made this conclusion that aluminum phosphate sealing was an effective method to improve the erosion resistances of oxide coatings. The alumina coating shows no effect on wear resistance in pH-1 value and chromia coatings shows good slurry erosion resistance even at low pH values. Wear characteristics of CrNrNbN superlattice coatings through combined cathodic Arc unbalanced magnetron sputtered in alkaline slurry was studied by Wang et al. [247] and observed that the wear rate of the coating could be higher in high-angle erosive wear due to a change of dominant wear mechanism. This cannot be demonstrated here due to the limit of the current RCE system the incident angle of the particle impingement, as a result of sample rotation, was relatively low in such apparatus. In another work in year 1999 [248] they studied erosion of TiN coatings under sodium carbonate/bicarbonate buffer slurries containing alumina particles and find that the erosion resistance of the TiN coatings was significantly higher than uncoated mild or the AISI 304 stainless steel. Increment in particle erosion speed shows no significant effect on the erosion performance of the coating. Increment in particle erosion speed shows severe erosion of the uncoated mild and stainless steels. Zhao et al. [249] investigated Slurry erosion of plasma-sprayed ceramic coatings and concluded that Ceramic coatings, especially Cr_2O_3 and Al_2O_3, improved wear resistance compared with the base metal (SUS 329J1). A study on erosive wear behavior of atmospheric plasma sprayed and nano-structured alumina coatings was done by Singh et al. [250] and observed that in nano-structured alumina coatings results shows improvement of its erosion resistance as compared to CC. The improved erosion resistance for NC was also due its high hardness.

The literature presented above, it is understood that particles addition improves slurry erosion resistance but it start to reduce when particles start to pullout from base matrix. Deposition of single and multilayer coating improved slurry erosion resistance of MMCs.

2.6. On techniques of Design of Experiments (DOE), its implementation and other optimization techniques like Taugchi Optimization methods etc. and Multi-criteria decision making methods for analyzing results

As cited above that slurry erosion wear process in composites is a complex phenomenon involving number of operating variables like xxx. And it's interesting to understand slurry erosive wear behavior of MMCs under such variable conditions. The experimental simulation under laboratory conditions could be easy designed using design of experiment techniques like Taugchi. Taguchi is a power full tool of Design of experiment and it works on orthogonal array. Data acquiring through taguchi technique was in a systematic/controlled way to understand the influence of operating parameters on output response parameters, which was unknown function of these operating variables. The important stage in the process is selection of factors which have effects on the slurry erosion wear process. An orthogonal array was created with the help of taguchi techniques to consider the effect of several factors on the target value and defines the plan of experiments. To overcome these problems, Taguchi et.al [251,252] advocated the use of orthogonal arrays discovered a new experiment design. In Taguchi optimization technique output is converted into signal-to-noise ratio of orthogonal arrays to the robust design of product and process. The output response of factors is measured in mean value and therefore, the output response can be reproducible in this procedure. Various researchers [253-257] have applied the Taguchi method to design the products and influence of process parameters. Taguchi experimental strategy is based on parameter design, simultaneously study effect of various parameters and their interactions on output of engineering processes. Taguchi is a systematic approach and it is inexpensive simultaneously it is easy to operate.

Basavarajappa and Chandramohan [258] used Taguchi method to study the effect of operating parameters on the wear rate and also found that the sliding distance was the parameter which has highest physical and statistical significance on the wear rate. Patnaik et al. [259] has demonstrated the use of Taguchi method for studying the effects of various parameters and their interactions in a number of engineering processes and successfully applied Taguchi design for parametric appraisal in wire electrical discharge machining process, drilling of metal matrix composites. Parametric study of slurry-erosion of hydro-turbine steels using taguchi technique was done by Grewal et al.[10] and found that the particle size and impact velocity was most significant factor in the erosion response of bare steels. In the case of the coating particle size

was found less significant factor. Yoganandh et al. [260] applied orthogonal array for erosive wear behavior of nickel-based high alloy white cast iron under mining conditions and reported that impact velocity was found to be the most significant parameter or the velocity and slurry concentration interaction showed a significant effect on erosive wear.

Shannon et al. [261] introduced information theory which known as entropy method. The amount of information acquired by people is one of the factors for evaluation accuracy and reliability of information. In the information theory, the entropy is measured with the index of disorder of system. If the index is less, the information provided by the index was more, so the index should has more effect during evaluation, the weights should be larger[262]. Therefore the entropy can determine weights for factors. The entropy weight is determined by the matrix constructed based on the monitoring indicators of the factors. The evaluation result can be more objective because the weights of factors can avoid the subjective factor. Chen et al. [263] applied entropy weight coefficients for the attributes of a model for the ground water quality assessment. In another study Zhi-hong et al. [264] used the entropy method for determination of weight of evaluating factors in water quality assessment of a river. The results are found more accurate after implementation of entropy weight of each criterion and outcomes were more subjectivity of expert evaluation. Chowdhury and Husain [265] applied entropy and fuzzy set theories are applied in a multi-criteria decision making technique for determination of health risk management of different water treatment. In their study, the weights of the attributes are determined based on the concept of entropy determining the objective weight of the attributes. Jahan et al. [266] reviewed the material screening and choosing methods in which considered a variety of quantitative selection procedures and the systematic evolution and concludes that multi criteria decision making approach has the potential to greatly improve the material selection methodology. Jahan et al. [267] proposed a model for material selection procedure with material selection problem including their qualitative properties or user-interaction aspects. This procedure uses linear assignment method and multi criteria decision making process to rank the materials.

It is understood from above present literature that optimization technique utilization for optimize process parameters is necessary and influence of these parameters affect the output results. In multi-criteria decision making situation, optimal solution is formulated by optimization techniques.

2.7. Research Gaps

The literature review as presented above on particulate reinforced MMCs reveals the following knowledge gap, that enable us to materialized the objectives of the present research work: .

- ✓ The literatures reported significant work on various wear characteristics of metals, alloys and homogeneous materials using coating. However, lesser research work is there on the slurry erosion wear performance of multilayer coating on surface of metal matrix composites and their homogeneous composites.
- ✓ There have been fewer attempts to explore the potential of industrial wastes like marble dust and synthesize multilayer surface coated metal matrix composites for wear resistance applications.
- ✓ Various researchers' works using acidic and base slurry but the effect of pH value on slurry erosion and corrosion has not been reported so far.
- ✓ Research worldwide on slurry erosion wear behavior of metal matrix composites using heat treatment were significantly reported by various researchers along with statistical techniques whereas impact of various crucial factors that plays vital role during wear of coating was scarcely available.
- ✓ Taguchi method, in spite of being simple, efficient and systematic approach to optimize designs for performance, quality and cost, was used rarely across numerous applications worldwide. Its implementation in parametric appraisal of wear processes has hardly been reported.

2.8. Proposed objective for the research work

The detailed objectives are as follows:

1. To synthesize a series of uncoated and multilayered coated granite powder filled metal matrix composites
2. To characterize the physical and mechanical properties of the uncoated and multilayered coated on the particulate filled metal alloy composites
3. To determine the fracture toughness or stress intensity factor (SIF) of uncoated and multilayered coated particulate filled metal matrix composites with different crack lengths
4. To analyze the dynamic mechanical and corrosive behavior of the proposed alloy composites

5. To determine the slurry erosive wear characteristics of proposed composites under different operating conditions
6. Finally, the optimal performance analysis of particulate filled alloy composites for analysis of physical, mechanical, fracture toughness and wear analysis of the said composites using ENTROPY-VIKOR method

The next chapter discusses details of (i) materials (i.e. matrix, reinforcement, and coating), (ii) the formulations, (iii) the fabrication technique of alloyed composites, (iv) the coating method employed for preparation of the specimen. It also discuss characterization methodology like physical, mechanical, fracture, thermo-mechanical, corrosive, slurry-erosive etc. It also presents Taguchi DOE methods and VIKOR multi-criteria-decision-making approach for formulation ranking.

*****

Chapter 3

MATERIALS AND METHODS

Introduction

This chapter discusses (i) materials used in this research work i.e. matrix, reinforcement, and coating material, (ii) the formulation designed for the investigation (iii) the fabrication technique employed for preparation of alloyed composites, (iv) the surface modification or coating techniques employed to obtain single/multi-layer coating over the fabricated MMCs, (v) the physical, mechanical, thermo-mechanical characterizations, slurry erosive wear behavior and corrosion analysis of the MMCs under investigation, (vi) the Taguchi DOE technique to design the experimental runs matrix, (vii) VIKOR (ViseKriterijumska Optimizacija I Kompromisno Resenje) MCDM (Multi-criteria decision making) technique to obtain optimal ranking of formulations based on their physical, mechanical, corrosion, slurry erosion wear rate etc.

3.1 Matrix material

The matrix phase in any composite material system plays vital role by (i) holding the reinforcing phase and protecting them from environment degradation (ii) acts as medium to pass stresses to reinforcing phase thereby avoid catastrophic failure of matrix. In this research work, two grades of aluminum alloy viz. AA 1050 and AA 5083 are used as matrix material [217, 268]. The respective chemical composition of the said grades is cited in Table 3.1 and Table 3.2 highlights their physical/mechanical properties.

AA 1050 grade reported [217] to exhibits excellent corrosion resistance, high ductility, highly reflective finish and good formability. This aluminum alloy is typically used in chemical process plant equipment, food industry containers, pyrotechnic powder, architectural flashings, lamp reflectors and cable sheathing industries etc. [217].

AA 5000 series comprises of high magnesium, manganese and chromium alloying element. In AA 5083 alloy posses high strength, high resistance to sea water and industrial chemical environments. It is widely used in marine, food industry, ship building, unfired welded pressure vessels and for other structural applications etc. [268].

Table 3.1 Chemical Composition of AA 1050 and AA 5083 [217,268]

Element		Al	Si	Fe	Cu	Mn	Mg	Zn	Ti	Cr
wt. %	**AA 1050**	Balance	0.08	0.23	0.01	0.03	0.03	0.01	0.03	-
	AA 5083	Balance	0.4	0.4	0.1	0.4 -1	4.0-4.9	0.25	0.15	0.25

Table 3.2 Engineering properties of AA 1050 and AA 5083 [217,268]

Properties	**AA 1050**	**AA 5083**
Density	2.71 g/cc	2.66 g/cc
Poisson Ratio	0.32	0.33
Melting Point	650ºC	650°C
Modulus of Elasticity	71 GPa	70.3 GPa
Thermal Conductivity	222 W/m-K	117 W/m-K
Electrical Resistivity	0.028e-06 ohm-cm	5.9e-006 ohm-cm
Tensile Strength	145 MPa	317 MPa
Shear Strength	50 MPa	190 MPa
Hardness	35 Hv	96 Hv

3.2 Reinforcement material

In this research work, granite powder dust is used as reinforcing phase in AA 1050 and AA 5083 matrix phase. The fine granite powder is the by-product of crushing/cutting/polishing of granite stone. The granite power comprises of mixture of various oxides as listed in Table 3.3 and its mechanical properties are summarizes in Table 3.4.

Table 3.3 Chemical composition of Granite powder [269]

Element	SiO_2	Al_2O_3	K_2O	Na_2O	CaO	FeO	Fe_2O_3	MgO	TiO_2	MnO
wt.%	72.04	14.42	4.12	3.69	1.82	1.68	1.22	0.71	0.30	0.05

Table 3.4 Physical and Mechanical properties of granite powder [269]

Mechanical properties	Granite Powder
Density	2.9 Kg/m^3
Melting Point	1260°C
Modulus of Elasticity	70 GPa
Thermal Conductivity	48 W/m.K
Tensile Strength	39 MPa
Hardness	1161 H_V

3.3 Coating material

The fabricated particulate filled aluminum alloyed composites are coated with chromium nitride (CrN) and silicon nitride (SiN) in this research work. Chromium nitride coating has high hardness, toughness, high cohesive strength, low coefficient of friction, excellent corrosion and abrasive wear resistance. Chromium nitride coating uniformly spread over the substrate and typically the thickness is 1-5 micron for different application.

Silicon nitride coating has for high-temperature oxidation/corrosion protection, optically transparent and wear resistance. Silicon nitride coating typically used in engine, airframe components and thermal protection system components etc.

3.4 Formulation of the investigated MMCs

The MMCs for investigation is formulated as per Table 3.5. There are three sets of each base alloy. The first set comprises of granite dust particulate (0, 2, 4, 6 wt.%) filled aluminum alloy composite, second set comprises of coating of CrN over the first set and third set comprises of coating of SiN + CrN over first set.

Table 3.5 Designations and detailed compositions

Designation	Nomenclature	Composition-1	Designation	Nomenclature	Composition-2
1050GD-0	A-1	AA1050 + 0 wt.% Granite Dust	5083GD-0	B-1	AA5083 + 0 wt.% Granite Dust
1050GD-2	A-2	AA1050 + 2 wt.% Granite Dust	5083GD-2	B-2	AA5083 + 2 wt.% Granite Dust

1050GD-4	A-3	AA1050 + 4 wt.% Granite Dust	5083GD-4	B-3	AA5083 + 4 wt.% Granite Dust
1050GD-6	A-4	AA1050 + 6 wt.% Granite Dust	5083GD-6	B-4	AA5083 + 6 wt.% Granite Dust
Coated		**CrN**	**Coated**		**CrN**
S1050GD-0	A-5	AA1050 + 0 wt.% Granite Dust	S5083GD-0	B-5	AA5083 + 0 wt.% Granite Dust
S1050GD-2	A-6	AA1050 + 2 wt.% Granite Dust	S5083GD-2	B-6	AA5083 + 2 wt.% Granite Dust
S1050GD-4	A-7	AA1050 + 4 wt.% Granite Dust	S5083GD-4	B-7	AA5083 + 4 wt.% Granite Dust
S1050GD-6	A-8	AA1050 + 6 wt.% Granite Dust	S5083GD-6	B-8	AA5083 + 6 wt.% Granite Dust
Coated		**SiN & CrN**	**Coated**		**SiN & CrN**
M1050GD-0	A-9	AA1050 + 0 wt.% Granite Dust	M5083GD-0	B-9	AA5083 + 0 wt.% Granite Dust
M1050GD-2	A-10	AA1050 + 2 wt.% Granite Dust	M5083GD-2	B-10	AA5083 + 2 wt.% Granite Dust
M1050GD-4	A-11	AA1050 + 4 wt.% Granite Dust	M5083GD-4	B-11	AA5083 + 4 wt.% Granite Dust
M1050GD-6	A-12	AA1050 + 6 wt.% Granite Dust	M5083GD-6	B-12	AA5083 + 6 wt.% Granite Dust

**G-0, G-2, G-4and G-6 indicate granite powder reinforcement, S indicate single layer coating on other hand M indicate multilayer coating, 5083 & 1050 indicate grade of aluminum alloy

3.5. Fabrication technique

The designed formulations are fabricated using high temperature vacuum casting machine (Figure 3.1). The sequences of activities performed for fabrication are listed below:

1. The graphite crucible is preheated (about 200°C) first to prevent oxidation of base material (i.e. aluminum alloy) and its easy melting.

2. Thereafter pieces of base material are put inside the crucible. Future, crucible is heated till 650°C. This melts the base material.
3. The reinforcing phase (i.e. granite powder) is added to the molten base alloy slowly and mechanical stirrer at 400 rpm is used to mix the ingredients at least for 5 minutes. To ensure proper wettability between ingredients 1 wt.% magnesium power is added to the mixture. This step continues for another 10 minutes. Thus, homogeneity in the mixture is ensured.
4. Now plunger is opened so that molten metal automatically poured into the molds (made of rectangular stainless steel) for solidification. The mold is kept in the room for around 20 minutes so as to achieve proper curing.
5. When the room temperature of casting is obtained the specimen samples are prepared as per characterization or testing methods with the help of diamond cutter.

Figure 3.1 High temperature vacuum casting machine and cast iron Mold

3.6. Coating Deposition

Single layer (chromium nitride) and multilayer (silicon nitride/chromium nitride) coatings are deposited on prepared granite reinforced aluminum alloy composites by thermal vapor deposition process using High Temperature Vacuum Box Coater (Model BC-300) supplied by Hind High Vacuum Co.(P) Ltd. Bangalore, India (Figure 3.2). The process conditions and values

of related parameters are listed in Table 3.6. Chromium and silicon powder (100 μm) of 99.8 % purity supplied by Alfa Alsar is used as coating material. Prior to coating deposition, the samples are mirror-polished using Meta Serve 250 machine supplied by Buhler. The polished surface reported to improve the adherence between the coating and composite samples surface. Samples are ultrasonically cleaned in acetone and alcohol progressively, each for 5 min., and dried for approximately 20 min. in a pre-vacuum dryer. The vacuum of 10^{-6} bar is maintained in high temperature vacuum box coater machine. Pure chromium and silicon pallet is placed into a tungsten boat and sample is placed on sample holder. High current (50-75 A) is supplied to tungsten boat at voltage 12 V for evaporation of coating material, and then the flow of nitrogen gas is released into the chamber; consequently nitride layer gets deposited over the sample surface. The coating thickness is shown by the control panel; which depends upon deposition rate of coating. The change in resonance frequency of piezoelectric sensor is represent coating thickness and the reason behind this change of resonance frequency is deposition of coating material on the surface of piezoelectric sensor.

Table 3.6 PVD coating conditions

Coating Temperature (˚C)	Total gas pressure (Pa)	Voltage (V)	Cathode current (A)	Coating Rate (A˚/min)	Source to substrate distance (mm)
200	1.5	12	50-75	1	200

Figure 3.2 Thermal Vapor Deposition Machine

3.7 Physical characterization and Mechanical characterization

3.7.1 Density and void fraction

Density and void fraction is an important parameter for determination of mechanical and wear properties. The theoretical density of the alloy uncoated and coated composite materials can be easily described in the Eq. 3.1 given by the Agarwal and Broutman [15]. Experimental density of composites can be determined by the water immersion technique.

$$\rho_{ct} = \frac{1}{\frac{W_m}{\rho_m} + \frac{W_f}{\rho_f}} \tag{3.1}$$

Where,

ρ_{ct} = theoretical density of composites

W_m = Weight fraction of Matrix

ρ_m = density of matrix

W_f = Weight fraction of fillers

ρ_f = density of fillers

The voids content in composites can be calculated by the Eq. 3.2

$$V_v = \frac{\rho_{ct} - \rho_{ce}}{\rho_{ct}} \tag{3.2}$$

Where

V_v = Void Fraction

ρ_{ct} = Theoretical density of composites

ρ_{ce} = Experimental density of composites

3.5.2 Flexural test

Flexural strength is an important property of any structural material and it represents the ability of material to withstand the bending before reaching breaking point. Conventionally three point bending test is conducted for finding out the material bending property. Flexural strength is carried out according to ASTM standard E-290 [270] using the universal testing machine (UTM) by Aimil Ltd., India. During flexural test the span length is taken 40 mm with a cross head speed

of 1 mm/min is maintained throughout the test with sample dimension of 60×10×10 mm^3 respectively. The flexural strength (*F.S.*) of composite specimen is determined using the Eq. 3.3.

$$F.S. = \frac{3FL}{2bd^2} \tag{3.3}$$

Where,

F= Applied central load (N)

L= Test span of the sample (m)

b= Width of the specimen (m)

d= Thickness of specimen under test (m)

3.5.3 Hardness Test

Micro-hardness measurement is carried out as per ASTM Standard E-92 [271] using a micro-hardness tester as shown in Figure 3.3. A right pyramid diamond indenter with square base and with an angle 136° is used for forced into the material under a load F. After removal of load indenter impression left on the surface of material and two diagonals X and Y of the indentation are measured or their arithmetic mean L is calculated. In the present study, the load considered F = 50N and Vickers hardness number is calculated using the Eqs. 3.4 and 3.5.

Figure 3.3 Micro-hardness Tester

$$H_V = 0.1889\frac{F}{L^2} \tag{3.4}$$

$$\text{And} \qquad L = \frac{X + Y}{2} \tag{3.5}$$

Where,

F is the applied load (N)

L is the diagonal of square impression (mm)

X is the horizontal length (mm)

Y is the vertical length (mm).

3.5.4 Impact Test

Impact test is done as per ASTM E-23[272] using impact tester (Figure 3.4) on the composite specimens. The pendulum impact testing machine ascertain the notch impact strength of the material by shattering the V-notched specimen with a pendulum hammer measuring the spent energy and relating it to the cross section of the specimen.

Figure 3.4 Impact testing machine

The specimen size is 64 × 12.7 × 3.2 mm^3 with 2 mm depth of notch (notch angle 45°) respectively. The machine is adjusted such that the hammer on the free hanging pendulum just barely contacts the specimen (zero position). The specimen is clamped in a square support and is

struck at their central point by a hemispherical bolt of diameter 5 mm. The respective values of impact energy for different specimens are recorded directly from the dial indicator.

3.5.5 Fracture Test

Fracture test is done as per ASTM E-399 [273] using same universal testing machine. For fracture analysis the samples are prepared with different crack lengths using wire electrical discharge machine and provided in the middle of the sample, thereafter sample is mounted on universal testing machine and carried out the tensile test. After test, breaking load and stress intensity factor are determined using Eqs. 3.6 and 3.7 for all granite powder reinforced composites and single / multilayer coating on granite powder reinforced alloy composites for different crack lengths.

$$K_I = \frac{P}{B\sqrt{W}}\gamma(\beta) \tag{3.6}$$

$$\gamma(\beta) = \frac{\sqrt{2\tan\frac{\pi a}{2W}}}{\cos\frac{\pi a}{2W}}\left[0.75 + 2.02\left(\frac{a}{W}\right) + 0.37\left(1-\sin\frac{\pi a}{3W}\right)^3\right] \tag{3.7}$$

Whereas K= Stress intensity factor, P is maximum load (stress), B is thickness of specimen, W is width of specimen and a is crack length and γ(β)= function of crack length and specimen width

3.6 Dynamic Mechanical Analysis (DMA)

Dynamic Mechanical Analysis is carried out using dynamic mechanical analyzer provided by Perkin Elmer-8000 as shown in Figure 3.5 at constant frequency (1 Hz) with temperature range of 30-250ºC under three point bending configuration.

Figure 3.5 Dynamic Mechanical Analyzer

A static force of 1 N is applied at the mid-point of the specimen and the span length is fixed at 25 mm. load pointer is roller supported type to provide uniform loading on the material and to inhibit friction effects. The sample size for dynamic mechanical analysis test is 27.5 × 10 × 1.5 mm^3.

3.7 Scratch Test

Scratch test is carried out as per ASTM standard C1624 [274] using scratch tester 101 (DUCOM Figure 3.6) equipped with Optical microscope, acoustic emission detection system and tangential friction force sensors. Rockwell-C type diamond indenter with tip radius 200 µm and tip angle is 120º. In scratch test 20 N constant load is applied with scratch speed 0.1 mm/min. for scratch length of 5 mm. Measured outputs from the scratch test are width and depth of indentation along with length of scratch. As normal load is applied traction force is generated and plastic deformation of coating started their sudden increase in traction force. The sudden increment in traction force is indication of coating failure. The width of scratch is observed with the help of optical microscope.

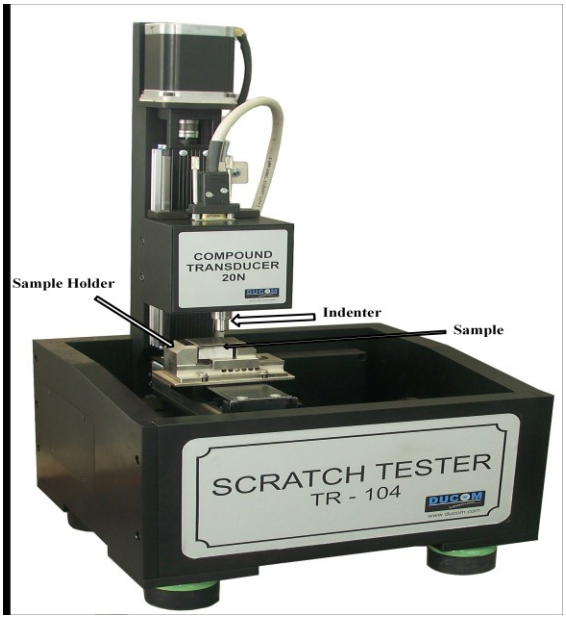

Figure 3.6 Scratch Tester

3.8 Scanning electron microscopy

The worn surfaces of wear samples are examined directly by scanning electron microscope NOVA-500 shown in Figure 3.7. Micrographs are taken at 20 kV accelerating voltage. The slurry erosion wear features such as micro cutting, micro ploughing, particle out, brittle failure is observed from the SEM micrographs.

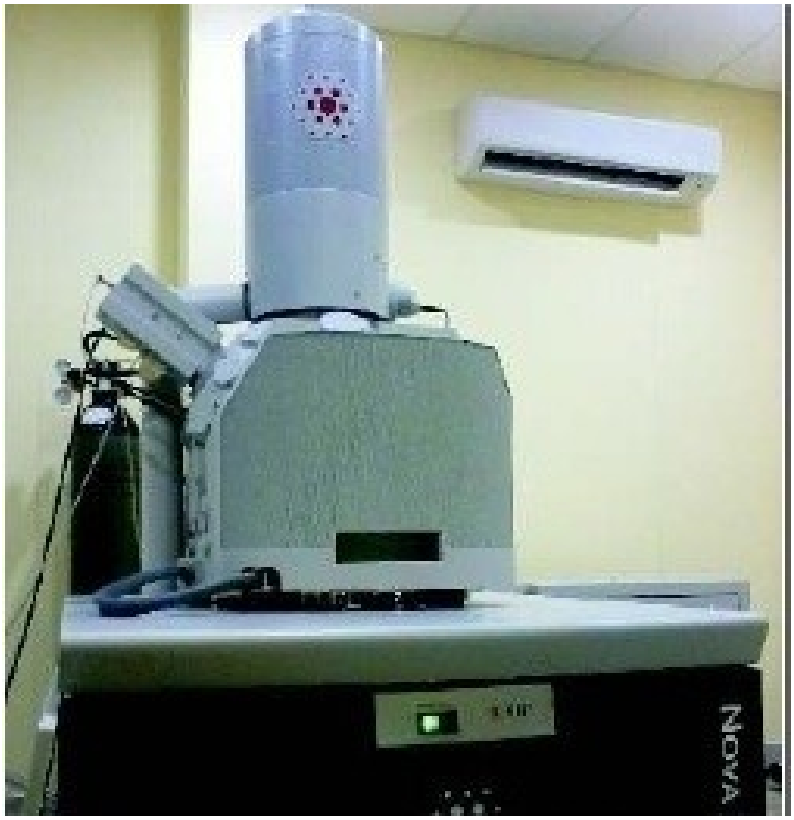

Figure 3.7 Scanning electron microscopes (NOVA-500) along with EDAX

3.9 Atomic Force microscopy (AFM)

The surface morphology of uneroded samples and eroded samples are analyzed using D3100 AFM equipped with a Nanoscope 5 electronic from Bruker Nanoscope TM manufacturer (Figure 3.8). The images are recorded in ambient conditions (25°C and 30% relative humidity) and in soft intermittent contact mode. In contact mode a cantilever silicon probe is utilized for mapping of surface. The scan rate is adjusted in the range of 0.4-0.5 Hz depending on the image quality. Surface area scan by silicon probe is 2 × 2 μm for surface mapping. For acquisition of surface morphology, amplitude error and height images are recorded on several areas of film surface. AFM data measured for uneroded and eroded samples as a three-dimensional projection which emphasizes the nanometer-scale precision of the instrument in the vertical *z* direction (height).

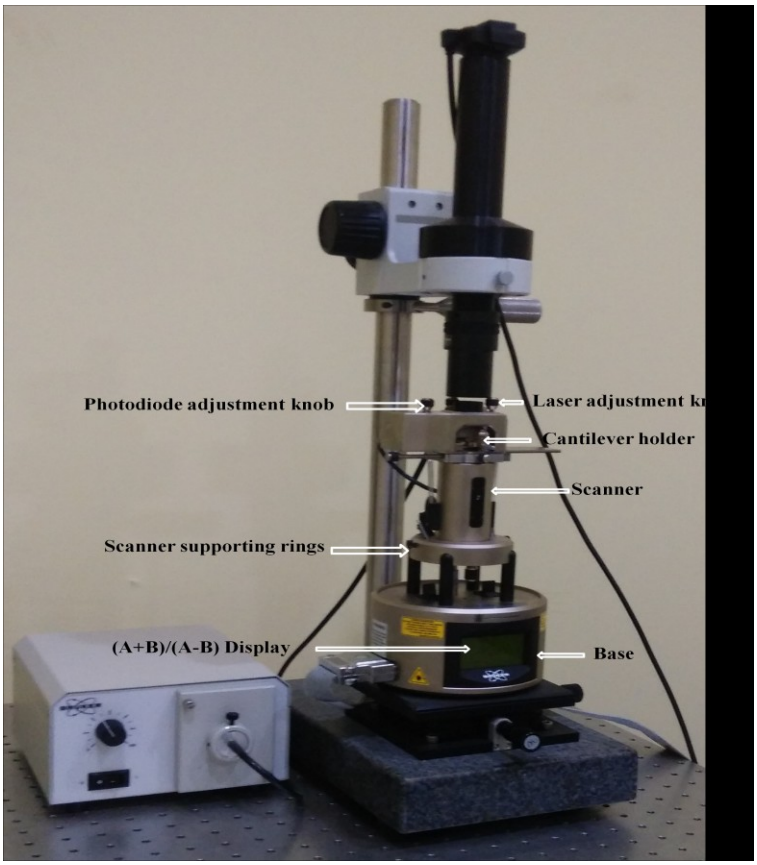

Figure 3.8 Atomic Force Microscope

3.10 Corrosion test

Salt spray corrosion test is carried out as per ASTM standard B117 [275] using corrosion tester model 606 supplied by ERICHSEN shown in Figure 3.9. This equipment provides a controlled corrosive environment and exposed the corrosion resistance information of metal specimen kept in test chamber. The apparatus have a fog chamber, salt solution reservoir, a supply of suitably conditioned compressed air, one or more atomizing nozzles, specimen holders, provision for heating the chamber, and necessary control panel. Fog of solution accumulates on the surface of specimens and exposed corrosion resistance information. Fog of solution that fall from the specimens will not return to the solution reservoir for re-spraying. Salt spray results is correlated with the prediction of performance of specimens in the natural environments when used as stand-alone data.

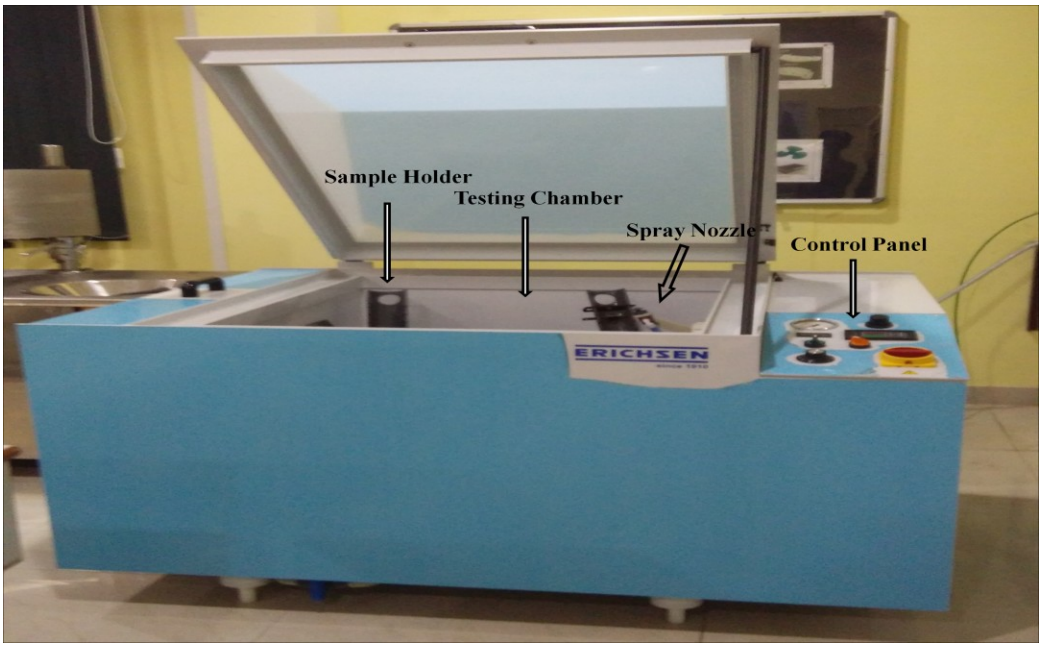

Figure 3.9 Corrosion Tester

3.11 Slurry Erosion test

The slurry-erosion experiments are conducted as per ASTM standard G-134[276]. A jet-type slurry erosion test rig supplied by DUCOM (TR-411) (Figure 3.10) is used for experiments. Slurry jet erosion tester consists following components, erodent tank, water jet motor, erodent motor, rectangular water tab, sample holder, filtration unit, control panel. Erodent tank contain 60 kg erodent, and discharge of erodent controlled by centrifugal pump driven by 3HP/1435 rpm electric motor. The water jet motor 2 HP/1415 rpm is used for different velocity and slurry concentration. Erodent particles fell down form erodent tank to mixing chamber. The particles are mixed with the water and form slurry and the jet is discharged to the samples through a nozzle of diameter 4 mm. The sample holder enables holding the samples at various impact angles (15-90°) within an accuracy of ±1°. The standoff distance between the nozzle and the specimen is kept fixed at 25 mm for all tests. The sample is eroded during the test for 10 minute and to measure the amount of erosion, the weight loss of the samples is measured using a precision weighing balance with 0.1 mg accuracy and converted to equivalent volume loss using the densities. All the samples are cleaned carefully with acetone prior to each weight measurement.

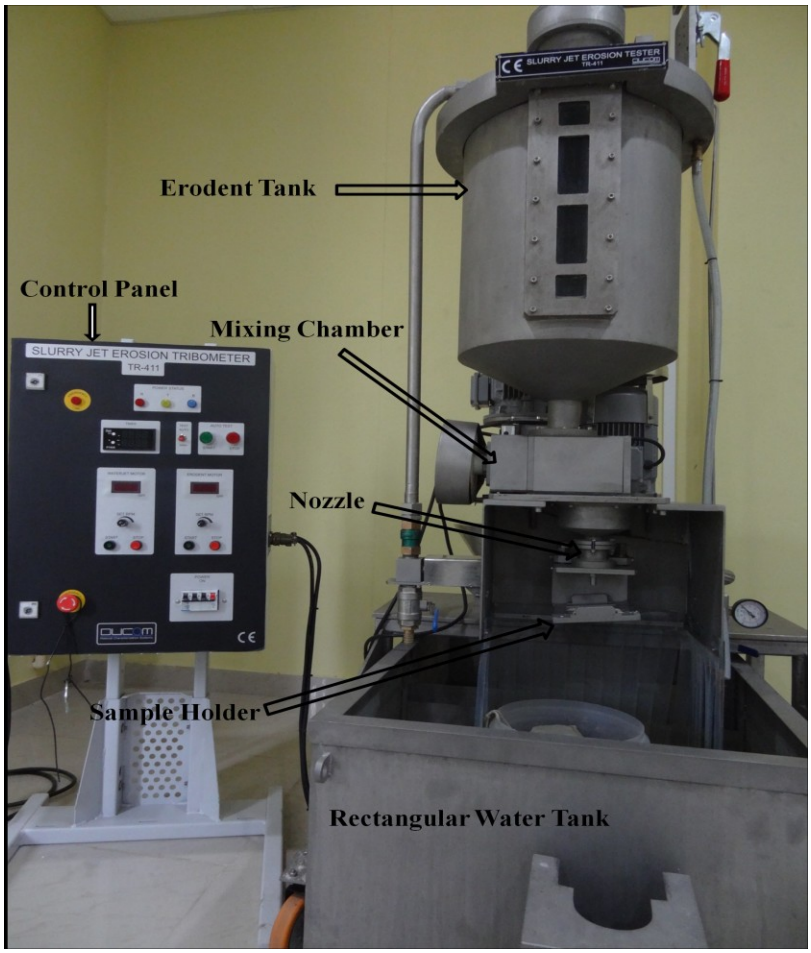

Figure 3.10 Slurry Jet Erosion Tester

3.12 Process optimization and Taguchi method

Taguchi design of experiment is used in the present research works to obtain accurate experimental results. Taguchi method provides the designer with a systematic and efficient approach for experimentation to determine near optimum settings of design parameters for performance and cost.

Table 3.7 Control Factor and levels used in Taguchi design

Control Factor	Levels				Unit
	I	II	III	IV	
Filler Content (A)	0	2	4	6	wt.%
Impact Velocity (B)	10	15	20	25	m/sec.
Impingement Angle (C)	30	45	60	75	Degree
Erodent Discharge (D)	160	200	240	280	g/min.

This method involves laying out the experimental conditions using specially constructed tables known as 'orthogonal arrays'. Use of orthogonal arrays significantly reduces the number of experimental configurations to be studied. The conclusions drawn from small scale experiments are valid over the entire experimental region spanned by the control factors and their settings. The most important stage in the design of experiment lies in the selection of the control factors. Therefore, initially a large number of factors are included so that non-significant variables can be excluded at the earliest opportunity. In Taguchi orthogonal L_{16} (4^4) orthogonal array design is: the first column is assigned to filler content, the second column to impact velocity, the third column to impingement angle, the forth column to erodent discharge respectively at constant stand-off distance (15 mm) for all the test runs to estimate the slurry erosion rate.

Table 3.8 Taguchi Orthogonal array design L_{16} (4^4)

S. No.	Filler Content	Impact Velocity	Impingement Angle	Erodent Discharge
1.	0	10	30	160
2.	0	15	45	200
3.	0	20	60	240
4.	0	25	75	280
5.	2	10	45	240
6.	2	15	30	280
7.	2	20	75	160
8.	2	25	60	200
9.	4	10	60	280
10.	4	15	75	240
11.	4	20	30	200
12.	4	25	45	160
13.	6	10	75	200
14.	6	15	60	160
15.	6	20	45	280
16.	6	25	30	240

The control factors and the parameter settings for slurry erosion test are given in Table 3.7. Table 3.8 presents the selected levels for various control factors. The tests are conducted as per the experimental design given in Table 3.7 [277]. Three samples replica are tested at each combination of factor settings as per L_{16}orthogonal array design [277,278]. For the better slurry erosion wear performance smaller-the-better characteristic S/N ratio is adopted and computed as logarithmic transformation of loss function (Eq. (3.8)).

Smaller-the-better characteristic:

$$S/N = -10\log\frac{1}{n}(\sum y_i^2) \tag{3.8}$$

Whereas, 'n' is the number of experiments in the L_{16} orthogonal array design and y_i is the measured values (i.e. erosion wear rate).

3.13 Optimization of physical, mechanical and slurry erosion wear behavior of the proposed composites using ENTROPY-VIKOR method

The present study is aimed to determine the ranking of different formulations based upon different decisive parameters using entropy and VIKOR hybrid technique. The entropy method is applied in order to prioritize the criterions by assigning weight. Thereafter, VIKOR method is applied to rank the alternatives. The evaluation methodology consists of the following three basic phases viz.

Phase I: Identification of the criterions, alternatives and construction of decision matrix.

Phase II: Determination of weight of individual criterion using entropy method.

Phase III: Ranking of the alternatives using VIKOR method.

Phase I: Identification of the criterions, alternatives and construction of decision matrix.

First the various criterions and alternatives of the problem are identified and a decision matrix of criterions and alternatives is formulated based on the information available regarding the problem. If the number of alternative is M and the number of criterions are N then the decision matrix having an order of M × N is represented as:

$$D_{M\times N} = \begin{bmatrix} x_{11} & x_{12} & \cdots & x_{1N} \\ x_{21} & x_{22} & \cdots & x_{2N} \\ \vdots & \vdots & \cdots & \vdots \\ x_{M1} & x_{M2} & \cdots & x_{MN} \end{bmatrix} \tag{3.9}$$

Where, an element x_{ij} (for i=1, 2... M; j = 1, 2... N), of the decision matrix $D_{M\times N}$ represents the actual value of the i^{th} alternative in term of j^{th} criterion.

Phase II: Determination of weight of individual criterion using entropy method.

The weights of various criterions are determined by the entropy method. First of all the projection value (ρ_{ij}) for each alternative is calculated as:

$$\rho_{ij} = \frac{x_{ij}}{\sum_{i=1}^{M} x_{ij}} \tag{3.10}$$

After the calculation of projection value, entropy of each criterion is calculated as:

$$\mathrm{E}_j = -\varsigma \sum_{j=1}^{N} \rho_{ij} \ln(\rho_{ij}) \tag{3.11}$$

where k is a constant and calculated as, $\varsigma = \frac{1}{\ln(M)}$

Next the dispersion value (ψ_j) of each criterion is calculated as:

$$\psi_j = 1 - \mathrm{E}_j \tag{3.12}$$

Finally the weight of each criterion is calculated as:

$$\omega_j = \frac{\psi_j}{\sum_{j=1}^{N} \psi_j} \tag{3.13}$$

VIKOR method

After the development of decision matrix, values of benefit $\left(x_{ij}\right)_{\max}$ and cost $\left(x_{ij}\right)_{\min}$ criterion is obtained as:

$$\left(x_{ij}\right)_{\max} = {}^{\max}_{i} x_{ij} = \max\left[x_{ij}, i = 1, 2..M\right]$$

$$\left(x_{ij}\right)_{\min} = {}^{\min}_{i} x_{ij} = \min\left[x_{ij}, i = 1, 2..M\right] \tag{3.14}$$

After this, the values of utility measure (α_i) and regret measure (β_i) are determined by using weights as:

$$\alpha_i = \sum_{j=1}^{N} \frac{\varpi_j \left[\left(x_{ij}\right)_{\max} - x_{ij}\right]}{\left[\left(x_{ij}\right)_{\max} - \left(x_{ij}\right)_{\min}\right]}, \textit{ if } j \textit{ is benefit criteria}$$

$$\alpha_i = \sum_{j=1}^{N} \frac{\varpi_j \left[x_{ij} - \left(x_{ij}\right)_{\min}\right]}{\left[\left(x_{ij}\right)_{\max} - \left(x_{ij}\right)_{\min}\right]}, \textit{ if } j \textit{ is cost criteria} \text{ , for j = 1, 2. . . N} \tag{3.15}$$

$$\beta_i = Max^x \ of \left\{ \frac{\varpi_j \left[\left(x_{ij}\right)_{\max} - x_{ij} \right]}{\left[\left(x_{ij}\right)_{\max} - \left(x_{ij}\right)_{\min} \right]} \right\}, \text{ for j = 1, 2. . . N} \quad (3.16)$$

Finally VIKOR index (Ω_i) is calculated as:

$$\Omega_i = \xi \left(\frac{\left(\alpha_i - \alpha_i^-\right)}{\left(\alpha_i^+ - \alpha_i^-\right)} \right) + \left(1-\xi\right) \left(\frac{\left(\beta_i - \beta_i^-\right)}{\left(\beta_i^+ - \beta_i^-\right)} \right) \quad (3.17)$$

Where,

$\alpha_i^+ = {}^{\max}_{i}\alpha_i = \max\left[\alpha_i, i = 1, 2...M\right]$; $\alpha_i^- = {}^{\min}_{i}\alpha_i = \min\left[\alpha_i, i = 1, 2...M\right]$

$\beta_i^+ = {}^{\max}_{i}\beta_i = \max\left[\beta_i, i = 1, 2...M\right]$; $\beta_i^- = {}^{\min}_{i}\beta_i = \min\left[\beta_i, i = 1, 2...M\right]$

ξ is introduced as weight for the maximum value of utility and $(1-\xi)$ is the weight of the individual regret and normally its value of ξ is taken as 0.5.

According to the value of VIKOR index alternatives are arranged in the ascending order and the best alternative is the one having the minimum value of Ω_i.

Summary of the Chapter

This chapter highlight below information:

I. The detailed description of materials used in this research work i.e. matrix, reinforcement, and coating material,
II. The details of the formulation designed for the investigation
III. The details of the fabrication technique employed for preparation of alloyed composites,
IV. The details of the surface modification or coating techniques employed to obtain single/multi-layer coating over the fabricated MMCs,
V. The details of methodology of physical, mechanical, thermo-mechanical characterizations, slurry erosive wear behavior and corrosion analysis of the MMCs under investigation,
VI. The details of Taugchi DOE technique to design the experimental runs matrix, and VIKOR, MCDM technique to obtain optimal ranking of formulations based on their physical, mechanical, corrosion, slurry erosion wear rate etc.

The next chapter presents discussion on results of physical and mechanical characteristics of the alloyed composites (coated/uncoated) under investigation.

******

Chapter 4

ANALYSIS OF PHYSICAL AND MECHANICAL CHARACTERISATION OF FABRICATIED GRANITE PARTICULATE FILLED ALLOYED COMPOSITES (COATED/UNCOATED)

This chapter deals with the behaviour of material (under investigation) under different loading conditions and responses in terms of strains, so as to understand deflection, deformation and failure etc. The variations in physical/mechanical characteristics with-respect-to filler-content variations in the alloyed composites (coated/uncoated) are discussed in length.

PART-I: Analysis of Physical and Mechanical characteristics of uncoated / single-layer coated / multi-layered coated granite particulate filled AA1050 alloyed composites

4.1. Physical characterization of the investigated composites

Density and void content of uncoated/single layer /Multilayer surface coating on granite powder filled alloyed composites are investigated at room temperature. The amount of void formation in the uncoated and coated granite powder filled alloy composites is predicted theoretically and experimentally. The presence of pre-existing void decline the mechanical properties of composites, to get better mechanical and fracture properties reduce the amount of void presence in the composites. The density of composites is measured by weighing polished cubes of the as-processed and extruded samples in air and when immersed in distilled water. The densities, derived from the recorded weights, are then compared to the theoretical rule of mixtures densities from which the volume content of porosity is calculated by Agarwal and Broutman [15] proposed formula.

The properties of particulate filled metal alloyed composites is depended on the relative proportion of matrix and reinforcing materials, distribution of reinforcing particles and interface bonding between the particle and matrix. The voids significantly affected some of the mechanical properties and even the performance of composites due to the stress concentration at that point where the specimen easily breaks under the loading condition. The knowledge of void content is desirable for estimation of the quality of the composites. It is understandable that a good composite should have fewer voids. The theoretical and experimental density with void content of granite powder filled aluminium metal alloyed composites. It is observed from the

Figure 4.1 that void content increases with the addition of granite powder in alloy matrix material. The possible reason might be attributed to fact that lower density may be attributed to insufficient bonding at interface of matrix and ceramic particulates that left voids, the agglomeration of particulates while solidifying may be created intra-particulate voids because of insufficient bonding with matrix material. The possible error may be the fabrication methodology resulted into voids contents [45]. Higher void content in composites are undesirable and represents inferior quality; as such composite materials affects various properties and performance while in service. Therefore, it can be said that a basic criterion with which to evaluate their quality is the density of composites.

Table 4.1 Physical and Mechanical characteristics of uncoated / single-layer coated / multi-layered coated granite particulate filled AA1050 alloyed composites

Nomenclature	Composite designation	Void content (%)	Flexural strength (MPa)	Hardness (Hv)	Impact Strength (J)
A-1	1050G-0	4.09	327.3	32	41
A-2	1050G-2	5.75	297.1	36.2	42
A-3	1050G-4	9.73	231.8	51.2	45
A-4	1050G-6	9.74	211.8	61.2	46
A-5	S1050G-0	3.73	355.29	87	44
A-6	S1050G-2	4.69	308.73	99	44
A-7	S1050G-4	6.63	263.66	113	51
A-8	S1050G-6	8.13	242.19	123	53
A-9	M1050G-0	3.23	395.13	93	45
A-10	M1050G-2	4.13	323.69	105	46
A-11	M1050G-4	5.49	286.13	127	52
A-12	M1050G-6	6.37	253.16	139	58

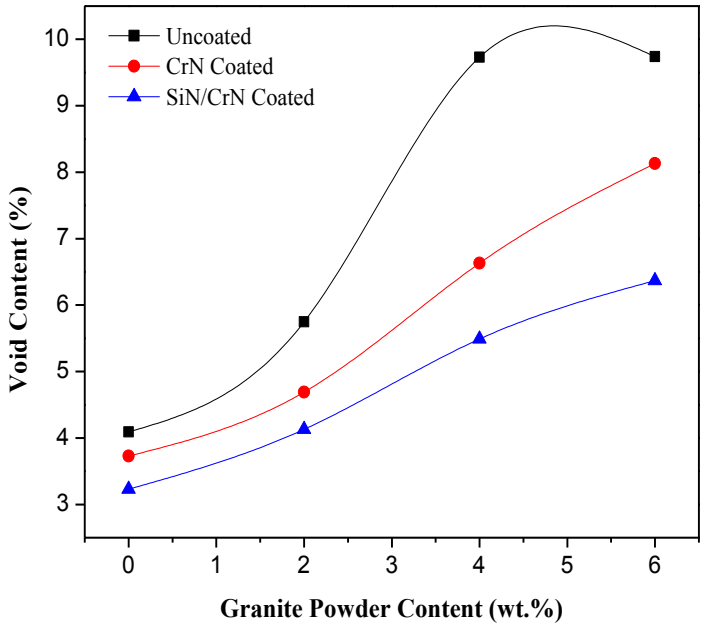

Figure 4.1 Effect of reinforcement and coating on void content

4.2 Adhesion properties of single-layer coated / multi-layered coated granite particulate filled AA1050 alloyed composites

The Figure 4.2(a-b) shows the results of scratch tests for single and multilayer coatings. This enables determination of adhesion properties between coating and substrate.

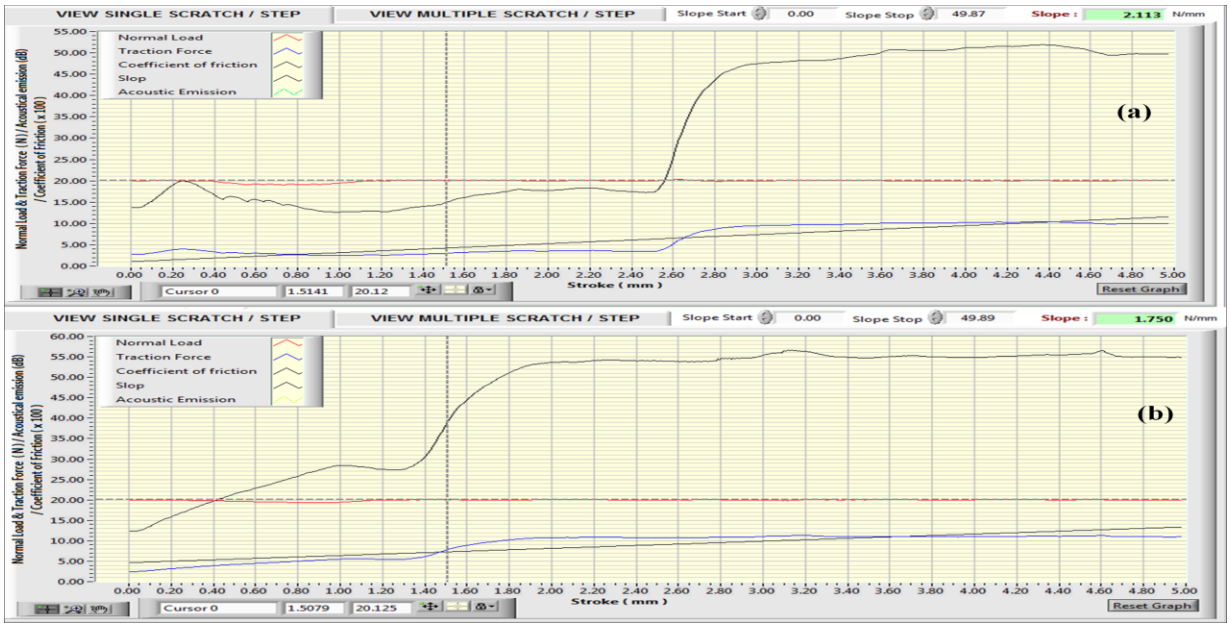

Figure 4.2 Scratch test results for (a) single and (b) multilayer coating

The change in traction force is observed with stroke length represents the cohesive failure i.e. failure within the coating. The failure of coating may be due to the plastic deformation of coating. The slope between normal load and traction force represent the failure of coating and change in slope, which may be due to adhesive failure between coating and substrate interfaces.

4.3. Hardness of uncoated / single-layer coated / multi-layered coated granite particulate filled AA1050 alloyed composites

The hardness of a material is the ability of a material to resist the penetration by an indenter under action of load. The indenter is made of hard material like diamond, hardened steel etc. The tip of the indenters may be conical, pyramidal, or spherical in shape. Since indentation tests are relatively easy to perform (macro-indentations require only limited specimen preparation), they are often used to obtain quick estimates of strength. Figure 4.3 presented the hardness of uncoated, single layer and multilayer coated on granite powder reinforced aluminium matrix composites. It is revealed that hardness increased (linearly) with increased in the content of granite powder reinforcement in aluminium matrix alloy.

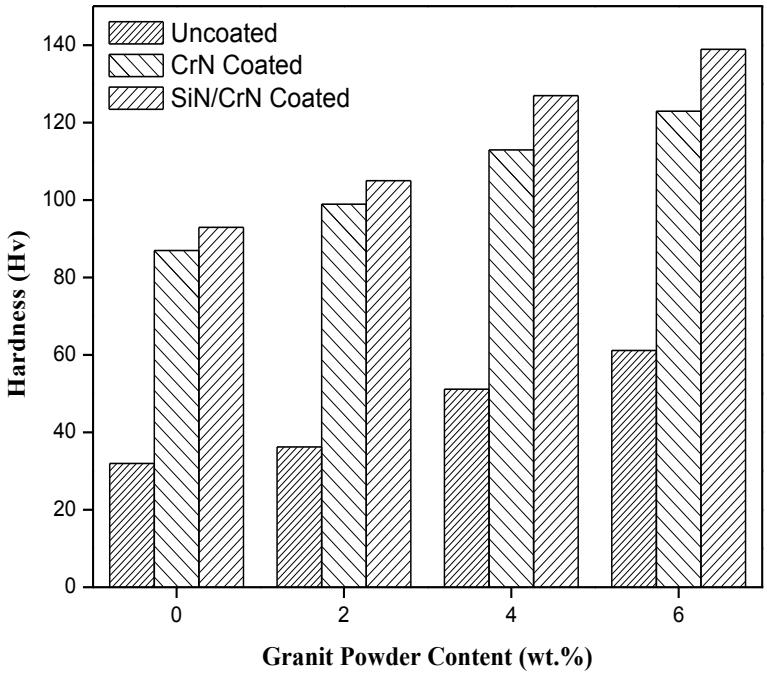

Figure 4.3 Effect of reinforcement and coating on hardness

The increased in hardness is quite obvious and expected since granite powder is combination of different hard dispersed ceramic materials and contributes effectively to increase hardness of the composites. Therefore, from Figure 4.3 it is clearly observed that for uncoated particulate filled alloy composites (0-6 wt.% granite powder) the hardness gradually increases from 32 Hv to 61.2 Hv respectively. Hence, addition of granite powder improved from 0 wt.% to 2 wt.% is ~ 12%, again on further addition of granite powder from 2 wt.% to 4 wt.% is ~ 29% and on further addition of granite powder from 4 wt.% to 6 wt.% the hardness improved to ~16% respectively [118]. This dispersion effect is expected to maintain a higher environment temperature instead of elevated temperature because the particles may not react with the matrix phase. Similar, trend also reported by Mummery and Derby [279] and Divecha et al. [280] in the hardness of the composite with hard dispersoids. Maximum hardness is observed for uncoated aluminium alloyed composites reinforced with 6 wt.% granite powder.

However, in single layer (CrN) and multilayer coating (SiN/CrN) on the particulate filled aluminium alloyed composites by keeping coating thickness remaining constant in all the proposed particulate filled alloy composites (Figure 4.3). It is observed that CrN coating on 0 wt.% granite powder reinforced aluminium alloyed composites and SiN/CrN coating on same 0 wt.% granite powder reinforced aluminium alloyed composites the hardness increased by ~171.8% and 190% respectively (Figure 4.3). Similarly, single and multilayered coating on 2wt.% granite powder reinforced aluminium alloyed composites the hardness increased by 173% and 193% respectively(Figure 4.3). However, same single and multilayer coating on 4 wt.% granite powder reinforced aluminium alloyed composites hardness increased to 162% and 181% respectively and same as in case of 6 wt.% granite powder reinforced aluminium alloy composites the hardness is increases by 151% and 163% respectively for single and multilayered coating (Figure 4.3). The improvement in hardness of single layer coating due to the promising hardness of chromium nitride coating on the other hand in multilayer coating CrN/SiN stack is attributed to many interfaces that blocked the micro-crack movements across interfaces due to differences in the shear module of the individual layer material [281,282]. From the graph it is also observed that hardness magnitude for multilayered coating samples are higher than single layer coating samples. The increase of the hardness can be attributed to the formation of CrN/SiN hard phases, which are homogeneously dispersed in the matrix.

4.4. Flexural strength of uncoated / single-layer coated / multi-layered coated granite particulate filled AA1050 alloyed composites

Figure 4.4 shows the flexural strength of the uncoated and coated granite powder filled 1050 aluminium alloyed composites. It is clearly observed from Figure 4.4 that as the reinforcement weight percentage increases in the alloy composites the flexural strength gradually decreased irrespective of coating effect. From this analysis it is observed that for uncoated particulate filled composites the flexural strength decreasing rate for 2 wt.% granite powder filled alloy composites is 28% but on further addition of granite powder the decreasing rate was slightly reduced to approximately 15% for 4 wt.% granite powder filled composite and on further addition of 6 wt.% granite powder in the base matrix material the strength reduced to 10% (Figure 4.4). Therefore, the decreasing rate of flexural strength is maximum initially up to 2 wt.% granite powder filled alloy composite and then the decreasing rate was continued but gradual decreasing in flexural strength of the uncoated composites. The possible reason for decrease of flexural strength with the increased in filler content in the alloy composites may be lead to poor strength between matrix and filler material, hence decreased the effectiveness of stress transfer between them [283-285].

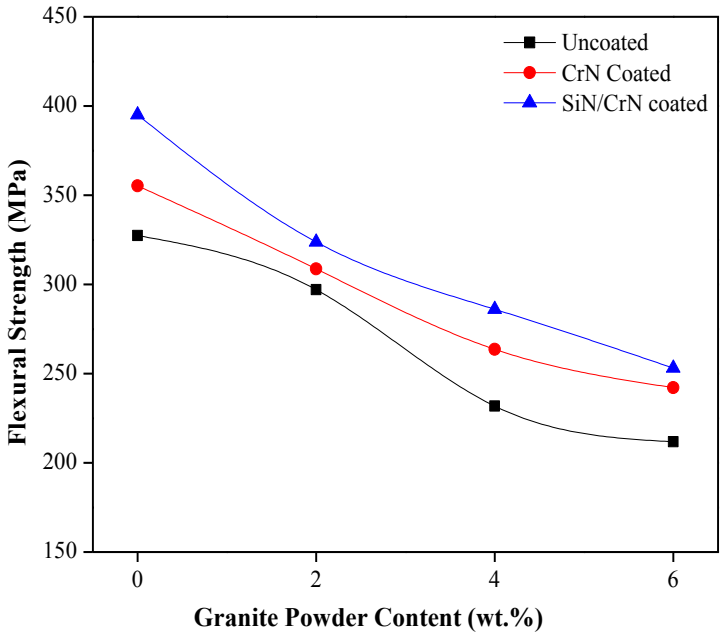

Figure 4.4 Effect of reinforcement and coating on flexural strength

However, as far as single layered coating and multilayered coating on the granite powder filled alloy composites also are shown same in trend like uncoated alloy materials but with higher flexural strength (Figure 4.4). The enhancement of flexural strength on single and multilayered coating on 0 wt.% granite powder reinforced aluminium alloyed composites are 8% and 17% respectively, 2 wt.% granite powder reinforced aluminium alloyed composites the enhancement rate is 4% and 8% respectively, 4 wt.% granite powder reinforced aluminium alloyed composites is 12% and 16% respectively and 6 wt.% granite powder reinforced aluminium alloyed composites the enhancement is up to 13% and 19% respectively [103]. The magnitude of flexural strength is maximum for multilayer coated samples and minimum for uncoated samples.

4.5. Impact strength of uncoated / single-layer coated / multi-layered coated granite particulate filled AA1050 alloyed composites

Impact strength is the amount of impact energy absorb during the impact test. Figure 4.5 shows the effect of impact strength on granite powder filled aluminum alloyed composites. It is observed that as the reinforcement increases the impact energy of the composites also increases. The percentage increased in the impact energy from 2 wt.% to 6 wt.% granite powder filled aluminum alloyed composites are ~ 3%, ~ 6% and ~ 2% respectively.

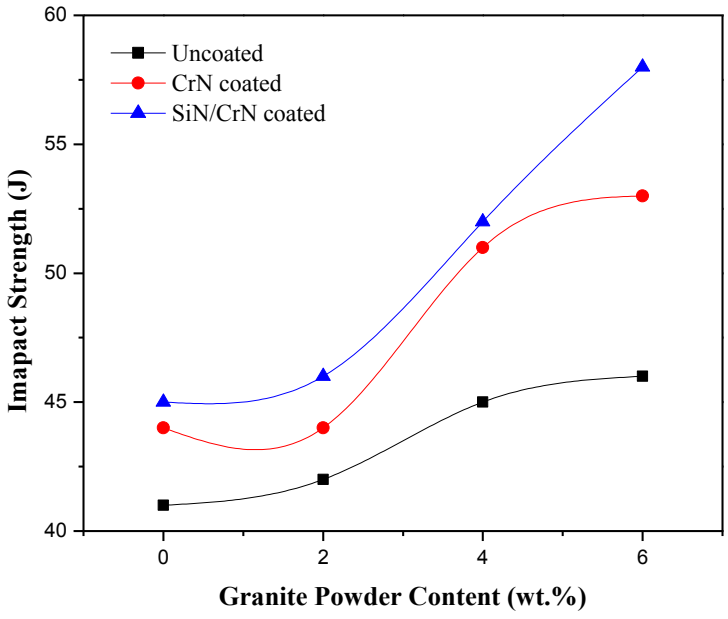

Figure 4.5 Effect of reinforcement and coating on impact strength

The increased in impact energy might be due to the fact that the particle size displayed positive effect on the impact energy of the composites as reported by Bindumadhavan et al. [286] and Patnaik et al. [287]. Similarly, when we move toward single layer and multilayer coating on the above sets of composites the impact energy increases with respective to uncoated granite filled aluminum alloy composites. The Impact energy increased for single layer and multilayer coated samples may be attributed the synergy effect of coating stiffness, coating material and reinforcement etc. The maximum magnitude of impact energy is higher for multilayer coating samples then uncoated granite powder reinforced samples.

PART-II: Analysis of Physical and Mechanical characteristics of uncoated / single-layer coated / multi-layered coated granite particulate filled AA 5083 alloyed composites

4.6. Physical characterization of the investigated composites

Density and void content of uncoated / single-layer coated / multi-layered surface coating on granite powder filled alloy composites are investigated at room temperature. The amount of void formation in the uncoated / single-layer coated / multi-layered surface coating on granite powder filled alloy composites is predict theoretically and experimentally. The presence of pre-existing void decline the mechanical and fracture properties of composites, to get better mechanical and fracture properties reduce the amount of void presence in the composites. The density of composites is measured by weighing polished cubes of the as-processed and extruded samples in air and when immersed in distilled water. The densities, derived from the recorded weights, are then compared to the theoretical rule of mixtures densities from which the volume content of porosity is calculated by Agarwal and Broutman [15] proposed formula.

The properties of particulate filled metal alloy is depended on the relative proportion of matrix and reinforcing materials, distribution of reinforcing particles and interface bonding between the particle and matrix. The voids significantly affected some of the mechanical properties and even the performance of composites due to the stress concentration at that point where the specimen easily breaks under the loading condition. The knowledge of void content is desirable for estimation of the quality of the composites. It is understandable that a good composite should have fewer voids. The theoretical and experimental density with void content of granite powder filled aluminium metal alloy composites.

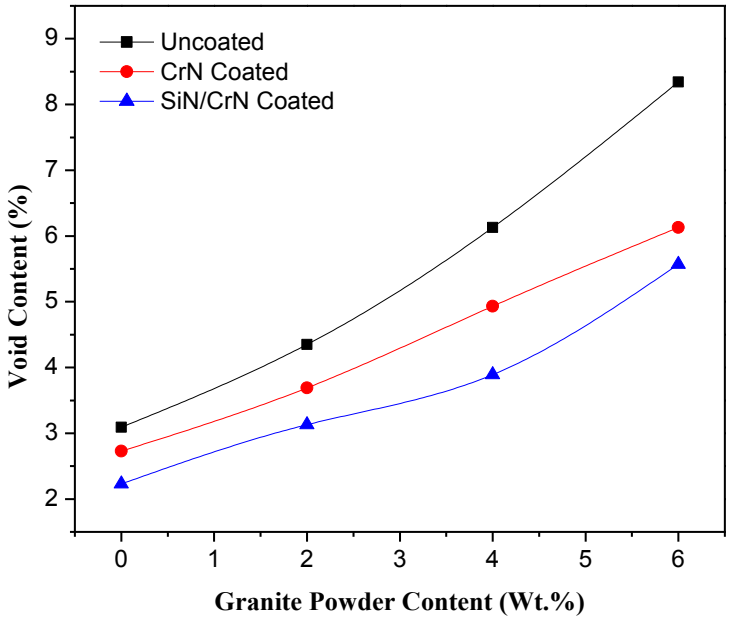

Figure 4.6 Effect of reinforcement and coating on void content

Table 4.2 Physical and Mechanical characteristics of uncoated / single-layer coated / multi-layered coated granite particulate filled AA5083 alloyed composites

Nomenclature	Composite designation	Void content (%)	Flexural strength (MPa)	Hardness (Hv)	Impact Strength (J)
B-1	5083G-0	3.09	375.13	68	57
B-2	5083G-2	4.35	355.19	78	61
B-3	5083G-4	6.13	335.33	91	66
B-4	5083G-6	8.34	315.93	107	69
B-5	S5083G-0	2.73	395.29	193	59
B-6	S5083G-2	3.69	376.36	213	62
B-7	S5083G-4	4.93	353.17	236	72
B-8	S5083G-6	6.13	339.9	259	75
B-9	M5083G-0	2.23	411.13	213	61
B-10	M5083G-2	3.13	401.36	237	64
B-11	M5083G-4	3.89	386.15	253	77
B-12	M5083G-6	5.57	369.19	279	80

It is observed from the Figure 4.6 that void content increases with the addition of granite powder in alloy matrix material. The possible reason might be attributed to fact that lower density may be attributed to insufficient bonding at interface of matrix and ceramic particulates that left voids, the agglomeration of particulates while solidifying may be created intra-particulate voids because of insufficient bonding with matrix material. The possible error may be the fabrication methodology resulted into voids contents [45]. Higher void content in composites are undesirable and represents inferior quality; as such composite materials affects various properties and performance while in service. Therefore, it can be said that a basic criterion with which to evaluate their quality is the density of composites.

4.7 Adhesion properties of single-layer coated / multi-layered coated granite particulate filled AA5083 alloyed composites

The scratch tests results of single and multilayer coating are shown in Figures 4.7 (a) and (b). This enables determination of adhesion properties between coating and substrate. The change in traction force is observed with stroke length represents the cohesive failure i.e. failure within the coating. The failure of coating may be due to the plastic deformation of coating. The slope between normal load and traction force represent the failure of coating and change in slope, which may be due to adhesive failure between coating and substrate interfaces.

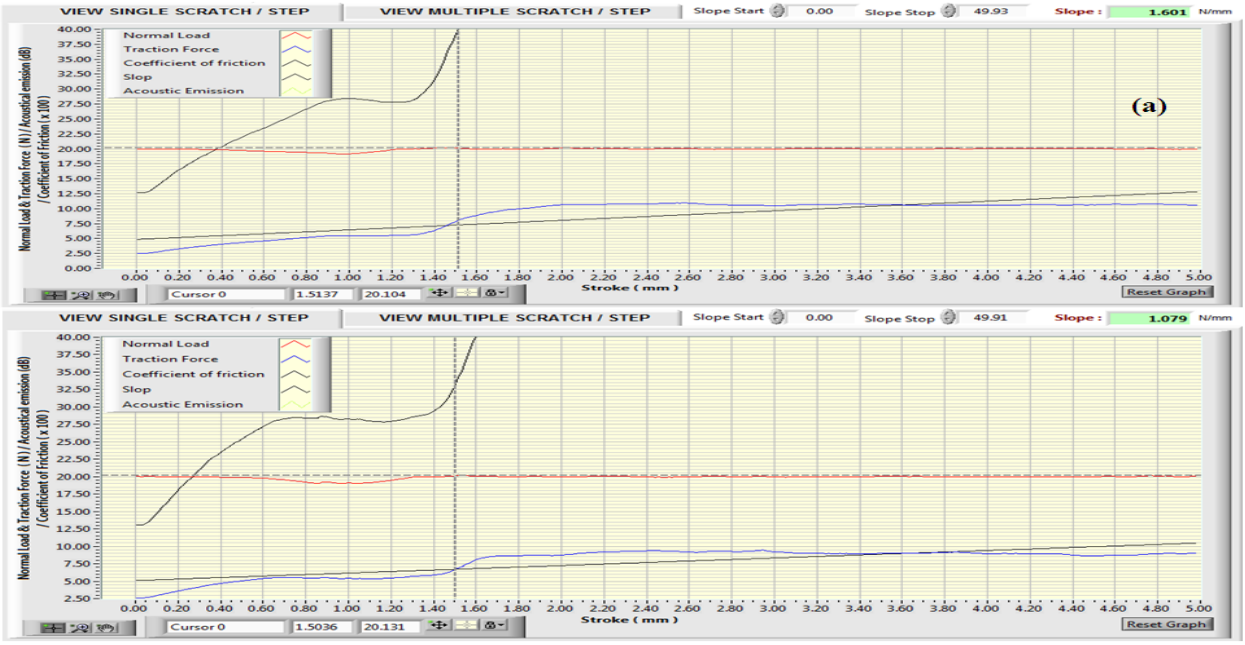

Figure 4.7 Scratch test results for (a) single and (b) multilayer coating

4.8. Hardness of uncoated / single-layer coated / multi-layered coated granite particulate filled AA5083 alloyed composites

Figure 4.8 shows the variation of hardness variation for uncoated and coated granite powder reinforced aluminum alloy composites. From the graph it is observed that hardness is increases with incorporation of granite powder into 5083 aluminum alloy. It further increases with deposition of single layer (chromium nitride) and multilayer (silicon nitride/chromium nitride) coating on granite particulate reinforced 5083 alloyed composites. The hardness of pure 5083 aluminum alloy is found 68 Hv and after addition of 2 wt.% granite powder it increases linearly ~ 12 % on further addition of 2 wt.% granite powder it increases ~ 14 % on further addition of 2 wt.% granite powder it increases ~ 15 % and found 107 Hv. The reason behind the increment in hardness after addition of granite powder into base matrix may be granite powder is mixture of different hard oxides. These hard oxides are dispersed in to base matrix homogeneously and impart strength to base matrix. Similar, results are reported Park et al. [103] and Hunt et al. [288] for particulate reinforced metal matrix composites.

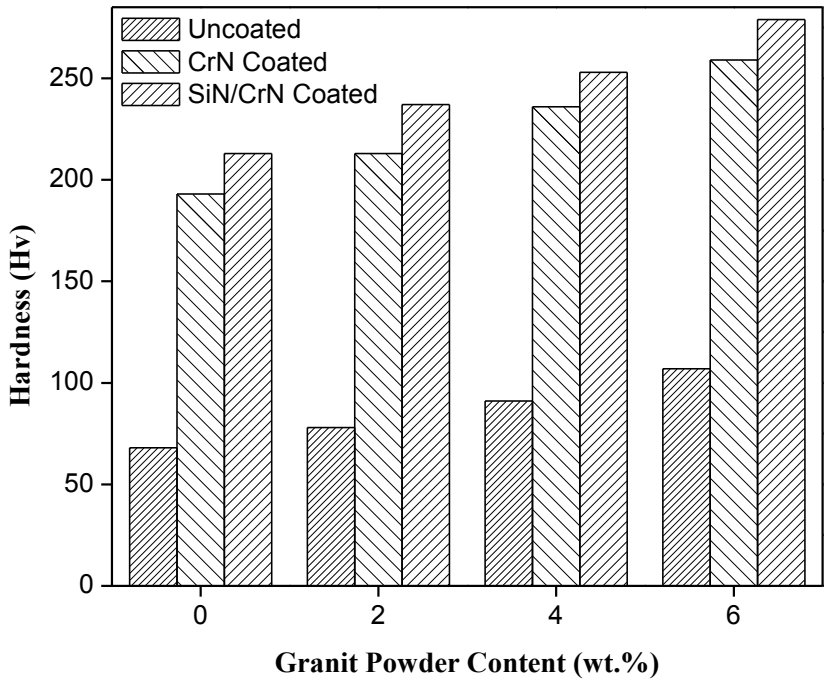

Figure 4.8 Effect of reinforcement and coating on hardness

After deposition of single layer (chromium nitride) coating and multilayer (silicon nitride/chromium nitride) coating hardness is significantly improved. The deposition of CrN coating on pure 5083 aluminum alloy it increases ~147% and after deposition of SiN/CrN coating it increases ~ 213 %. Similarly, after deposition of single layer (chromium nitride) and multilayer (silicon nitride/chromium nitride) coating on 2 wt.% granite powder reinforced aluminum alloy composites the hardness increases by ~ 173 % and 204 % respectively, same as in case of 4 wt.% granite powder reinforced aluminum alloy composites the hardness increases by ~159 % and 174 % respectively and same again in case of 6 wt.% granite powder reinforced aluminum alloy composites the hardness increases by ~ 142 % and 151 % respectively (Figure 4.8). The improvement in hardness of single layer coating due to the promising hardness of chromium nitride coating on the other hand in multilayer coating CrN/SiN stack is attributed to many interfaces that blocked the micro-crack movements across interfaces due to differences in the shear module of the individual layer material [281,282]. From the graph it is also observed that hardness magnitude for multilayered coating samples shows higher than single layer coating samples. The increase of the hardness can be attributed to the formation of CrN/SiN hard phases, which are homogeneously dispersed in the matrix.

4.9. Flexural strength of uncoated / single-layer coated / multi-layered coated granite particulate filled AA5083 alloyed composites

Flexural strength of the uncoated and coated granite powder filled 5083 aluminium alloy composites shown in Figure 4.9. From Figure 4.9 it is clearly observed that incorporation of granite powder into base matrix lead to decrement in flexural strength with deposition of coating on above set of composites the decrement rate is less. The amount in decrement in flexural strength after incorporation of granite powder is observed 19%. From this analysis it is observed that for uncoated particulate filled composites the flexural strength decreasing rate for 2 wt.% granite powder filled alloy composites is 5% but on further addition of granite powder the decreasing rate is slightly reduced to approximately 6% for 4 wt.% granite powder filled composite and on further addition of 6 wt.% granite powder in the base matrix material the strength reduced to 6%. Therefore, the decreasing rate of flexural strength is linearly for the uncoated composites. The possible reason for decrease of flexural strength with the increased in filler content in the alloy composites may be lead to poor strength between matrix and filler material, hence decreased the effectiveness of stress transfer between them [283-285].

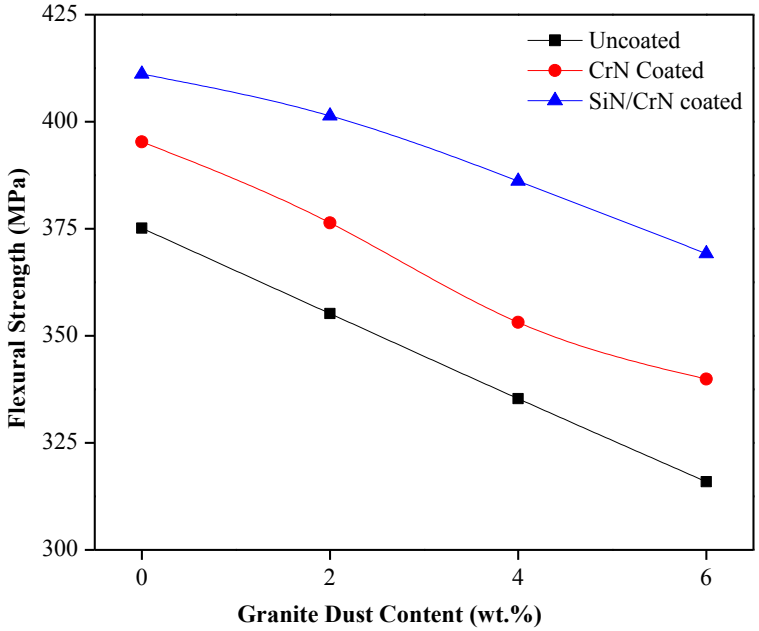

Figure 4.9 Effect of reinforcement and coating on flexural strength

However, as far as single layered coating and multilayered coating on the granite powder filled alloy composites also are shown same in trend like uncoated alloy materials but with higher flexural strength (Figure 4.9). The enhancement of flexural strength on single and multilayered coating on 0 wt.% granite powder reinforced aluminium alloy composites are 5% and 9% respectively, 2 wt.% granite powder reinforced aluminium alloy composites the enhancement rate is 6% and 12% respectively, 4 wt.% granite powder reinforced aluminium alloy composites is 5% and 13% respectively and 6 wt.% granite powder reinforced aluminium alloy composites the enhancement is up to 7% and 14% respectively [103]. The magnitude of flexural strength is maximum for multilayer coated samples and minimum for uncoated samples.

4.10. Impact strength of uncoated / single-layer coated / multi-layered coated granite particulate filled AA5083 alloyed composites

Impact strength variation with reinforcement and coating for 5083 aluminium alloy is present in Figure 4.10. From the graph it is observed that addition of granite particles improve the absorption of impact energy for aluminium alloy composites and it further improved by deposition of single and multilayer coating. The amount of energy absorption is improves from 57 joule to 69 joule by incorporation of granite powder into base matrix. The percentage

increases in impact energy from 2 wt.% to 6 wt.% granite powder filled aluminium alloy composites are ~ 6%, ~ 8% and ~ 4% respectively (Figure 4.10). The increase in impact strength is due to the presence of hard particle which impart strength to soft matrix and also with increase in quartz content reduces the inter particle between these hard particles causing increase in the dislocation pile up and there is a restriction to the plastic flow. This may attribute to embitterment effect; the granite powder in unfilled 5083 alloy ceases dislocation movement in the matrix, thereby decreases the number of local stress concentration sites. These results are in accordance with those obtained by Seah et al. [289], Sharma et al. [67] and Kataih et al. [64] reported similar findings for particulate filled metal matrix composites. When we observed the impact strength of single layer and multilayer coating on the above sets of composites the impact energy increased. After deposition of single layer coating impact energy improved 20% for above sets of composites but it further improved by deposition of multilayer coating and improvement in impact energy is 23% for above sets of composites. The Impact energy increased for single layer and multilayer coated samples may be attributed the synergy effect of coating stiffness, coating material and reinforcement etc. The maximum magnitude of impact energy is found for multilayer coating samples and minimum for uncoated granite powder reinforced samples.

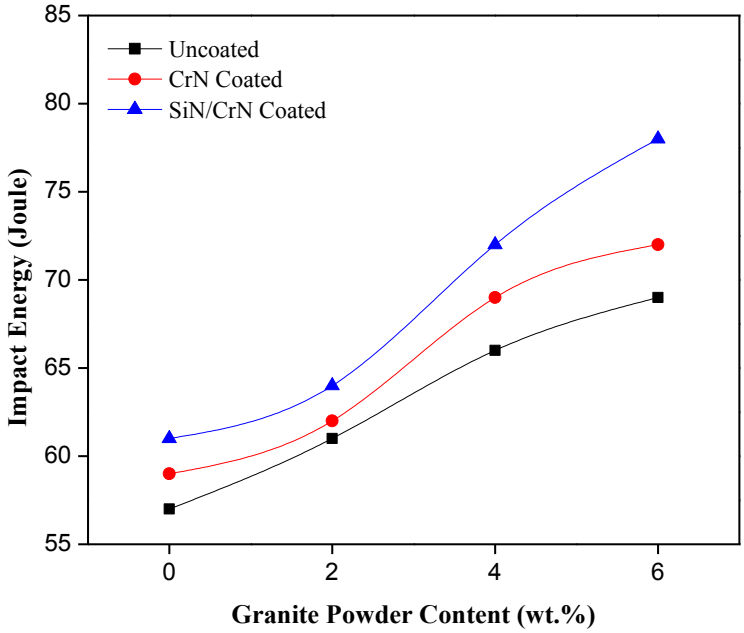

Figure 4.10 Effect of reinforcement and coating on impact strength

Chapter Summary

The results discussed above clearly indicates that reinforcement of granite particulate in AA1050 and AA5083 alloy significantly improves flexural, micro-hardness and impact strength of the resultant alloyed composites. The same properties further observed to be multitude with single /multi layered coating of CrN, SiN materials.

The next chapter presents the Stress intensity factor and Dynamic-mechanical analysis of single/multi layer coated and uncoated granite particulates filled aluminium alloy composites.

****

Chapter 5

ANALYSIS OF FRACTURE AND THERMO-MECHANICAL CHARACTERISATION OF FABRICATIED GRANITE PARTICULATE FILLED ALLOYED COMPOSITES (COATED/UNCOATED)

This chapter presents the thermo-mechanical and fracture analysis of multilayer and single layer surface coating on granite powder filled composites. The relative effects of multilayer, single layer coating and addition of filler content on thermo-mechanical and fracture properties of the composites have also been discussed.

PART-I: Analysis of Stress intensity factor and Thermo-Mechanical properties of uncoated / single-layer coated / multi-layered coated granite particulate filled AA1050 alloyed composites

5.1. Stress intensity factor of uncoated / single-layer coated / multi-layered coated granite particulate filled AA1050 alloyed composites

Fracture is the separation of material into two or more pieces under the action of load in the presence of pre-existing crack. As material is brittle than fracture occurs before plastic deformation, if there has been extensive plastic deformation preceding fracture, the material is considered ductile. Fracture occurs as soon as critical stress has been reached up to plastic deformation. The magnitude of stress intensity factor (K) of Multilayer surface coating of marble dust and alumina filled alloy composites is evaluated experimentally. Figures 5.1 to 5.3 show the graph for stress intensity for uncoated, single layer and multilayer coating on granite powder filled aluminium alloy composites. From the Figure 5.1 it is reveal that the magnitude of stress intensity factor is higher as compared to unreinforced aluminium alloy composites. This may be attributed to the enhancement of interfacial bonding between matrix-particulate. It is reported in literature [41] that the magnitude of stress intensity factors are governed by difference in the mechanical properties between contacting materials, crack length, interface curvatures and loading conditions. Figure 5.1 shows stress intensity factor of particulate filled aluminium alloyed composites in four different crack lengths. From this study it is observed that with the increased in crack length the stress intensity also increases and for 0 wt.% granite filled aluminium alloy is shown minimum stress intensity factor whereas 6 wt.% granite filled alloy composite have maximum stress intensity factor. The crack growth is not only depends on the matrix material, but also affected other factors such

as reinforcing material, their size and shape, percentage reinforcement and properties respectively. Hence, it is very difficult to conclude a specific cause specifically particulate filled alloy composites [290-292]. Figure 5.1 observed that at point 1 (i.e. at crack length 1) the SIF is increases with the increases in filler content from 0 to 2 wt.% is ~ 15%, from 2 to 4 wt.% the SIF is 5%, and further increased in filler content from 4 to 6 wt.% the SIF is 5% respectively. Similar, observations are also reported for other three different crack length with the varying in filler percentages in the alloy composites (Figure 5.1). The maximum stress intensity magnitude is found for 6 wt.% granite powder reinforced aluminium alloy composites for all crack length [287].

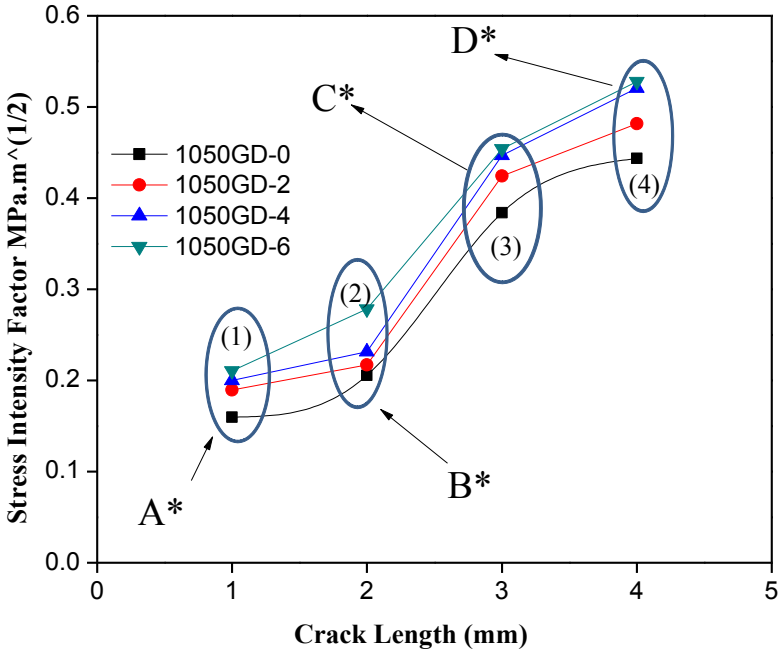

A* = SIF 0 to 2 wt.% (15%) > SIF 2 to 4 wt.% (5%) > SIF 4 to 6 wt.% (5%)

B* = SIF 0 to 2 wt.% (5%) > SIF 2 to 4 wt.% (6%) > SIF 4 to 6 wt.% (16%)

C* = SIF 0 to 2 wt.% (9%) > SIF 2 to 4 wt.% (5%) > SIF 4 to 6 wt.% (2%)

D* = SIF 0 to 2 wt.% (8%) > SIF 2 to 4 wt.% (7%) > SIF 4 to 6 wt.% (2%)

Figure 5.1 Effect of reinforcement on stress intensity factor

The effect of single and multilayer coated granite powder reinforced aluminium alloy composites on stress intensity factor are shown in Figures 5.2 and 5.3 respectively. The stress intensity factor for 1 mm crack length of single layer chromium nitride coating is increased by ~16%, 5%, 6% on the reinforcement of granite powder from 0 wt.%, 2 wt. %, 4wt.% and 6 wt.% in aluminium alloyed composites respectively. The stress intensity factor for 2 mm

crack length of single layer chromium nitride coating is increases by ~ 6%, 6%, 16% on the reinforcement of granite powder from 0 wt.%, 2 wt.-%, 4 wt.-% and 6 wt.% in aluminium alloyed composites respectively (Figure 5.2). The stress intensity factor for 3 mm crack length for single layer chromium nitride coating enhanced by ~ 10%, 5%, 2% on the reinforcement of granite powder from 0 wt.%, 2 wt.%, 4 wt.% and 6 wt.% in aluminium alloyed composites respectively. The stress intensity factor for 4 mm crack length single layer chromium nitride coating enhanced by ~ 8%, 7%, 2% on the reinforcement of granite powder from 0 wt.%, 2 wt.%, 4wt.% and 6 wt.% in aluminium alloyed composites respectively. Similar observation is observed by Lee et al. [293] and Chan et al [294].

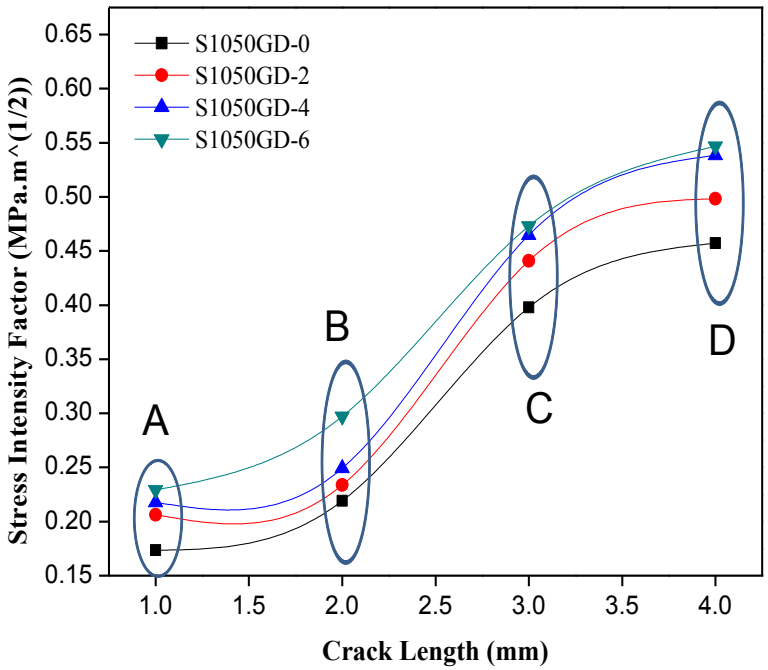

Figure 5.2 Effect of reinforcement and coating on stress intensity factor (CrN coating)

The stress intensity factor increased for multilayer coated aluminium alloyed composites reinforced with 0 wt.%, 2 wt.%, 4wt.% and 6 wt.% granite powder by ~ 16%, 5%, 4% for crack length 1 mm respectively (Figure 5.3). The stress intensity factor increased for multilayer coated aluminium alloyed composites reinforced with 0 wt.%, 2 wt.%, 4 wt.% and 6 wt.% granite powder by ~ 7%, 6%, 15% for crack length 2 mm respectively. The stress intensity factor increased for multilayer coated aluminium alloy composites reinforced with 0 wt.%, 2 wt.%, 4wt.% and 6 wt.% granite powder by ~ 10%, 4%, 3% for crack length 3 mm respectively. The stress intensity factor increased for multilayer coated aluminium alloyed

composites reinforced with 0 wt.%, 2 wt.%, 4wt.% and 6 wt.% granite powder by ~ 8%, 4%, 5% for crack length 4 mm respectively. Both graph shows enhancement in magnitude of stress intensity with respect to crack length. This may be attributed to the enhancement of interfacial bonding between coating and granite powder reinforced aluminium alloy composites. The enhancement in stress intensity factor is due to synergy effect of coating and reinforcement (Figure 5.3). Also it is known that single and multilayer coating is hard and its stiffness Lee et al. [293] and Chan et al [294].

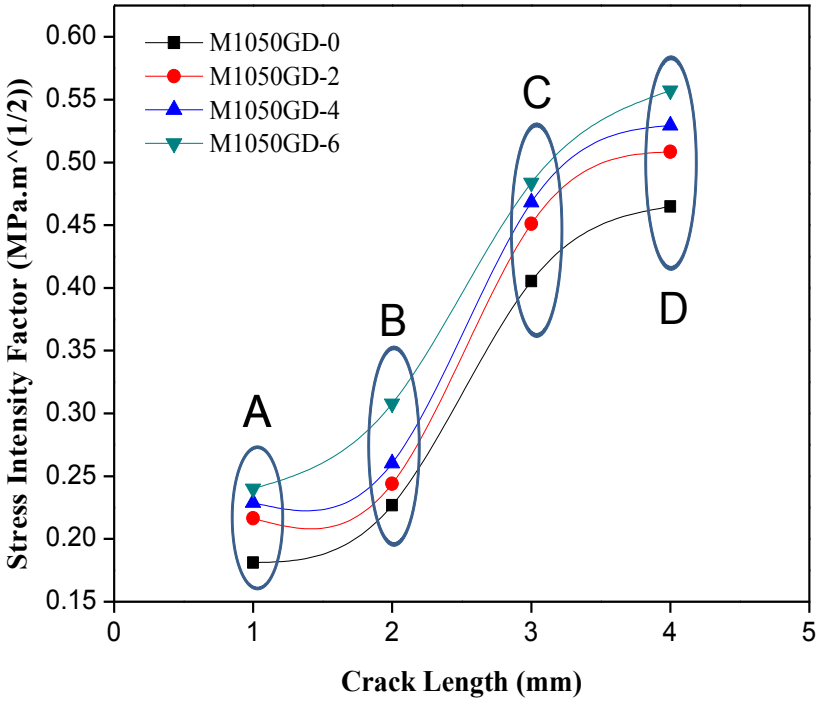

Figure 5.3 Effect of reinforcement and coating on stress intensity factor (SiN/CrN coating)

5.2. Thermo-mechanical analysis of uncoated / single-layer coated / multi-layered coated granite particulate filled AA1050 alloyed composites

The aspects of dynamic mechanical properties viz. storage-modulus (E'), loss-modulus (E") and loss-tangent factor (Tan δ) of the investigated granite powder reinforced aluminum metal matrix composites are carried out as a function of temperature in order to evaluate thermo-mechanical response of the composites. Dynamic mechanical properties of granite powder reinforced and unreinforced aluminum alloy are evaluated using three point bending test with the increasing in temperature in the range of 29-250ºC. Figure 5.4(a-c) shows the variation of storage modulus (E') for uncoated, chromium nitride coating, silicon nitride/chromium nitride

coating on granite powder reinforced aluminum alloy composites. From Figure 5.4a, it is observed that storage modulus (E') representing the stiffness of the visco-elastic material and has been observed to undergo consistent decay with the increasing in temperature from 29-250ºC. From Figure 5.4a, it is revealed that storage modulus decay with increment in temperature. The magnitude of storage modulus is higher as compare to unreinforced aluminium alloy. Maximum decay in storage modulus is observed for 6 wt.% granite powder reinforced composites and minimum decay in storage modulus is observed for unreinforced aluminium alloyed composites. The incorporation of granite powder particle enhanced stiffness of composites. The increased in E' in such cases may be attributed to thermally induced phase transformations leading to hardening of the composites. Similar, observations are also reported by Patnaik.et al. [287] and Zang et al. [299] for particulate filled metal alloyed composites.

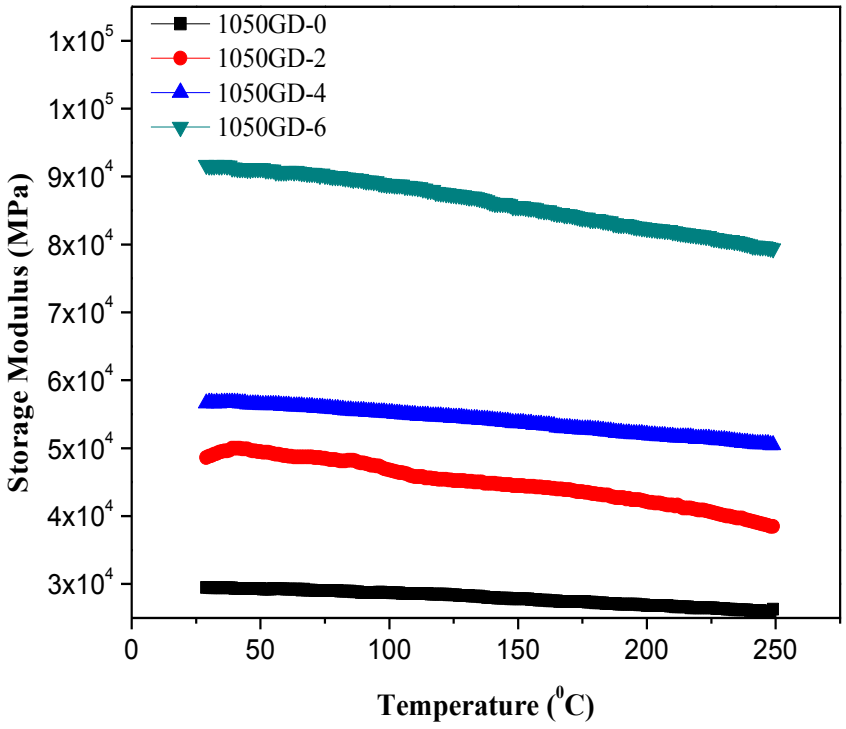

Figure 5.4a Variation of storage modulus with temperature for granite powder reinforced aluminium alloyed composites

The variation of storage modulus with temperature for chromium nitride coating on granite powder reinforced aluminium alloyed composites is shown in Figure 5.4b. Storage modulus is decreased with the increase in temperature range from 29-250ºC. The degradation

of storage modulus depended on temperature and its slope of degradation is less as compared to uncoated granite powder reinforced aluminium alloyed composites. This may be due to high stiffness of chromium nitride coating and as well as high melting point of the coating materials.

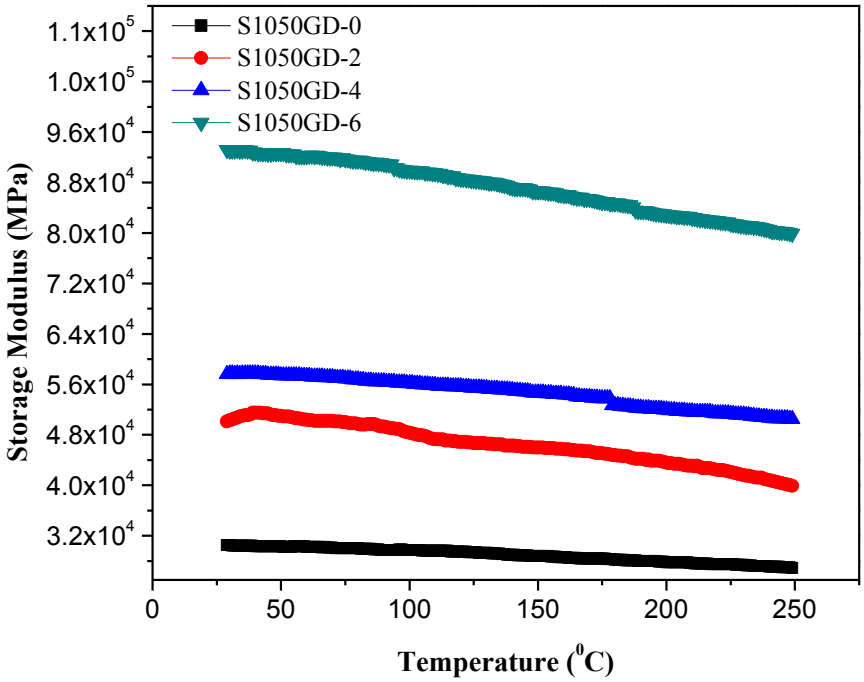

Figure 5.4b Variation of storage modulus with temperature for chromium nitride coating on granite powder reinforced aluminium alloyed composites

Figure 5.4c shows the effect of temperature on storage modulus for multilayered (silicon nitride/chromium nitride) coating on granite powder reinforced aluminium alloyed composites. The degradation in stiffness of silicon nitride/chromium nitride coating on granite powder reinforced aluminium alloyed composites is enhance for temperature range of 29-250ºC. The degradation slope of stiffness of silicon nitride/chromium nitride coating on granite powder reinforced aluminium alloyed composites is less. This may be due to the fact that the stiffness of multilayer coating is high due to proper adhesion between both coating materials and along with the high melting point of the coating materials. Similar, observation is observed by Gupta et al. [300] for multilayer coating on steel substrate samples. The minimum storage modulus magnitude is observed for uncoated and maximum for multilayer coated granite powder reinforced aluminium alloyed composites.

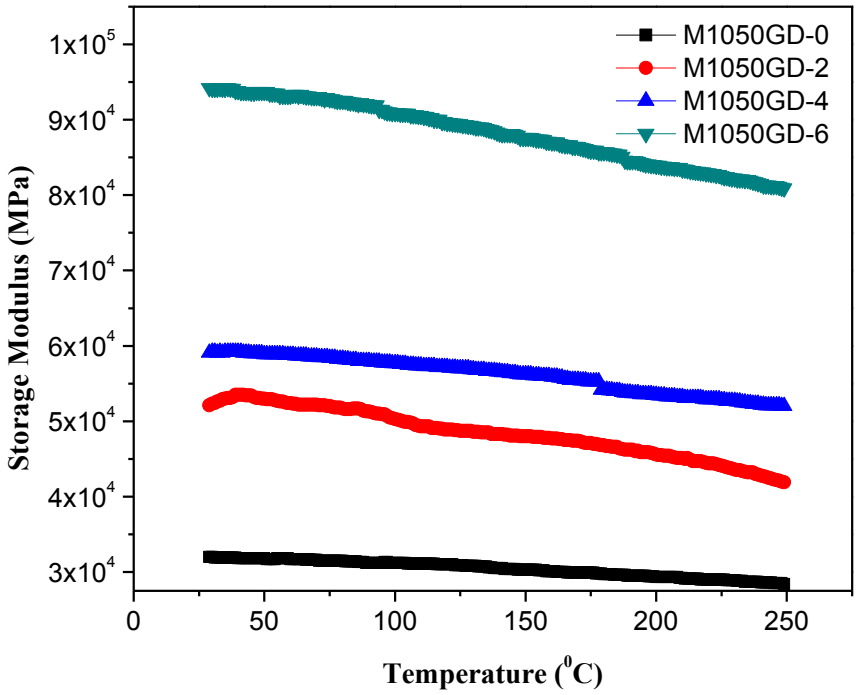

Figure 5.4c Variation of storage modulus with temperature for silicon nitride/chromium nitride coating on granite powder reinforced aluminium alloyed composites

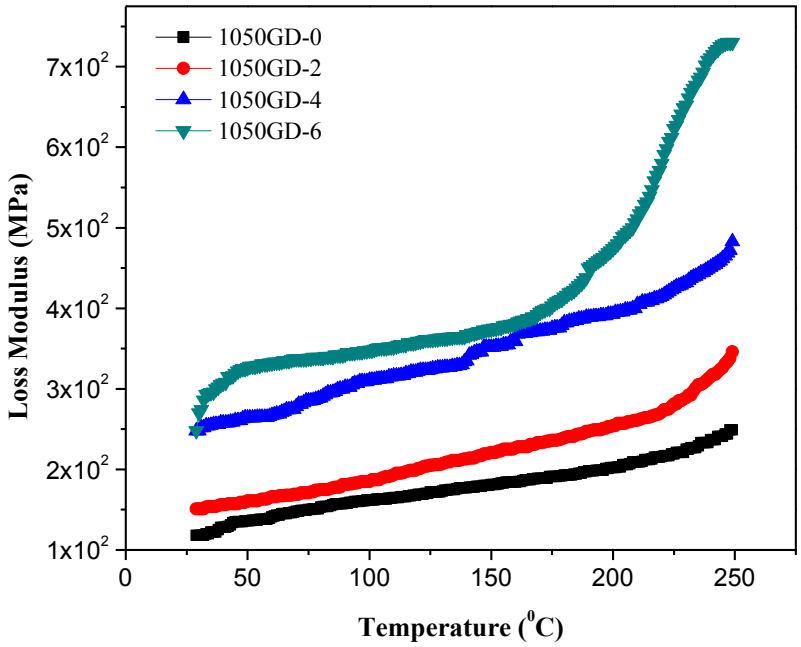

Figure 5.5a Variation of loss modulus with temperature for granite powder reinforced aluminium alloyed composites

The loss modulus for uncoated, single layer and multilayer coating on granite powder reinforced aluminium alloyed composites is shown in Figure 5.5(a-c). From Figure 5.5a it is reveals that with the increased in temperature, loss modulus magnitude is enhance in the order of 6 wt.% granite powder > 4 wt.% granite powder > 2 wt.% granite powder > 0 wt.% granite powder respectively and which had contributed to the reinforcement effects imparted by the particulates allowing enhanced stress transfer ability across the interface.

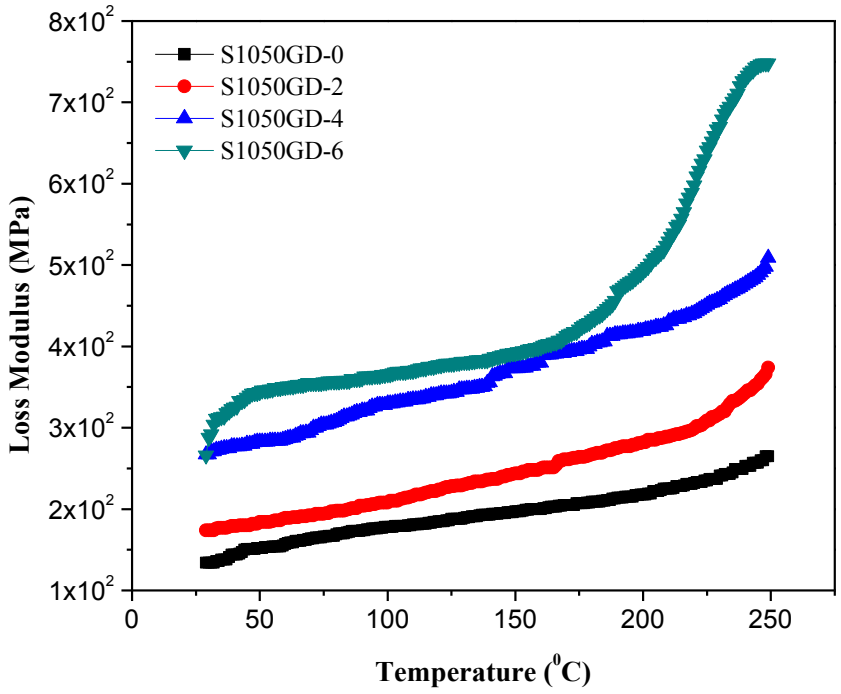

Figure 5.5b Variation of loss modulus with temperature for chromium nitride coating on granite powder reinforced aluminium alloyed composites

Figure 5.5b shows the effect of temperature on loss modulus for single layer coating on granite powder reinforced aluminium alloyed composites. The loss modulus magnitude is increases with increment in temperature range. Stress is properly transferred from coating material to base material due to proper adhesion between the coating and base materials. Figure 5.5c shows variation in loss modulus with-respective-to temperature for multilayer coating on granite powder reinforced aluminium alloyed composites. It is observed that from Figure 5.5c the loss modulus decreased as coating thickness is increase. The results reveal the substrate effect has significant influence on the dynamic properties of thin films. The loss modulus magnitude is decreases in order uncoated > single layer coated > multilayer coated granite powder reinforced aluminium alloyed composites.

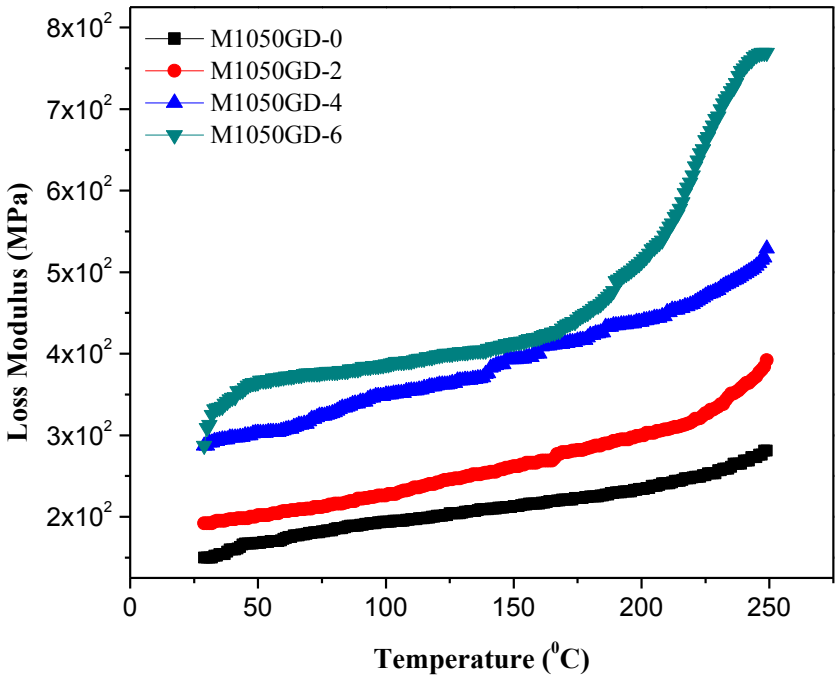

Figure 5.5c Variation of loss modulus with temperature for silicon nitride/chromium nitride coating on granite powder reinforced aluminium alloyed composites

The damping factor (Tan δ) indicates the recoverable energy in terms of mechanical damping or internal friction in terms of visco-elastic system. The variation of Tan δ of the composites as a function of temperature is shown in Figure 5.6(a-c) for uncoated / single-layer coated / multi-layered coated granite particulate filled AA1050 alloyed composites. It is observed that Tan δ enhance with temperature as stiffness decreased leading to higher damping of granite powder reinforced composites. The difference in the stiffness of the particle and matrix material is expected to help in providing high damping at high temperature by causing deformation along the particle-matrix interface (Figure 5.6a). The damping factor for single and multilayer coating is observed higher as compared to uncoated granite powder reinforced aluminium alloyed composites (Figures 5.6b-c). The Improvement in damping factors is due to the difference in stiffness of substrate and coating materials. Similar, results is reported by Cox et al. [301] and Licitra et al. [302] for damping behaviour of metal matrix composites and Gupta et al. [300] for multilayer coated steel substrate.

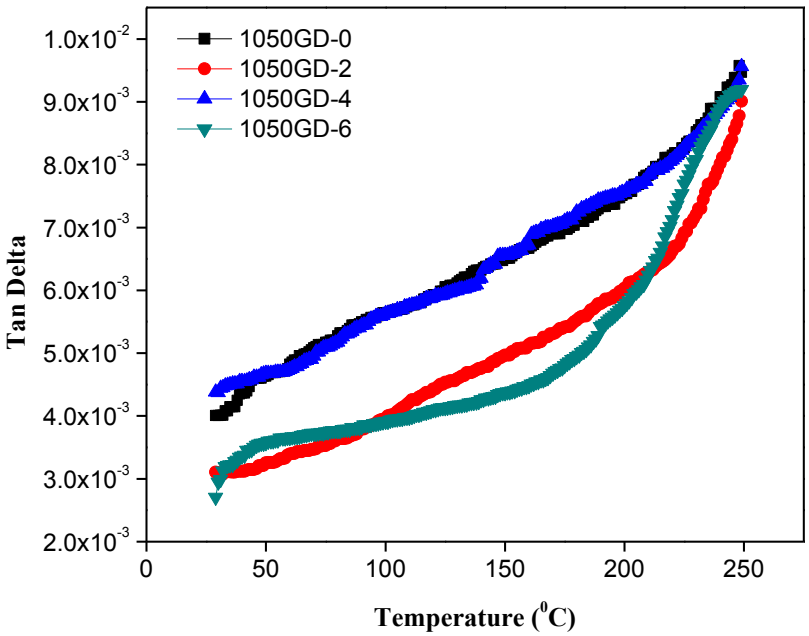

Figure 5.6a Variation of Tan Delta with temperature for granite powder reinforced aluminium alloyed composites

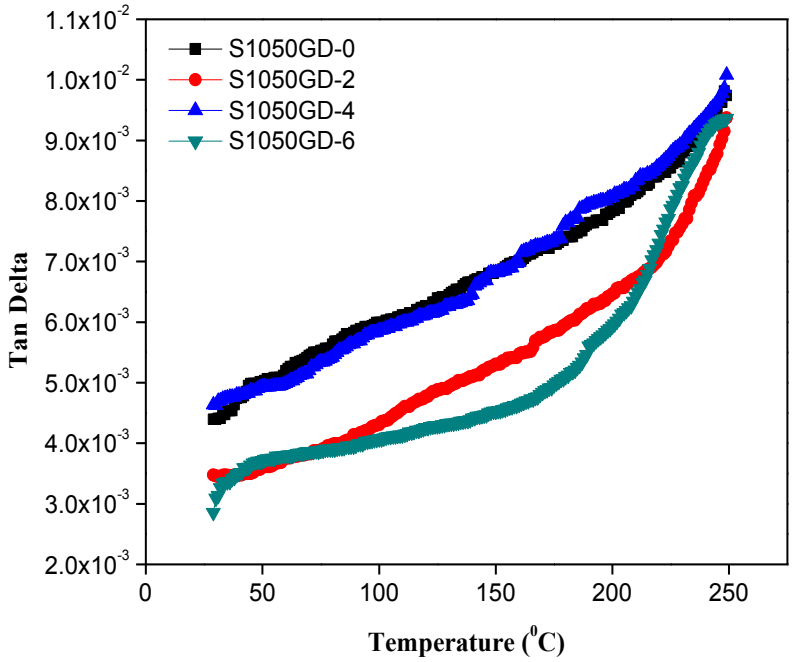

Figure 5.6b Variation of Tan Delta with temperature for chromium nitride coating on granite powder reinforced aluminium alloyed composites

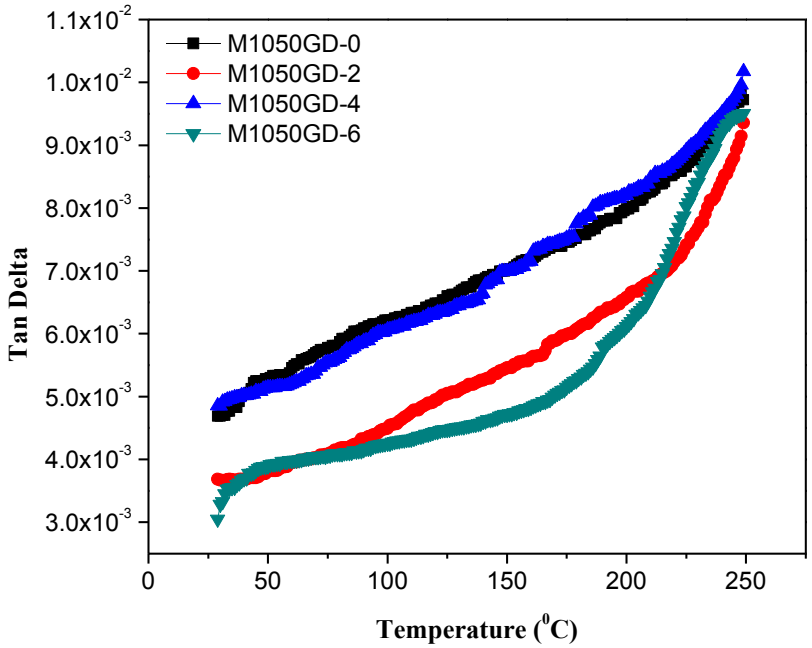

Figure 5.6c Variation of Tan Delta with temperature for silicon nitride/chromium nitride coating on granite powder reinforced aluminium alloyed composites

PART-II: Analysis of Stress intensity factor and Thermo-Mechanical properties of uncoated / single-layer coated / multi-layered coated granite particulate filled AA5083 alloyed composites

5.3 Stress intensity factor of uncoated / single-layer coated / multi-layered coated granite particulate filled AA5083 alloyed composites

The values of mode I stress intensity factors (SIF) is calculated for uncoated, single layer and multilayer coating on granite powder filled aluminium alloy composites shown in Figure 5.7 to Figure 5.9. In literature it is reported that the magnitude of stress intensity factor depends on the mechanical properties of the matrix and reinforcement, crack length, and loading conditions. The interface between the matrix and the reinforcement plays an important role in determining stress intensity factor at different crack length [42]. Figure 5.7 shows stress intensity factor of particulate filled aluminium alloy composites in four different crack lengths. From this study it is observed that with the increase in crack length the stress intensity also increases and for 0 wt.% granite filled aluminium alloy shows minimum stress intensity factor whereas 6 wt.% granite filled alloy composite have maximum stress intensity factor.

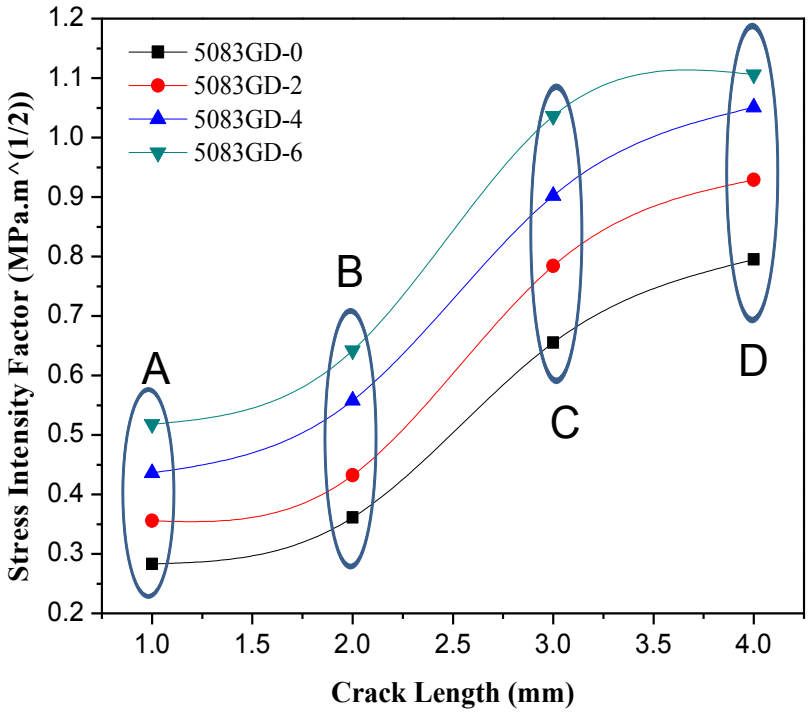

Figure 5.7 Effect of reinforcement on stress intensity factor

The crack growth behaviour is not only depends on the matrix material, but also affected other factors such as reinforcing material, their size and shape, percentage reinforcement and properties respectively. Hence, it is very difficult to conclude a specific cause specifically particulate filled alloy composites [290-292]. From Figure 5.7 it is observed that at point 1 (i.e at crack length 1mm) the SIF is increased with the increased in filler content from 0 to 2 wt.% is ~ 20%, from 2 to 4 wt.% the SIF is 18%, and further increased in filler content from 4 to 6 wt.% the SIF is 16% respectively. When we observed point 2 (i.e at 6 wt.%) the SIF is increased with the increase in crack length from 1 to 2 mm is 19%, from 2 to 3 mm the SIF is 38%, and further increased in crack length from 4 to 6 mm the SIF is 6% respectively. This may attribute to enhancement of interfacial bonding between matrix-particulate. It is reported in literatures that the magnitude of stress intensity factors are governed by difference in the mechanical properties between contacting materials, crack length, interface curvatures and loading conditions by Singh and Prasad [295], Somekawa et al. [296], Hemanth [297]. Similar observations are reported for other three different crack length with the varying in filler percentages in the alloy composites (Figure 5.7). The maximum stress intensity magnitude is observed for 6 wt. % granite powder reinforced aluminium alloy composites for all crack length [287,110]. The SIF values obtained for

different compositions are in the agreement with the values given by the Agrawal and Sun [110].

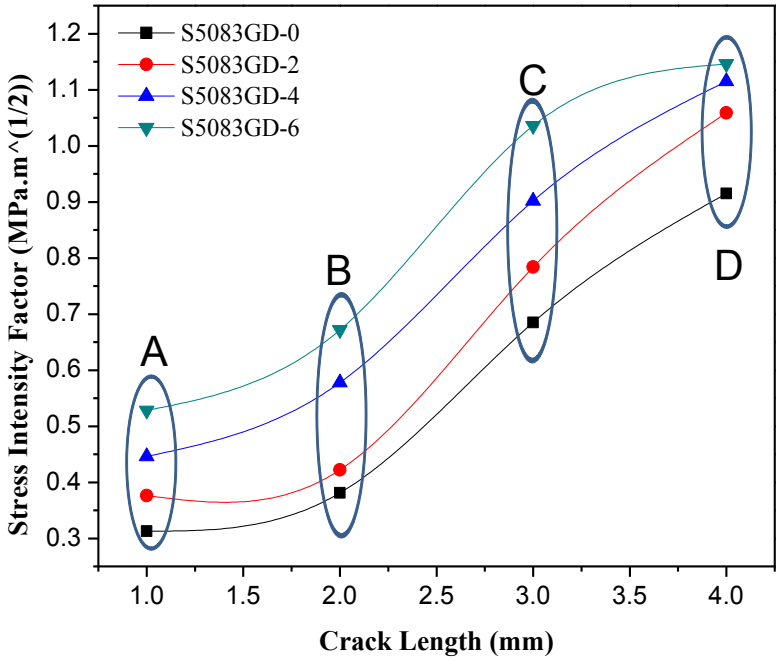

Figure 5.8 Effect of reinforcement and coating on stress intensity factor (CrN coating)

Stress intensity factor graph of single and multilayer coated granite powder reinforced aluminium alloyed composites is shown in Figure 5.8 and Figure 5.9 respectively. The stress intensity factor for 1 mm crack length of single layer chromium nitride coating is increased by ~17%, 16%, 15% on the reinforcement of granite powder from 0 wt.%, 2 wt.-%, 4wt.-% and 6 wt.% in aluminium alloyed composites respectively (Figure 5.8). The stress intensity factor for 2 mm crack length of single layer chromium nitride coating is increased by ~ 10%, 27%, 14% on the reinforcement of granite powder from 0 wt.%, 2 wt.-%, 4wt.-% and 6 wt.% in aluminium alloyed composites respectively. The stress intensity factor for 3 mm crack length for single layer chromium nitride coating enhanced by ~ 13%, 13%, 13% on the reinforcement of granite powder from 0 wt.%, 2 wt.-%, 4wt.-% and 6 wt.% in aluminium alloyed composites respectively. The stress intensity factor for 4 mm crack length single layer chromium nitride coating enhanced by ~ 13%, 5%, 3% on the reinforcement of granite powder from 0 wt.%, 2 wt.-%, 4wt.-% and 6 wt.% in aluminium alloyed composites respectively (Figure 5.8). Similar observation is observed by Lee et al. [293] and Chan et al [294].

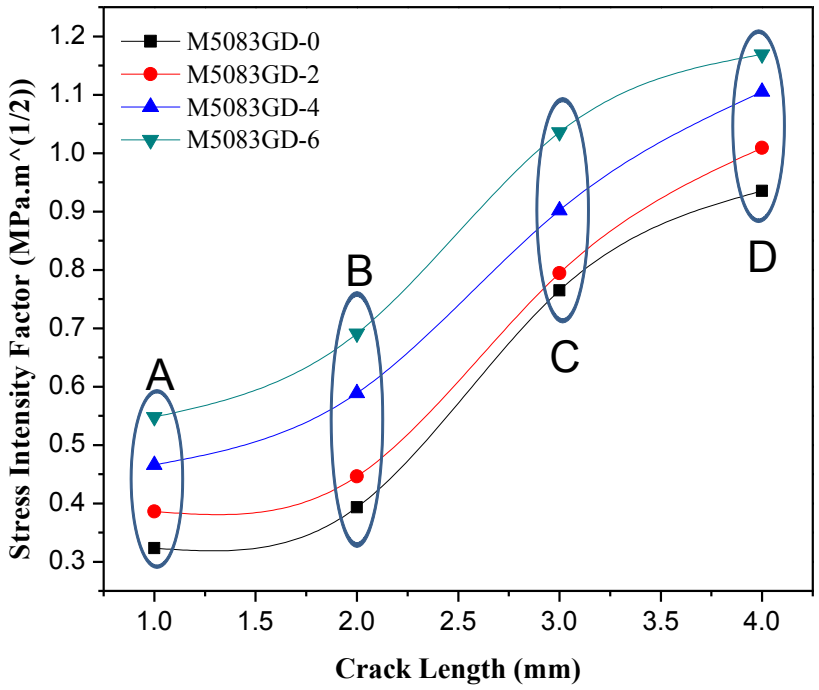

Figure 5.9 Effect of reinforcement and coating on stress intensity factor (SiN/CrN coating)

The stress intensity factor increases for multilayer coated aluminium alloyed composites reinforced with 0 wt.%, 2 wt.%, 4wt.% and 6 wt.% granite powder by ~ 16%, 17%, 15% for crack length 1 mm respectively (Figure 5.9). The stress intensity factor increased for multilayer coated aluminium alloyed composites reinforced with 0 wt.%, 2 wt.%, 4 wt.% and 6 wt.% granite powder by ~ 12%, 24%, 15% for crack length 2 mm respectively. The stress intensity factor increased for multilayer coated aluminium alloyed composites reinforced with 0 wt.%, 2 wt.%, 4 wt.% and 6 wt.% granite powder by ~ 4%, 12%, 13% for crack length 3 mm respectively (Figure 5.9). The stress intensity factor increased for multilayer coated aluminium alloyed composites reinforced with 0 wt.%, 2 wt.%, 4 wt.% and 6 wt.% granite powder by ~ 7%, 8%, 5% for crack length 4 mm respectively. Both graph shows enhancement in magnitude of stress intensity with respect to crack length. This may be attributed to the enhancement of interfacial bonding between coating and granite powder reinforced aluminium alloyed composites. The enhancement in stress intensity factor is due to synergy effect of coating and reinforcement. Also it is known that single and multilayer coating is hard and its stiffness Lee et al. [293] and Chan et al [294].

5.4 Thermo-mechanical analysis of uncoated / single-layer coated / multi-layered coated granite particulate filled AA5083 alloyed composites

Dynamic Mechanical Analysis (DMA) of the composites have been carried out to characterize storage modulus (E'), loss modulus(E") and damping factor (tan δ) as a function of temperature in order to evaluate thermo-mechanical response of different particulate filled ZA alloy composites. The variation of E', E" and tan δ are shown in Figure 5.10(a-c). Storage modulus (E') representing the stiffness of the visco-elastic material and has been observed to undergo consistent decay with increasing temperature in the range of 29-250ºC irrespective of the compositions (Figure 5.10a).

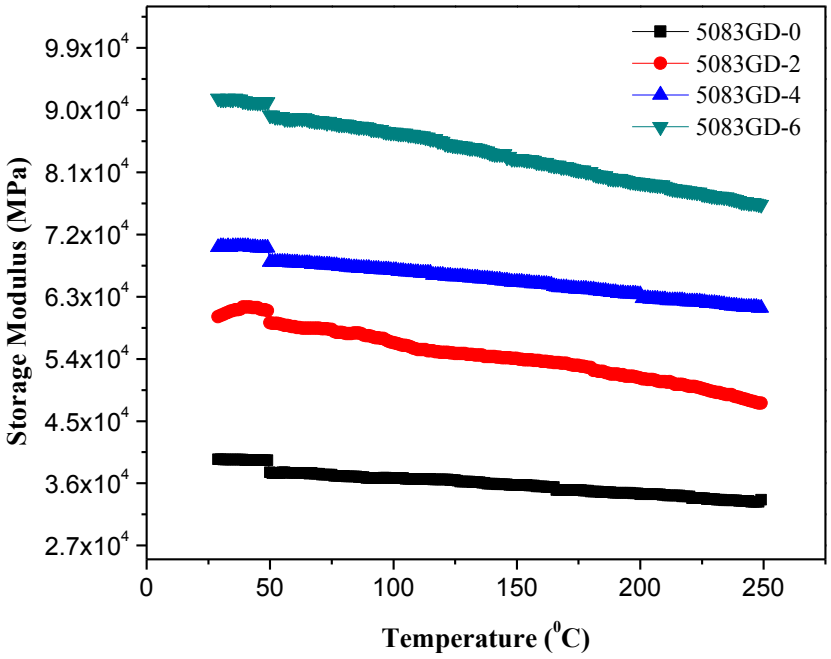

Figure 5.10a Variation of storage modulus with temperature for granite powder reinforced aluminium alloy composites

Figure 5.10(a-c) shows the variation of storage modulus (E') for uncoated, chromium nitride coating, silicon nitride/chromium nitride coating on granite powder reinforced aluminium alloyed composites. From Figure 5.10a, it is observed that storage modulus (E') representing the stiffness of the visco-elastic material and has been observed to undergo consistent decay with the increasing in temperature from 29-250ºC. From Figure 5.10a, it is reveals that storage modulus is decay with increment in temperature and maximum decay in storage modulus is observed for 6 wt.% granite powder reinforced composites on other hand

minimum decay in storage modulus is observed for unreinforced aluminium alloy composites.

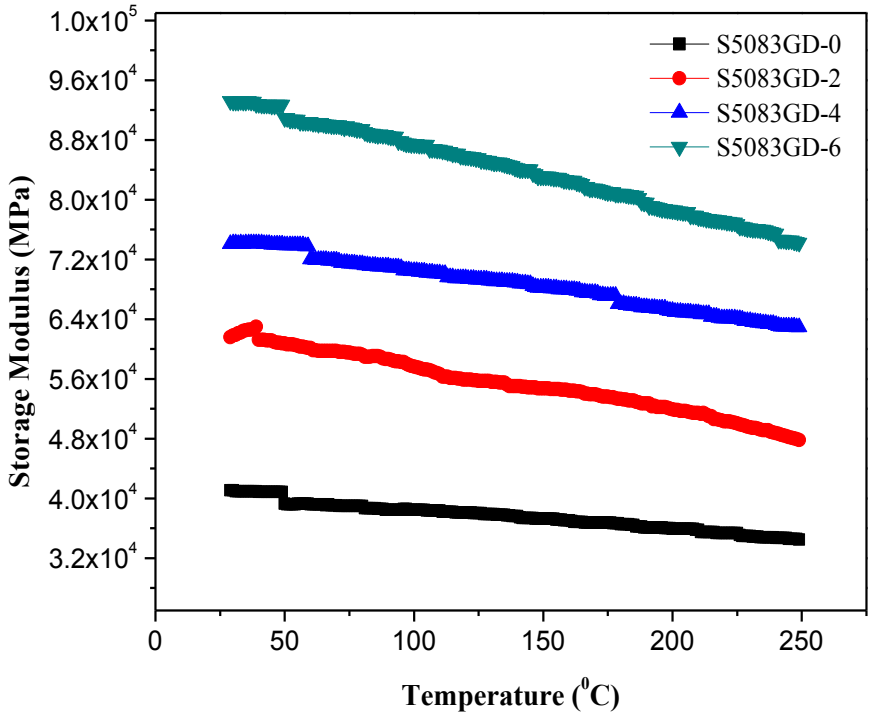

Figure 5.10b Variation of storage modulus with temperature for chromium nitride coating on granite powder reinforced aluminium alloy composites

The decay in storage modulus magnitude depend on the incorporation of granite powder particle as particle incorporated in base matrix it enhanced stiffness of composites. The increased in E' in such cases may be attributed to thermally induced phase transformations leading to hardening of the composites. Similar, observations are reported by Patnaik.et al. [287] and Zang et al. [299] for particulate filled metal alloy composites. The variation of storage modulus with temperature for chromium nitride coating on granite powder reinforced aluminium alloy composites has shown in Figure 5.10b. Storage modulus is decreased with the increase in temperature range from 29-250ºC. The degradation of storage modulus depended on temperature and its slope of degradation is less as compared to uncoated granite powder reinforced aluminium alloy composites. This may be due to high stiffness of chromium nitride coating and as well as high melting point of the coating materials.

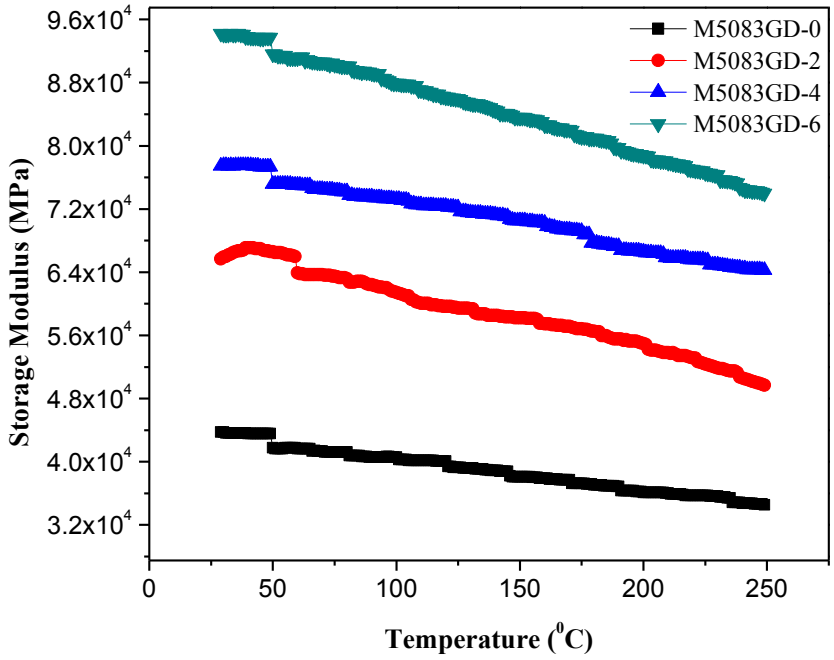

Figure 5.10c Variation of storage modulus with temperature for silicon nitride/chromium nitride coating on granite powder reinforced aluminium alloy composites

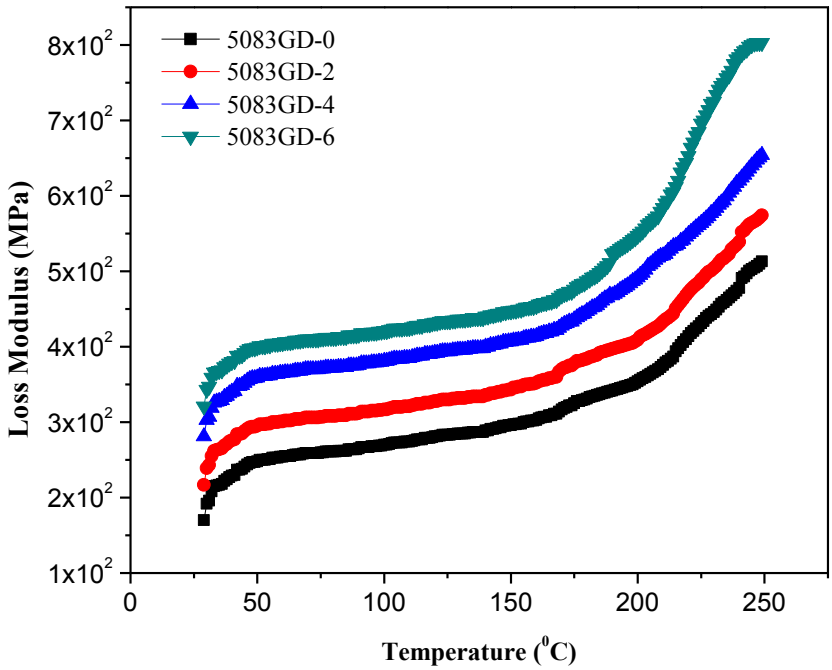

Figure 5.11a Variation of loss modulus with temperature for granite powder reinforced aluminium alloy composites

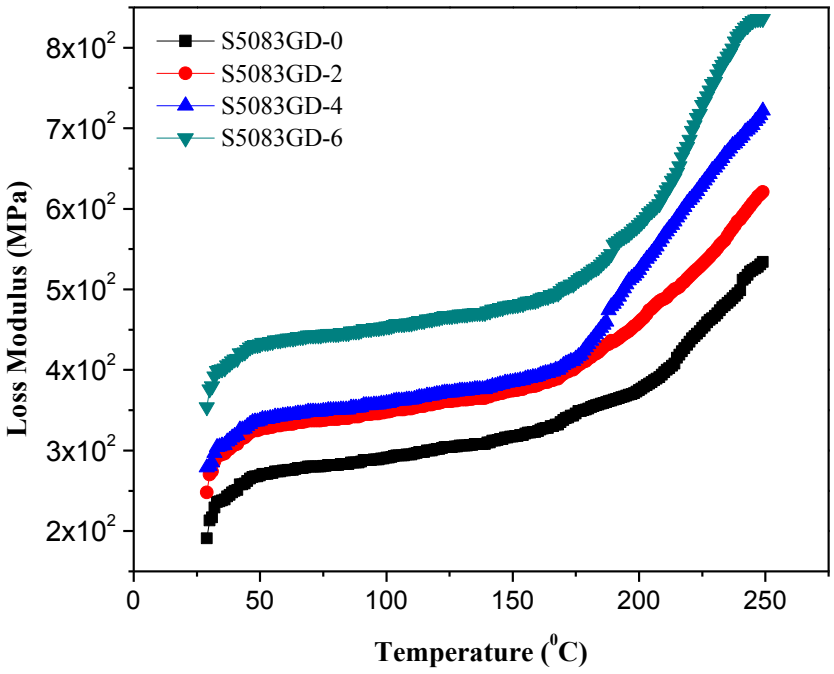

Figure 5.11b Variation of loss modulus with temperature for chromium nitride coating on granite powder reinforced aluminium alloy composites

The loss modulus for uncoated, single layer and multilayer coating on granite powder reinforced aluminium alloyed composites is shown in Figure 5.11 (a-c). From Figure 5.11a it is reveals that with the increase in temperature, loss modulus magnitude is enhance in the order of 6 wt.% granite powder > 4 wt.% granite powder > 2 wt.% granite powder > 0 wt.% granite powder respectively and which has contributed to the reinforcement effects imparted by the particulates allowing enhanced stress transfer ability across the interface. Figure 5.11b shows the effect of temperature on loss modulus for single layer coating on granite powder reinforced aluminium alloyed composites. The loss modulus magnitude is increased with increment in temperature range. Stress is properly transferred from coating material to base material due to proper adhesion between the coating and base materials. Figure 5.11c shows variation in loss modulus with-respective-to temperature for multilayer coating on granite powder reinforced aluminium alloy composites. It is observed that from Figure 5.11c the loss modulus decreases as coating thickness is increases. The results reveal the substrate effect has significant influence on the dynamic properties of thin films. The loss modulus magnitude is decreases in order uncoated > single layer coated > multilayer coated granite powder reinforced aluminium alloyed composites.

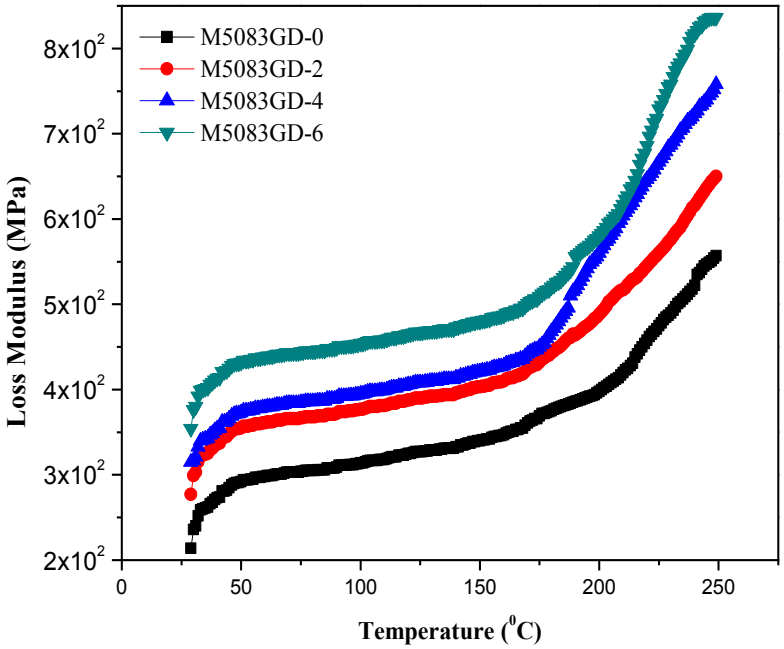

Figure 5.11c Variation of loss modulus with temperature for silicon nitride/chromium nitride coating on granite powder reinforced aluminium alloy composites

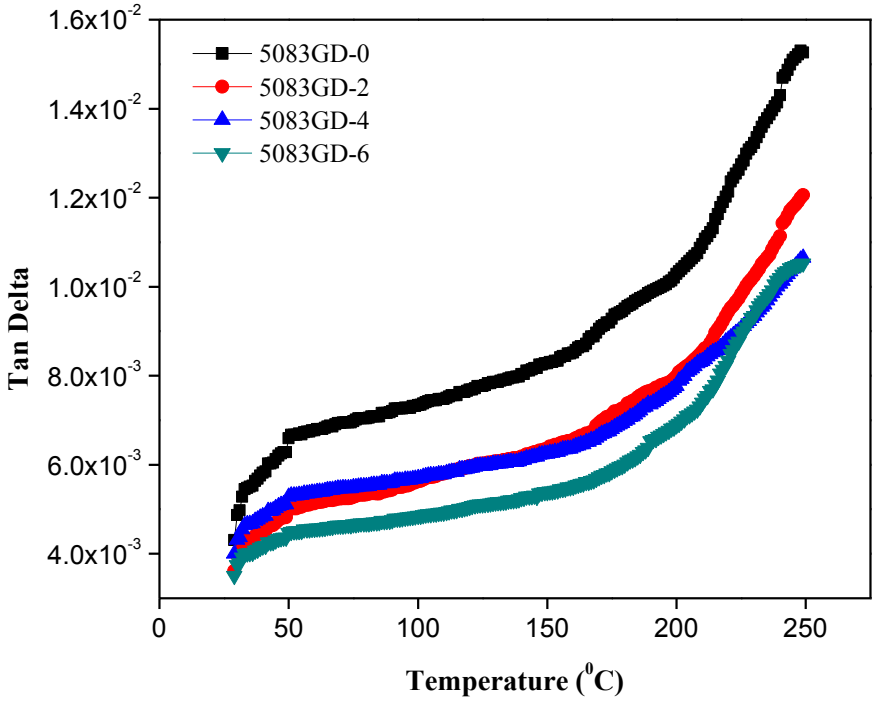

Figure 5.12a Variation of Tan Delta with temperature for granite powder reinforced aluminium alloy composites

The damping factor (Tan δ) indicates the recoverable energy in terms of mechanical damping or internal friction in terms of visco-elastic system. The variation of Tan δ of the composites as a function of temperature is shown in Figure 5.12(a-c) for uncoated, single layer and multilayer coating on granite powder reinforced aluminium alloyed composites. It is observed that Tan δ is enhance with temperature as stiffness decreased leading to higher damping of granite powder reinforced composites (Figure 5.12a). The difference in the stiffness of the particle and matrix material is expected to help in providing high damping at high temperature by causing deformation along the particle-matrix interface. The damping factor for single and multilayer coating is observed higher as compared to uncoated granite powder reinforced aluminium alloyed composites (Figure 5.12b). The Improvement in damping factors is due to the difference in stiffness of substrate and coating materials. Similar, results reported by Cox et al. [301] and Licitra et al. [302] for damping behaviour of metal matrix composites and Gupta et al. [300] for multilayer coated steel substrate (Figure 5.12c).

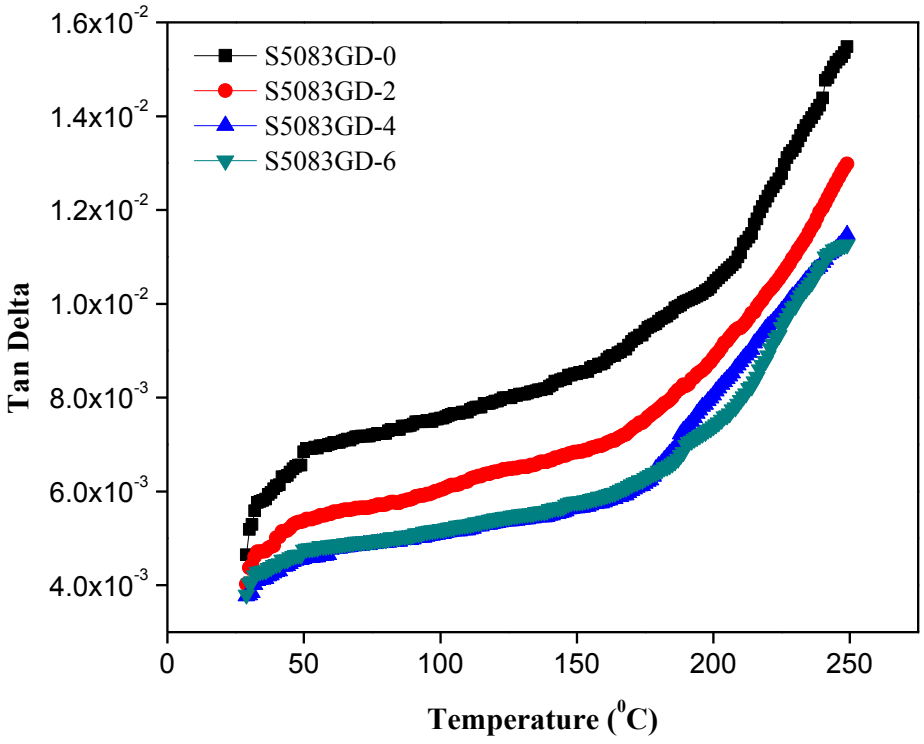

Figure 5.12b Variation of Tan Delta with temperature for chromium nitride coating on granite powder reinforced aluminium alloy composites

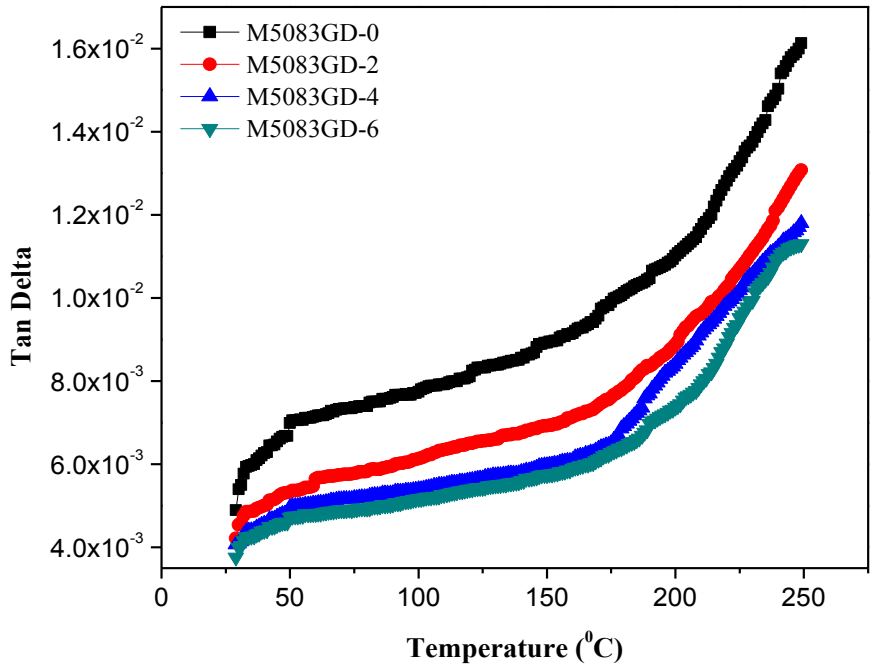

Figure 5.12c Variation of Tan Delta with temperature for silicon nitride/chromium nitride coating on granite powder reinforced aluminium alloy composites

Chapter Summary

This chapter has provided:

- The magnitude of stress intensity factor for the all compositions is well remains above unfilled aluminium alloy composition. Stress intensity factor increased with crack length and also with weight fraction of granite particulate in base matrix.
- Similarly, the magnitude of stress intensity factor enhanced after deposition of single and multilayer coating on granite particulate filled aluminium alloy composites and crack length also.
- Thermo- mechanical analysis of uncoated and coated granite powder reinforced aluminium alloy composites with variation in temperature range.

The next chapter presents the slurry erosion test results for the composites under investigation and the Taugchi DOE technique used for designing experiment runs.

****

Chapter 6

SLURRY EROSION AND CORROSION WEAR BEHAVIOUR OF FABRICATIED GRANITE PARTICULATE FILLED ALLOYED COMPOSITES (COATED/UNCOATED)

This chapter presents the slurry erosion and corrosion wear behaviour of single and multilayer surface coating on granite powder filled alloyed composites. The following results are discussed in brief: (i) the steady state slurry erosion wear behavior and the hierarchy of operating factors (like impact velocity, impingement angle, abrasive size and slurry concentration etc.) controlling wear behavior using Taugchi DOE approach; this followed by surface morphology studies of wear samples using SEM and AFM, (ii) Corrosion wear behavior of under operating conditions like time, pH value of solution etc.

PART-I:

Slurry erosive and corrosion wear behaviour of uncoated / single-layer coated / multi-layered coated granite particulate filled AA1050 alloyed composites

6.1. Steady state erosion of uncoated / single-layer coated / multi-layered coated granite particulate filled AA1050 alloyed composites

Erosion wear phenomenon may use air or water as a medium. When air is used as a medium, it is termed as air-jet erosive wear, alternatively when water is used as medium; it is termed as slurry -jet erosive wear. In slurry erosion wear, there is repeated impact of hard abrasive particle along with water (known as silt) on the surface of the specimen. The rate of slurry erosion is reported [6-14] to be governed by parameters like impact velocity of slurry, impingement angle, slurry concentration, particle shape and size. High rate of erosion may results in functionality failure of the parts in machines along with regular wear/tear/deformation failure.

In the present work, steady state slurry erosion wear rate behaviour of the investigated composites as a function of impact velocity (i.e. 10 m/sec. to 25 m/sec.), erodent discharge (160 g/min. to 280 g/min.) and impingement angle (30-75°) under constant operating conditions are discussed briefly.

6.1.1. Effect of impact velocity on reinforcement and coating

The effect of impact velocity variations on slurry erosion rate of uncoated and coated granite powder reinforced aluminium alloyed composites is shown in Figure 6.1. The parameters kept constant during steady state test runs are impingement angle of 45°, erodent discharge of 160 g/min. and time of 10 min. The impact velocity may be varied from 10-25 m/sec. in-order-to obtain slurry erosion rate of investigated composites. From Figure 6.1 it is observed that slurry erosion rate increases with impact velocity variations for all sets of composites. It further decreases with filler content in respective sets. The rate is observed to be higher for uncoated then single layer then multi-layer alloyed composites. This is in accordance with the power relation between erosion rate and impact velocity as proposed by Hutching I et al. [306]. Similar, observations are reported by other scholars like Patnaik et al. [287] and Ramesh et al. [72] while reported the erosion wear of ZA-27 and 6061 alloy composites respectively.

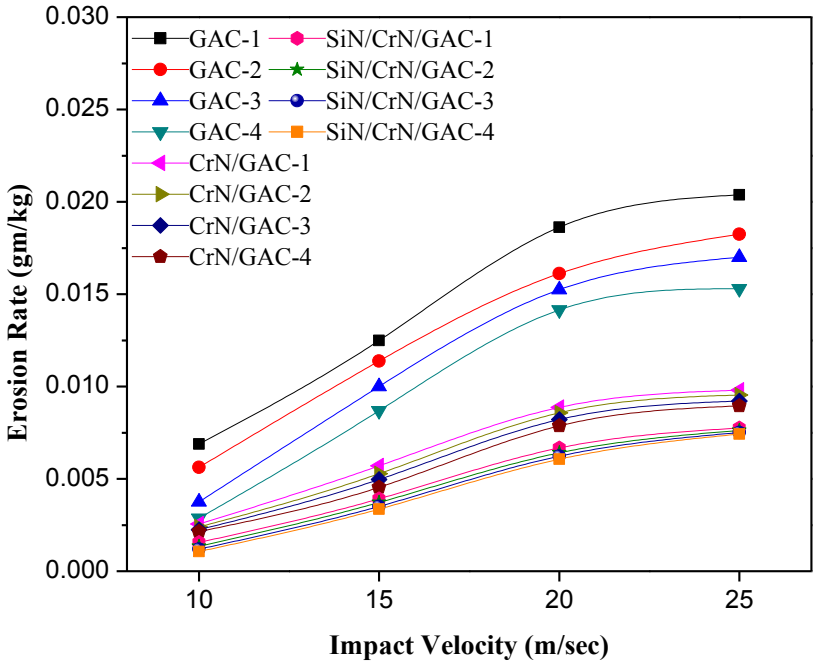

Figure 6.1 Variations in Erosion rate with impact velocity for uncoated / single-layer coated / multi-layered coated granite particulate filled AA1050 alloyed composites

The coating of ceramic materials on granite particulate filled composites observed to be improved. For example, single layer coating of CrN enhances the erosion rate with velocity this may attributed to high hardness and less deformability nature of the coating. Further, composites having multilayer (Silicon nitride/chromium nitride) coating shows enhanced erosion rate with velocity then other set of composites under investigations. In such coating-composite system the hardness is much higher than single layered due to multiphase diffusion of one layer over the other. The multi-deposition of hard coating layer further manifolds hardness magnitude as a result resistance to wear phenomenon is increased, consequently erosion wear behaviour observed to be improved. Similar, results are reported by Bhandari et al. [12] found while studying the Al_2O_3 and Al_2O_3–$13TiO_2$ coated CF8M steel under slurry erosion and Goyal et al. [9] reported similar observation for Cr_2O_3 coated hydro-turbine steel.

6.1.2. Effect of slurry concentration on reinforcement and coating

The effect of slurry concentration on erosion rate of uncoated and coated granite powder reinforced aluminum alloyed composites is shown in Figure 6.2. The erosion rate is computed keeping constant parameters like impact velocity (=15 m/sec.), impingement angle (=75°) and time (=10 min.) and varying the slurry concentration (16-28 g/lts). The variation in slurry concentration is obtained by varying erodent discharge (160-280 gms) in flowing water. From Figure 6.2 it is observed that mass loss for uncoated granite powder reinforced composites increases with slurry concentration. This may attributed to increase in the impacting erodent quantity or concentration per unit target surface area. Further, with increase in granite particulate content in respective formulations, the erosion rate observed to be diminished by small magnitude. The similar results are reported by various scholars like Das et al. [8] while investigating erosion wear rate of Al-SiC composite; Ramesh et al. [72] while investigating 6061 ally; Saini et al. [303] and Finnie [305] reported similar linear response of the volume wear loss of the material with slurry concentration.

Coating of chromium nitride and silicon nitride/chromium nitride over the granite particulate reinforced aluminium alloy composites observed lesser slurry erosive wear rate at all concentration of slurry. It is reported that hardness of single layer (CrN) coating is three times higher than any oxide layer. This may attributed to higher hardness, toughness and corrosion resistance of ceramic coating materials. Such an attribute is higher in case of multi layered

coating (SiN/CrN) then single (CrN) coating due to multiphase combination of different coatings over granite particulate filled alloyed composites. The multi-layered coating forms stable, corrosive resistant thin film over substrate thereby enhancing the slurry erosion resistance of the coated alloyed composites. However, the increase in mass loss with slurry concentration can be attributed to fact that, increase in the abrasive particle concentration in the slurry, enhances the probability of erodent impingement on the target specimen surfaces that consequently leading to increase the deterioration of material from its surfaces. Such observations are made by various scholars [9-14].

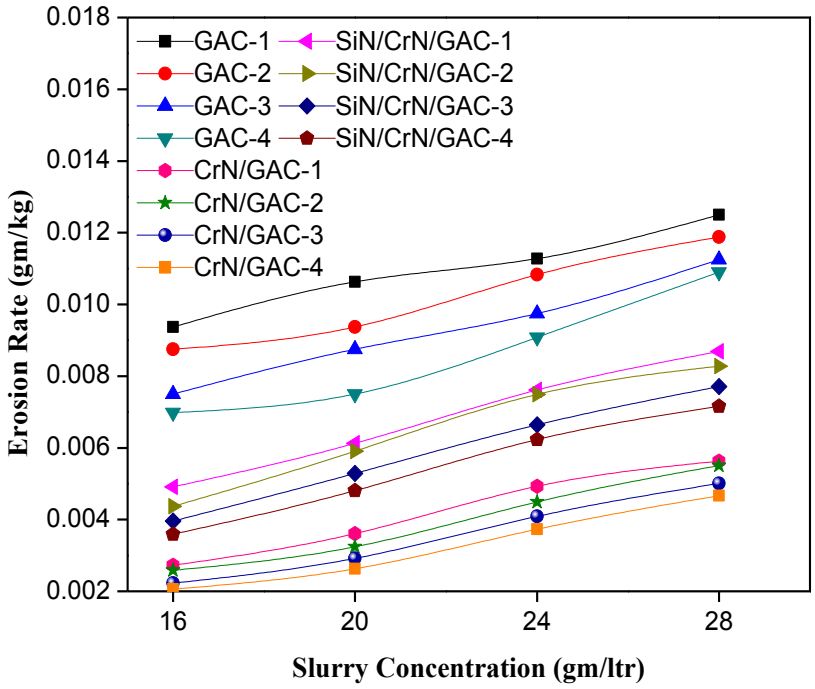

Figure 6.2 Variations in Erosion rate with Slurry concentration for uncoated / single-layer coated / multi-layered coated granite particulate filled AA1050 alloyed composites

6.1.3. Effect of impingement angle on reinforcement and coating

The effect of erodent impingement angle on erosion rate of uncoated and coated granite powder reinforced aluminum alloyed composites is shown in Figure 6.3. The erosion rate is computed keeping constant parameters like impact velocity (=15 m/sec.), slurry concentration (16 g/lts), time (=10 min.) and varying impingement angle (from 30° to 75°). The Figure 6.3 shows that the erosion rate increases with impingement angle upto 60° thereafter it diminishes, irrespective of

the formulations. This may attribute to domination of presence of micro-cutting erosive mechanism rather than plastic deformation erosive mechanism at impingement angle lesser then 60°. And vice-versa as the angle of impingement further increases. Similar observations are made by patnaik et al. [287] while studying erosion behavior for titania reinforced MMCs.

The erosion rate diminishes with particulate content in respective formulation. It observed to be higher for uncoated particulate filled alloyed composites then single coating then multi-layered coating in order. This may be attributed to hardness, toughness and deformation properties of the coating materials. As hardness of coating increases its scratch, abrasion resistance and plastic deformation properties are enhanced simultaneously. Similar results are reported in literatures [304].

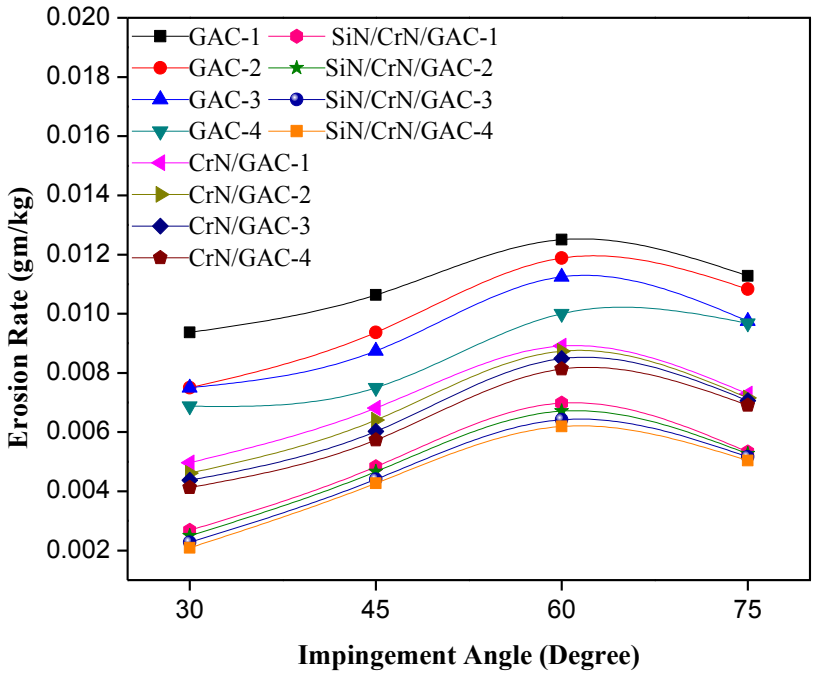

Figure 6.3 Variations in Erosion rate with Impingement angle for uncoated / single-layer coated / multi-layered coated granite particulate filled AA1050 alloyed composites

6.2. Taguchi experimental results for uncoated / single-layer coated / multi-layered coated granite particulate filled AA1050 alloyed composites

The overall mean S/N ratio of the wear rate is found to be 38.01, 49.02, 50.94 db for uncoated, single layer coated, multilayer coated granite powder reinforced aluminium alloyed composites respectively **(**Table 6.1**)**. The analysis is made using the popular software specifically used for

design of experiment applications known as MINITAB 15. Thus factorial design incorporates a simple means of testing for the presence of the interaction effects.

The main effect plots in Figure 6.4(a-c) shown the effects of individual control factors on the erosive wear of the composite can be clearly seen. Maximum S/N ratio corresponds to minimum wear rate and minimum S/N ratio corresponds to maximum wear rate. Thus from Figure 6.4a, it is observed that wear loss decreases (maximum S/N ratio) with increased in impact velocity at level-1 (at 10 m/sec.), filler content at level-4 (at 6 wt.%), impingement angle at level-4 (at 75°) and erodent discharge at level-2 (at 200 g/min.) respectively. Moreover, the granite particles act as resistance to further destructive action of abrasion by wear debris. Analysis of the result lead to the conclusion that factor combination of A_1, B_4, C_4, and D_2 gives minimum erosion rate for uncoated granite filled metal alloy composites. This analysis established that wear rate also depended upon the types of filler, filler content and fabrication methodology.

Thus from Figure 6.4b, it is observed that wear loss decreases (maximum S/N ratio) with increase in impact velocity at level-1 (at 10 m/sec.), filler content at level-4 (at 6 wt.%), impingement angle at level-3 (at 60°), and erodent discharge at level-4 (at 280 g/min.) respectively. Moreover, the granite particles act as resistance to further destructive action of abrasion by wear debris. Analysis of the result lead to the conclusion that factor combination of A_1, B_4, C_3, and D_4 gives minimum erosion rate for uncoated granite filled metal alloy composites. This analysis established that wear rate also depended upon the types of filler, coating material and deposition technique.

Thus from Figure 6.4c, it is observed that wear loss decreases (maximum S/N ratio) with increase in impact velocity at level-1 (at 10 m/sec.), filler content at level-4 (at 6 wt.%), impingement angle at level-3 (at 60°), and erodent discharge at level-4 (at 280 g/min.) respectively. Moreover, the granite particles act as resistance to further destructive action of abrasion by wear debris. Analysis of the result lead to the conclusion that factor combination of A_1, B_4, C_3, and D_4 gives minimum erosion rate for uncoated granite filled metal alloy composites. This analysis established that wear rate also depended upon the types of filler, coating material and deposition technique.

Table 6.1 S/N ratio of wear rate of uncoated, single layer coated, multilayer coated granite dust reinforced aluminium alloyed composites

S. No	Filler Content (wt.%)	Impact Velocity (m/sec)	Impingement Angle (Degree)	Erodent Discharge (gm/min)	Erosion Rate (uncoated)	S/N Ratio (db)	Erosion Rate (Single layer coated)	S/N Ratio (db)	Erosion Rate (Multilayer coated)	S/N Ratio (db)
1.	0	10	30	160	0.005625	40.91	0.0032750	49.69	0.0032500	49.76
2.	0	15	45	200	0.005000	40.00	0.0039425	48.08	0.0040000	47.95
3.	0	20	60	240	0.009583	32.76	0.0044250	47.08	0.0046510	46.64
4.	0	25	75	280	0.008571	32.39	0.0048728	46.24	0.0053750	45.39
5.	2	10	45	240	0.003750	40.91	0.0022330	53.02	0.0025000	52.04
6.	2	15	30	280	0.003571	40.00	0.0027271	51.28	0.0028750	50.82
7.	2	20	75	160	0.006875	39.17	0.0046380	46.67	0.0043800	47.17
8.	2	25	60	200	0.010000	33.97	0.0041500	47.63	0.0045900	46.76
9.	4	10	60	280	0.002857	41.93	0.0022650	52.89	0.0016070	55.87
10.	4	15	75	240	0.005417	37.72	0.0032580	49.74	0.0017080	55.35
11.	4	20	30	200	0.006000	38.41	0.0041560	47.62	0.0025500	51.86
12.	4	25	45	160	0.015000	32.39	0.0044645	47.00	0.0026130	51.65
13.	6	10	75	200	0.002500	46.02	0.0021500	53.35	0.0016250	55.78
14.	6	15	60	160	0.006250	40.00	0.0031425	50.05	0.0018269	54.76
15.	6	20	45	280	0.004286	38.41	0.0035403	49.01	0.0023182	52.69
16.	6	25	30	240	0.009167	33.15	0.004051	47.84	0.0029480	50.60

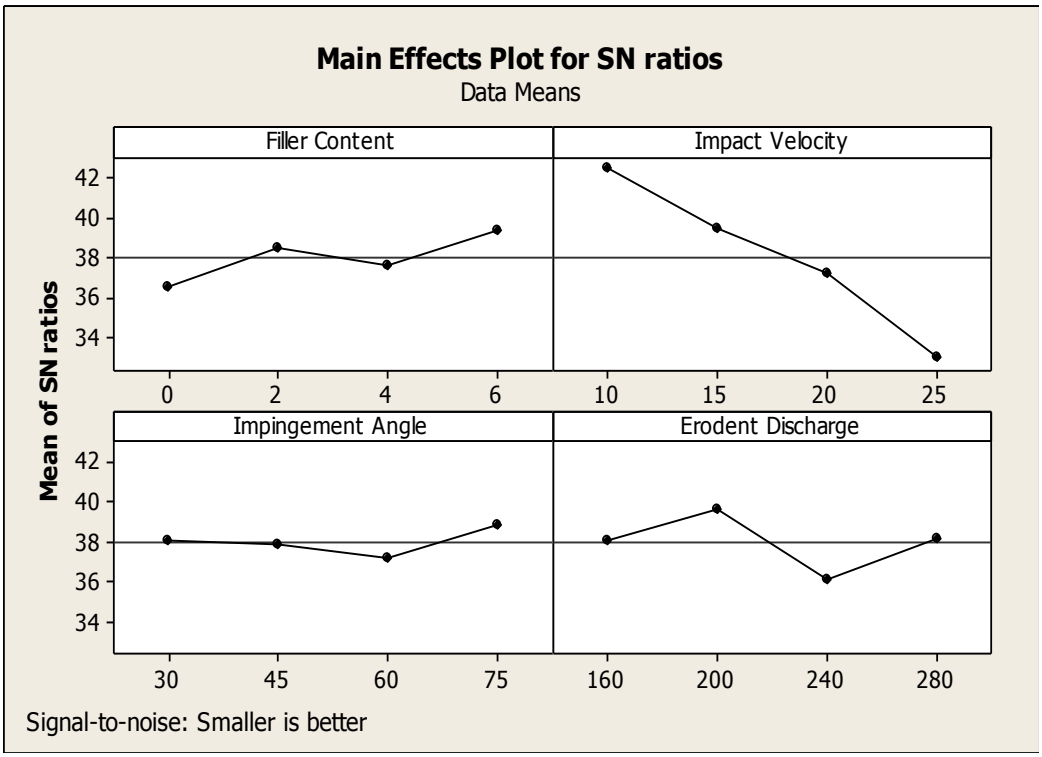

Figure 6.4a Effect of control factors on the Erosion rate of granite filled aluminium alloyed composites

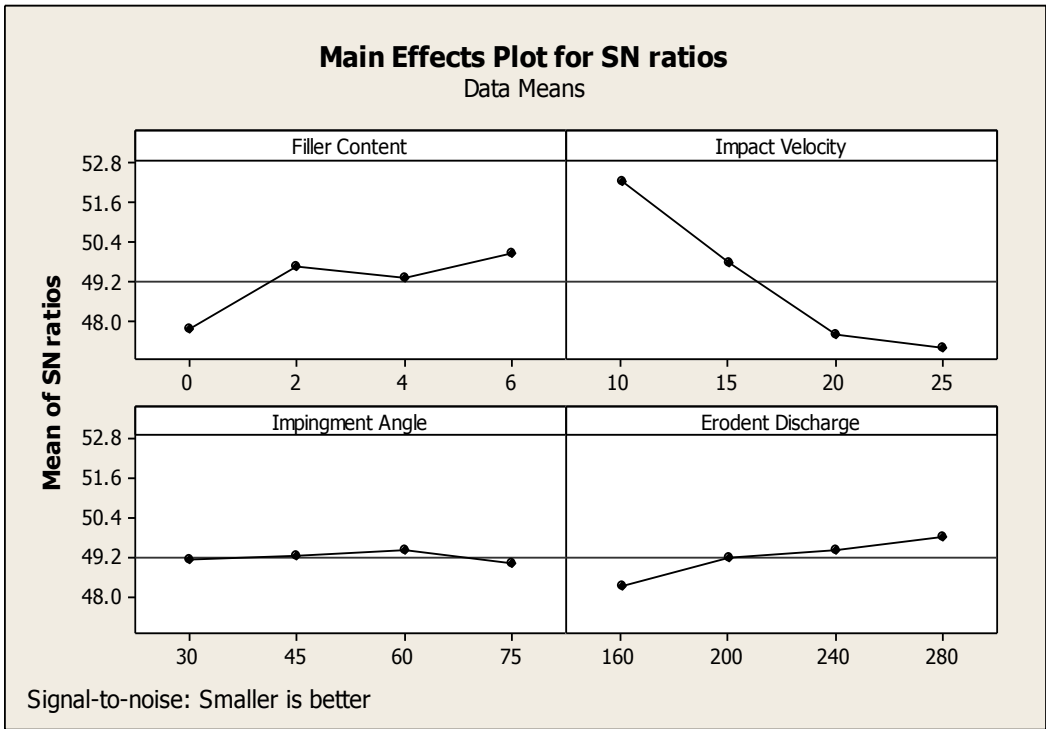

Figure 6.4b Effect of control factors on the Erosion rate of Single layer coated granite filled aluminium alloyed composites

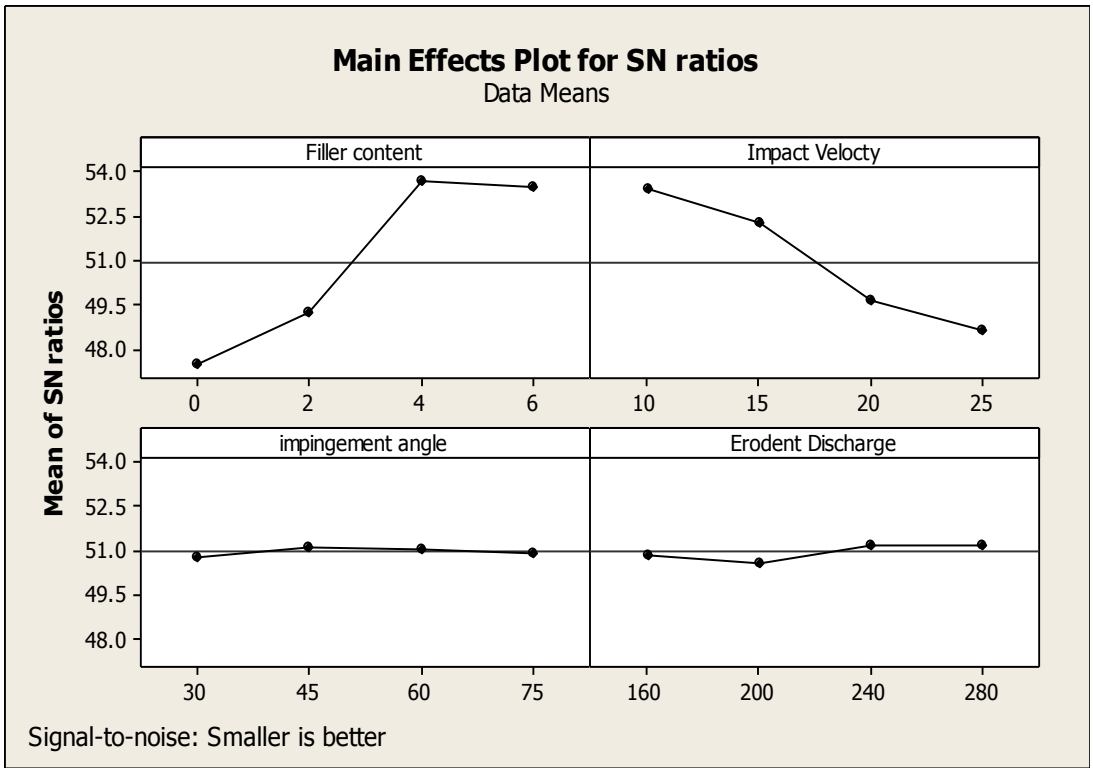

Figure 6.4c Effect of control factors on the Erosion rate of multilayer coated granite filled aluminium alloyed composites

6.3 ANOVA Analysis

In order to understand impact of various factors effect on the output performance, it is desirable to perform analysis of variance (ANOVA) to find out the order of significant factors. Table 6.2 (a-c) shows results of the ANOVA with the specific wear rate. This analysis is undertaken for a level of significance is 95%. The last column of the table is indicated the order of significance among factors.

From Table 6.2a, it can be observed that the impact velocity ($p = 0.006$), filler content ($p = 0.059$), erodent discharge ($p = 0.179$), impingement angle ($p = 0.842$) have positive influence on slurry erosion rate. Among these factors, impact velocity is indicated the most significant effect on wear rate and impingement angle is observed to be less significant effect on wear rate for uncoated granite powder reinforced composites.

Table 6.2a ANOVA table of uncoated granite filled aluminium alloyed composites for wear rate

Source	DF	Seq SS	Adj SS	Adj MS	F	P	Rank	%
Filler Content	3	18.230	18.230	6.077	10.74	0.041	3	7.63
Impact Velocity	3	190.677	190.677	63.559	112.39	0.001	1	79.85
Impingement Angle	3	5.563	5.563	1.854	3.28	0.178	4	2.33
Erodent Discharge	3	24.352	24.352	8.117	14.35	0.028	2	10.19
Error	3	1.697	1.697	0.566				
Total	15	240.519						

On other hand from Table 6.2b, it can be observed that granite filled aluminium alloyed composites the impact velocity (p = 0.001), erodent discharge (p = 0.028), filler content (p = 0.041), impingement angle (p = 0.178) have positive influence on slurry erosion rate. Among these factor, impact velocity indicated most significant effect on wear rate and impingement angle indicated less significant effect on wear rate for single layer coated granite powder reinforced composites.

Table 6.2b ANOVA table of Single layer coated granite filled aluminium alloyed composites for wear rate

Source	DF	Seq SS	Adj SS	Adj MS	F	P	Rank	%
Filler Content	3	12.0029	12.0029	4.0010	8.14	0.059	2	14.61
Impact Velocity	3	64.9072	64.9072	21.6357	44.04	0.006	1	79.06
Impingement Angle	3	0.4034	0.4034	0.1345	0.27	0.842	4	0.48
Erodent Discharge	3	4.7972	4.7972	1.5991	3.25	0.179	3	5.83
Error	3	1.4738	1.4738	0.4913				
Total	15	83.5846						

Again from Table 6.2c, it can be observe that the filler content (p = 0.003), impact velocity (p = 0.008), erodent discharge (p = 0.662), impingement angle (p = 0.931) have influence on slurry erosion rate. Among these factors, multilayer coated filler content indicated most significant effect on wear rate and impingement angle indicated less significant effect on wear rate for multilayer coated granite powder reinforced composites.

Table 6.2c ANOVA table of Multilayer coated granite filled aluminium alloyed composites for wear rate

Source	DF	Seq SS	Adj SS	Adj MS	F	P	Rank	%
Filler Content	3	116.789	116.789	38.9295	69.98	0.003	1	65.91
Impact Velocity	3	59.178	59.178	19.7258	35.46	0.008	2	33.40
Impingement Angle	3	0.230	0.230	0.0767	0.14	0.931	4	0.13
Erodent Discharge	3	0.986	0.986	0.3287	0.59	0.662	3	0.56
Error	3	1.669	1.669	0.5563				
Total	15							

6.4 Confirmation Experiment

The confirmation experiment is performed with a new combination of factors and levels used during the wear test. The purpose of confirmation experiment is to evaluate the optimum condition for wear test with optimal levels of selecting parameters. It established relationship between theoretical value and experimental value of slurry erosion wear. The estimated S/N ratio for slurry erosion wear can be calculated by predictive equation: (Eqs. 6.1 and 6.2)

$$\eta = \eta_m + \sum_{i=1}^{n} (\bar{\eta}_1 - \eta_m) \tag{6.1}$$

$$\eta = \bar{T} + (\bar{A}_3 - \bar{T}) + (\bar{B}_3 - \bar{T}) + (\bar{C}_4 - \bar{T}) + (\bar{D}_4 - \bar{T}) \tag{6.2}$$

In this study the confirmation has been performed by taking an arbitrary set of factor combination $A_3B_3C_4D_4$for uncoated, single layer coated, multilayer coated granite filled aluminium alloyed composites. A new combination of factor levels is use to predict deposition rate through prediction equation and it is found to be 37.7874, 48.1692 and 52.5630 db for uncoated, single layer coated, multilayer coated samples respectively. For each performance measure, an experiment is conducted for a different factors combination and compared with the results obtained from the predictive equation as shown in Table 6.3 Actual runs are performed to verify the results obtained by above equations are acceptable or not. It is found that when actual runs have been performed on above factor settings an error of 5.17%, 2.59% and 2.32% for uncoated, single layer coated, multilayer coated granite filled aluminium alloyed composites and are well within the reasonable limits. The error can be reduced further by increasing the number

of experimental runs. This verifies that the predicted values are reliable and testified the validity of this model for predicting the performance output on the basis of input characteristics.

Table 6.3 Results of the confirmation experiments for wear rate of uncoated, single layer coated, multilayer coated granite filled aluminium alloyed composites

	Optimum control parameters		Error
	Prediction	Experimental	
Level	$A_3B_3C_4D_4$	$A_3B_3C_4D_4$	%
S/N ratio for wear rate (db) for uncoated granite dust reinforced aluminium alloyed composites	37.7874	35.8342	5.17
S/N ratio for wear rate (db) for single layer coated granite dust reinforced aluminium alloyed composites	48.1692	46.9531	2.59
S/N ratio for wear rate (db) for multilayer coated granite dust reinforced aluminium alloyed composites	52.5630	51.3679	2.32

6.5 Microstructure analysis of the worn surface by varying impact velocity

SEM image for uncoated, single layer and multilayer coated eroded samples for two different velocities were shown in Figure 6.5(a-f). Figure 6.5(a) and Figure 6.5(b) indicate the micrographs obtained by impact velocity at 25 m/sec. and 10 m/sec. for 6 wt.% granite powder reinforced and unreinforced samples. From the image it is observed that at higher impact velocity extensive plastic deformation with characteristics as deep craters, plates and lips can be observed. The characteristics of the eroded surface is observed that severe plastic deformation occurred and materials were displaced randomly first before being removed. The embedded erosive erodent particles are also found over the eroded composite surface and indicate the soft/ductile nature of the alloy. On the other hand, with decreased in impact velocity (10 m/sec), at lower impingement angle (45°) and slurry concentration the erosion rate indicated lowest among unfilled composites.

When we observed the eroded surface of single layer coated samples the SEM image is shown in Figures 6.5(c) and 6.5(d) for same experiments velocity 25 m/sec and 10 m/sec. Single layer coated samples wear rate are less as compared to uncoated sample due to high hardness of deposited layer. An increased in hardness below the eroded surface due to work-hardening also

helps in explaining the erosion mechanism (plastic deformation) proposed. With further continuation of the impact process, brittleness of the material could be increased due to extensive work-hardening. This would result into the removal of material from the surface in the form of small fragments as illustrated. From SEM image it also evident that amount of craters, plates and lips are less as compared to SEM image of uncoated samples.

Again multilayer coated eroded samples the SEM image is shown in Figures 6.5(e) and 6.5(f) for velocity 25 m/sec and 10 m/sec. Multilayer coated samples wear rate is less as compared to uncoated sample due to hardness of layer as deposit layer is removed than particles strike on the surface of granite reinforced composites. An increase in hardness below the eroded surface due to work-hardening also helps in explaining the erosion mechanism (plastic deformation) proposed. With further continuation of the impact process, brittleness of the material could increase due to extensive work-hardening. This would result in the removal of material from the surface in the form of small fragments as illustrated from SEM image (figure 6.5(e) and 6.5(f)) it evident that amount of craters, plates and lips are less as compared to SEM image of uncoated samples

From all SEM images it is also observed that the surface eroded at slow-impact velocity is less plastically deformed in comparison with one eroded at high velocity. The removal of material through platelet mechanism is comparatively a slow process [311,312]. It requires higher number of impacts in comparison with micro-cutting or ploughing for the final detachment of the material. After the formation of platelets the continuous impacts of subsequent particle would result in flattening of the platelets [313,314]. When strain value of surface exceed to a limit cracks were generated. This process will eventually result in the removal of material in the form of small fragments, indicating the presence of fatigue phenomena. Along with platelet mechanism, extensive plastic deformation is also playing a significant role in the erosion process at high velocity. The supporting trend in erosion rates is already discussed in section 6.1.1 for appeared observation of SEM images.

Uncoated

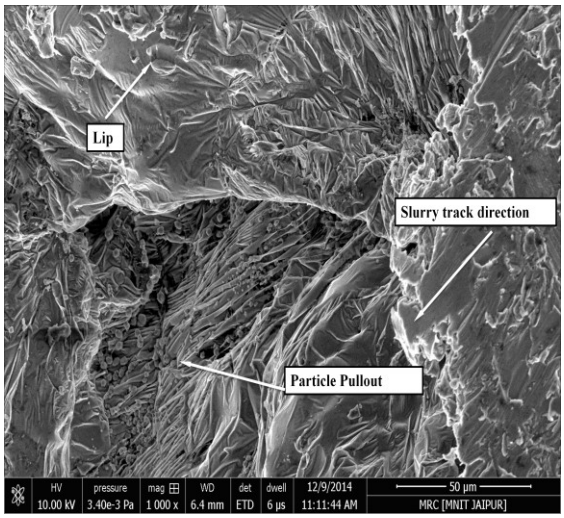

(a) 6 wt.% GD, impact velocity 25 m/sec., impingement angle 45°, erodent discharge 160 g/min., time 10 min.

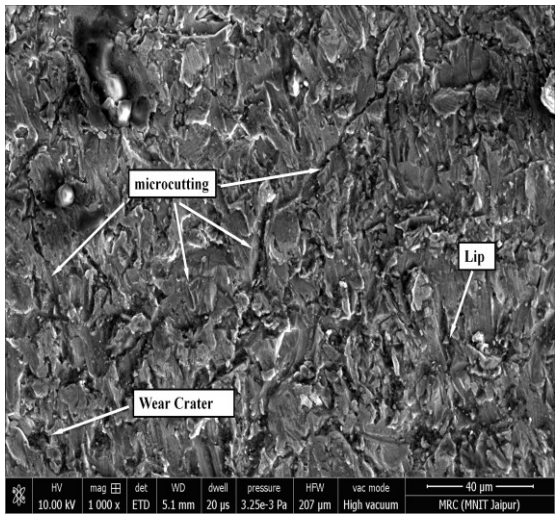

(b) 0 wt.% GD, impact velocity 10 m/sec., impingement angle 45º, erodent discharge 160 g/min., time 10 min

Single layer coated

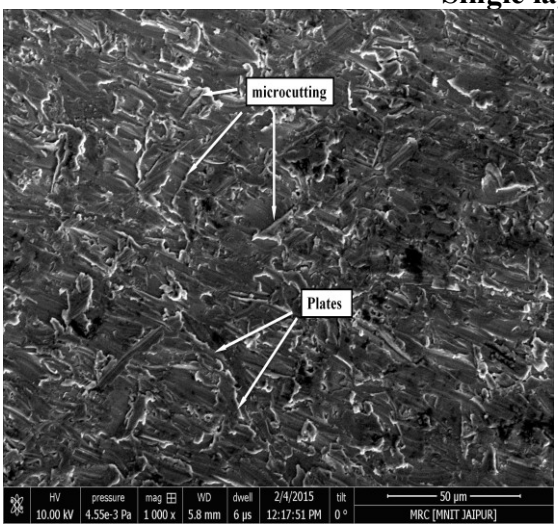

(c) Single layer coated 4 wt.% GD, impact velocity 25 m/sec., impingement angle 45º, erodent discharge 160 g/min., time 10 min

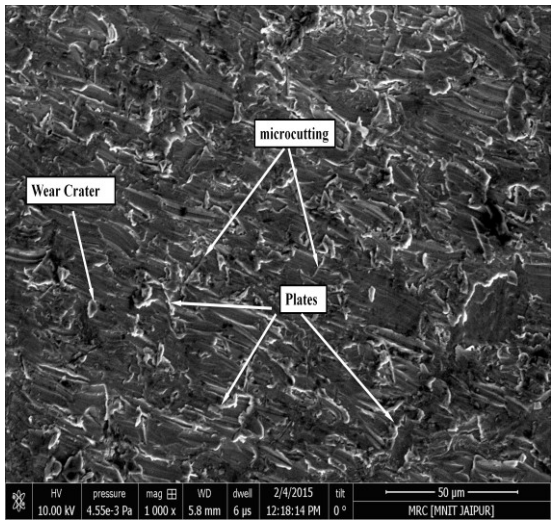

(d) Single layer coated 0 wt.% GD, impact velocity 10 m/sec., impingement angle 45º, erodent discharge 160 g/min., time 10 min

Multilayer coated

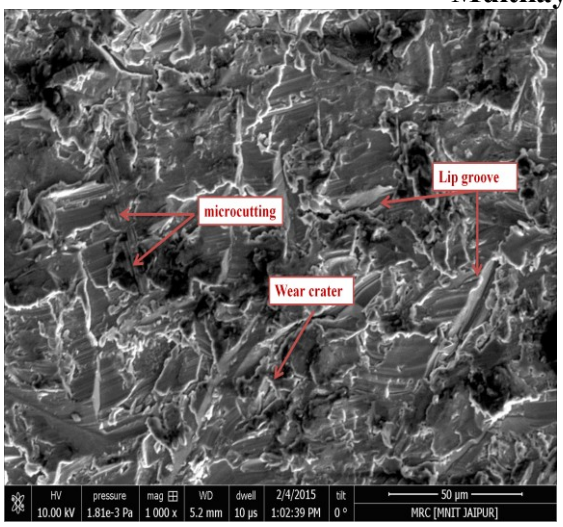

(e) Multilayer coated 0 wt.% GD, impact velocity 25 m/sec., impingement angle 45º, erodent discharge 160 g/min., time 10 min

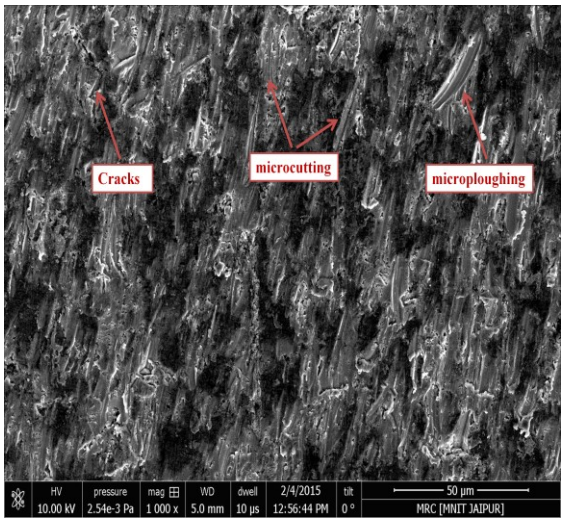

(f) Multilayer coated 6 wt.% GD, impact velocity 10 m/sec., impingement angle 45º, erodent discharge 160 g/min., time 10 min

Figure 6.5 SEM image of uncoated, single layer coated, multilayer coated eroded sample

6.6 Microstructure analysis of the worn surface by varying slurry concentration

The effect of slurry concentration on the erosion mechanism can be observed from Figure 6.6(a-f) for uncoated, single layer coated and multilayer coated samples. Figure 6.6(a) and Figure 6.6(b) represent the eroded surface SEM image of uncoated granite powder reinforced aluminium alloyed composites for lower and higher slurry concentration. For the images it is replicate that as the slurry concentration is increases the rate of impingement particles per unit are increased. The material removal took place through platelet mechanism at normal impacts and ploughing along with Micro-cutting process (Mcp) at acute impingement angle. However, it is to be noticed that intensity of the slurry concentration is significantly affected. At lower concentration the amount of micro-ploughing is less as slurry concentration increase ploughing effect increase and wear crater also. The SEM image of Figure 6.6(c) and Figure 6.6(d) of single layer coated granite powder reinforced aluminium alloyed composites for same experiments. We found that scratch generated by impingement of hard abrasive particles is seemed to less as compared to uncoated samples. Hardness of coating is only parameter which ensures scratch and abrasion resistance and it represents high resistance for plastic deformation during contact events. Single layer (chromium nitride) coating was three times harder than oxides coating.

When we observed the SEM image 6.6(e) and 6.6(f) of multilayer coated granite powder reinforced aluminium alloyed composites for same experiments. We found that scratch generated by impingement of hard abrasive particles was seemed to less as compared to uncoated and single layer coated samples. As hardness increased its scratch and abrasion resistance properties enhanced simultaneously its resistance for plastic deformation also increased. The supporting trend in erosion rates was already discussed in section 6.1.2 for appeared observation of SEM images.

uncoated

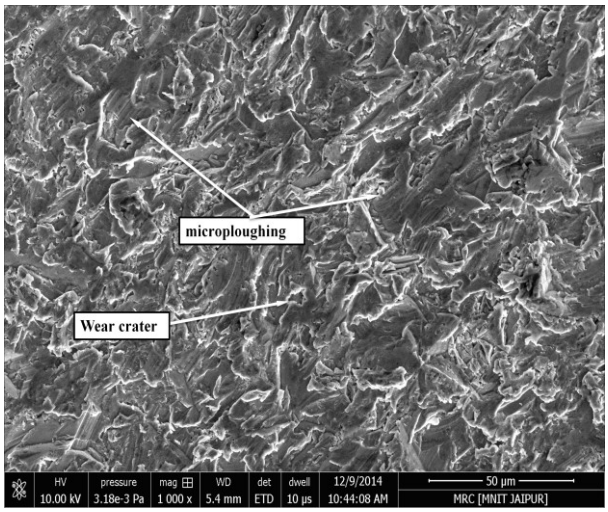

(a) 6 wt.% GD, impact velocity 15 m/sec., impingement angle 75º, erodent discharge 200 g/min., time 10 min.

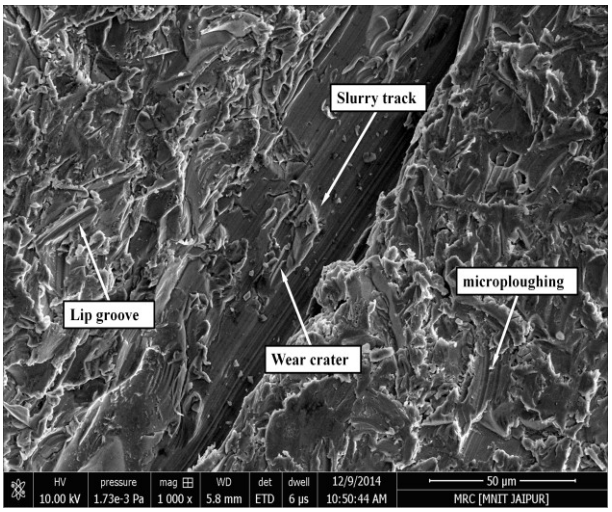

(b) 0 wt.% GD, impact velocity 15 m/sec., impingement angle 75º, erodent discharge 280 g/min., time 10 min.

Single layer coated

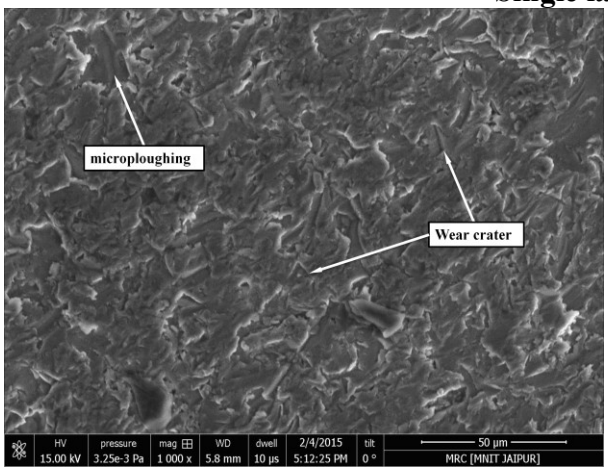

(a) Single layer coated 6 wt.% GD, impact velocity 15 m/sec., impingement angle 75º, erodent discharge 240 g/min., time 10 min

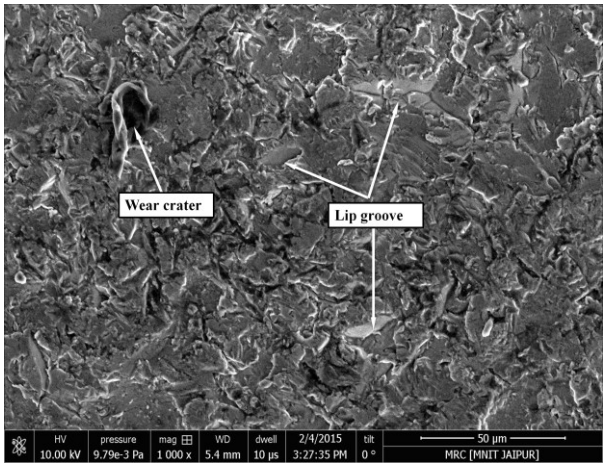

(b) Single layer coated 2 wt.% GD, impact velocity 15 m/sec., impingement angle 75º, erodent discharge 160 g/min., time 10 min

Multilayer coated

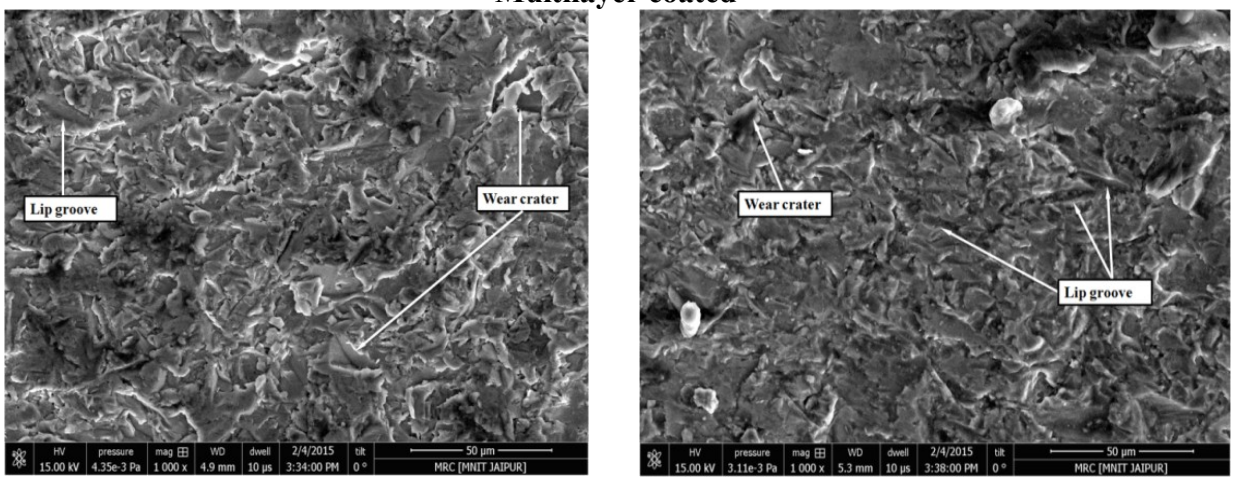

(a) Multilayer coated 4 wt.% GD, impact velocity 15 m/sec., impingement angle 75º, erodent discharge 200 g/min, time 10 min

(b) Multilayer coated 0 wt.% GD, impact velocity 15 m/sec., impingement angle 75º, erodent discharge 160 g/min, time 10 min

Figure 6.6 SEM image of uncoated, single layer coated, multilayer coated eroded sample

6.7 Microstructure analysis of the worn surface by varying impingement angle

Effect of impingement angle on erosion mechanism shown in Figure 6.7(a-f) by uncoated, single layer coated, multilayer coated eroded samples for two different angles. From the SEM it was observed that the surface impacted at normal impingement angle showed the presence of platelets and plastically deformed target surface. The impact energy of the particles would make the material to deform plastically. This plastically deformed material would tend to flow outward and get accumulated around the impact crater. During subsequent impacts, this deformed material would get removed in the form of small fragments as discussed in preceding subsection. For surfaces impacted at acute angle, major material removal mechanisms were ploughing and mixed cutting-ploughing mode. Hutching [315] and Levy [316-318] have shown that with the impact of round particles such as sphere, the material displaces and get accumulated at the end from where the particle leaves. This mechanism of material removal is generally known as ploughing. However, in our work, in addition to ploughing observed at acute impingement angle, the primary mode of material removal is the mixture of ploughing and micro-cutting mechanism. This mechanism is significantly different from what the earlier researchers have proposed, which the authors have named to be mixed cutting and ploughing (Mcp).

Uncoated

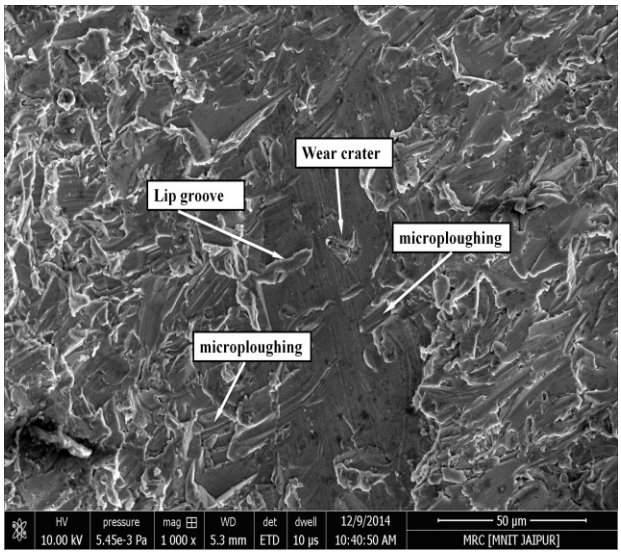

(a) 0 wt.% GD, impact velocity 15 m/sec., impingement angle 60º, erodent discharge 160 g/min, time 10 min

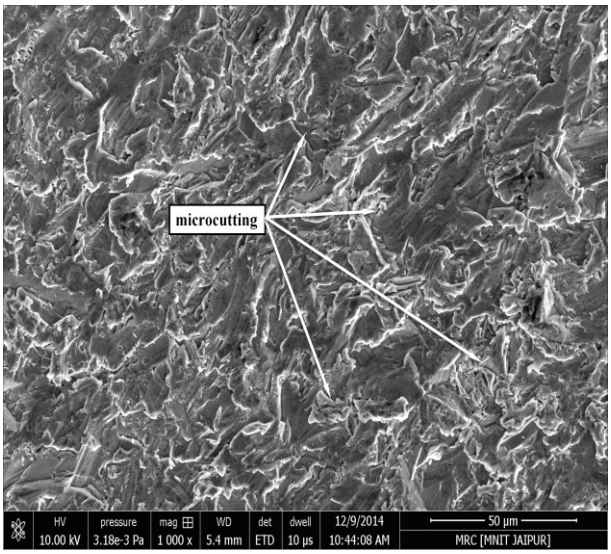

(b) 0 wt.% GD, impact velocity 15 m/sec., impingement angle 30º, erodent discharge 160 g/min, time 10 min

Single layer coated

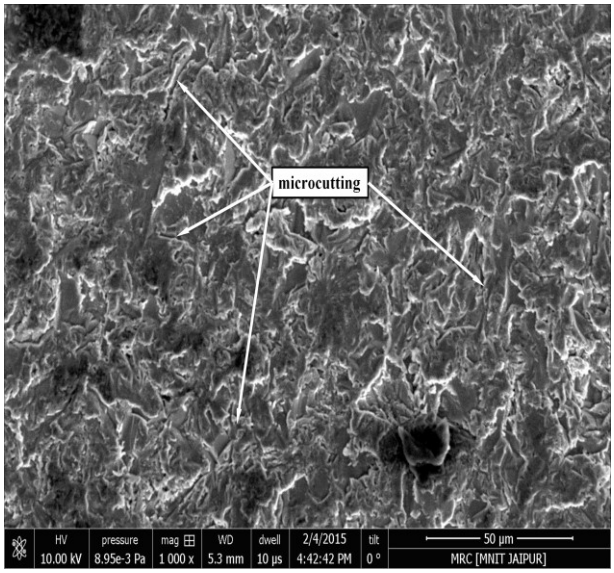

(a) Single layer coated 6 wt.% GD, impact velocity 15 m/sec., impingement angle 45º, erodent discharge 160 g/min, time 10 min

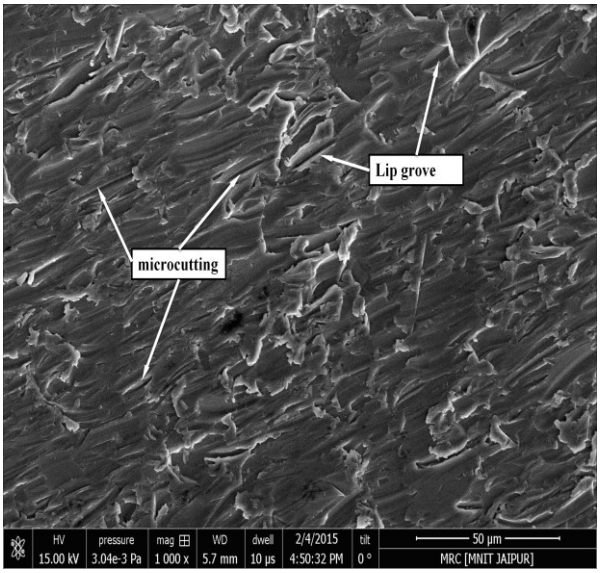

(b) Single layer coated 0 wt.% GD, impact velocity 15 m/sec., impingement angle 75º, erodent discharge 160 g/min, time 10 min

Multilayer coated

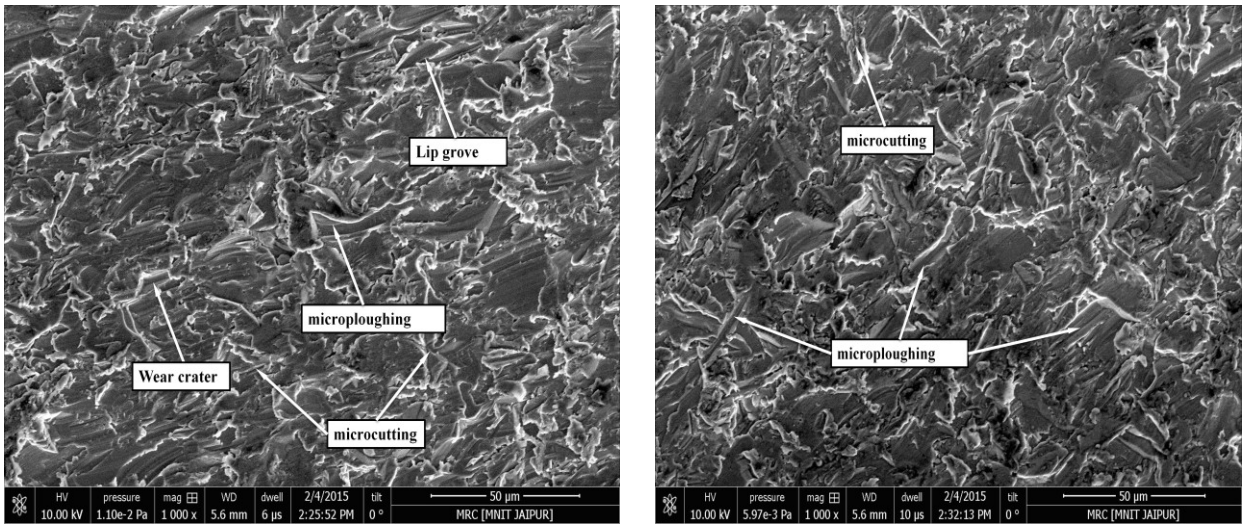

(a) Multilayer coated 4 wt.% GD, impact velocity 15 m/sec., impingement angle 45º, erodent discharge 160 g/min, time 10 min

(b) Multilayer coated 2 wt.% GD, impact velocity 15 m/sec., impingement angle 75º, erodent discharge 160 g/min, time 10 min

Figure 6.7 SEM image of uncoated, single layer coated, multilayer coated eroded sample

The SEM micrographs shown in Figure 6.7 clearly indicate the presence of Mcp mode. Moreover, the presence of this mode is more preferential than pure ploughing or micro-cutting. In continuation to the discussion of Sect. 6.1.3, the reason for the lower erosion rates for normal impingement angles in comparison with acute angle impingement could be easily explained in terms of erosion mechanism. Platelet mechanism as explained earlier is a slow process involving combined plastic deformation and fatigue phenomena. In contrast to it, micro-cutting and Mcp are more efficient mechanisms for the removal of material. This explains the cause as to why the erosion rates were higher at low impingement angles rather than at normal impact angle. This observation appears to be supporting the trend in erosion rates as discussed in Sect. 6.1.3.

6.8 AFM analysis of worn surfaces

The removal of material during wear leads to alternations in surface topology. Atomic force microscopy in contact mode served to evaluate the topology characterization of plain and worn surfaces. It is worth mentioning that all roughness values are given in terms of Ra which represents the arithmetic mean of height deviations from the mean profile value shown in Table 6.4. Figure 6.8 represents the AFM image of plain and worn surface of uncoated and coated

granite powder reinforced aluminium alloyed composites. It is notice that nearly no surface defecates found in uncoated granite powder reinforced unworn surface samples. Worn surfaces samples show grooves, micro-ploughing and lip formation features of material removal or slurry track direction, which shows good agreement with results obtained from FE-SEM image of worn surfaces (Figure 6.7). All the eroded surface AFM image for lower impact velocity, impingement angle 45º, erodent discharge 160 g/min. for uncoated and coated granite particulate reinforced aluminium alloyed composites. AFM image of uneroded and eroded samples are compared and after slurry erosion the surface roughness value of increase and it depends on the erosion mechanism. The microstructure and surface roughness of uncoated 0 wt.% granite powder reinforced aluminium alloyed worn surface for operating condition impact velocity 10 m/sec., impingement angle 45º, erodent discharge 160 g/min shown in the SEM image 5.6(b) and AFM image 6.8(e) respectively. In SEM image Deep groove lip formation, micro cutting and wear craters features is found which show good agreement with AFM image. The roughness value of these features is found higher from AFM image due to the lower hardness of base material. On other hand the SEM image 5.6(d) and AFM image 6.8(m) of single layer coated samples above says set composites for same operating condition. In SEM image Deep groove lip formation, micro cutting and wear craters features is found which show good agreement with AFM image but roughness value is lower due to hardness of single layer coating. Multilayer coated 6 wt.% granite powder reinforced aluminium alloyed worn surface for operating condition impact velocity10 m/sec., impingement angle 45º, erodent discharge 160 g/min shown in the SEM image 5.6(f) and AFM image 6.8(X) respectively. In SEM image Deep groove lip formation, micro cutting and wear craters features is found which show good agreement with AFM image but roughness value is lower due to high hardness of multilayer coating.

AFM image (a-h), (i-p) and (q-x) are for uncoated, single layer and multilayer coated granite powder reinforced aluminium alloy composites respectively. AFM image (a-d), it can be observed that the addition of granite particle reduced the surface roughness value (8.85-5.75nm). However, on coating of single and multilayer on these samples the surface roughness is decreased as shown in AFM image (i-l) (6.36-4.95nm) and (q-t) (4.54-2.53nm) respectively. When we observed the AFM image of eroded surface the roughness value is higher as compared to uneroded surface roughness value. The surface roughness value of eroded surface is higher due to presence of peaks and valleys resulting from severe plastic deformation mechanism. For

(e-h) AFM image shows that surface roughness value of eroded surface is reduced (338-176nm). The reduction in surface roughness value is due to the addition of granite particle and it can be proved that addition of granite particle reduced the slurry erosion wear rate discuss in section 3.1.1 When we observed the eroded surface AFM image (m-p) & (u-x) of single and multilayer coating the surface roughness value is reduced (130 to 87.6 nm) & (66.1-39.9nm) respectively. The reduction in surface roughness value is due to the deposition of surface coating and it can be proved that deposition of coating reduced the slurry erosion wear rate discuss in section 3.1.1. Similar observation for AFM surface mapping before and after erosion reported by Iwai et al.[247] and Lopez et al.[186].

Table 6.4 Surface roughness for plain surface and worn surface of uncoated, single layer coated, multilayer coated granite filled aluminium alloyed composites

S. No.	Designation	Plain Surface Roughness (Ra)	Worn Surface Roughness (Ra)
Uncoated			
1	1050GD-0	8.85 nm	338 nm
2	1050GD-2	7.13 nm	248 nm
3	1050GD-4	6.13 nm	216 nm
4	1050GD-6	5.75 nm	176 nm
Single layered CrN Coated			
5	S1050GD-0	6.36 nm	130 nm
6	S1050GD-2	5.91 nm	110 nm
7	S1050GD-4	5.34 nm	97.4 nm
8	S1050GD-6	4.95 nm	87.6 nm
Multilayered SiN & CrN Coated			
9	M1050GD-0	4.54 nm	66.1 nm
10	M1050GD-2	3.73 nm	59.3 nm
11	M1050GD-4	2.93 nm	46.1 nm
12	M10550GD-6	2.53 nm	39.9 nm

Uneroded Surface **Eroded surface**

(a)

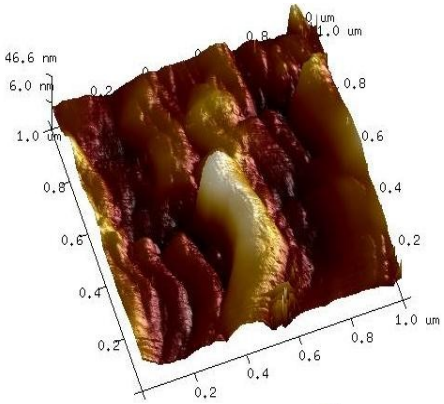

(e)

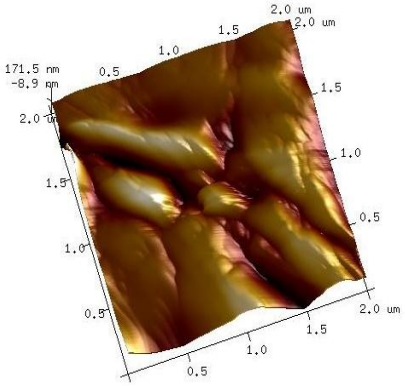

(b)

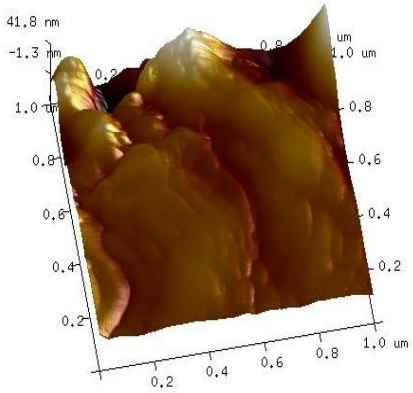

(f)

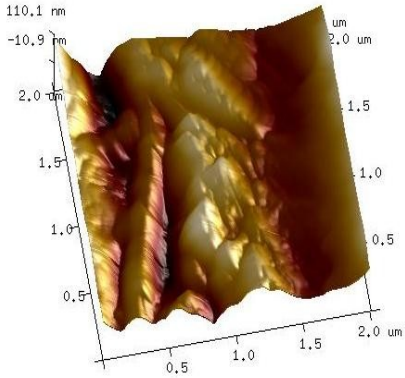

(c)

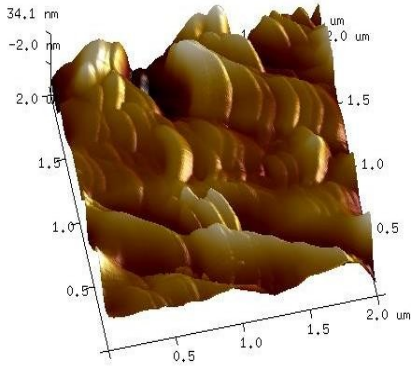

(g)

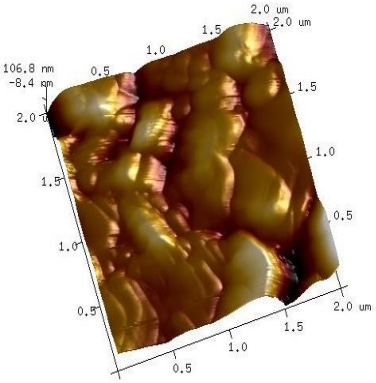

(d)

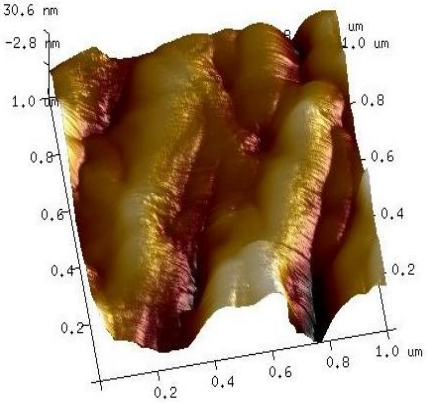

(h)

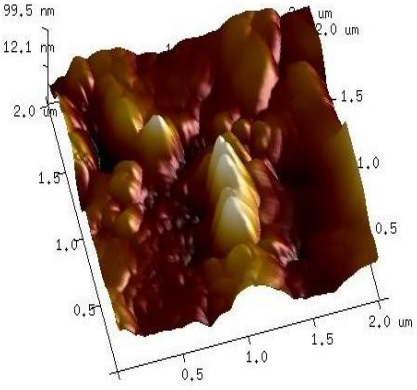

(i)

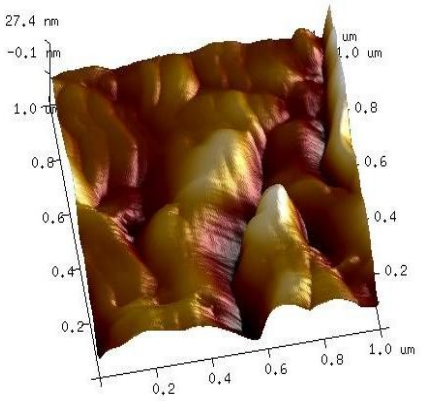
27.4 nm
-0.1 nm
1.0 um
0.8
0.6
0.4
0.2
0.2
0.4
0.6
0.8
1.0 um

(m)

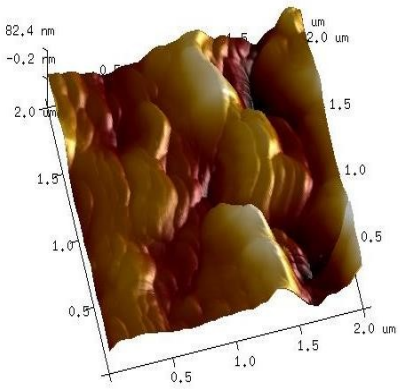
82.4 nm
-0.2 nm
2.0 um
1.5
1.0
0.5
0.5
1.0
1.5
2.0 um

(j)

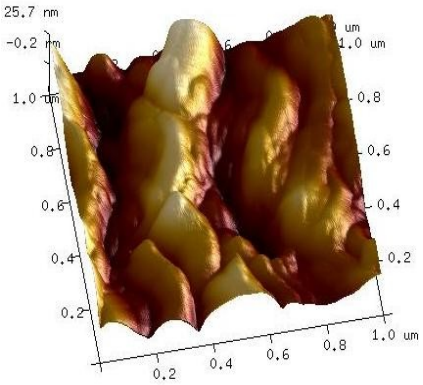
25.7 nm
-0.2 nm
1.0 um
0.8
0.6
0.4
0.2
0.2
0.4
0.6
0.8
1.0 um

(n)

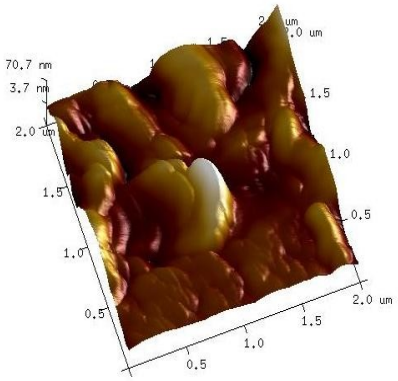
70.7 nm
3.7 nm
2.0 um
1.5
1.0
0.5
0.5
1.0
1.5
2.0 um

(k)

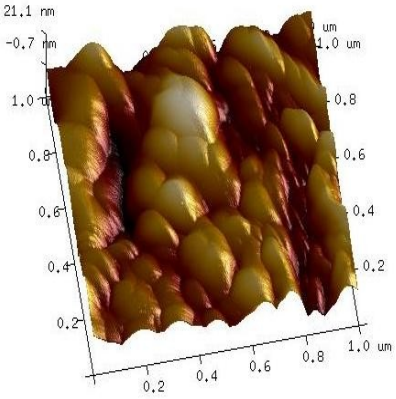
21.1 nm
-0.7 nm
1.0 um
0.8
0.6
0.4
0.2
0.2
0.4
0.6
0.8
1.0 um

(o)

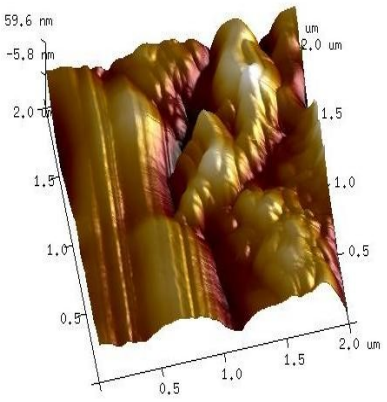
59.6 nm
-5.8 nm
2.0 um
1.5
1.0
0.5
0.5
1.0
1.5
2.0 um

(l)

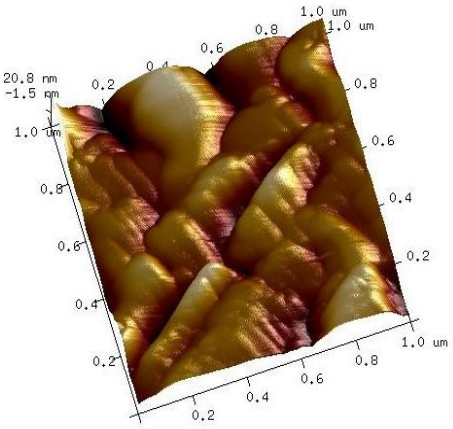
20.8 nm
-1.5 nm
1.0 um
0.8
0.6
0.4
0.2
0.2
0.4
0.6
0.8
1.0 um

(p)

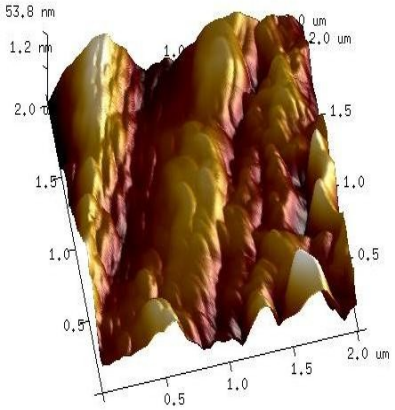
53.8 nm
1.2 nm
2.0 um
1.5
1.0
0.5
0.5
1.0
1.5
2.0 um

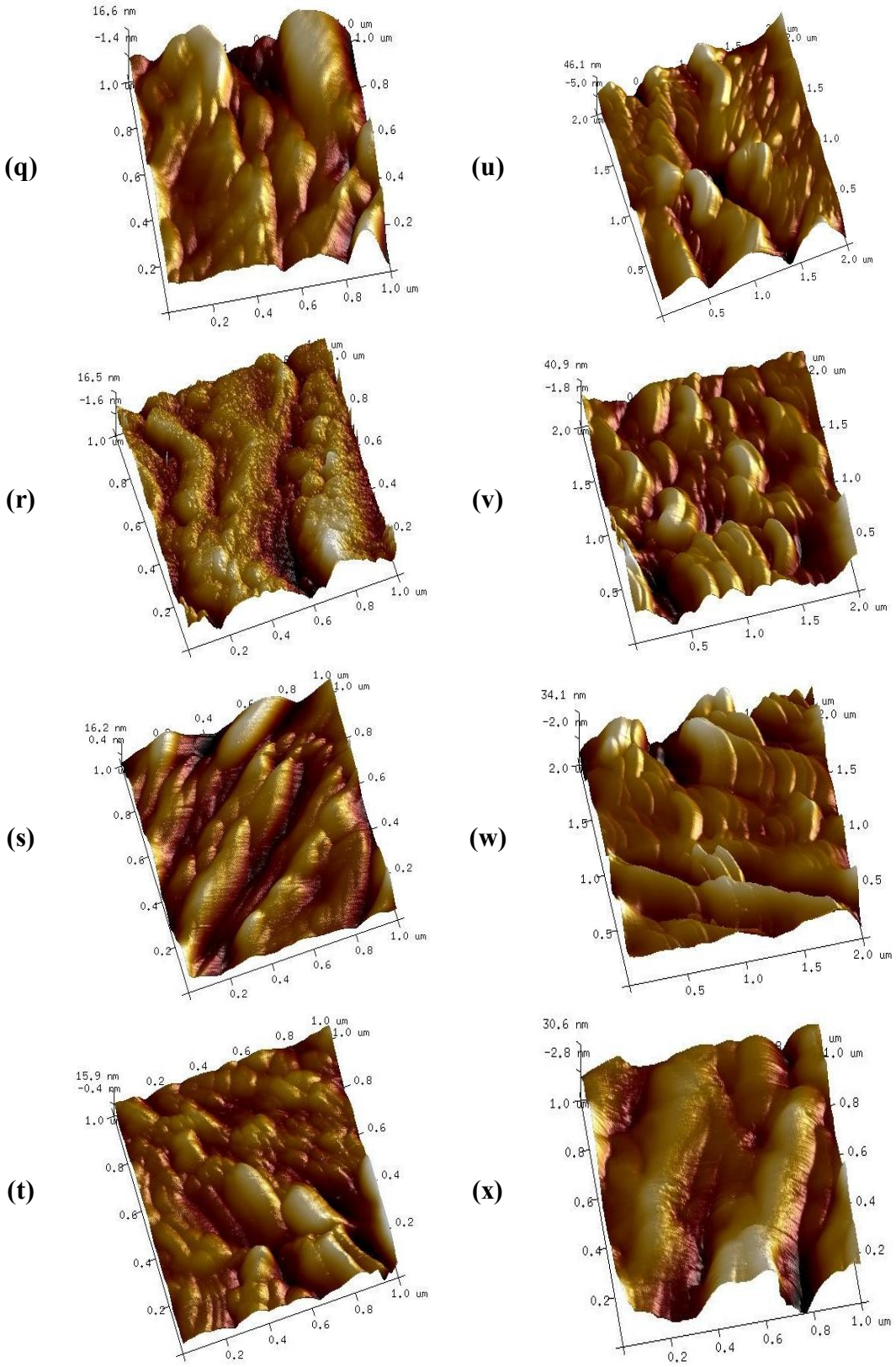

Figure 6.8 AFM image of plain and worn out surfaces for uncoated and coated granite particulate reinforced aluminum alloyed composites

6.9 Corrosion rate variation with time

Figure 6.9 shows the corrosion rate variation with time for uncoated, single layer and multilayer coated granite powder reinforced aluminium alloy composites. It is observed, that that corrosion rate decreases with time for uncoated, single layer and multilayer coated granite particulate reinforced aluminium alloy composites in order. The corrosion rate further decreases with filler content irrespective of formulations. This may attributed to the formation of protective oxide layer on the upper surface of the samples with time that proves to be much harder than the original surface thereby inhibiting corrosion. Similar observations are reported by Seetharaman et al. [182] and Pardo et al. [176] for AA2024 aluminium alloy and AZ92 magnesium alloy respectively.

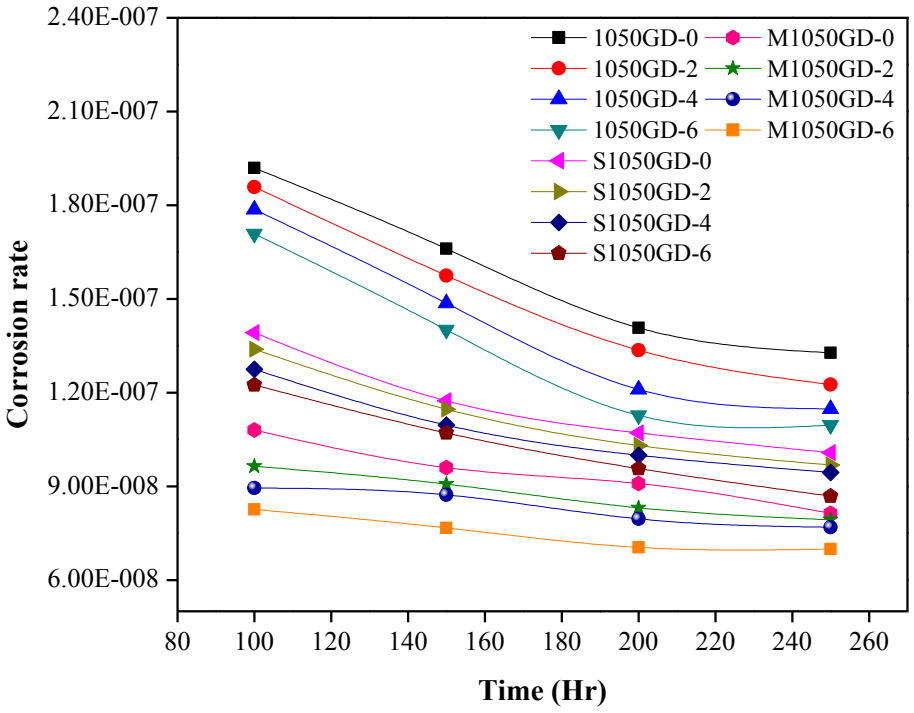

Figure 6.9 Variations in corrosion rate with time for uncoated / single-layer coated / multi-layered coated granite particulate filled AA1050 alloyed composites

6.10 Corrosion rate variation with pH

The Figure 6.10 shows the corrosion rate variation with pH of the solution for uncoated, single layer and multilayer coated granite powder reinforced aluminium alloy composites. It is observed, that that corrosion rate increases with pH of the solution for uncoated, single layer and multilayer coated granite particulate reinforced aluminium alloy composites in order. It is observed that corrosion rate increases with pH value of the solution irrespective of the formulation. However, the same observed to be decreasing with filler content at a particular pH of solution. This may attributed to the fact that as the pH value increases the number of free ions impact on the surface becomes high and it further enhances corrosion rate of samples material. Similar observation are reported by Lopez et al. [186] for TiN coated stainless steel and Jegadeeswaran et al. [205] for HVOF sprayed Al_2O_3 + CoCrAlTaY on Ti-31 alloy.

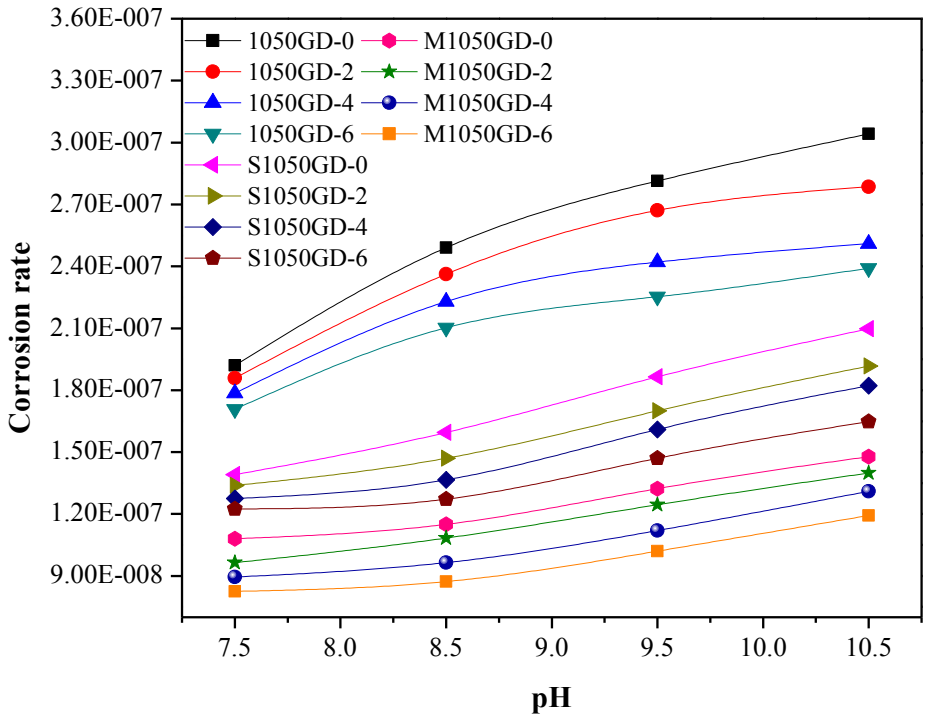

Figure 6.10 Variation in corrosion rate with pH for uncoated / single-layer coated / multi-layered coated granite particulate filled AA1050 alloyed composites

PART-II

Slurry erosive and corrosion wear behaviour of uncoated / single-layer coated / multi-layered coated granite particulate filled AA5083 alloyed composites

6.11. Steady state erosion of uncoated / single-layer coated / multi-layered coated granite particulate filled AA5083 alloyed composites

Erosion wear phenomenon may use air or water as a medium. When air is used as a medium, it is termed as air-jet erosive wear, alternatively when water is used as medium; it is termed as slurry -jet erosive wear. In slurry erosion wear, there is repeated impact of hard abrasive particle along with water (known as silt) on the surface of the specimen. The rate of slurry erosion is reported [6-14] to be governed by parameters like impact velocity of slurry, impingement angle, slurry concentration, particle shape and size. High rate of erosion may results in functionality failure of the parts in machines along with regular wear/tear/deformation failure.

In the present work, steady state slurry erosion wear rate behaviour of the investigated composites as a function of impact velocity (i.e. 10 m/sec. to 25 m/sec.), erodent discharge (160 g/min. to 280 g/min.) and impingement angle (30-75°) under constant operating conditions are discussed briefly.

6.11.1 Effect of impact velocity on reinforcement and coating

The variation of slurry erosion rate for impact velocity (10-25 m/sec) with constant parameters (time 10 minute, impingement angle 45º, erodent discharge 160 g/min) is shown in Figure 6.11 From the Figure 6.11 it is observed that slurry erosion rate increases with impact velocity for uncoated and coated aluminium alloyed composites. Hutching et al. [4] reported that the impact velocity is proportional to the erosion rate and as impact velocity increases slurry erosion rate but it also depends on the hardness of samples. From Figure 6.11 it is reveals that for unreinforced composites shows maximum erosion rate and it is decreases with the granite particulate addition into matrix material. Patnaik et al. [287] and Ramesh et al.[72] observed similar observation for ZA-27 and 6061 alloy composites respectively. After deposition of single layer (chromium nitride) coating on above said set of granite reinforced samples erosion rate is enhance with respect to increment in velocity. Single layer coated sample shows less wear as compared to uncoated samples.

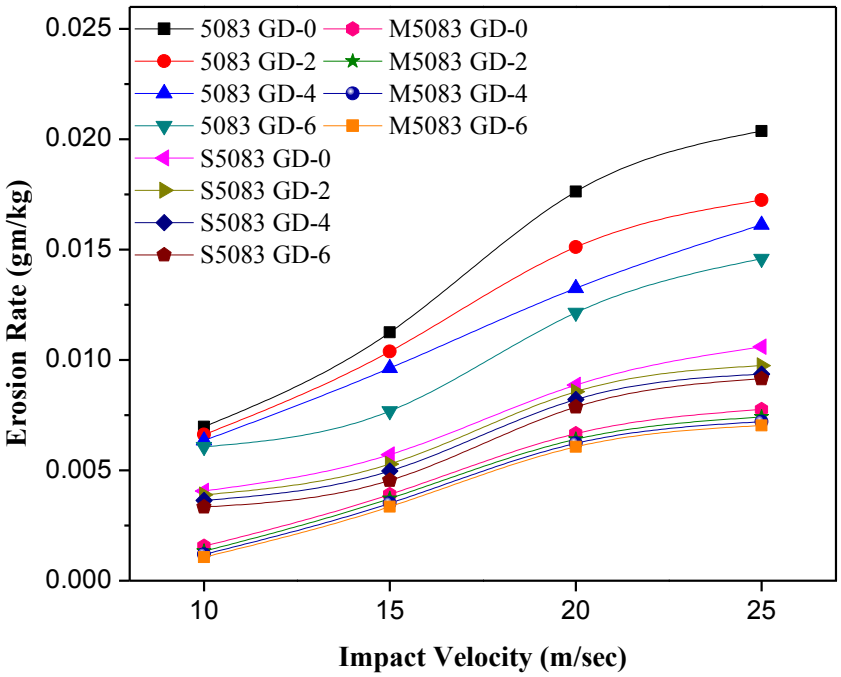

Figure 6.11 Variations in Erosion rate with impact velocity for uncoated / single-layer coated / multi-layered coated granite particulate filled AA5083 alloyed composites

The reduction in erosion rate may be attributed to the deposited hard coating and its less deformation. On further deposition of multilayer (Silicon nitride/chromium nitride) coating on above said set of granite reinforced samples erosion rate is enhance with respect to increment in velocity as compared to single layer coated granite reinforced samples. However, multilayer (Silicon nitride/chromium nitride) coated samples the hardness is still higher as compared to single layer particulate filled composites. Multilayer coating is multiphase diffusion of two coating materials and formed harder surface that's why erosion rate is minimum for multilayer coated samples. Similar erosion pattern are reported by Ramesh et al. [219] for uncoated aluminium alloy and Grewal et al. [237] for WC-Co-Cr coated steel samples. Decay in erosion rate with respect to impact velocity followed the order: Multilayer coated< single layer coated<uncoated aluminium alloy.

6.11.2 Effect of slurry concentration on reinforcement and coating

The effect of slurry concentration on erosion rate of uncoated / single-layer coated / multi-layered coated granite particulate filled AA5083 alloyed composites has been presented in Figure

6.12. From Figure 6.12 it is observed that mass loss for uncoated granite powder reinforced composites increases with slurry concentration. This may attributed to increase in the impacting erodent quantity or concentration per unit target surface area. Further, with increase in granite particulate content in respective formulations, the erosion rate observed to be diminished by small magnitude. The similar results are reported by various scholars like Das et al. [8] while investigating erosion wear rate of Al-SiC composite; Ramesh et al. [72] while investigating 6061 ally; Saini et al. [303] and Finnie [305] reported similar linear response of the volume wear loss of the material with slurry concentration.

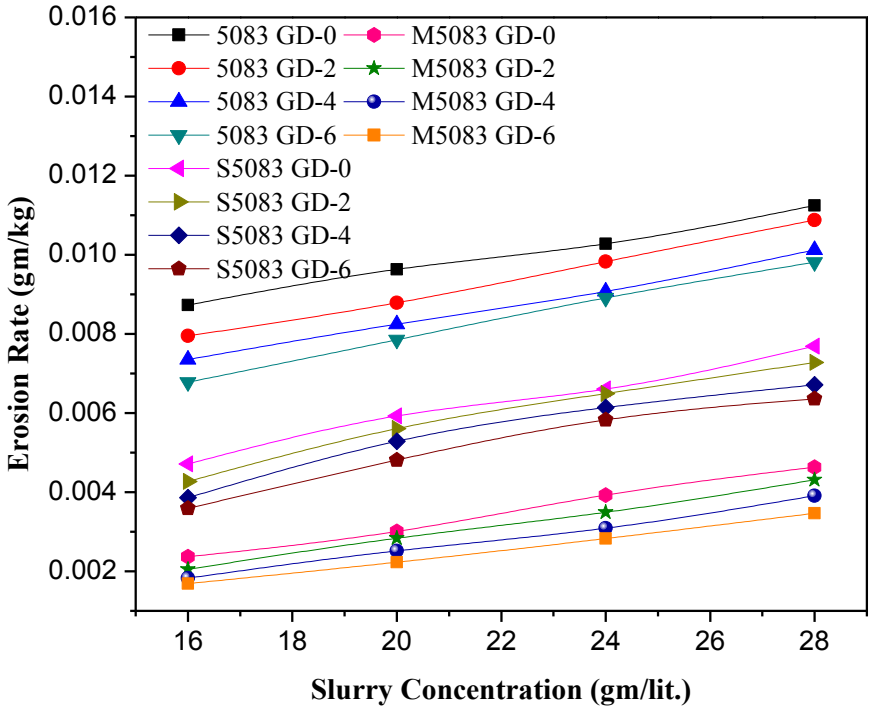

Figure 6.12 Variation in Erosion rate with Slurry concentration for uncoated / single-layer coated / multi-layered coated granite particulate filled AA5083 alloyed composites

Chromium Nitride and silicon nitride/chromium nitride coated granite powder reinforced aluminium alloy composites indicated less slurry erosive wear loss for all the slurry concentration studied. The improvement in the slurry erosion resistance of the coatings can be attributed to the following reasons. Single layer chromium nitride coating has good hardness and high toughness and corrosion resistance. Chromium nitride hardness is three times higher as compared to oxides. Multilayer Silicon/chromium nitride hardness improved due to multiphase

combination of different coating and form stable thin film which are corrosion protective in nature thereby enhancing the slurry erosion resistance of the coatings. Similar observation is reported for slurry concentration observed by [2]. However, the increased mass loss with increase in slurry concentration of all the studied materials can be attributed to fact that, increased abrasive particle concentration in the slurry enhanced the probability of more impingements on the surfaces leading to increased deterioration of material from its surfaces. For all slurry concentration wear rate in ascending order follows as Multilayer coated <Single layer coated<Uncoated Granite powder reinforced aluminium alloyed composites.

6.11.3 Effect of impingement angle on reinforcement and coating

The impingement angle of the erodent plays a significant role in the erosion process, which can affect the mechanism of erosion significantly. The effect of erodent impingement angle on erosion rate of uncoated and coated granite powder reinforced aluminium alloyed composites is shown in Figure 6.13. The erosion rate is computed keeping constant parameters like impact velocity (=15 m/sec.), slurry concentration (16 g/lts), time (=10 min.) and varying impingement angle (from 30° to 75°). From the graph it is observed that erosion rate is increases with increment in impingement angle up to 60º after that it slow down for all granite reinforced and unreinforced composites. The increment in erosion rate at lower angle is due to presence of micro cutting erosion mechanism and it slow down because at higher angle plastic deformation of surface erosion mechanism obtained. From the graph it is also observed that maximum erosion rate for unreinforced aluminium composites and it is decreases with addition of granite powder into aluminium matrix. The similar erosion pattern for impingement angle for titania reinforced is found by Patnaik et al. [287].

As observed from this analysis the slurry erosion rate trend of single layer coated sample it shows similar trend as uncoated granite powder reinforced aluminium alloyed composites but it seems to less. The decay in erosion rate is due to its hardness and toughness of coating and corrosion resistance. The plastic deformation of hard coated surface is less. Similar observation is reported by [235,238]. Again multilayer coated granite reinforced aluminium alloyed composites shows similar trend of slurry erosion rate for all impingement angle. Slurry erosion rate of multilayer coated samples is less as compared to uncoated and single layer coated granite powder reinforced aluminium alloyed composites. As hardness of coating increased its scratch and abrasion resistance properties enhanced simultaneously its resistance for plastic deformation

also increased. Uncoated sample indicated maximum wear for impingement angle than single layer (chromium nitride) coated, multilayer (silicon nitride/chromium nitride) coated in descending order.

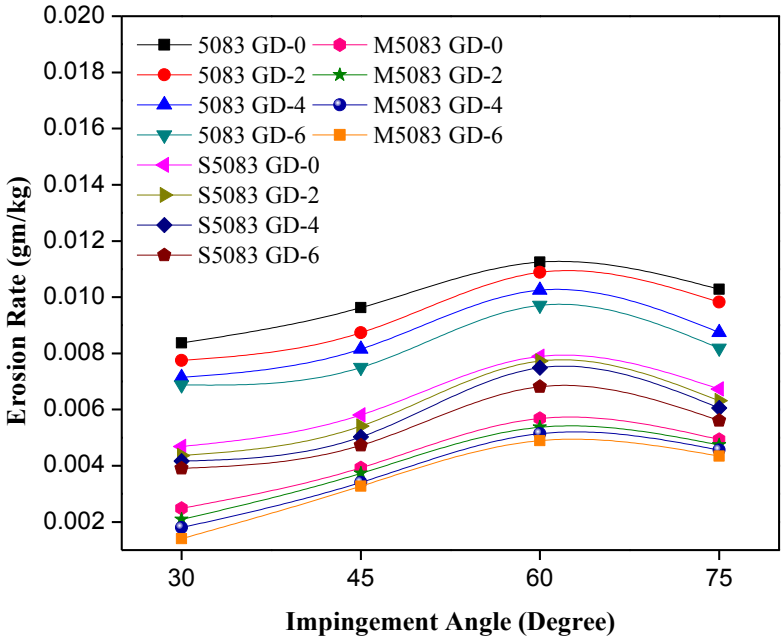

Figure 6.13 Variation in Erosion rate with Impingement angle for uncoated / single-layer coated / multi-layered coated granite particulate filled AA5083 alloyed composites

6.12. Taguchi experimental results for uncoated / single-layer coated / multi-layered coated granite particulate filled AA5083 alloyed composites

The overall mean S/N ratio of the wear rate is found to be 43.89, 49.30, 51.06 db for uncoated, single layer coated, multilayer coated granite powder reinforced aluminium alloyed composites respectively (Table 6.5). The analysis is made using the popular software specifically used for design of experiment applications known as MINITAB 15. Thus factorial design incorporates a simple means of testing for the presence of the interaction effects. The main effect plots in Figure 6.14(a-c) shown the effects of individual control factors on the erosive wear of the composite can be clearly seen. Maximum S/N ratio corresponds to minimum wear rate and minimum S/N ratio corresponds to maximum wear rate. Figure 6.14a effect of control factors on the erosion rate of granite filled aluminium alloyed composites.

Thus from Figure 6.14a, it is observed that wear loss decreases (maximum S/N ratio) with increased in impact velocity at level-1 (at 10 m/sec.), filler content at level-4 (at 6 wt.%), Impingement angle at level-4 (at 75º) and Erodent Discharge at level-4 (at 280 g/min.) respectively. Moreover, the granite particles act as resistance to further destructive action of abrasion by wear debris. Analysis of the result lead to the conclusion that factor combination of A_1, B_4, C_4, and D_4gives minimum erosion rate for uncoated granite filled metal alloy composites. This analysis is established that wear rate also depended upon the types of filler and fabrication methodology.

Thus from Figure 6.14b, it is observed that wear loss decreases (maximum S/N ratio) with increase in impact velocity at level-1 (at 10 m/sec.), filler content at level-4 (at 6 wt.%), Impingement angle at level-3 (at 60º), and Erodent Discharge at level-4 (at 280 gm/min) respectively. Moreover, the granite particles act as resistance to further destructive action of abrasion by wear debris. Analysis of the result lead to the conclusion that factor combination of A_1, B_4, C_3, and D_4 gives minimum erosion rate for uncoated granite filled metal alloy composites. This analysis established that wear rate also depended upon the types of filler, filler content, coating material and deposition methodology. Thus from Figure 6.14c, it is observed that wear loss decreases (maximum S/N ratio) with increase in impact velocity at level-1 (at 10 m/sec.), filler content at level-4 (at 6 wt.%), Impingement angle at level-2 (at 45º), and Erodent Discharge at level-3 (at 240 gm/min) respectively. Moreover, the granite particles act as resistance to further destructive action of abrasion by wear debris. Analysis of the result lead to the conclusion that factor combination of A_1, B_4, C2, and D3gives minimum erosion rate for uncoated granite filled metal alloy composites. This analysis established that wear rate also depended upon the types of filler, filler content, coating material and deposition technique.

Table 6.5 S/N ratio of wear rate of uncoated / single-layer coated / multi-layered coated granite particulate filled AA5083 alloyed composites

S. No	Filler Content (wt.%)	Impact Velocity (m/sec)	Impingement Angle (Degree)	Erodent Discharge (g/min)	Erosion Rate (uncoated)	S/N Ratio (db)	Erosion Rate (Single layer coated)	S/N Ratio (db)	Erosion Rate (Multilayer coated)	S/N Ratio (db)
1.	0	10	30	160	0.005167	45.74	0.0031950	49.91	0.0032100	49.87
2.	0	15	45	200	0.005239	45.62	0.0038945	48.19	0.004060	47.83
3.	0	20	60	240	0.008489	41.42	0.0043925	47.15	0.0046210	46.71
4.	0	25	75	280	0.009679	40.28	0.0047628	46.44	0.0053350	45.46
5.	2	10	45	240	0.0035969	48.88	0.0021930	53.18	0.0024040	52.38
6.	2	15	30	280	0.0037963	48.41	0.0026971	51.38	0.0028150	51.01
7.	2	20	75	160	0.006579	43.64	0.0046980	46.56	0.0043600	47.21
8.	2	25	60	200	0.089893	20.93	0.0041094	47.72	0.0045309	46.88
9.	4	10	60	280	0.0027969	51.07	0.0021950	53.17	0.0016050	55.89
10.	4	15	75	240	0.0050297	45.97	0.0032160	49.85	0.0017010	55.39
11.	4	20	30	200	0.0057319	44.83	0.0040960	47.75	0.0025100	52.01
12.	4	25	45	160	0.010945	39.22	0.0043695	47.19	0.0025110	52.00
13.	6	10	75	200	0.0024637	52.17	0.0021500	53.35	0.0016150	55.84
14.	6	15	60	160	0.006012	44.42	0.0031425	50.06	0.0018169	54.81
15.	6	20	45	280	0.0041696	47.60	0.0035403	49.02	0.0022982	52.77
16.	6	25	30	240	0.0079136	42.03	0.0040115	47.93	0.0028380	50.94

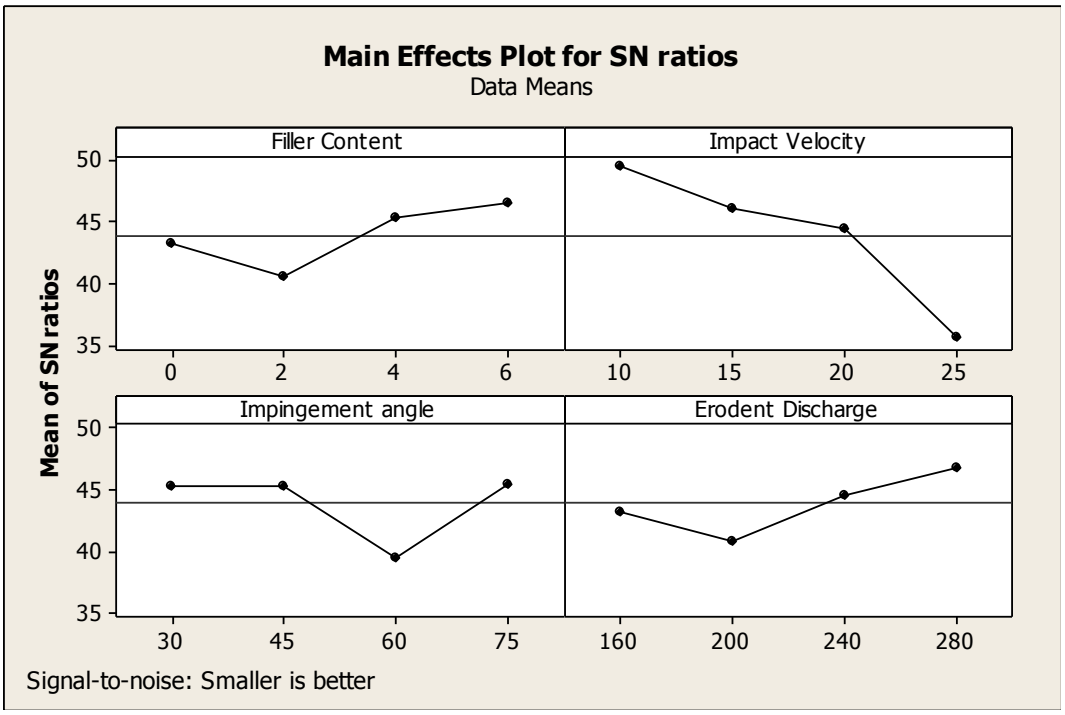

Figure 6.14a Effect of control factors on the Erosion rate of uncoated granite filled aluminium alloyed composites

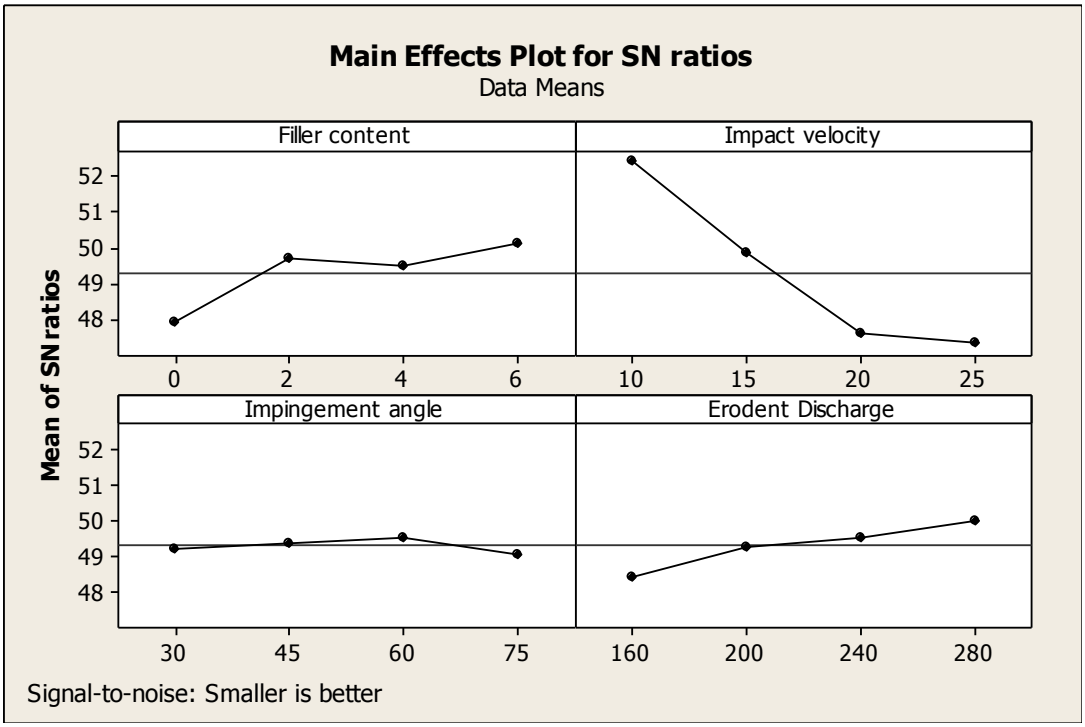

Figure 6.14b Effect of control factors on the Erosion rate of Single layer coated granite filled aluminium alloyed composites

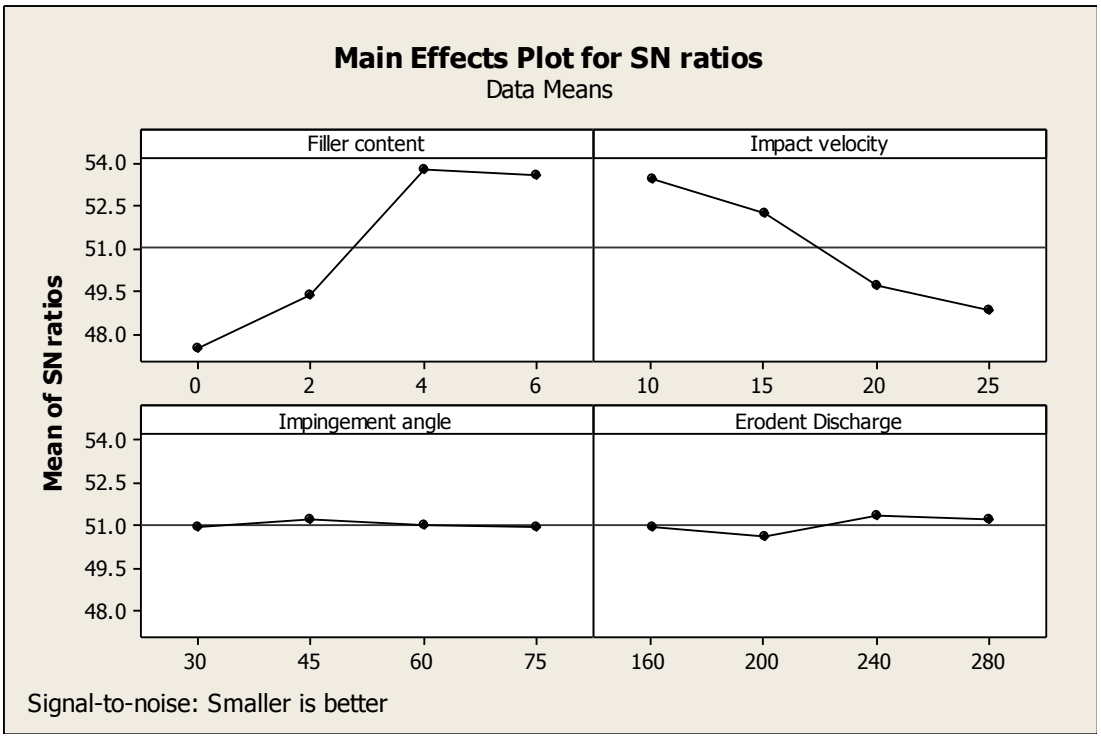

Figure 6.14c Effect of control factors on the Erosion rate of multilayer coated granite filled aluminium alloyed composites

6.13 ANOVA Analysis

In order to understand impact of various factors effect on the output performance, it is desirable to perform analysis of variance (ANOVA) to find out the order of significant factors. Table 6.6 (a-c) shows results of the ANOVA with the specific wear rate. This analysis is undertaken for a level of significance is 95 %. The last column of the table is indicated the order of significance among factors.

From Table 6.6a, it can be observed that the impact velocity (p = 0.104), filler content (p = 0.484), erodent discharge (p = 0.524), impingement angle (p = 0.416) have positive influence on slurry erosion rate. Among these factors, impact velocity is indicated the most significant effect on wear rate and erodent discharge is observed to be less significant effect on wear rate for uncoated granite powder reinforced composites.

On other hand from Table 6.6b, it can be observed that granite filled aluminium alloyed composites the impact velocity (p = 0.005), erodent discharge (p = 0.161), filler content (p = 0.066), impingement angle (p = 0.801) have positive influence on slurry erosion rate. Among these factor, impact velocity indicated most significant effect on wear rate and impingement

angle indicated less significant effect on wear rate for single layer coated granite powder reinforced composites.

Again from Table 6.6c, it can observe that the filler content (p = 0.004), impact velocity (p = 0.010), erodent discharge (p = 0.636), impingement angle (p = 0.951) have influence on slurry erosion rate. Among these factors, multilayer coated filler content indicated most significant effect on wear rate and impingement angle indicated less significant effect on wear rate for multilayer coated granite powder reinforced composites.

Table 6.6a ANOVA table of uncoated granite filled aluminium alloyed composites for wear rate

Source	DF	Seq SS	Adj SS	Adj MS	F	P	Rank	%
Filler Content	3	84.55	84.55	28.18	1.05	0.484	3	12.36
Impact Velocity	3	418.72	418.72	139.57	5.21	0.104	1	61.36
Impingement Angle	3	104.81	104.81	34.94	1.30	0.416	2	15.31
Erodent Discharge	3	74.43	74.43	24.81	0.93	0.524	4	10.95
Error	3	80.35	80.35	26.78				
Total	15	762.85						

Table 6.6b ANOVA table of Single layer coated granite filled aluminium alloyed composites for wear rate

Source	DF	Seq SS	Adj SS	Adj MS	F	P	Rank	%
Filler Content	3	10.9105	10.9105	3.6368	7.48	0.066	2	13.07
Impact Velocity	3	66.7411	66.7411	22.2470	45.79	0.005	1	80.05
Impingement Angle	3	0.4942	0.4942	0.1647	0.34	0.801	4	0.59
Erodent Discharge	3	5.2283	5.2283	1.7428	3.59	0.161	3	6.27
Error	3	1.4576	1.4576	0.4859				
Total	15	84.8316						

Table 6.6c ANOVA table of Multilayer Coated granite filled aluminium alloyed composites for wear rate

Source	DF	Seq SS	Adj SS	Adj MS	F	P	Rank	%
Filler Content	3	119.229	119.229	39.743	59.89	0.004	1	66.99
Impact Velocity	3	57.241	57.241	19.080	28.75	0.010	2	28.80
Impingement Angle	3	0.213	0.213	0.071	0.11	0.951	4	0.12
Erodent Discharge	3	1.286	1.286	0.429	0.65	0.636	3	0.72
Error	3	1.991	1.991	0.664				
Total	15	179.960						

6.14 Confirmation Experiment

The confirmation experiment is performed with a new combination of factors and levels used during wear test. The purpose of confirmation experiment is to evaluate the optimum condition for wear test with optimal levels of selecting parameters. It established relationship between theoretical value and experimental value of slurry erosion wear. The estimated S/N ratio for slurry erosion wear can be calculated by predictive equation: (Eqs. 6.3 and 6.4)

$$\eta = \eta_m + \sum_{i=1}^{n} (\bar{\eta}_1 - \eta_m) \tag{6.3}$$

$$\eta = \bar{T} + (\bar{A}_3 - \bar{T}) + (\bar{B}_3 - \bar{T}) + (\bar{C}_4 - \bar{T}) + (\bar{D}_4 - \bar{T}) \tag{6.4}$$

In this study the confirmation has been performed by taking an arbitrary set of factor combination $A_3B_3C_4D_4$for uncoated, single layer coated, multilayer coated granite filled aluminium alloyed composites. A new combination of factor levels is used to predict deposition rate through prediction equation and it is found to be 37.7874, 48.1692 and 52.5630 db for uncoated, single layer coated, multilayer coated samples respectively. For each performance measure, an experiment is conducted for a different factors combination and compared with the result obtained from the predictive equation as shown in Table 6.7. Actual runs are performed to verify if the results obtained by above equations are acceptable. It is found that when actual runs have been performed on above factor settings an error of 4.38%, 2.67% and 2.63% for uncoated, single layer coated, multilayer coated granite filled aluminium alloyed composites and it well

within the reasonable limits. The error can be reduced if the number of runs are enhanced. This verifies that the predicted values are reliable and testified the validity of this model for predicting the performance output on the basis of input characteristics.

Table 6.7 Results of the confirmation experiments for wear rate of uncoated / single-layer coated / multi-layered coated granite particulate filled AA5083 alloyed composites

	Optimum control parameters		Error
	Prediction	Experimental	
Level	$A_3B_3C_4D_4$	$A_3B_3C_4D_4$	%
S/N ratio for wear rate (db) for uncoated granite dust reinforced aluminium alloyed composites	48.2561	46.1413	4.38
S/N ratio for wear rate (db) for single layer coated granite dust reinforced aluminium alloyed composites	50.3332	48.9873	2.67
S/N ratio for wear rate (db) for multilayer coated granite dust reinforced aluminium alloyed composites	52.6549	51.2671	2.63

6.15 Microstructure analysis of the worn surface by varying impact velocity

SEM image for uncoated, single layer and multilayer coated eroded samples for two different velocities were shown in Figure 6.15(a-f). Figure 6.15(a) and 6.15(b) indicates the micrographs obtained by impact velocity at 25 m/sec. and 10 m/sec. for 0 wt.% granite powder reinforced and unreinforced samples. From the image it is observed that at higher impact velocity extensive plastic deformation with characteristics as deep craters, plates and lips can be observed. The characteristics of the eroded surface is observed that severe plastic deformation occurred and materials were displaced randomly first before being removed. The embedded erosive erodent particles are also found over the eroded composite surface and indicate the soft/ductile nature of the alloy.

Uncoated

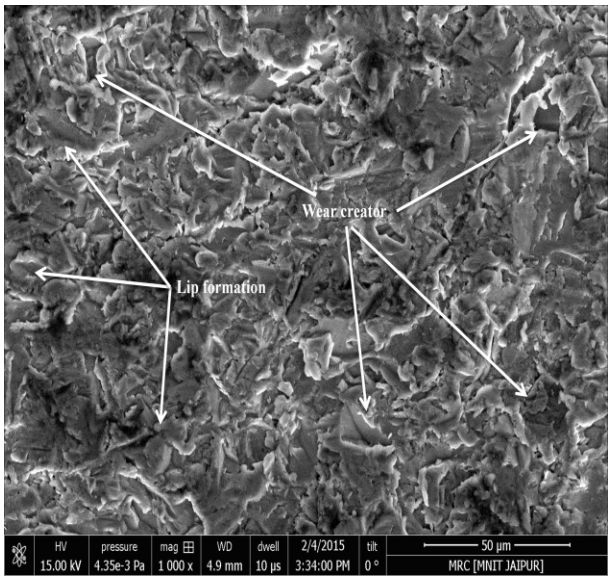

a. Uncoated impact velocity 10 m/sec., impingement angle 45º, erodent discharge 160 g/min., time 10 min

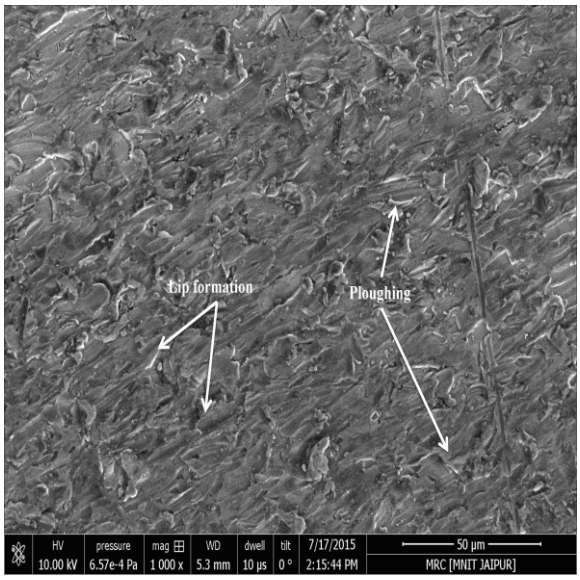

b. Uncoated impact velocity 25 m/sec., impingement angle 45º, erodent discharge 160 g/min., time 10 min

Single layer coated

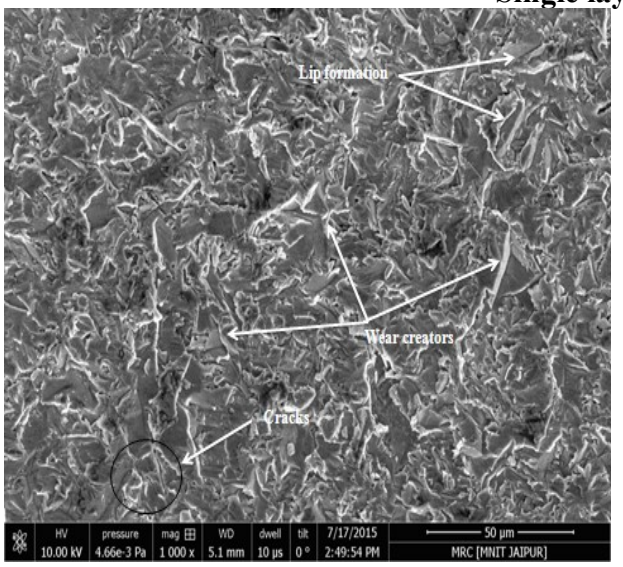

c. Single layer coated impact velocity 10m/sec., impingement angle 45º, erodent discharge 160 g/min., time 10 min

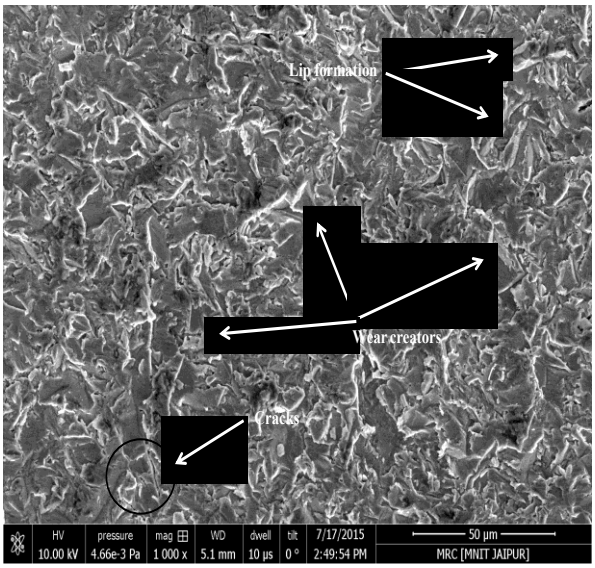

d. Single layer coated impact velocity 25 m/sec., impingement angle 45º, erodent discharge 160 g/min., time 10 min

Multilayer coated

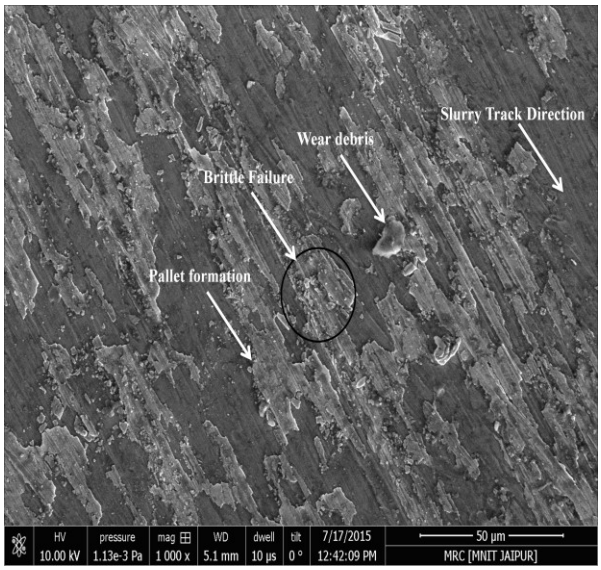

e. Multilayer coated impact velocity 10 m/sec., impingement angle 45º, erodent discharge 160 g/min, time 10 min

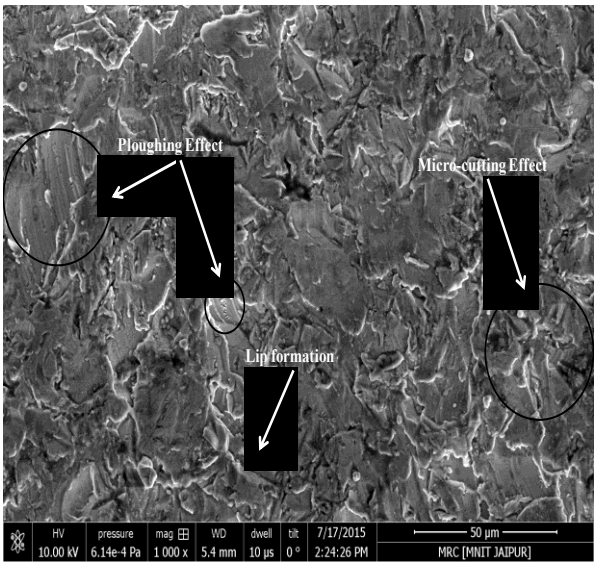

f. Multilayer coated impact velocity 25 m/sec., impingement angle 75º, erodent discharge 160 g/min, time 10 min

Figure 6.15 SEM image of uncoated, single layer coated, multilayer coated eroded sample

On the other hand, with decreased in impact velocity (10 m/sec), at lower impingement angle (45°) and slurry concentration the erosion rate indicated lowest among unfilled composites. The eroded surface of single layer coated samples, SEM image shown in Figures 6.15(c) and 6.15(d) for same experiments velocity 25 m/sec and 10 m/sec. Single layer coated samples the wear rate are less as compared to uncoated sample due to high hardness of deposited layer. An increased in hardness below the eroded surface due to work-hardening also helps in explaining the erosion mechanism (plastic deformation) proposed. With further continuation of the impact process, brittleness of the material could be increased due to extensive work-hardening. This would result into the removal of material from the surface in the form of small fragments as illustrated. From SEM image it also evident that amount of craters, plates and lips are less as compared to SEM image of uncoated samples.

Again multilayer coated eroded samples SEM image shown in Figures 6.15(e) and 6.15(f) for velocity 25 m/sec and 10 m/sec. Multilayer coated samples wear rate is less as compared to uncoated sample due to hardness of layer as deposit layer is removed than particles strike on the surface of granite reinforced composites. An increase in hardness below the eroded surface due to work-hardening also helps in explaining the erosion mechanism (plastic

deformation) proposed. With further continuation of the impact process, brittleness of the material could increase due to extensive work-hardening. This would result in the removal of material from the surface in the form of small fragments as illustrated from SEM image (Figures 6.15(e) and 6.15(f)) it evident that amount of craters, plates and lips are less as compared to SEM image of uncoated samples

From all SEM images it is also observed that the surface eroded at slow-impact velocity is less plastically deformed in comparison with one eroded at high velocity. The removal of material through platelet mechanism is comparatively a slow process [305,306]. It requires higher number of impacts in comparison with micro-cutting or ploughing for the final detachment of the material. After the formation of platelets the continuous impacts of subsequent particle would result in flattening of the platelets [307,308]. When strain value of surface exceed to a limit cracks were generated. This process will eventually result in the removal of material in the form of small fragments, indicating the presence of fatigue phenomena. Along with platelet mechanism, extensive plastic deformation is also playing a significant role in the erosion process at high velocity. The supporting trend in erosion rates is already discussed in section 6.9.1 for appeared observation of SEM images.

6.16 Microstructure analysis of the worn surface by varying slurry concentration

The effect of slurry concentration on the erosion mechanism can be observed from Figure 6.16(a-f) for uncoated, single layer coated and multilayer coated samples. Figure 6.16(a) and 6.16(b) represents the eroded surface SEM image of uncoated granite powder reinforced aluminium alloyed composites for lower and higher slurry concentration. For the images it is observed that as the slurry concentration is increases the rate of impingement particles per unit are increased. The material removal took place through platelet mechanism at normal impacts and ploughing along with Micro-cutting process (Mcp) at acute impingement angle. However, it is to be noticed that intensity of the slurry concentration is significantly affected. At lower concentration the amount of micro-ploughing is less as slurry concentration increase ploughing effect increase and wear crater also. When we observed the SEM image 6.16(c) and 6.16(d) of single layer coated granite powder reinforced aluminium alloyed composites for same experiments. We found that scratch generated by impingement of hard abrasive particles is seemes to less as compared to uncoated samples. Hardness of coating is only parameter which

ensures scratch and abrasion resistance and it represents high resistance for plastic deformation during contact events. Single layer (chromium nitride) coating is three times harder than oxides coating.

Uncoated

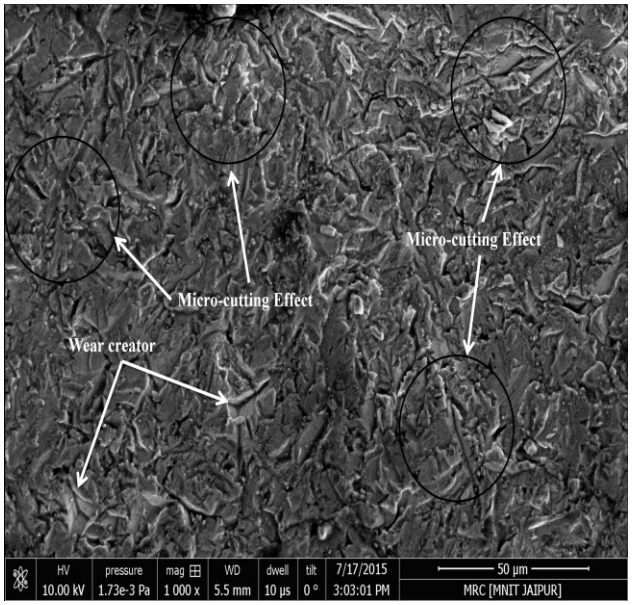

a. Uncoated, impact velocity 15 m/sec, impingement angle 75^0, erodent discharge 200 g/min, time 10 min

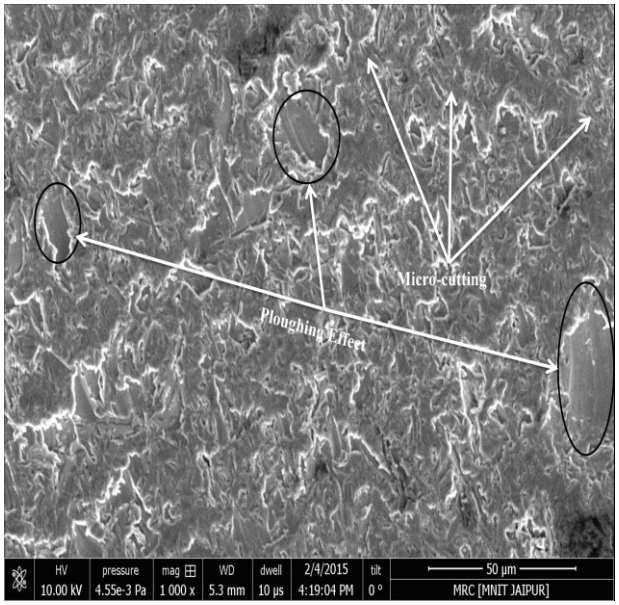

b. Uncoated, impact velocity 15 m/sec, impingement angle 75^0, erodent discharge 280 g/min, time 10 min

Single layer coated

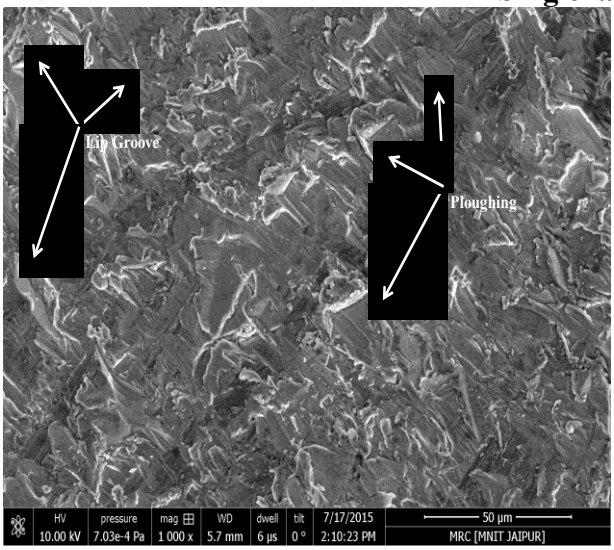

c. Single layer coated, impact velocity 15 m/sec, impingement angle 75^0, erodent discharge 160 g/min, time 10 min

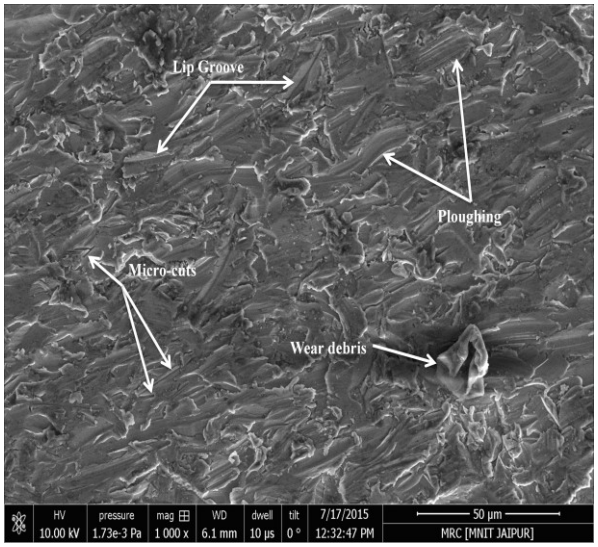

d. Single layer coated, impact velocity 15 m/sec, impingement angle 75^0, erodent discharge 280 g/min, time 10 min

Multilayer coated

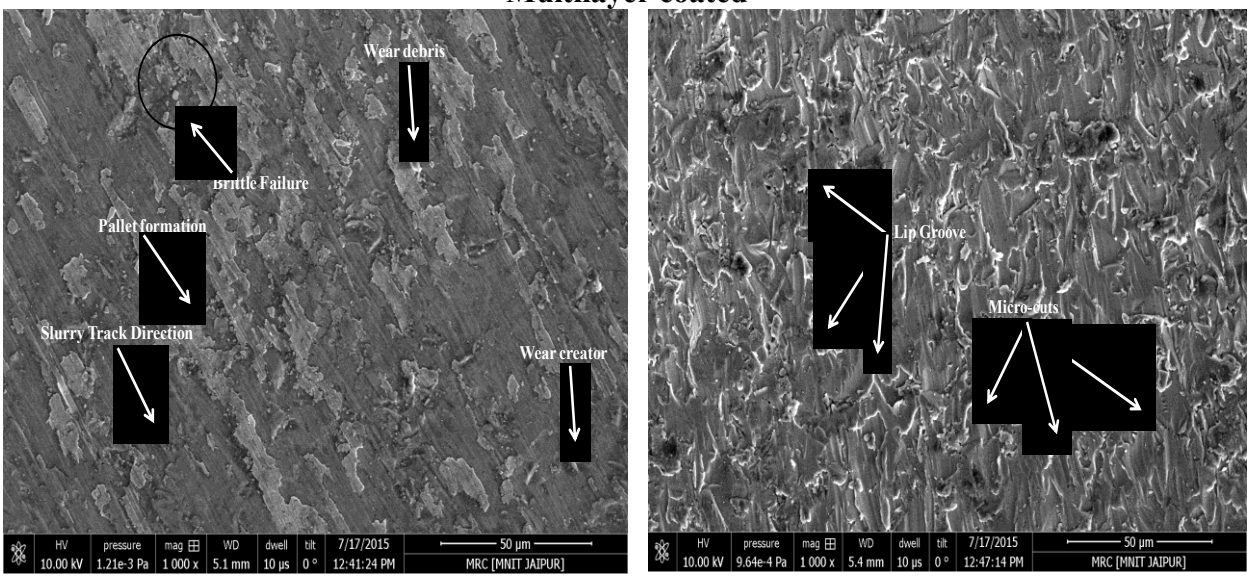

e. Multilayer coated, impact velocity 15 m/sec, impingement angle 75^0, erodent discharge 160 g/min, time 10 min

f. Multilayer coated, impact velocity 15 m/sec, impingement angle 75^0, erodent discharge 240 g/min, time 10 min

Figure 6.16 SEM image of uncoated, single layer coated, multilayer coated eroded sample

When we observed the SEM image 6.16(e) and 6.16(f) of multilayer coated granite powder reinforced aluminium alloyed composites for same experiments. We found that scratch generated by impingement of hard abrasive particles are seem to less as compared to uncoated and single layer coated samples. As hardness increased its scratch and abrasion resistance properties enhanced simultaneously its resistance for plastic deformation also increased. The supporting trend in erosion rates are already discussed in section 6.9.2 for appeared observation of SEM images.

6.17 Microstructure analysis of the worn surface by varying impingement angle

Effect of impingement angle on erosion mechanism shown in Figure 6.17(a-f) by uncoated, single layer coated, multilayer coated eroded samples for two different angles. From the SEM it is observed that the surface impacted at normal impingement angle showed the presence of platelets and plastically deformed target surface. The impact energy of the particles would make the material to deform plastically. This plastically deformed material would tend to flow outward and get accumulated around the impact crater. During subsequent impacts, this deformed material would get removed in the form of small fragments as discussed in preceding subsection. For surfaces impacted at acute angle, major material removal mechanisms were ploughing and mixed cutting-ploughing mode. Hutching [309] and Levy [310-312] have shown that with the

impact of round particles such as sphere, the material displaces and get accumulated at the end from where the particle leaves. This mechanism of material removal is generally known as ploughing. However, in our work, in addition to ploughing observed at acute impingement angle, the primary mode of material removal was the mixture of ploughing and micro-cutting mechanism. This mechanism was significantly different from what the earlier researchers have proposed, which the authors have named to be mixed cutting and ploughing (Mcp).

Uncoated

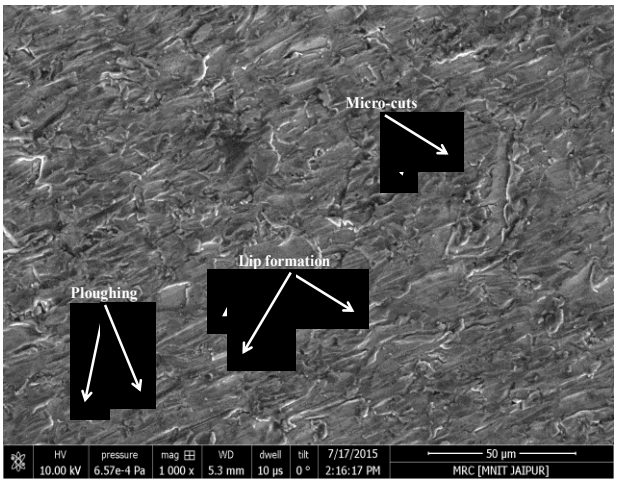

a. Uncoated, impact velocity 15 m/sec., impingement angle 30º, erodent discharge 280 g/min, time 10 min

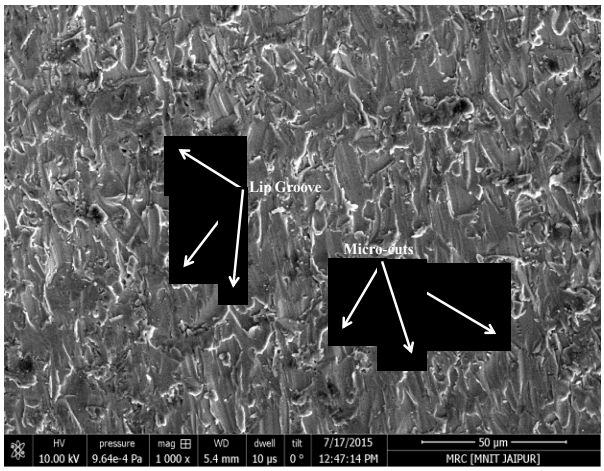

b. Uncoated, impact velocity 15 m/sec., impingement angle 60º, erodent discharge 200 g/min, time 10 min

Single layer coated

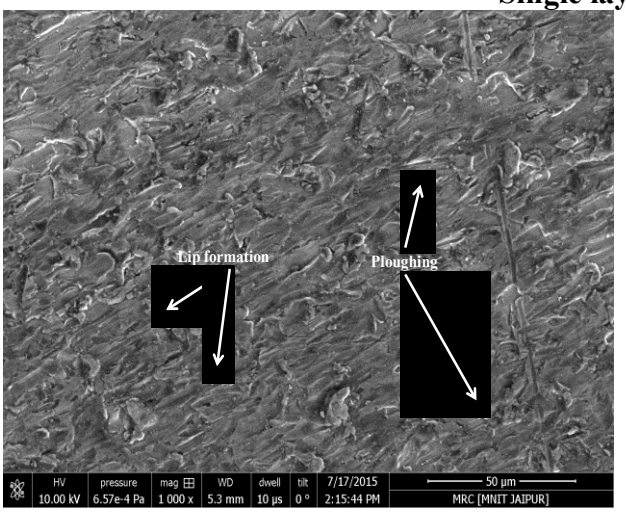

c. Single layer coated impact velocity 15 m/sec, impingement angle 45º, erodent discharge 240 g/min, time 10 min

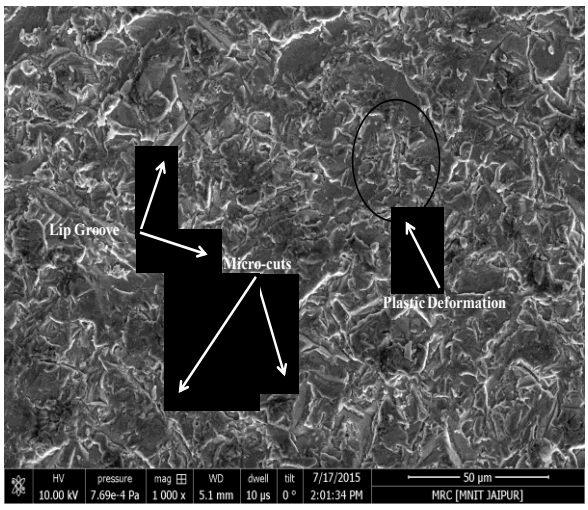

d. Single layer coated impact velocity 15 m/sec, impingement angle 75º, erodent discharge 200 g/min, time 10 min

Multilayer coated

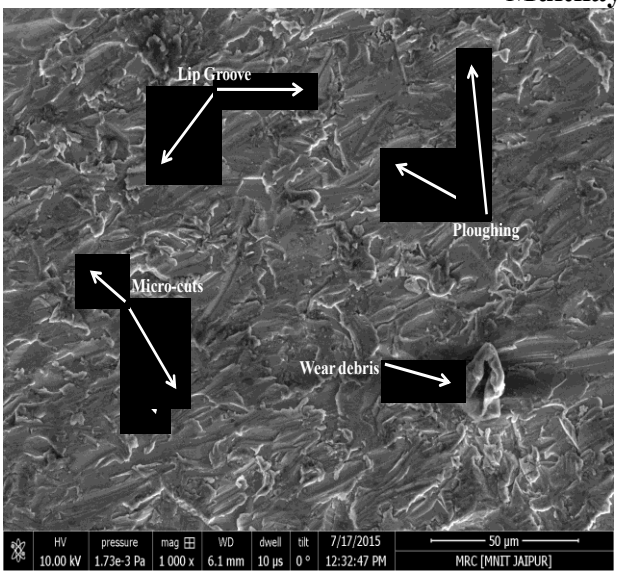

e. Multilayer coated impact velocity 25 m/sec., impingement angle 75º, erodent discharge 280 g/min, time 10 min

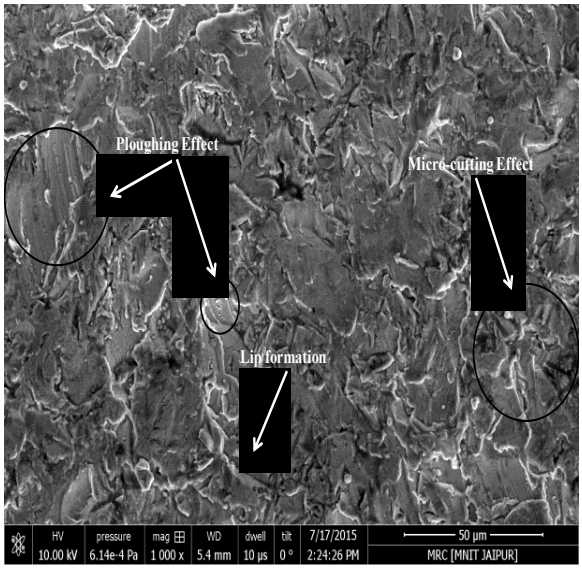

f. Multilayer coated impact velocity 25 m/sec., impingement angle 75º, erodent discharge 160 g/min, time 10 min

Figure 6.17 SEM image of uncoated, single layer coated, multilayer coated eroded sample

The SEM micrographs shown in Figure 6.17 clearly indicate the presence of Mcp mode. Moreover, the presence of this mode was more preferential than pure ploughing or micro-cutting. In continuation to the discussion of Sect. 6.9.3, the reason for the lower erosion rates for normal impingement angles in comparison with acute angle impingement could be easily explained in terms of erosion mechanism. Platelet mechanism as explained earlier is a slow process involving combined plastic deformation and fatigue phenomena. In contrast to it, micro-cutting and Mcp are more efficient mechanisms for the removal of material. This explains the cause as to why the erosion rates were higher at low impingement angles rather than at normal impact angle. This observation appears to be supporting the trend in erosion rates as discussed in Sect. 6.1.3.

6.18 AFM analysis of worn surfaces

The removal of material during wear leads to alternations in surface topology. Atomic force microscopy in contact mode served to evaluate the topology characterization of plain and worn surfaces. It is worth mentioning that all roughness values are given in terms of Ra which represents the arithmetic mean of height deviations from the mean profile value shown in Table

6.8. Figure 6.18 represents the AFM image of plain and worn surface of uncoated and coated granite powder reinforced aluminium alloyed composites. It is notice that nearly no surface defecates found in uncoated granite powder reinforced unworn surface samples. Worn surfaces samples show grooves, micro-ploughing and lip formation features of material removal or slurry track direction, which shows good agreement with results obtained from FE-SEM image of worn surfaces (Figure 6.16). The entire eroded surfaces AFM image for lower impact velocity, impingement angle 45º, erodent discharge 160 g/min for uncoated and coated granite powder reinforced aluminium alloyed composites.

Table 6.8 Surface roughness for plain surface and worn surface of uncoated, single layer coated, multilayer coated granite filled aluminium alloy composites

S. No.	Designation	Plain Surface Roughness (Ra)	Worn Surface Roughness (Ra)
Uncoated			
1	5083GD-0	15.9 nm	308 nm
2	5083GD-2	13.1 nm	268 nm
3	5083GD-4	11.7 nm	236 nm
4	5083GD-6	10.3 nm	196 nm
Single layered CrN Coated			
5	S5083GD-0	8.36 nm	140 nm
6	S5083GD-2	7.91 nm	119 nm
7	S5083GD-4	7.08 nm	99.4 nm
8	S5083GD-6	6.58 nm	89.6 nm
Multilayered SiN & CrN Coated			
9	M5083GD-0	6.13 nm	69.1 nm
10	M5083GD-2	5.43 nm	59.3 nm
11	M5083GD-4	3.93 nm	46.1 nm
12	M5083GD-6	2.93 nm	33.9 nm

AFM image of uneroded and eroded samples are compared and after slurry erosion the surface roughness value of increase and it depends on the erosion mechanism. The microstructure and surface roughness of uncoated 0 wt.% granite powder reinforced aluminium alloyed worn surface for operating condition impact velocity 10m/sec, impingement angle 45º,

erodent discharge 160 g/min shown in the SEM image 3(b) and AFM image 9(e) respectively. In SEM image Deep groove lip formation, micro cutting and wear craters features was found which show good agreement with AFM image. The roughness value of these features was found higher from AFM image due to the lower hardness of base material. On other hand the SEM image 3(d) and AFM image 9(m) of single layer coated samples above says set composites for same operating condition. In SEM image Deep groove lip formation, micro cutting and wear craters features was found which show good agreement with AFM image but roughness value is lower due to hardness of single layer coating. Multilayer coated 6 wt.% granite powder reinforced aluminium alloy worn surface for operating condition impact velocity10 m/sec, impingement angle 45º, erodent discharge 160 g/min shown in the SEM image 3(f) and AFM image 9(X) respectively. In SEM image Deep groove lip formation, micro cutting and wear craters features was found which show good agreement with AFM image but roughness value is lower due to high hardness of multilayer coating.

AFM image (a-h), (i-p) and (q-x) are for uncoated, single layer and multilayer coated granite powder reinforced aluminium alloyed composites respectively. AFM image (a-d), it can be observed that the addition of granite particle reduced the surface roughness value (15.9-10.3nm). However, on coating of single and multilayer on these samples the surface roughness is decreased as shown in AFM image (i-l) (8.36-6.58nm) and (q-t) (6.13-2.93nm) respectively. When we observed the AFM image of eroded surface the roughness value is higher as compared to uneroded surface roughness value. The surface roughness value of eroded surface is higher due to presence of peaks and valleys resulting from severe plastic deformation mechanism. For (e-h) AFM image shows that surface roughness value of eroded surface is reduced (308-196nm). The reduction in surface roughness value is due to the addition of granite particle and it can be proved that addition of granite particle reduced the slurry erosion wear rate discuss in section 6.9.1 When we observed the eroded surface AFM image (m-p) & (u-x) of single and multilayer coating the surface roughness value is reduced (140-89.6nm) & (69.1-33.9nm) respectively. The reduction in surface roughness value is due to the deposition of surface coating and it can be proved that deposition of coating reduced the slurry erosion wear rate discuss in section 3.1.1. Similar observation for AFM surface mapping before and after erosion reported by Iwai et al.[247] and Lopez et al.[186].

Uneroded Surface **Eroded surface**

(a)

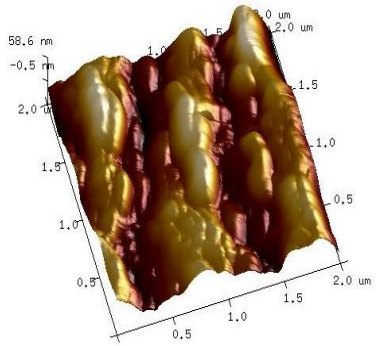

(e)

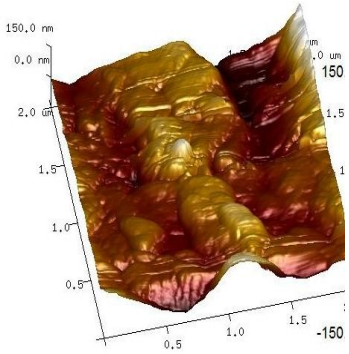

(b)

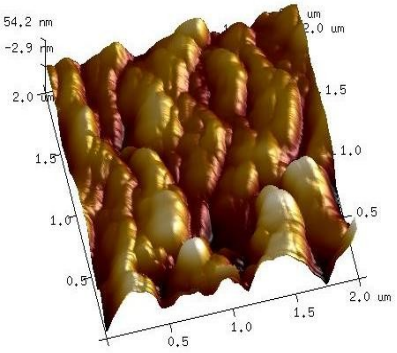

(f)

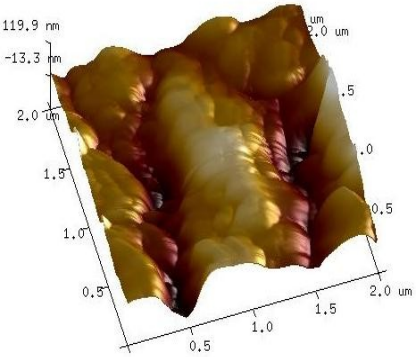

(c)

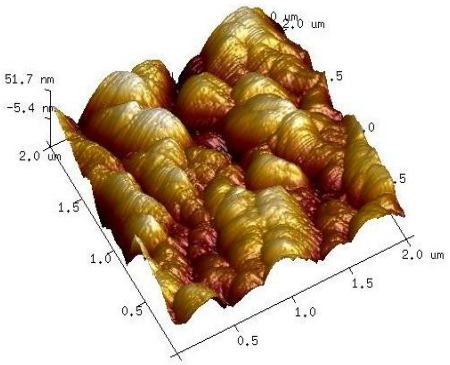

(g)

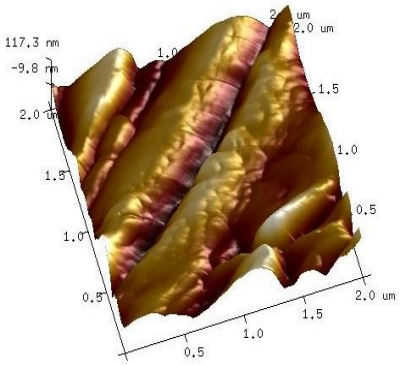

(d)

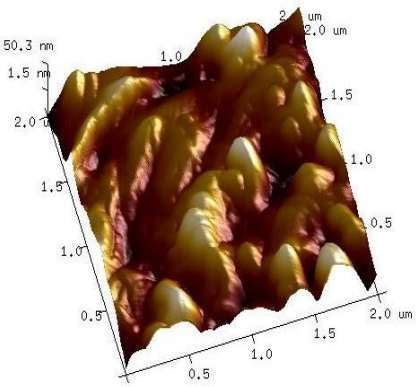

(h)

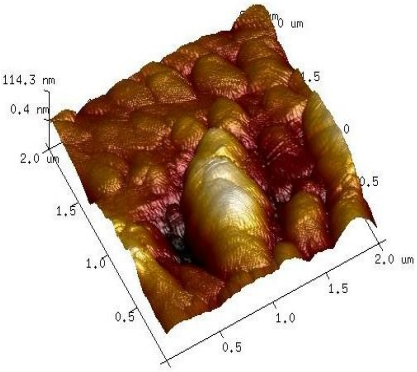

(i)

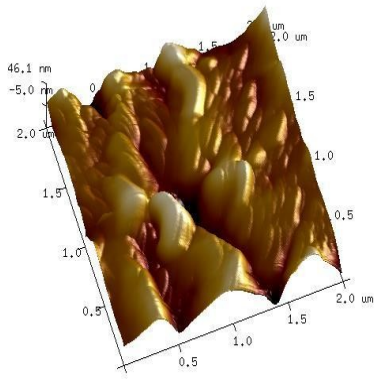
46.1 nm
-5.0 nm
2.0 um
1.5
1.0
0.5
2.0 um

(m)

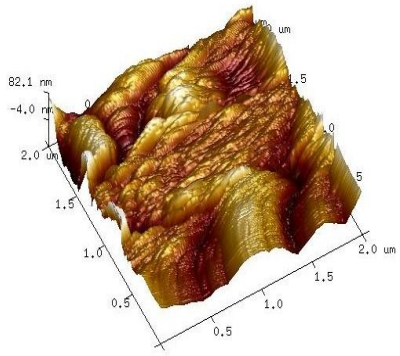
82.1 nm
-4.0 nm
2.0 um
1.5
1.0
0.5
2.0 um

(j)

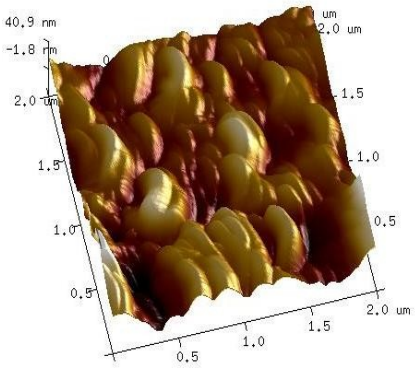
40.9 nm
-1.8 nm
2.0 um
1.5
1.0
0.5
2.0 um

(n)

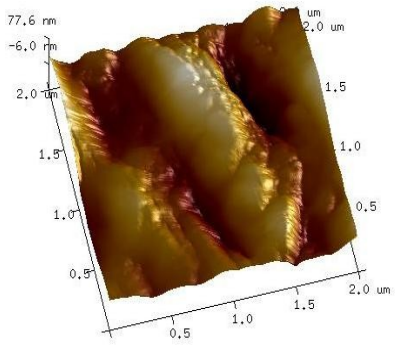
77.6 nm
-6.0 nm
2.0 um
1.5
1.0
0.5
2.0 um

(k)

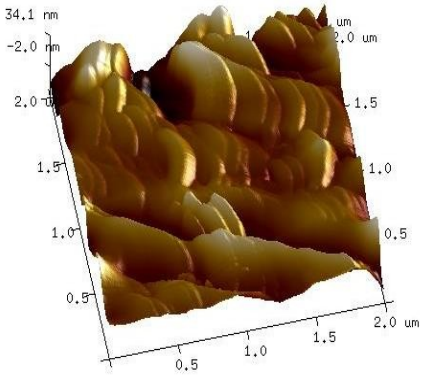
34.1 nm
-2.0 nm
2.0 um
1.5
1.0
0.5
2.0 um

(o)

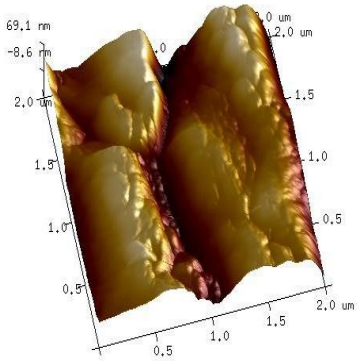
69.1 nm
-8.6 nm
2.0 um
1.5
1.0
0.5
2.0 um

(l)

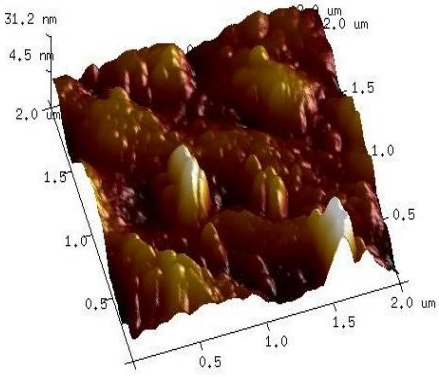
31.2 nm
4.5 nm
2.0 um
1.5
1.0
0.5
2.0 um

(p)

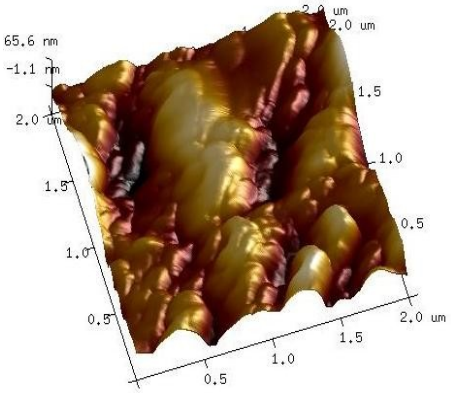
65.6 nm
-1.1 nm
2.0 um
1.5
1.0
0.5
2.0 um

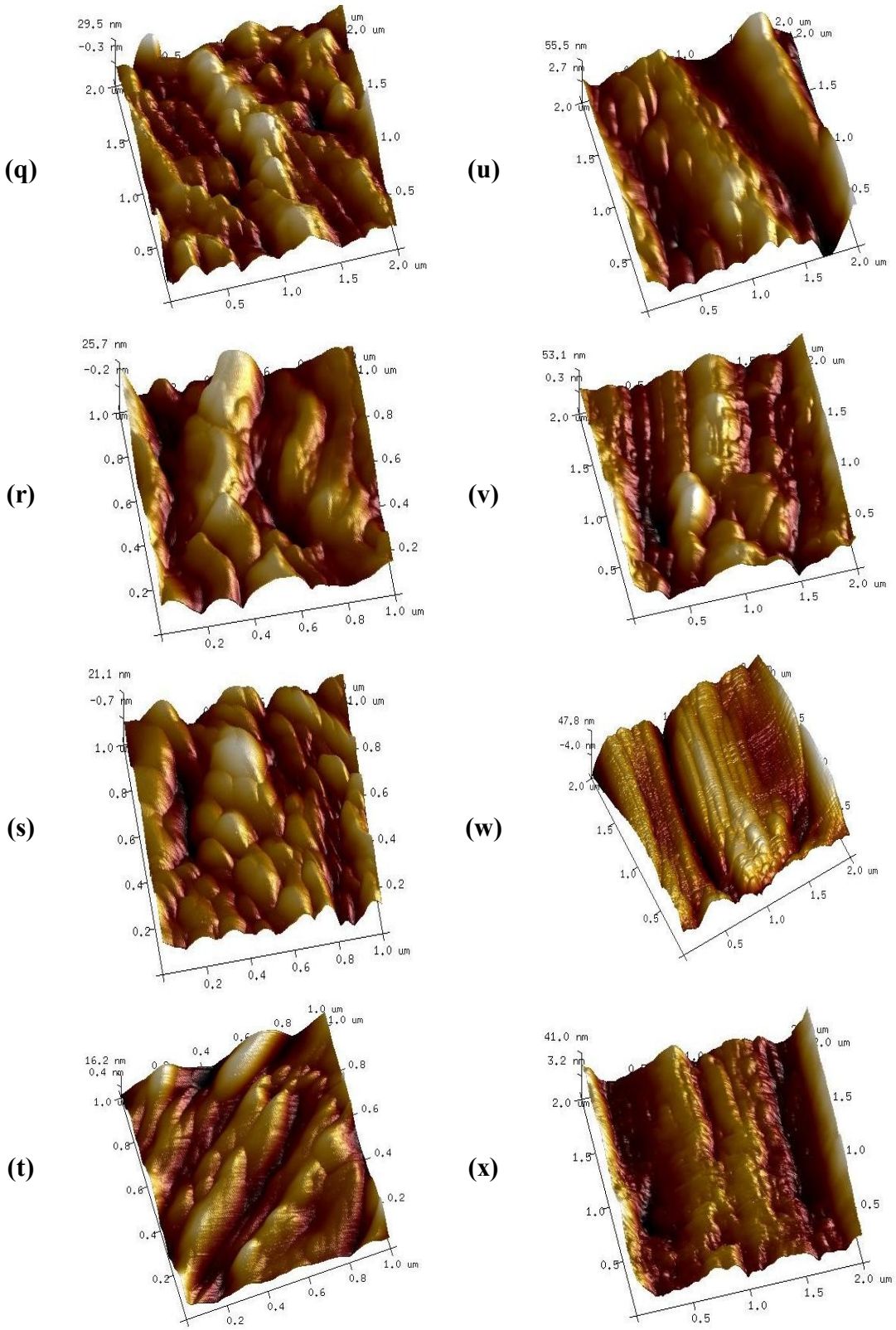

Figure 6.18 AFM image of plain and worn out surfaces for uncoated and coated granite particulate reinforced aluminum alloyed composites

6.19 Corrosion rate variation with time

Corrosion rate variation with time for uncoated, single layer and multilayer coated granite powder reinforced aluminium alloyed composites is shown in Figure 6.19. From the graph it is observed that corrosion rate is decreased with increment in time for uncoated single layer and multilayer coated granite powder reinforced aluminium alloyed composites. Uncoated granite powder reinforced aluminium alloyed composites shows high corrosion rate and multilayer coated granite powder reinforced aluminium alloyed composites shows less corrosion rate. Corrosion rate is decreases after addition of granite powder into base matrix and possible reason behind the decrement in corrosion rate as the time increased a protection layer of oxides was formed on the upper surface of samples and it is much harder as compared to original surface.

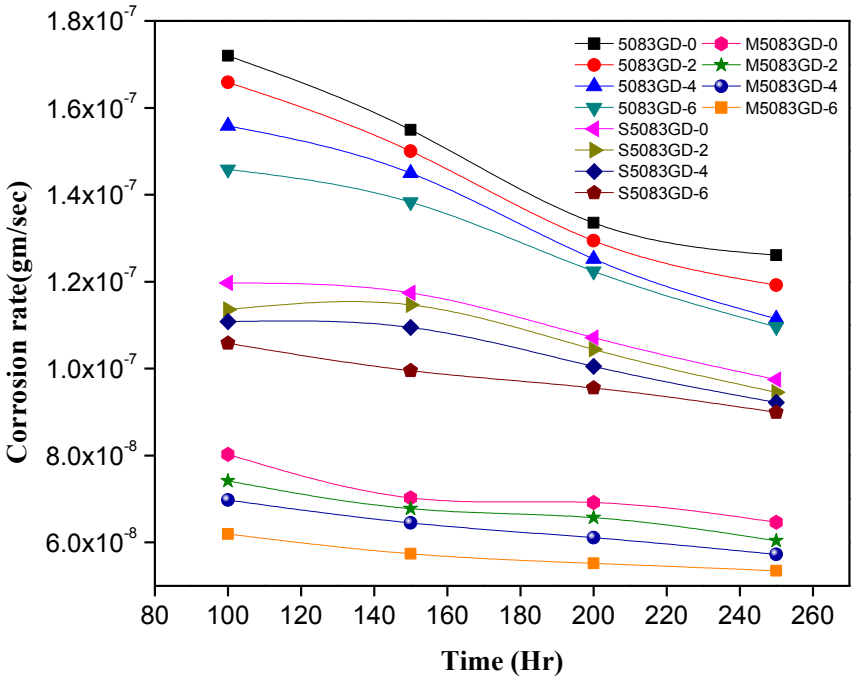

Figure 6.19 Variation in corrosion rate with time for uncoated, Chromium nitride coated and silicon nitride/chromium nitride coated granite dust reinforced aluminium alloyed composites

Similarly, corrosion rate is decreased with an increment in time for single layer and multilayer coated granite powder reinforced aluminium alloyed composites. The possible reason behind the reduction in corrosion rate as the time increased a protection layer of oxides is formed on the upper surface of samples and it is much harder as compared to original surface. This hard

layer of oxides reduced the corrosion rate of the uncoated single layer and multilayer coated granite powder reinforced aluminium alloyed composites. Similar observation is observed by Seetharaman et al.[182] and Pardo et al.[176] for AA2024 aluminium alloy or AZ92 magnesium alloy respectively.

6.20 Corrosion rate variation with pH

Figure 6.20 shows the variation in corrosion rate with increment in pH value of solution for uncoated, single layer and multilayer coated granite powder reinforced aluminium alloyed composites. From the graph it was revealed that corrosion rate is function of pH value and it increases with increment in pH value of solution for uncoated, single layer and multilayer coated granite powder reinforced aluminium alloyed composites. Uncoated granite powder reinforced aluminium alloyed composites shows higher corrosion rate and multilayer coated granite powder reinforced aluminium alloyed composites shows minimum corrosion rate is observed.

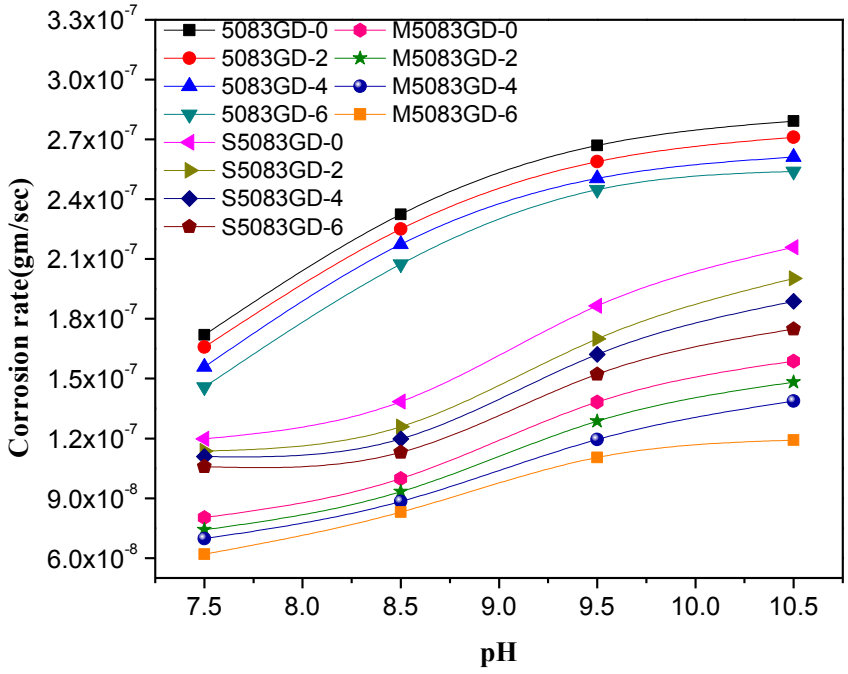

Figure 6.20 Variation in corrosion rate with pH for uncoated, Chromium nitride coated and silicon nitride/chromium nitride coated granite dust reinforced aluminium alloyed composites

Corrosion rate increased with pH value of solution but it decreased with addition of granite particles into base matrix material in increasing trend with pH value of solution. Highest

corrosion rate is observed at 10.5 pH of solution and lowest at 7.5 pH of solution for all set of composition. Form the fig. for uncoated granite powder filled aluminium alloyed composites it seems that corrosion rate increased 7.5 pH value of solution to 9.5 pH value of solution but at 10.5 pH value of solution corrosion rate is constant. The possible reason behind the increment in corrosion rate may be as the pH value increased the number of free ions impact on the surface is more and it enhanced the carrion rate of samples.

Similarly corrosion rate is increased with increment in pH value of solution for single layer and multilayer coated granite powder reinforced aluminium alloyed composites. The possible reason behind the increment in corrosion rate may be as the pH value increased the number of free ions impact on the surface was more and it enhanced the carrion rate of single layer and multilayer coated samples. Similar observation is observed by Lopez et al.[186] for TiN coated stainless steel and Jegadeeswaran et al.[198] for HVOF Sprayed Al_2O_3+CoCrAlTaY on Ti-31 Alloy.

Chapter summary

1. The erosion rate increases with velocity but decreases with addition of granite particulate in both base matrix material. The erosion resistance enhance with deposition of CrN and SiN coating on granite particulate reinforced alloyed composites.
2. The erosion rate increases with slurry concentration but decreases with addition of granite particulate in both base matrix material and it further improved with deposition of single layer and multilayer coating on granite particulate reinforced alloyed composites.
3. Taguchi analysis and ANOVA Analysis is perform to evaluate the significant level or factor in slurry erosion wear of uncoated / single layer / multilayer coated granite particulate reinforced alloyed composites.
4. The surface morphologies of eroded uncoated / single layer / multilayer coated granite particulate reinforced alloyed composites using scanning electron microscope (SEM) and Atomic force microscope (AFM).
5. The corrosion rate decreases with time and corrosion rate increases with pH value of the solution for both coated and uncoated granite particulate reinforced alloyed composites.

The next chapter briefly discusses the ranking of the fabricated composites by using ENTROPY-VIKOR approach under a set of conflicting performance defining criteria.

******

Chapter 7

Selection of Optimal Formulation by Using Entropy-VIKOR Method

Introduction

As in the previous chapter, the various properties of materials such as slurry erosion, corrosion performance, mechanical, fracture, thermo-mechanical properties etc. which contribute to the selection process of materials are evaluated. It is observed that no composite showed the best performance when all the above said individual performance defining attributes (PDAs) are taken into account simultaneously. The estimation obtained from such PDAs and formulation of desired optimal selection depends on the multi-level and multi-factor features, so such difficulties can be regarded as (MCDM) [313]. Selection of appropriate ingredients for multiple criteria decision-making is such as weight fraction addition of granite powder for a successful fabrication of composites and selection of proper coating material to protect the surface from damages, characterization and performance evaluation of a large number of composites. Identifying these evaluation criteria, defining the effects of them on each other, assessing their importance, and choosing a best among many alternatives is a well-designed MCDM [314-318].

The complications involved in slurry erosive performance evaluation of composite wear materials are usually not easy to be overcome not only because of the complex mechanical characteristics, but also because of their compositional variations that comprises distinct materials. The use of distinct materials is strongly affected the slurry erosive performance due to the several operating parameters such as impact velocity, impingement angle, slurry concentration. The complication in slurry erosive wear performance evaluation arises more as the same composition the wear composite materials yield different results with different manufacturing conditions [319]. Intrinsically non-deterministic nature of wear processes further adds complexities in the evaluation of wear composites materials.

The PDAs which fundamentally are manifestations of some other material, process and operational mechanism induced sub-attributes/variables whose actual influential modes are highly grey and hence the predictive accuracy regarding the performance trends of such multi-phase composites becomes probabilistic.

7.1 Evaluation methodology

All performance defining criteria or attributes is must be satisfied to obtain an optimal solution of many decision making problems. However, sometimes these performance defining criteria or attributes are must be satisfied, conflict. The multi-criteria decision making (MCDM) methods are commonly used to solve this type of problems, where number of performance defining criteria or attributes are more. For this, Entropy method is used to determine the weight of different criteria, and the best alternative is selected by VIKOR method.

The evaluation methodology consists of the following three basic phases viz.

Phase I: Identification of the criterions, alternatives and construction of decision matrix.

Phase II: Determination of weight of individual criterion using entropy method.

Phase III: Ranking of the alternatives using VIKOR method.

In the first phase the different alternatives PDAs which is used in the evaluation of optimal formulation and a decision hierarchy is constructed. In the next phase weight is assigned to each PDA by using Entropy technique. In last phase best alternate is determine by using VIKOR method.

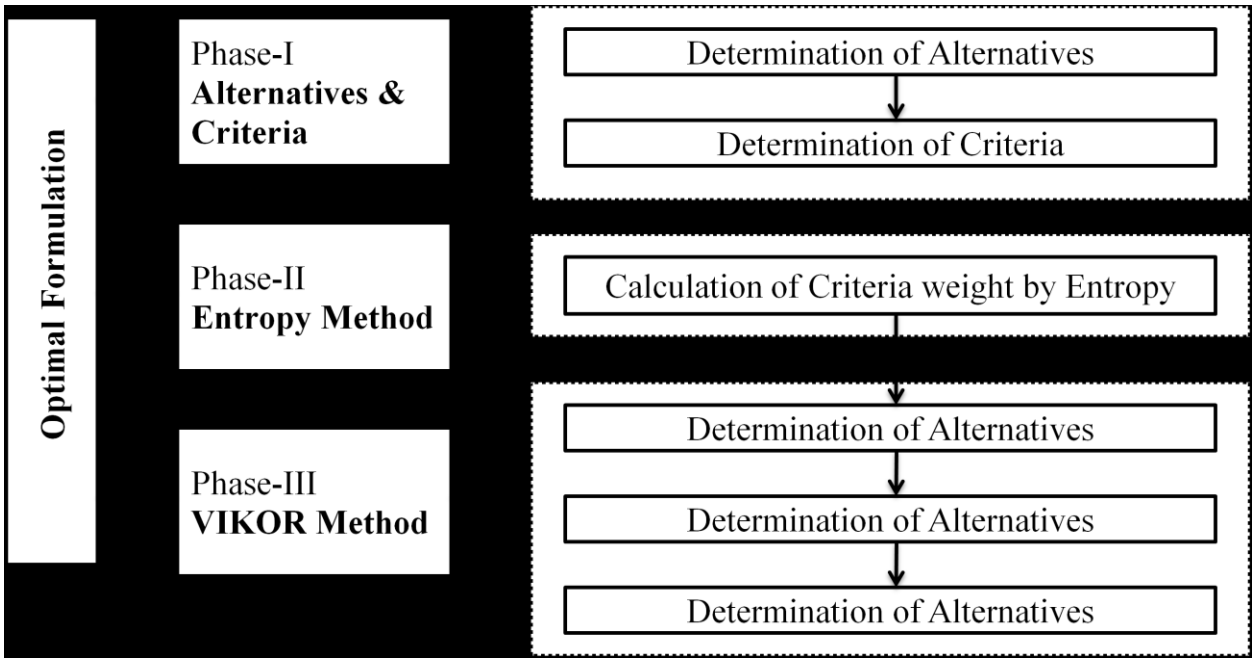

Figure7.1 Flow chart used in the VIKOR optimization technique

7.1.1 Phase I: Identification of PDAs

In the first phase the various PDAs or criteria used in the performance evaluation of wear composites materials are identified. The eight identified PDAs are physical performance, mechanical performance, wear performance, corrosion performance and fracture performance, are briefly described in Table 7.1 and depicted in Figure 7.1.

Table 7.1 Description of the different performance defining attributes

Performance defining Attribute(PDA)	**Description of the individual PDA**	**Performance implications of different PDA**
PDA-1	The void content in the composites is calculated using the following equation: $V_v = \frac{\rho_{ct} - \rho_{ce}}{\rho_{ct}}$, where, ρ_{ce} is the experimental and ρ_{ct} is the theoretical density of the composite.	Lower is good
PDA-2	Hardness as a measure of resistance to indentation under loads is measure on a digital hardness tester.	Higher is good
PDA-3	Flexural strength as a measure of resistance to bend under action of load on universal testing machine	Higher is good
PDA-4	Impact strength as ability of material to resist the sudden impact of load on impact tester	Higher is good
PDA-5	It is the energy absorbed by the composite upto its fracture. The tests are done as per ASTM D 256 using an impact tester machine	Higher is good
PDA-6	It is the removal of the material from the surface when slurry strikes the surface at 45° with impact velocity 10m/sec and erodent discharge 160 gm/min	Lower is good
PDA-7	It is the removal of the material from the surface when slurry strikes the surface at 45° with impact velocity 25m/sec and erodent discharge 160 gm/min	Lower is good
PDA-8	It is the removal of the material from the surface when slurry strikes the surface at 75° with impact velocity	Lower is good

	15m/sec and erodent discharge 160 gm/min	
PDA-9	It is the removal of the material from the surface when slurry strikes the surface at 75° with impact velocity 15m/sec and erodent discharge 280 gm/min	Lower is good
PDA-10	It is the removal of material from the surface when fog strikes the surface at .The tests are done as per ASTM D 256 using corrosion tester	Lower is good

7.1.2 Phase II: Determination of criteria weights

Due to the diverse significance of the PDAs in the performance evaluation of wear materials, one cannot assume that each PDA is of equal importance. There are many methods that can be employed to determine weights [320] such as the weighted least square method, eigen-vector method, entropy method, and linear programming techniques for Multi-dimensional of Analysis Preference (LINMAP). The selection of method depends on the nature of problems.

Shannon et al. [261] introduced information theory which known as entropy method. The amount of information acquired by people is one of the factors for evaluation accuracy and reliability of information. In the information theory, the entropy is measured with the index of disorder of system. If the index is less, the information provided by the index is more, so the index should has more effect during evaluation, the weights should be larger[262]. Therefore the entropy can determine weights for factors. The entropy weight is determined by the matrix constructed based on the monitoring indicators of the factors. The evaluation result can be more objective because the weights of factors can avoid the subjective factor. Chen et al. [263] applied entropy weight coefficients for the attributes of a model for the ground water quality assessment. In another study Zhi-hong et al. [264] used the entropy method for determination of weight of evaluating factors in water quality assessment of a river. The results are found more accurate after implementation of entropy weight of each criterion and outcomes are more subjectivity of expert evaluation. Chowdhury and Husain [265] applied entropy and fuzzy set theories are applied in a multi-criteria decision making technique for determination of health risk management of different water treatment. In their study, the weights of the attributes are determined based on the concept of entropy determining the objective weight of the attributes.

7.1.3 Phase III: Ranking of the alternatives using VIKOR method.

VIKOR method has been widely used as an applicable technique to implement within MCDM [321-323]. The main focus of VIKOR method is on ranking and selection from a set of alternatives in the presence of conflicting criteria. The compromise solution, whose foundation is established by Yu [324] and Zeleny [325], is a feasible solution, which is the closest to the ideal, and here "compromise" means an agreement established by mutual concessions. The VIKOR method determines the compromise ranking list and the compromise solution by introducing the multi-criteria ranking index based on the particular measure of "closeness" to the "ideal" solution [326]. The multi-criteria measure for compromise ranking is developed from the Lp-metric used as an aggregating function in a compromise programming method [327]. VIKOR method is proposed to derive the preference order of open pit mines equipment by Bazzazi et al. [326] and Jahan et al. [327] presented a comprehensive VIKOR method for material selection. A fuzzy VIKOR method on entropy measure for objective weighting for a best supplier selection is develope by Shemshadi et al. [329]. Kuo and Liang [328] integrated a VIKOR with GRA technique to evaluate a service quality of airports under fuzzy environment. Yuenur and Demirer [330] proposed an extended VIKOR method to solve the insurance company problem under fuzzy environment. Ju and Wang [331] presented an extension of VIKOR method for multiple criteria group decision making problem under linguistic information. Wan et al. [332] developed an extended VIKOR method for multi-attribute group decision making with triangular intuitionists fuzzy numbers. Chang [333] applied a fuzzy VIKOR method for the evaluation of hospital service quality in Taiwan. Kim and Chung [334] proposed a fuzzy VIKOR modal to estimate the approach for assessing the vulnerability of the water supply to climate change and variability in South Korea.

The steps followed in the VIKOR optimization technique are as follows:

Step I: After identifying the performance defining criterion (PDCs) and alternatives of the problem, a decision matrix is created. The Description of the different performance defining criteria's is given in Table 7.1. If the number of alternative is P and the number of performance defining criterion are Q then the decision matrix having an order of $P \times Q$ is represented as:

$$D_{P\times Q}=\begin{bmatrix} a_{11}a_{12}\ldots a_{1N} \\ a_{21}a_{22}\ldots a_{2N} \\ \ldots\ldots\ldots\ldots \\ \ldots\ldots\ldots\ldots \\ a_{M1}a_{M2}\ldots a_{MN} \end{bmatrix} \tag{7.1}$$

Where, an element a_{ij} of the decision matrix $D_{P\times Q}$ represents the actual value of the i^{th} alternative in term of j^{th} PDC. The decision matrix is presented in Table 7.6.

Step II: The weights of various criterions are determined by the entropy method. First of all the projection value (ρ_{ij}) for each alternative is calculated as:

$$\rho_{ij}=\frac{x_{ij}}{\sum_{i=1}^{M}x_{ij}} \tag{7.2}$$

The projection value (ρ_{ij}) is represent in table

Step III: After the calculation of projection value, entropy of each criterion is calculated as:

$$E_j=-\varsigma\sum_{j=1}^{N}\rho_{ij}\ln(\rho_{ij}) \tag{7.3}$$

where k is a constant and calculated as, $\varsigma=\frac{1}{\ln(M)}$

The Entropy of each criteria (E_j) is represent in table

Step IV: Next the dispersion value (ψ_j) of each criterion is calculated as:

$$\psi_j=1-E_j \tag{7.4}$$

Finally the weight of each criterion is calculated as:

$$\omega_j=\frac{\psi_j}{\sum_{j=1}^{N}\psi_j} \tag{7.5}$$

The Weight of each criteria (ψ_j) is represent in table

Step V: After the development of decision matrix, values of benefit $(x_{ij})_{\max}$ and cost $(x_{ij})_{\min}$ criterion is obtained as:

$$(x_{ij})_{\max}=\overset{\max}{i}x_{ij}=\max[x_{ij},i=1,2..M]$$

$$\left(x_{ij}\right)_{\min} = {}^{\min}_{i} x_{ij} = \min\left[x_{ij}, i = 1, 2..M\right] \tag{7.6}$$

The Decision matrix is represent in table

Step VI: After this, the values of utility measure (α_i) and regret measure (β_i) are determined by using weights as:

$$\alpha_i = \sum_{j=1}^{N} \frac{\varpi_j \left[\left(x_{ij}\right)_{\max} - x_{ij}\right]}{\left[\left(x_{ij}\right)_{\max} - \left(x_{ij}\right)_{\min}\right]}, \; if \;\; j \; is \; benefit \; criteria$$

$$\alpha_i = \sum_{j=1}^{N} \frac{\varpi_j \left[x_{ij} - \left(x_{ij}\right)_{\min}\right]}{\left[\left(x_{ij}\right)_{\max} - \left(x_{ij}\right)_{\min}\right]}, \; if \;\; j \; is \; \text{cost} \; criteria \;\; , \text{ for j = 1, 2. . . N} \tag{7.7}$$

$$\beta_i = Max^{x} \; of \left\{ \frac{\varpi_j \left[\left(x_{ij}\right)_{\max} - x_{ij}\right]}{\left[\left(x_{ij}\right)_{\max} - \left(x_{ij}\right)_{\min}\right]} \right\}, \text{ for j = 1, 2. . . N} \tag{7.8}$$

Finally VIKOR index (Ω_i) is calculated as:

$$\Omega_i = \xi\left(\frac{\left(\alpha_i - \alpha_i^{-}\right)}{\left(\alpha_i^{+} - \alpha_i^{-}\right)}\right) + \left(1 - \xi\right)\left(\frac{\left(\beta_i - \beta_i^{-}\right)}{\left(\beta_i^{+} - \beta_i^{-}\right)}\right) \tag{7.9}$$

Where,

$$\alpha_i^{+} = {}^{\max}_{i}\alpha_i = \max\left[\alpha_i, i = 1, 2...M\right]; \; \alpha_i^{-} = {}^{\min}_{i}\alpha_i = \min\left[\alpha_i, i = 1, 2...M\right]$$

$$\beta_i^{+} = {}^{\max}_{i}\beta_i = \max\left[\beta_i, i = 1, 2...M\right]; \; \beta_i^{-} = {}^{\min}_{i}\beta_i = \min\left[\beta_i, i = 1, 2...M\right]$$

ξ is introduced as weight for the maximum value of utility and $(1-\xi)$ is the weight of the individual regret and normally its value of ξ is taken as 0.5.

According to the value of VIKOR index alternatives are arranged in the ascending order and the best alternative is the one having the minimum value of Ω_i.

The α_i, β_i, Ω_i values and ranking of the alternatives is represent in table

7.2 Evaluation of ranking of the alternatives

7.2.1 Evaluation of ranking of type-1 uncoated and coated granite particulate reinforced 1050 aluminum alloyed composites wear material

The description of the ten selected performance defining attributes and their experimental data's of the type-1 wear material investigated composites are given in Table 7.1 and Table 7.2.

Table 7.2 Experimental data of type-1 wear material

Composite designation	C-1	C-2	C-3	C-4	C-5	C-6	C-7	C-8	C-9	C-10
A-1	4.09	32	327.3	41	0.159	0.00688	0.02038	0.00937	0.0125	1.92E-07
A-2	5.75	36.2	297.1	42	0.189	0.00562	0.01825	0.00875	0.01188	1.86E-07
A-3	9.73	51.2	231.8	45	0.199	0.00375	0.017	0.0075	0.01125	1.79E-07
A-4	9.74	61.2	211.8	46	0.21	0.00287	0.01529	0.00698	0.0109	1.71E-07
A-5	3.73	87	355.29	44	0.173	0.00256	0.00981	0.00491	0.00869	1.39E-07
A-6	4.69	99	308.73	44	0.206	0.00239	0.00954	0.00437	0.00828	1.34E-07
A-7	6.63	113	263.66	51	0.218	0.00224	0.00921	0.00396	0.00771	1.28E-07
A-8	8.13	123	242.19	53	0.229	0.00214	0.00895	0.00359	0.00716	1.23E-07
A-9	3.23	93	395.13	45	0.181	0.00156	0.00776	0.00273	0.00563	8.86E-08
A-10	4.13	105	323.69	46	0.216	0.00134	0.00762	0.00259	0.00551	8.53E-08
A-11	5.49	127	286.13	52	0.229	0.00119	0.00751	0.00223	0.00501	8.08E-08
A-12	6.37	139	253.16	58	0.241	0.00107	0.00743	0.00206	0.00467	7.86E-08

Table 7.3 Projection value (ρ_{ij}) data of type-1 wear material

Composite designation	C-1	C-2	C-3	C-4	C-5	C-6	C-7	C-8	C-9	C-10
A-1	0.0570	0.03000	0.09362	0.07231	0.06489	0.20470	0.14688	0.15875	0.12623	0.12112
A-2	0.0802	0.03393	0.08498	0.07407	0.07714	0.16721	0.13153	0.14824	0.11977	0.11737
A-3	0.1356	0.04800	0.06630	0.07936	0.08122	0.11157	0.12252	0.12703	0.11349	0.11292
A-4	0.1358	0.05737	0.06058	0.08112	0.08571	0.08539	0.11019	0.11822	0.10989	0.10786
A-5	0.0520	0.08156	0.10162	0.07760	0.07061	0.07616	0.07070	0.08316	0.08769	0.08768
A-6	0.0654	0.09281	0.08831	0.07760	0.08408	0.07111	0.06875	0.07401	0.08347	0.08456
A-7	0.0924	0.10594	0.07541	0.08994	0.08897	0.06664	0.06637	0.06707	0.07779	0.08074
A-8	0.1133	0.11531	0.06927	0.09347	0.09346	0.06367	0.06450	0.06081	0.07218	0.07758
A-9	0.0450	0.08719	0.11302	0.07936	0.07387	0.04641	0.05592	0.04629	0.05679	0.05588
A-10	0.0575	0.09844	0.09258	0.08112	0.08816	0.03986	0.05491	0.04388	0.05559	0.05380
A-11	0.0765	0.11906	0.08184	0.09171	0.09346	0.03541	0.05412	0.03777	0.05059	0.05096
A-12	0.0888	0.13032	0.07241	0.10229	0.09836	0.03184	0.05354	0.03489	0.04781	0.04958

Table 7.4 Entropy of each criteria (E_j) data of type-1 wear material

Composite designation	C-1	C-2	C-3	C-4	C-5	C-6	C-7	C-8	C-9	C-10
A-1	-0.1635	-0.1057	-0.2217	-0.1899	-0.1779	-0.3249	-0.2879	-0.2929	-0.2619	-0.2557
A-2	-0.2029	-0.1148	-0.2095	-0.1927	-0.1976	-0.2997	-0.2668	-0.2829	-0.2549	-0.2518
A-3	-0.2712	-0.1457	-0.1799	-0.2087	-0.2039	-0.2468	-0.2578	-0.2677	-0.2469	-0.2468
A-4	-0.2719	-0.1639	-0.1698	-0.2037	-0.2107	-0.2169	-0.2439	-0.2598	-0.2428	-0.2404
A-5	-0.1538	-0.2047	-0.2323	-0.1986	-0.1876	-0.1968	-0.1876	-0.2068	-0.2137	-0.2199
A-6	-0.1786	-0.2209	-0.2143	-0.1986	-0.2088	-0.1879	-0.1847	0.1927	-0.2078	-0.2088
A-7	-0.2209	-0.2378	-0.1949	-0.2166	-0.2157	-0.1829	-0.1846	-0.1897	-0.1987	-0.2038
A-8	-0.2468	-0.2499	-0.1849	-0.2254	-0.2287	-0.1758	-0.1768	-0.1708	-0.1899	-0.1984
A-9	-0.1399	-0.2127	-0.2464	-0.2087	-0.1976	-0.1449	-0.1678	-0.1427	-0.1629	-0.1625
A-10	-0.1649	-0.2282	-0.2203	-0.2037	-0.2141	-0.1286	-0.1599	-0.1378	-0.1656	-0.1579
A-11	-0.1967	-0.2538	-0.2048	-0.2191	-0.2217	-0.1188	-0.1578	-0.1277	-0.1508	-0.1579
A-12	-0.2156	-0.2656	-0.1901	-0.2332	-0.2289	-0.1098	-0.1567	-0.1177	-0.1489	-0.1489

Table 7.5 Weight of each criteria (ψ_j) data of type-1 wear material

Composite designation	C-1	C-2	C-3	C-4	C-5	C-6	C-7	C-8	C-9	C-10
A-1	0.0657	0.0428	0.0899	0.0765	0.07477	0.1368	0.1177	0.11757	0.10507	0.10288
A-2	0.0814	0.0465	0.0846	0.0779	0.07955	0.1207	0.1079	0.11388	0.10279	0.10168
A-3	0.1099	0.0586	0.0798	0.0809	0.08268	0.0989	0.1059	0.10576	0.09948	0.09919
A-4	0.1094	0.0659	0.0689	0.0819	0.08476	0.0857	0.0979	0.10178	0.09799	0.09669
A-5	0.0687	0.0826	0.0935	0.0798	0.07575	0.0789	0.0778	0.08527	0.08589	0.08879
A-6	0.0717	0.0888	0.0864	0.0798	0.08779	0.0756	0.0777	0.07754	0.08495	0.08468
A-7	0.0888	0.0959	0.0784	0.0876	0.08667	0.0726	0.0796	0.07298	0.07995	0.08177
A-8	0.0993	0.1006	0.0746	0.0898	0.08949	0.0708	0.0776	0.06854	0.07655	0.07989
A-9	0.0569	0.0898	0.0995	0.0809	0.07758	0.0578	0.0689	0.05719	0.06669	0.06488
A-10	0.0651	0.0918	0.0888	0.0819	0.08659	0.0519	0.0643	0.05599	0.06466	0.06379
A-11	0.0796	0.1019	0.0828	0.0889	0.08949	0.0479	0.0656	0.04979	0.06089	0.06149
A-12	0.0865	0.1068	0.0767	0.0938	0.09198	0.0446	0.0677	0.04762	0.05789	0.05997
E_j	0.9749	0.9689	0.9968	0.9978	0.99793	0.9357	0.9775	0.94996	0.97888	0.98087
ψ_j	0.0257	0.0339	0.0066	0.0027	0.00287	0.0679	0.0298	0.05039	0.02479	0.01973
Weight	0.0974	0.1327	0.0265	0.0084	0.01177	0.2657	0.1159	0.19409	0.08386	0.07597

Table 7.6 Decision matrix of type-1wear material

Composite designation	C-1	C-2	C-3	C-4	C-5	C-6	C-7	C-8	C-9	C-10
A-1	4.09	32	327.3	41	0.159	0.00688	0.02038	0.00937	0.0125	1.92E-07
A-2	5.75	36.2	297.1	42	0.189	0.00562	0.01825	0.00875	0.01188	1.86E-07
A-3	9.73	51.2	231.8	45	0.199	0.00375	0.017	0.0075	0.01125	1.79E-07
A-4	9.74	61.2	211.8	46	0.21	0.00287	0.01529	0.00698	0.0109	1.71E-07
A-5	3.73	87	355.29	44	0.173	0.00256	0.00981	0.00491	0.00869	1.39E-07
A-6	4.69	99	308.73	44	0.206	0.00239	0.00954	0.00437	0.00828	1.34E-07
A-7	6.63	113	263.66	51	0.218	0.00224	0.00921	0.00396	0.00771	1.28E-07
A-8	8.13	123	242.19	53	0.229	0.00214	0.00895	0.00359	0.00716	1.23E-07
A-9	3.23	93	395.13	45	0.181	0.00156	0.00776	0.00273	0.00563	8.86E-08
A-10	4.13	105	323.69	46	0.216	0.00134	0.00762	0.00259	0.00551	8.53E-08
A-11	5.49	127	286.13	52	0.229	0.00119	0.00751	0.00223	0.00501	8.08E-08
A-12	6.37	139	253.16	58	0.241	0.00107	0.00743	0.00206	0.00467	7.86E-08
MAX	9.73	139	395.13	58	0.241	0.00688	0.02038	0.00937	0.0125	1.92E-07
MIN	3.23	32	211.8	41	0.159	0.00107	0.00743	0.00206	0.00467	7.86E-08
Weight	0.0972	0.1302	0.0246	0.0084	0.0110	0.26157	0.11359	0.19407	0.08328	7.59E-02
MAX-MIN	6.5	107	183.33	17	0.082	0.00581	0.01295	0.00731	0.00783	1.13E-07

Table 7.7 α_i, β_i, Ω_i values and ranking of the alternatives.

Composite designation	α_i	β_i	Ω_i	Ranking
A-1	0.756882	0.26157	1	12
A-2	0.684757	0.20484	0.787789	11
A-3	0.616877	0.14442	0.476876	10
A-4	0.550979	0.13062	0.264393	09
A-5	0.343886	0.075663	0.224828	08
A-6	0.338969	0.081533	0.181876	07
A-7	0.353449	0.09857	0.167139	06
A-8	0.361849	0.110739	0.155615	05
A-9	0.163474	0.074231	0.132587	04
A-10	0.168836	0.088834	0.069254	03
A-11	0.189985	0.115607	0.043245	02
A-12	0.202254	0.13021	0.00024	01

7.2.2 Evaluation of ranking of type-2uncoated and coated granite particulate reinforced 5083 aluminum alloyed composites wear material

The description of the ten selected performance defining attributes and their experimental data's of the type-1 wear material investigated composites are given in Table 7.1 and Table 7.8.

Table 7.8 Experimental data of type-2wear material

Composite designation	C-1	C-2	C-3	C-4	C-5	C-6	C-7	C-8	C-9	C-10
B-1	3.09	68	375.13	57	0.283	0.00698	0.02038	0.00873	0.01125	1.72E-07
B-2	4.35	78	355.19	61	0.356	0.00662	0.01725	0.00795	0.01088	1.66E-07
B-3	6.13	91	335.33	66	0.436	0.00635	0.01613	0.00735	0.01012	1.56E-07
B-4	8.34	107	315.93	69	0.518	0.00607	0.01459	0.00678	0.00981	1.46E-07
B-5	2.73	193	395.29	59	0.313	0.00406	0.0106	0.00471	0.00769	1.20E-07
B-6	3.69	213	376.36	62	0.376	0.0039	0.00974	0.00427	0.00728	1.14E-07
B-7	4.93	236	353.17	72	0.446	0.00364	0.00936	0.00386	0.00671	1.06E-07
B-8	6.13	259	339.9	75	0.528	0.00334	0.00915	0.00359	0.00636	9.47E-08
B-9	2.23	213	411.13	61	0.323	0.00156	0.00776	0.00237	0.00463	6.08E-08
B-10	3.13	237	401.36	64	0.386	0.00134	0.00742	0.00205	0.00431	5.75E-08
B-11	3.89	253	386.15	77	0.466	0.00119	0.00721	0.00183	0.00391	5.31E-08
B-12	5.57	279	369.19	80	0.548	0.00107	0.00703	0.00169	0.00347	5.08E-08

Table 7.9 Projection value (ρ_{ij}) data of type-2wear material

Composite designation	C-1	C-2	C-3	C-4	C-5	C-6	C-7	C-8	C-9	C-10
B-1	0.0579	0.0354	0.0898	0.0709	0.05687	0.15149	0.14928	0.15829	0.13019	0.13266
B-2	0.0824	0.0357	0.0847	0.0759	0.07150	0.14589	0.12626	0.14409	0.12589	0.12797
B-3	0.1308	0.0408	0.0797	0.0829	0.08778	0.13768	0.11807	0.13320	0.11715	0.12036
B-4	0.1585	0.0487	0.0757	0.0893	0.10409	0.13168	0.10679	0.12287	0.11359	0.11259
B-5	0.0536	0.0867	0.0895	0.0747	0.06286	0.08803	0.07789	0.08557	0.08898	0.09239
B-6	0.0687	0.0956	0.0856	0.0772	0.07577	0.08456	0.07197	0.07783	0.08439	0.08765
B-7	0.0994	0.1097	0.0801	0.0896	0.08976	0.07895	0.06859	0.06998	0.07766	0.08209
B-8	0.1138	0.1163	0.0772	0.0934	0.10609	0.07249	0.06699	0.06509	0.07359	0.07309
B-9	0.0414	0.0956	0.0934	0.0759	0.06487	0.03388	0.05679	0.04295	0.05376	0.04693
B-10	0.0577	0.1064	0.0919	0.0797	0.07756	0.02906	0.05438	0.03751	0.04987	0.04469
B-11	0.0776	0.1137	0.0878	0.0959	0.09359	0.02585	0.05277	0.03319	0.04546	0.04098
B-12	0.1075	0.1258	0.0864	0.0996	0.11006	0.02307	0.05159	0.03069	0.04057	0.03929

Table 7.10 Entropy of each criteria (E_j) data of type-2wear material

Composite designation	C-1	C-2	C-3	C-4	C-5	C-6	C-7	C-8	C-9	C-10
B-1	-0.1639	-0.10659	-0.20951	-0.18777	-0.16298	-0.28787	-0.28895	-0.29178	-0.26595	-0.26799
B-2	-0.2043	-0.11794	-0.20277	-0.1958	-0.18868	-0.27863	-0.26288	-0.27939	-0.26089	-0.26308
B-3	-0.2467	-0.13068	-0.1958	-0.20537	-0.21357	-0.27299	-0.25289	-0.26889	-0.25504	-0.25469
B-4	-0.2879	-0.14589	-0.18874	-0.21089	-0.23567	-0.26896	-0.23889	-0.25769	-0.24699	-0.24581
B-5	-0.1505	-0.21292	-0.21608	-0.19183	-0.17393	-0.21598	-0.19867	-0.21056	-0.21589	-0.22021
B-6	-0.1892	-0.22488	-0.20992	-0.19775	-0.19509	-0.20889	-0.18886	-0.19805	-0.20866	-0.21384
B-7	-0.2184	-0.23788	-0.20207	-0.21624	-0.21617	-0.20047	-0.18369	-0.18607	-0.19887	-0.20521
B-8	-0.2467	-0.25029	-0.19743	-0.22144	-0.23799	-0.19028	-0.18106	-0.17777	-0.19209	-0.19198
B-9	-0.1316	-0.22488	-0.22108	-0.1958	-0.17779	-0.11459	-0.16298	-0.13519	-0.15797	-0.14357
B-10	-0.1666	-0.23840	-0.21801	-0.2016	-0.19873	-.102828	-0.15829	-0.12398	-0.14954	-0.13839
B-11	-0.1894	-0.24709	-0.21313	-0.22482	-0.22179	-0.09467	-0.15578	-0.11299	-0.14065	-0.13087
B-12	-0.2338	-0.26038	-0.20753	-0.22977	-0.24489	-0.08768	-0.15277	-0.10679	-0.12909	-0.12706

Table 7.11 Weight of each criteria (ψ_j) data of type-2wear material

Composite designation	C-1	C-2	C-3	C-4	C-5	C-6	C-7	C-8	C-9	C-10
B-1	0.0657	0.04288	0.08407	0.07556	0.06586	0.11499	0.11465	0.11785	0.10681	0.10786
B-2	0.0818	0.04788	0.08594	0.07889	0.07594	0.12076	0.10579	0.11331	0.10498	0.10588
B-3	0.0998	0.05277	0.07891	0.08264	0.08588	0.10989	0.10152	0.10809	0.10109	0.10879
B-4	0.1159	0.05889	0.07949	0.08486	0.09479	0.10739	0.09628	0.10366	0.09938	0.09896
B-5	0.0606	0.08529	0.08951	0.07719	0.06998	0.08608	0.07988	0.08597	0.08668	0.08862
B-6	0.0736	0.09044	0.08471	0.07957	0.07809	0.08407	0.07579	0.07989	0.08388	0.08586
B-7	0.0877	0.09576	0.08314	0.08705	0.08696	0.0806	0.07398	0.07487	0.07987	0.08257
B-8	0.0998	0.10069	0.07945	0.08907	0.09578	0.07658	0.07289	0.07157	0.07729	0.07699
B-9	0.0528	0.09044	0.08896	0.07889	0.07409	0.04609	0.06568	0.05407	0.06309	0.05777
B-10	0.0669	0.09595	0.08779	0.08125	0.07977	0.04138	0.06367	0.04955	0.06018	0.05566
B-11	0.0760	0.09949	0.08576	0.09067	0.08925	0.03797	0.06279	0.04578	0.05660	0.05266
B-12	0.0940	0.10479	0.08359	0.09246	0.09777	0.03539	0.06144	0.04296	0.05198	0.05142
E_j	0.9754	0.96809	0.99888	0.99784	0.99179	0.93249	0.97257	0.94409	0.97182	0.96657
ψ_j	0.02756	0.03695	0.00122	0.00246	0.00865	0.06776	0.02788	0.05590	0.02888	0.03389
Weight	0.09481	0.12498	0.00418	0.00845	0.02979	0.23406	0.09558	0.19306	0.09898	0.11698

Table 7.12 Decision matrix of type-2wear material

Composite designation	C-1	C-2	C-3	C-4	C-5	C-6	C-7	C-8	C-9	C-10
B-1	3.09	68	375.13	57	0.283	0.00698	0.02038	0.00873	0.01125	1.72E-07
B-2	4.35	78	355.19	61	0.356	0.00662	0.01725	0.00795	0.01088	1.66E-07
B-3	6.13	91	335.33	66	0.436	0.00635	0.01613	0.00735	0.01012	1.56E-07
B-4	8.34	107	315.93	69	0.518	0.00607	0.01459	0.00678	0.00981	1.46E-07
B-5	2.73	193	395.29	59	0.313	0.00406	0.0106	0.00471	0.00769	1.20E-07
B-6	3.69	213	376.36	62	0.376	0.0039	0.00974	0.00427	0.00728	1.14E-07
B-7	4.93	236	353.17	72	0.446	0.00364	0.00936	0.00386	0.00671	1.06E-07
B-8	6.13	259	339.9	75	0.528	0.00334	0.00915	0.00359	0.00636	9.47E-08
B-9	2.23	213	411.13	61	0.323	0.00156	0.00776	0.00237	0.00463	6.08E-08
B-10	3.13	237	401.36	64	0.386	0.00134	0.00742	0.00205	0.00431	5.75E-08
B-11	3.89	253	386.15	77	0.466	0.00119	0.00721	0.00183	0.00391	5.31E-08
B-12	5.57	279	369.19	80	0.548	0.00107	0.00703	0.00169	0.00347	5.08E-08
MAX	8.34	279	411.13	80	0.548	0.00698	0.02038	0.00873	0.01125	1.72E-07
MIN	2.23	68	315.93	57	0.283	0.00107	0.00703	0.00169	0.00347	5.08E-08
Weight	0.095	0.125	0.0042	0.0085	0.0298	0.23406	0.09515	0.19311	0.098697	1.17E-01
MAX-MIN	6.11	211	95.2	23	0.265	0.00591	0.01335	0.00704	0.00778	1.21E-07

Table 7.13 α_i, β_i, Ω_i values and ranking of the alternatives.

Composite designation	α_i	β_i	Ω_i	Ranking
B-1	0.753876	0.23406	0.99999	12
B-2	0.719570	0.2198	0.92282	11
B-3	0.710399	0.2091	0.87895	10
B-4	0.712319	0.19842	0.84456	09
B-5	0.436097	0.11842	0.34068	08
B-6	0.434589	0.112079	0.31796	07
B-7	0.439409	0.10178	0.28737	06
B-8	0.444880	0.113088	0.33014	05
B-9	0.163616	0.08585	0.49999	04
B-10	0.172338	0.100062	0.09704	03
B-11	0.183808	0.109535	0.05057	02
B-12	0.217248	0.12493	0.00325	01

7.2.3 Evaluation of ranking of all type uncoated and coated granite particulate reinforced aluminum alloyed composites wear material

The description of the ten selected performance defining attributes and their experimental data's of the type-1 wear material investigated composites are given in Table 7.1 and Table 7.14.

Table 7.14 Experimental data of all wear material

Composite designation	C-1	C-2	C-3	C-4	C-5	C-6	C-7	C-8	C-9	C-10
B-1	3.09	68	375.13	57	0.283	0.00698	0.02038	0.00873	0.01125	1.72E-07
B-2	4.35	78	355.19	61	0.356	0.00662	0.01725	0.00795	0.01088	1.66E-07
B-3	6.13	91	335.33	66	0.436	0.00635	0.01613	0.00735	0.01012	1.56E-07
B-4	8.34	107	315.93	69	0.518	0.00607	0.01459	0.00678	0.00981	1.46E-07
B-5	2.73	193	395.29	59	0.313	0.00406	0.0106	0.00471	0.00769	1.20E-07
B-6	3.69	213	376.36	62	0.376	0.0039	0.00974	0.00427	0.00728	1.14E-07
B-7	4.93	236	353.17	72	0.446	0.00364	0.00936	0.00386	0.00671	1.06E-07
B-8	6.13	259	339.9	75	0.528	0.00334	0.00915	0.00359	0.00636	9.47E-08
B-9	2.23	213	411.13	61	0.323	0.00156	0.00776	0.00237	0.00463	6.08E-08
B-10	3.13	237	401.36	64	0.386	0.00134	0.00742	0.00205	0.00431	5.75E-08
B-11	3.89	253	386.15	77	0.466	0.00119	0.00721	0.00183	0.00391	5.31E-08
B-12	5.57	279	369.19	80	0.548	0.00107	0.00703	0.00169	0.00347	5.08E-08
A-1	4.09	32	327.3	41	0.159	0.00688	0.02038	0.00937	0.0125	1.92E-07
A-2	5.75	36.2	297.1	42	0.189	0.00562	0.01825	0.00875	0.01188	1.86E-07
A-3	9.73	51.2	231.8	45	0.199	0.00375	0.017	0.0075	0.01125	1.79E-07
A-4	9.74	61.2	211.8	46	0.21	0.00287	0.01529	0.00698	0.0109	1.71E-07
A-5	3.73	87	355.29	44	0.173	0.00256	0.00981	0.00491	0.00869	1.39E-07
A-6	4.69	99	308.73	44	0.206	0.00239	0.00954	0.00437	0.00828	1.34E-07
A-7	6.63	113	263.66	51	0.218	0.00224	0.00921	0.00396	0.00771	1.28E-07
A-8	8.13	123	242.19	53	0.229	0.00214	0.00895	0.00359	0.00716	1.23E-07
A-9	3.23	93	395.13	45	0.181	0.00156	0.00776	0.00273	0.00563	8.86E-08
A-10	4.13	105	323.69	46	0.216	0.00134	0.00762	0.00259	0.00551	8.53E-08
A-11	5.49	127	286.13	52	0.229	0.00119	0.00751	0.00223	0.00501	8.08E-08
A-12	6.37	139	253.16	58	0.241	0.00107	0.00743	0.00206	0.00467	7.86E-08

Table 7.15 Projection value (ρ_{ij}) data of all wear material

Composite designation	C-1	C-2	C-3	C-4	C-5	C-6	C-7	C-8	C-9	C-10
B-1	0.0245	0.0206	0.0474	0.0416	0.0381	0.0875	0.0740	0.0764	0.0606	0.0597
B-2	0.0345	0.0237	0.0449	0.0445	0.0479	0.0830	0.0626	0.0696	0.0586	0.0576
B-3	0.0487	0.0276	0.0424	0.0482	0.0587	0.0796	0.0586	0.0643	0.0545	0.0541
B-4	0.0662	0.0325	0.0399	0.0504	0.0697	0.0761	0.0530	0.0594	0.0529	0.0506
B-5	0.0217	0.0586	0.0500	0.0431	0.0421	0.0509	0.0385	0.0412	0.0414	0.0415
B-6	0.0293	0.0647	0.0476	0.0453	0.0506	0.0489	0.0354	0.0374	0.0392	0.0394
B-7	0.0392	0.0717	0.0446	0.0526	0.0600	0.0457	0.0340	0.0338	0.0362	0.0369
B-8	0.0487	0.0786	0.0430	0.0547	0.0711	0.0419	0.0332	0.0314	0.0343	0.0329
B-9	0.0177	0.0647	0.0520	0.0445	0.0435	0.0196	0.0282	0.0207	0.0249	0.0211
B-10	0.0249	0.0720	0.0507	0.0467	0.0520	0.0168	0.0269	0.0179	0.0232	0.0200
B-11	0.0309	0.0768	0.0488	0.0562	0.0627	0.0149	0.0262	0.0160	0.0211	0.0184
B-12	0.0442	0.0847	0.0467	0.0584	0.0738	0.0134	0.0255	0.0148	0.0187	0.0176
A-1	0.0325	0.0097	0.0414	0.0299	0.0214	0.0863	0.0740	0.0820	0.0673	0.0666
A-2	0.0457	0.0110	0.0376	0.0307	0.0254	0.0705	0.0663	0.0766	0.0640	0.0646
A-3	0.0773	0.0155	0.0293	0.0328	0.0268	0.0470	0.0617	0.0657	0.0606	0.0621
A-4	0.0774	0.0186	0.0268	0.0336	0.0283	0.0360	0.0555	0.0611	0.0587	0.0593
A-5	0.0296	0.0264	0.0449	0.0321	0.0233	0.0321	0.0356	0.0430	0.0468	0.0482
A-6	0.0372	0.0301	0.0390	0.0321	0.0277	0.0300	0.0346	0.0383	0.0446	0.0465
A-7	0.0527	0.0343	0.0333	0.0372	0.0293	0.0281	0.0334	0.0347	0.0415	0.0444
A-8	0.0646	0.0373	0.0306	0.0387	0.0308	0.0268	0.0325	0.0314	0.0386	0.0427
A-9	0.0257	0.0282	0.0500	0.0328	0.0244	0.0196	0.0282	0.0239	0.0303	0.0307
A-10	0.0328	0.0319	0.0409	0.0336	0.0291	0.0168	0.0277	0.0227	0.0297	0.0296
A-11	0.0436	0.0386	0.0362	0.0380	0.0308	0.0149	0.0273	0.0195	0.0270	0.0280
A-12	0.0506	0.0422	0.0320	0.0423	0.0324	0.0134	0.0270	0.0180	0.0252	0.0273

Table 7.16 Entropy of each criteria (E_j) data of all wear material

Composite designation	C-1	C-2	C-3	C-4	C-5	C-6	C-7	C-8	C-9	C-10
B-1	-0.0909	-0.0801	-0.1448	-0.1329	-0.1248	-0.2133	-0.19268	-0.19658	-0.16990	-0.16881
B-2	-0.1166	-0.0886	-0.1395	-0.1385	-0.1459	-0.2066	-0.17354	-0.18587	-0.16628	-0.16615
B-3	-0.1474	-0.0996	-0.1339	-0.1461	-0.1664	-0.2015	-0.16628	-0.17681	-0.15865	-0.15777
B-4	-0.1799	-0.1113	-0.1286	-0.1505	-0.1859	-0.1966	-0.155651	-0.16791	-0.15547	-0.15107
B-5	-0.0837	-0.1665	-0.1497	-0.1354	-0.1334	-0.1516	-0.12589	-0.13791	-0.13198	-0.13646
B-6	-0.1034	-0.177	-0.149	-0.1409	-0.1511	-0.1476	-0.11841	-0.12863	-0.12709	-0.12889
B-7	-0.1268	-0.1888	-0.1388	-0.1548	-0.1688	-0.1409	-0.11495	-0.11477	-0.12033	-0.12805
B-8	-0.1474	-0.1999	-0.1354	-0.1594	-0.1879	-0.1329	-0.11312	-0.10879	-0.11598	-0.11667
B-9	-0.0714	-0.177	-0.1539	-0.1385	-0.1363	-0.0769	-0.10079	-0.08049	-0.09207	-0.08495
B-10	-0.0918	-0.1897	-0.1516	-0.1432	-0.1536	-0.0687	-0.09779	-0.07255	-0.08778	-0.07808
B-11	-0.1074	-0.1974	-0.1474	-0.1618	-0.1739	-0.0627	-0.09575	-0.06637	-0.08358	-0.07597
B-12	-0.1379	-0.2091	-0.1433	-0.1658	-0.1923	-0.0578	-0.09369	-0.06345	-0.07977	-0.07854
A-1	-0.1113	-0.0452	-0.1319	-0.1051	-0.0828	-0.2114	-0.19268	-0.20537	-0.18697	-0.18089
A-2	-0.1409	-0.0498	-0.1236	-0.1068	-0.0934	-0.1869	-0.17986	-0.19688	-0.17987	-0.17898
A-3	-0.1978	-0.0647	-0.1034	-0.1122	-0.0969	-0.1438	-0.17196	-0.17884	-0.16999	-0.17668
A-4	-0.1979	-0.0746	-0.0969	-0.1139	-0.1008	-0.1196	-0.16059	-0.17087	-0.16679	-0.16768
A-5	-0.1045	-0.0959	-0.1397	-0.1104	-0.0876	-0.1104	-.118798	-0.13574	-0.14396	-0.14645
A-6	-0.1255	-0.1054	-0.1269	-0.1104	-0.0994	-0.1054	-0.11697	-0.12486	-0.13877	-0.14689
A-7	-0.1551	-0.117	-0.1137	-0.1225	-0.1035	-0.1006	-0.11364	-0.11662	-0.13242	-0.13856
A-8	-0.1769	-0.1227	0.1067	-0.1258	-0.1075	-0.0971	-0.11169	-0.10879	-0.12689	-0.14698
A-9	-0.0939	-0.1007	-0.1499	-0.1122	-0.0905	-0.0769	-0.10091	-0.08943	-0.10608	-0.10708
A-10	-0.1128	-0.1098	-0.1309	-0.1139	-0.1028	-0.0687	-0.09983	-0.08586	-0.10408	-0.10407
A-11	-0.1368	-0.1255	-0.1207	-0.1247	-0.1075	-0.0627	-0.09839	-0.07688	-0.09750	-0.10332
A-12	-0.1509	-0.1338	-0.1106	-0.1338	-0.1112	-0.0578	-0.09775	-0.07496	-0.09265	-0.09873

Table 7.17 Weight of each criteria (ψ_j) data of all wear material

Composite designation	C-1	C-2	C-3	C-4	C-5	C-6	C-7	C-8	C-9	C-10
B-1	0.02863	0.02521	0.04599	0.04163	0.03974	0.06712	0.06069	0.06189	0.05347	0.05297
B-2	0.03688	0.02789	0.04385	0.04362	0.04588	0.06525	0.05467	0.05839	0.05238	0.05179
B-3	0.04634	0.03125	0.04268	0.04598	0.05237	0.06346	0.05366	0.05556	0.04999	0.04969
B-4	0.05658	0.03536	0.04077	0.04767	0.05848	0.06171	0.04898	0.05276	0.04894	0.04781
B-5	0.02614	0.05318	0.04721	0.04264	0.04199	0.04774	0.03958	0.04138	0.04156	0.04199
B-6	0.03255	0.05733	0.04599	0.04408	0.04752	0.04645	0.03719	0.03898	0.03997	0.04019
B-7	0.03994	0.05948	0.04683	0.04872	0.05343	0.04447	0.03617	0.03609	0.03777	0.03841
B-8	0.04634	0.06293	0.04559	0.05009	0.05938	0.04186	0.03559	0.03433	0.03678	0.03531
B-9	0.02248	0.05733	0.04866	0.04362	0.04292	0.02423	0.03165	0.02547	0.02897	0.02579
B-10	0.02891	0.05995	0.04761	0.04504	0.04856	0.02161	0.03065	0.02277	0.02749	0.02458
B-11	0.03385	0.06239	0.04691	0.05098	0.05466	0.01975	0.03009	0.02088	0.02559	0.02376
B-12	0.04348	0.06806	0.04513	0.0522	0.06055	0.01827	0.02969	0.01988	0.02347	0.02246
A-1	0.03531	0.01469	0.04474	0.03308	0.02589	0.06653	0.06069	0.06466	0.05778	0.05679
A-2	0.04454	0.01602	0.03879	0.03362	0.02939	0.05885	0.05660	0.06195	0.05537	0.05567
A-3	0.06263	0.02037	0.03255	0.03531	0.03055	0.04547	0.05410	0.05788	0.05347	0.05434
A-4	0.06302	0.02336	0.03056	0.03586	0.03173	0.03768	0.05055	0.05375	0.05239	0.05278
A-5	0.03806	0.03027	0.043861	0.03475	0.02755	0.03476	0.03738	0.04278	0.04517	0.04608
A-6	0.03866	0.03351	0.039838	0.03475	0.03186	0.03387	0.03669	0.03929	0.04367	0.04494
A-7	0.04878	0.03641	0.035678	0.03855	0.03286	0.03158	0.03577	0.03685	0.04158	0.04354
A-8	0.05675	0.03867	0.033591	0.03959	0.03375	0.03059	0.03508	0.03433	0.03956	0.04238
A-9	0.02971	0.03198	0.047108	0.03531	0.02848	0.02423	0.03165	0.02809	0.03337	0.03369
A-10	0.03573	0.03457	0.041159	0.03586	0.03237	0.02161	0.03139	0.02702	0.03287	0.03298
A-11	0.04298	0.03955	0.037787	0.03907	0.03375	0.01975	0.03098	0.02484	0.03068	0.03154
A-12	0.04756	0.04239	0.034666	0.04229	0.035	0.01827	0.03067	0.02279	0.02917	0.03098
E_j	0.9767	0.9526	0.9953	0.9937	0.9763	0.9434	0.978	0.9587	0.9801	0.9783
ψ_j	0.0233	0.0474	0.0047	0.0063	0.0237	0.0566	0.022	0.0413	0.0199	0.0217
Weight	0.0812	0.1651	0.0164	0.0219	0.0825	0.1971	0.0766	0.1439	0.0693	0.0756

Table 7.18 Decision matrix of all wear material

Composite designation	C-1	C-2	C-3	C-4	C-5	C-6	C-7	C-8	C-9	C-10
B-1	3.09	68	375.13	57	0.283	0.00698	0.02038	0.00873	0.01125	1.72E-07
B-2	4.35	78	355.19	61	0.356	0.00662	0.01725	0.00795	0.01088	1.66E-07
B-3	6.13	91	335.33	66	0.436	0.00635	0.01613	0.00735	0.01012	1.56E-07
B-4	8.34	107	315.93	69	0.518	0.00607	0.01459	0.00678	0.00981	1.46E-07
B-5	2.73	193	395.29	59	0.313	0.00406	0.0106	0.00471	0.00769	1.20E-07
B-6	3.69	213	376.36	62	0.376	0.0039	0.00974	0.00427	0.00728	1.14E-07
B-7	4.93	236	353.17	72	0.446	0.00364	0.00936	0.00386	0.00671	1.06E-07
B-8	6.13	259	339.9	75	0.528	0.00334	0.00915	0.00359	0.00636	9.47E-08
B-9	2.23	213	411.13	61	0.323	0.00156	0.00776	0.00237	0.00463	6.08E-08
B-10	3.13	237	401.36	64	0.386	0.00134	0.00742	0.00205	0.00431	5.75E-08
B-11	3.89	253	386.15	77	0.466	0.00119	0.00721	0.00183	0.00391	5.31E-08
B-12	5.57	279	369.19	80	0.548	0.00107	0.00703	0.00169	0.00347	5.08E-08
A-1	4.09	32	327.3	41	0.159	0.00688	0.02038	0.00937	0.0125	1.92E-07
A-2	5.75	36.2	297.1	42	0.189	0.00562	0.01825	0.00875	0.01188	1.86E-07
A-3	9.73	51.2	231.8	45	0.199	0.00375	0.017	0.0075	0.01125	1.79E-07
A-4	9.74	61.2	211.8	46	0.21	0.00287	0.01529	0.00698	0.0109	1.71E-07
A-5	3.73	87	355.29	44	0.173	0.00256	0.00981	0.00491	0.00869	1.39E-07
A-6	4.69	99	308.73	44	0.206	0.00239	0.00954	0.00437	0.00828	1.34E-07
A-7	6.63	113	263.66	51	0.218	0.00224	0.00921	0.00396	0.00771	1.28E-07
A-8	8.13	123	242.19	53	0.229	0.00214	0.00895	0.00359	0.00716	1.23E-07
A-9	3.23	93	395.13	45	0.181	0.00156	0.00776	0.00273	0.00563	8.86E-08
A-10	4.13	105	323.69	46	0.216	0.00134	0.00762	0.00259	0.00551	8.53E-08
A-11	5.49	127	286.13	52	0.229	0.00119	0.00751	0.00223	0.00501	8.08E-08
A-12	6.37	139	253.16	58	0.241	0.00107	0.00743	0.00206	0.00467	7.86E-08
MAX	9.74	279	411.13	80	0.548	0.00698	0.02038	0.00937	0.0125	1.92E-07
MIN	2.23	32	211.8	41	0.159	0.00107	0.00703	0.00169	0.00347	5.08E-08
Weight	0.0812	0.1651	0.0164	0.0219	0.0825	0.1971	0.0766	0.1439	0.0693	0.0756
MAX-MIN	7.51	247	199.33	39	0.389	0.00591	0.01335	0.00768	0.00903	1.42E-07

Table 7.19 α_i, β_i, Ω_i values and ranking of the alternatives.

Composite designation	α_i	β_i	Ω_i	Ranking
B-1	0.7526	0.1971	0.9021	23
B-2	0.6928	0.1851	0.8349	22
B-3	0.6473	0.1761	0.7842	20
B-4	0.6064	0.1668	0.7352	18
B-5	0.3719	0.0997	0.4498	12
B-6	0.3305	0.0944	0.4197	11
B-7	0.2832	0.0857	0.3266	6
B-8	0.2376	0.0757	0.2730	5
B-9	0.1500	0.0477	0.1454	4
B-10	0.1100	0.0344	0.0857	3
B-11	0.0687	0.0179	0.0508	2
B-12	0.0396	0.0361	0.0164	1
A-1	0.8557	0.1938	0.9511	24
A-2	0.7925	0.1623	0.8276	21
A-3	0.7256	0.1523	0.7619	19
A-4	0.6619	0.1456	0.7073	17
A-5	0.4622	0.1283	0.5464	16
A-6	0.4382	0.1203	0.5105	15
A-7	0.4249	0.111	0.4771	14
A-8	0.4141	0.1043	0.4523	13
A-9	0.3108	0.1243	0.4157	10
A-10	0.2969	0.1163	0.3775	9
A-11	0.2753	0.1016	0.3665	8
A-12	0.2621	0.0936	0.3367	7

Chapter Summery

This chapter has provided:

1. VIKOR Method is applied for the selection of optimal composition by strengthening with ENTROPY method.
2. ENTROPY method is used for the weight criteria of ten PDAs. These ten PDAs are very different in functioning, even though hybrid ENTROPY/VIKOR method gives the result for selection of composition i.e. appropriate or best composition for the wear application.
3. Based on final optimization by ENTROPY/VIKOR approach, ranking of wear composites is:
   Type-1 wear composites: A-12>A-11>A-10>A-9>A-8>A-7>A-6>A-5>A-4>A-3>A-2>A-1
   Type-2 wear composites: B-12>B-11>B-10>B-9>B-8>B-7>B-6>B-5>B-4>B-3>B-2>B-1
   Overall the ranking order was: B-12>B-11>B-10>B-9>B-8>B-7>A-12>A-11>A-10>A-9>B-6>B-5>A-8>A-7>A-6>A-5>A-4>B-4>A-3>B-3>A-2>B-2>B-1>A-1
   Thus it is concluded that the Multilayer coated 6 wt.% granite powder reinforced 5083 aluminum alloy composites i.e. B-12 based wear composition was adjusted to be optimal option.
4. The VIKOR method strengthened by ENTROPY is an effective tool for the ranking or selection of friction materials and should be helpful in the optimal wear composition selection without performing long and costly laboratory experiments. Thus performance evaluation of composite wear materials having various PDAs may be predicted with appreciable accuracy for designing wear material formulations.

Chapter 8

SUMMARY AND FUTURE SCOPE

Introduction

This chapter contains the summary of the work done along with objectives, conclusions based on the research work presented in this thesis followed by scope for future work in this field. The research reported in this thesis broadly consists of two parts:

- The first part provided the detail explanation of the matrix material, granite particulate filler material and coating technique. It also provided the fabrication technique and detail description of physical, mechanical, fracture and thermo-mechanical characterisations uncoated and coated granite particulate filled aluminium alloyed composites
- In this study the second part has reported the effect of granite particulate reinforcement and single, multilayer coating on slurry erosion wear characteristics of proposed metal alloyed composites. Simultaneously it also represent the effect of granite particulate reinforcement and single, multilayer coating on corrosion properties uncoated and coated granite particulate filled aluminium alloyed composites

8.1. Summary of research findings

The work in this thesis is initiated with a goal to find the influence of single layer and multilayer coating with waste granite particulate as reinforcement on physical, mechanical, fracture and slurry erosion wear, corrosion wear performance. Incorporation granite particulate as particulate fillers into alloyed metal matrix, shows the modified mechanical, fracture and improved slurry erosion wear, corrosion wear resistance. Further deposition of single layer and multilayer coating tailored the mechanical, fracture and improved slurry erosion wear, corrosion wear properties. This would lead to guidelines to select the appropriate formulation to achieve the best combination of performance properties in proposed materials.

Inclusion of granite particulate in alloy matrix decreased the load bearing capacity (Flexural strength) and improved the ability to withstand shock loading (Impact strength) of the composites. After deposition of single layer and multilayer coating on granite filled aluminium alloyed composites, the load bearing capacity (Flexural strength) and the ability to withstand shock loading (Impact strength) is improve. The decrement in strength due to incorporation of granite particle may be attributed to the presence of pores at the interface between the filler particles and the matrix, the interfacial adhesion may be too weak to transfer the stress and increment in strength after deposition of single layer and multilayer

coating due to the synergy effect of reinforcement and coating. The enhancement in impact strength after incorporation of granite particle may be attributed to the positive effect of granite particulate size and increment in strength after deposition of single layer and multilayer coating due to the synergy effect of reinforcement and coating.

Hardness values is enhance due to incorporation of granite particulate into base matrix and it further improved after deposition of single layer and multilayer coating on granite filled aluminium alloyed composites. The improvement in hardness value after incorporation of granite particle is quite obvious and expected since granite particulate is combination of different hard dispersed ceramic materials and contributes effectively to increase hardness of the composites, The improvement in hardness of single layer coating due to the promising hardness of chromium nitride coating on the other hand in multilayer coating CrN/SiN stack is attributed to many interfaces that blocked the micro-crack movements across interfaces due to differences in the shear module of the individual layer material.

The magnitude of stress intensity factor enhance with incorporation of granite particulate into base matrix but it remain higher as compared to unfilled metal matrix composites but it further improved after deposition of single layer and multilayer coating on granite filled aluminium alloyed composites. The increment in stress intensity factor after incorporation of granite particulate in to base matrix may be attributed to the enhancement of interfacial bonding between matrix and particulate. The fracture toughness decreases with increasing volume fraction of granite particulate reinforcement, a trend which is consistent regardless of the matrix temper and increment in stress intensity factor after deposition of single layer and multilayer coating due to the synergy effect of reinforcement and coating.

In present investigation it is notice that the uncoated granite filled aluminium alloyed composites shows higher void fraction as compared to single layer and multilayer coated granite filled aluminium alloyed composites. Among all set of composites, least value of void fraction is record for multilayer coated granite filled aluminium alloyed composites.

However, for the multilayer coated granite filled aluminium alloyed composites, minimum void fraction is observed. The presence of pores and voids in the composite structure significantly affect some of the mechanical properties and even the performance of the composites. Higher void contents usually mean lower fatigue resistance, greater susceptibility to water penetration and weathering. However, presence of void is unavoidable

in composite making granite particulate filled aluminium alloyed composites particularly through Liquid stir casting process.

The slurry erosion rates of multilayer coated granite particulate filled aluminium alloyed composites are found lower than single layer coated and uncoated granite particulate filled aluminium alloyed composites under similar test conditions. The incorporation granite particulate into base matrix improves the slurry erosion rate as compared to uncoated and improvement in slurry erosion resistance can be attributed to two reasons. One is the improvement in the hardness of the composite with addition of these hard filler particles. Secondly, during the erosion process, the filler particles absorb a good part of the kinetic and thermal energy associated with the erodent. This results in less amount of energy being available to be absorbed by the matrix body. These two factors together lead to the enhancement of erosion wear resistance of the composites. The improvement in slurry erosion resistance after deposition of single layer and multilayer coating can be attributed to two reasons. One is the improvement in the hardness of the composite and second during the erosion process, the coating absorbs a good part of the kinetic and thermal energy associated with the erodent. This results in less amount of energy being available to be absorbed by the matrix body.

The slurry erosion rates of uncoated and coated granite filled aluminium alloyed composites are found to be dependent on the impingement angle. The results of this research further suggest that, the slurry erosion rate was influenced by the nature of reinforcement material as well as coating material. In fact, the angle of impact determines the relative magnitude of the two components of the impact velocity namely, the component normal to the surface and parallel to the surface. Hence, as this angle changes the amount of sliding that takes place also changes the nature and magnitude of the stress system. Both of these aspects influence the slurry erosion wear rate of composite. This study therefore implies that composites with reinforcement and coating of different type material exhibited different angular dependency.

The corrosion rate of multilayer coated granite particulate filled aluminium alloyed composites are found lower than single layer coated and uncoated granite particulate filled aluminium alloyed composites for under similar test condition of time and pH value of solution. The incorporation of granite particulate into base matrix leads to increment in corrosion resistance it further improved after deposition of single layer and multilayer coating on granite particulate filled aluminium alloyed composites.

8.2. Conclusions

The experimental investigation of physical, mechanical, thermo-mechanical, corrosion wear and improved slurry erosion wear resistance of uncoated and coated granite particulate filled aluminium alloyed composites drawn specific conclusions which are presented below.

1. The addition of granite particle into base matrix enhance void content but after deposition of single layer and multilayer coating void content reduced but trend same as uncoated granite reinforced 1050 aluminum alloyed composites
2. The addition of granite particle into base matrix enhance void content but after deposition of single layer and multilayer coating void content reduced but trend same as uncoated granite reinforced 5083 aluminum alloyed composites.
3. The incorporation of granite particulate into aluminum matrix lead toward the decrement in flexural strength of composites. However, unfilled aluminum alloy indicated maximum flexural strength and 6 wt.% granite particulate reinforcement indicated minimum flexural strength. Single layer, multilayer coating enhanced flexural strength of granite reinforced 1050 aluminum alloyed composites but its trend shows slight decrement in flexural strength. Flexural Strength decreased (327.3-211.8 MPa) after addition of granite particle into base matrix, (355.2-242.1 MPa) after deposition of single layer coating and (395.3-253.2 MPa) after multilayer coating.
4. The incorporation of granite particulate into aluminum matrix lead toward the decrement in flexural strength of composites. However, unfilled aluminum alloy indicated maximum flexural strength and 6 wt.% granite particulate reinforcement indicated minimum flexural strength. Single layer, multilayer coating enhanced flexural strength of granite reinforced 5083 aluminum alloyed composites but its trend shows slight decrement in flexural strength. Flexural Strength decreased (375.1-315.9 MPa) after addition of granite particle into base matrix, (395.3-339.9 MPa) after deposition of single layer coating and (411.1-369.2 MPa) after multilayer coating.
5. Addition of granite particulate into base matrix enhanced hardness of composites and maximum hardness is found for 6 wt.% granite particulate 1050 aluminum alloyed composites but deposition of single layer and multilayer significantly enhanced hardness value of composites. Hardness enhanced (32 Hv-61.2 Hv) after addition of granite particle into base matrix, (87 Hv-123 Hv) after deposition of single layer coating and (93 Hv-139 Hv) after multilayer coating.

6. Addition of granite particulate into base matrix enhanced hardness of composites and maximum hardness is found for 6 wt.% granite particulate 5083 aluminum alloyed composites but deposition of single layer and multilayer significantly enhanced hardness value of composites. Hardness enhanced (68 Hv-107 Hv) after addition of granite particle into base matrix, (193 Hv-259 Hv) after deposition of single layer coating and (213 Hv-279 Hv) after multilayer coating.
7. Impact energy absorption value enhanced with addition of granite particulate into the base matrix material without coated. After deposition of single layer and multilayer coating the magnitude of impact energy improved slightly for granite particulate 1050 aluminum alloyed composites. Impact Strength enhanced (41-46 Joule) after addition of granite particle into base matrix, (44-53 Joule) after deposition of single layer coating and (45-58 Joule) after multilayer coating.
8. Impact energy absorption value enhanced with addition of granite particulate into the base matrix material without coated. After deposition of single layer and multilayer coating the magnitude of impact energy improved slightly for granite particulate 5083 aluminum alloyed composites. Impact Strength enhanced (57-69 Joule) after addition of granite particle into base matrix, (59-74 Joule) after deposition of single layer coating and (61-79 Joule) after multilayer coating.
9. The magnitude of stress intensity factor for the granite particulate reinforced aluminum alloyed composites are well remains above the unfilled 1050 aluminum alloyed composite. However, 6 wt.% granite particulate reinforced composites shows maximum magnitude of stress intensity factor for all crack lengths. Single and multilayer coating enhanced the magnitude of stress intensity factor slightly irrespective of crack lengths.
10. The magnitude of stress intensity factor for the granite particulate reinforced aluminum alloyed composites are well remains above the unfilled 5083 aluminum alloyed composite. However, 6 wt.% granite particulate reinforced composites shows maximum magnitude of stress intensity factor for all crack lengths. Single and multilayer coating enhanced the magnitude of stress intensity factor slightly irrespective of crack lengths.
11. Dynamic mechanical analysis (DMA) of uncoated, single layer coated and multilayer coated granite particulate reinforced aluminum alloyed composites have been carried out to investigate the variation of storage modulus (E'), loss modulus(E") and damping factor (Tan δ) as a function of temperature. Storage modulus is decreases with increment in temperature and loss modulus is increases with increment in temperature for uncoated,

single layer and multilayer coated particulate reinforced 1050 aluminum alloyed composites.

12. Dynamic mechanical analysis (DMA) of uncoated, single layer coated and multilayer coated granite particulate reinforced aluminum alloyed composites have been carried out to investigate the variation of storage modulus (E'), loss modulus(E") and damping factor (Tan δ) as a function of temperature. Storage modulus is decreases with increment in temperature and loss modulus is increases with increment in temperature for uncoated, single layer and multilayer coated particulate reinforced 5083 aluminum alloyed composites.
13. The S/N ratio is found to be 38.01, 49.02, 50.94 db for uncoated, single layer coated, multilayer coated granite particulate reinforced 1050 aluminum alloyed composites respectively. Utilizing the predictive equations is highly essential as it authenticates the result derived from ANNOVA, it is concluded from confirmation tests that for granite reinforced composites, the error associated in prediction and experimental largely lies in the range of 5.17%, 2.59% and 2.32% for uncoated, single layer coated and multilayer coated respectively, which is well within limits.
14. The S/N ratio is found to be 43.89, 49.30, 51.06 db for uncoated, single layer coated, multilayer coated granite particulate reinforced 5083 aluminum alloyed composites respectively. Utilizing the predictive equations is highly essential as it authenticates the result derived from ANNOVA, it is concluded from confirmation tests that for granite reinforced composites, the error associated in prediction and experimental largely lies in the range of 5.17%, 2.59% and 2.32% for uncoated, single layer coated and multilayer coated respectively, which is well within limits.
15. Slurry erosion rate is increased with impact velocity for all compositions but it decreases with addition of granite particulate. Granite particulate contains hard particles resist the impact of slurry. It also evident from the results as coating deposition increase wear performance is enhancing. Multilayer coated samples indicated minimum wear as compared to uncoated granite reinforced 1050 aluminum alloyed samples.
16. Slurry erosion rate is increases with impingement angle upto 60 degree after that increment in impingement angle its lower down for uncoated, single layer coated, multilayer coated granite particulate reinforced composites. Coating enhance erosion rate and multilayer coated samples indicated minimum wear as compared to single layer and uncoated granite reinforced 1050 aluminum alloyed composites.

17. Slurry erosion rate is linearly increase with increment in slurry concentration for uncoated, single layer coated, multilayer coated granite particulate reinforced 1050 aluminum alloyed composites. For uncoated samples as reinforcement incorporation increases erosion rate is decreases. Multilayer coated granite reinforced sample indicated minimum wear among all compositions.
18. Analysis of eroded surface of uncoated and coated samples exhibited mainly two types of erosion mechanism for material micro-cutting, micro-ploughing and plastic deformation which convert into fracture after repeated impact of hard abrasive particles.
19. Slurry erosion rate is increased with impact velocity for all compositions but it decreases with addition of granite particulate. Granite particulate contains hard particles resist the impact of slurry. It also evident from the results as coating deposition increase wear performance is enhancing. Multilayer coated samples indicated minimum wear as compared to uncoated granite reinforced 5083 aluminum alloyed samples.
20. Slurry erosion rate is increases with impingement angle upto 60 degree after that increment in impingement angle its lower down for uncoated, single layer coated, multilayer coated granite particulate reinforced composites. Coating enhance erosion rate and multilayer coated samples indicated minimum wear as compared to single layer and uncoated granite reinforced 5083 aluminum alloyed composites.
21. Slurry erosion rate is linearly increase with increment in slurry concentration for uncoated, single layer coated, multilayer coated granite particulate reinforced 5083 aluminum alloyed composites. For uncoated samples as reinforcement incorporation increases erosion rate is decreases. Multilayer coated granite reinforced sample indicated minimum wear among all compositions.
22. Analysis of eroded surface of uncoated and coated samples exhibited mainly two types of erosion mechanism for material micro-cutting, micro-ploughing and plastic deformation which convert into fracture after repeated impact of hard abrasive particles. And for coating samples brittle failure and pallet formation features is observed.
23. The corrosion rate is decreases with time but after addition of granite particle into base matrix it reduced, trend still same as unreinforced. Similarly after deposition of single layer and multilayer coating corrosion rate further decreased with decrement trend for all coated and uncoated 1050 granite reinforced aluminum alloyed composites sample.
24. The Corrosion rate is increases with pH value of solution but after addition of granite particle into base matrix it reduced, trend still same as unreinforced. Similarly after

deposition of single layer and multilayer coating corrosion rate further decreased with increment trend for all coated and uncoated 1050 granite reinforced aluminum alloyed composites sample.

25. The corrosion rate is decreases with time but after addition of granite particle into base matrix it reduced, trend still same as unreinforced. Similarly after deposition of single layer and multilayer coating corrosion rate further decreased with decrement trend for all uncoated and coated 5083 granite reinforced aluminum alloyed composites sample.
26. The Corrosion rate is increased with pH value of solution but after addition of granite particle into base matrix it reduced, trend still same as unreinforced. Similarly after deposition of single layer and multilayer coating corrosion rate further decreased with increment trend for all uncoated and coated 5083 granite reinforced aluminum alloyed composites sample.

    Finally, the calculation of ranking order by using VIKOR method for analysis of mechanical, physical, fracture, corrosion wear and slurry erosion wear behaviour of uncoated and coated granite particulate filled aluminum alloyed composites is done and the sequence of ranking is B-12>B-11>B-10>B-9>B-8>B-7>A-12>A-11>A-10>A-9>B-6>B-5>A-8>A-7>A-6>A-5>A-4>B-4>A-3>B-3>A-2>B-2>B-1>A-1. B-12(multilayer coated 6 wt.- % granite particulate reinforced 5083 aluminum alloyed composites) shows the optimal performance among all considered set of composition in this study.

8.3. Scope for future work

Further scope of research and development steps that would contribute to the subject of this research has been identified and some area for future work is as:

- The present investigation has been limited to stir casting process. The other casting techniques could be tried and analysed. This may lead to mixing weight fraction of granite particulate and a final conclusion can be drawn more effectively
- In present investigation thermal vapour vacuum coating has been utilized. The other coating techniques could be tried and analysed so that effect of coating thickness can be determined for some specific alloys used in different applications.
- Treatment of coating could be tried to analyse its effect on slurry erosion wear and corrosion wear.

- Corrosion is not investigated in this study in learns of mechanism of failure. It is proposed to investigate micro-galvanic corrosion that may occur between coating particles and base metal in the existence of corrosive environment.
- Cost analysis of these composites to assess their economic viability in various industrial applications can be investigated.

****

References

1. Energy Statistics 2013 report published by ministry of statistics and programme implementation government of india.
2. Ramesh CS, Kumar S, Devraj DS, Keshavmurthy R, Slurry Erosive Wear Behavior of Plasma Sprayed Inconel-718 Coatings on Al6061 Alloy, Journal of Minerals & Materials Characterization & Engineering, 2011, vol. 10, pp. 445-453.
3. Bhoi R, Ali SM, Potential of Hydro Power Plant in India and its Impact on Environment, International Journal of Engineering Trends and Technology, 2011, vol. 10, pp. 114-119.
4. Hemanth J "Abrasive and slurry wear behavior of chilled aluminum alloy (A356) reinforced with fused silica (SiO_2p) metal matrix composites" Composites Part-B, 2011, vol. 42, pp. 1826-1833.
5. Fang Q, Sidky PS, Hocking GM, Erosion resistance of continuously reinforced SiC-Ti-based metal matrix composites by a SiC water slurry jet, Wear, 1999, vol. 233, pp. 174-181.
6. Ramachandra M, Radhakrishna K, Effect of reinforcement of flyash on sliding wear, slurry erosive wear and corrosive behavior of aluminium matrix composite, Wear, 2007, vol. 262, pp. 1450-1462.
7. Das S, Saraswathi YL, Mondal DP, Erosive-corrosive wear of aluminum alloy composites: Influence of slurry composition and speed, Wear, 2006, vol. 261, pp. 180-190.
8. Das S, Mondal DP, Modi OP, Dasgupta R, Influence of experimental parameters on the erosive-corrosive wear of Al-SiC particle composite, Wear, 1999, vol. 231, pp. 195-205.
9. Goyal DK, Singh H, Kumar H, Sahni V, Slurry Erosive Wear Evaluation of HVOF-Spray Cr_2O_3 Coating on Some Turbine Steels, Journal of Thermal Spray Technology, 2011, vol. 21, pp. 838-851.
10. Grewal HS, Bhandari S, Singh H, Parametric Study of Slurry-Erosion of Hydroturbine Steels with and without Detonation Gun Spray Coatings using Taguchi Technique, Metallurgical and Materials Transactions A, 2012, vol. 43, pp. 3387-3401.
11. Shivamurthy RC, Kamraj M, Nagarajan R, Shariff SM, Padmanabham G, Slurry Erosion Characteristics and Erosive Wear Mechanisms of Co-Based and Ni-Based Coatings

Formed by Laser Surface Alloying, Metallurgical and Materials Transactions A, 2010, vol. 41A, pp. 470-486.

12. Bhandari S, Singh H, Kansal HK, Rastogi V, Slurry Erosion Behaviour of Detonation Gun Spray Al_2O_3 and Al_2O_3-13TiO_2-Coated CF8M Steel Under Hydro Accelerated Conditions, Tribology Letters, 2012, vol. 45, pp. 319-331.
13. Bhandari S, Singh H, Kansal HK, Rastogi V, Slurry Erosion Performance Study of Detonation Gun-Sprayed WC-10Co-4Cr Coatings on CF8M Steel Under Hydro-Accelerated Conditions, Journal of Thermal Spray Technology, 2012, vol. 21, pp. 1054-1064.
14. Manisekaran T, Kamraj M, Sharrif SM, Joshi SV, Slurry Erosion Studies on Surface Modified 13Cr-4Ni Steels: Effect of Angle of Impingement and Particle Size, Journal of Materials Engineering and Performance, 2007, vol. 16, pp. 567-572.
15. Agarwal BD, and Broutman LJ, Analyswas and performance of fiber composites, Second Edition. John Wiley and Sons, Inc.1990.
16. Mehrabian R, Riek RG, Flemings MC, Preparation and casting of Metal Particulate Non-Metal composites, Metallurgical Transactions A, 1974, vol. 5, pp. 1899-1905.
17. Eliasson J and Sandstorm R, Applications of Aluminium Matrix Composites, Transaction Technology publications, Switzerland, 1995, pp 3-36.
18. Lopez D, Sanchez C, Toro A, Corrosion-erosion behavior of TiN-coated stainless steels in aqueous slurries, Wear, 2005, vol. 258, pp. 684-692.
19. Durney LJ, Electroplating Engineering Handbook, Van Norstand, NY, USA, 1984.
20. Biestek T and Weber J, Electrolytic and Chemical Conversion Coating, Portcullis Press Ltd, Warsaw, Poland, 1976.
21. Tape NA, BakerEA,Jackson BC, Plating and Surface Finishing, October, 1976 pp. 30.
22. Ashby MF and Jones DR, Engineering Materials, Pergamon press, NY, USA, 1980.
23. Brooks CR, Heat Treatment of Ferrous Metals, Hemisphere Publishing Co., Washington, USA, 1979.
24. Dawes C and Tranter DF, 1983, Metal Progress, December, pp. 17.
25. Linial AV and Hunterman HE, Wear of Materials, ASME, NY, USA, 1979.
26. Bhattacharya S and Seaman FD, 1985, Laser Heat Treatment for Gear Application in Laser Processing of Materials, The Metallurgical Society of AIME, pp. 211.

27. Smidt FA, Ion Implantation for Material Processing, Noyes Data Corp, NJ, USA, 1983.
28. Miracle DB, Metal matrix composites- From science to technological significance, Journal of Composites Science and Technology, 2005, vol. 65, pp. 2526-2540.
29. Bunshah RF, Deposition Technologies for Films and Coatings, Noyes Publications, NJ, USA, 1982.
30. Vossen J and Kern W, Thin Film Processes, Academic Press, NY, USA, 1978.
31. Legg HS and Legg KO, Ion Beam Based Techniques for Surface Modification in Surface Modification Technologies, Marcell Dekker Inc, USA, 1989.
32. Blocher JM, Vapour Deposited Materials in Vapour Deposition, Willy, NY, USA, 1966.
33. Bhatt DG, Chemical Vapour Deposition, in "Surface Modification Technologies", by T. S. Sudarsan (ed), Marcell Dekker Inc, USA,1989.
34. Little RL, Welding and Welding Technology, TMH Publications, New Delhi, India, 1979.
35. Xiao-dong YU, Yang-wei W, Fu-chi W, Effect of particle size on mechanical properties of SiCp/5210 Al metal matrix composite, Transaction of Nonferrous Metals Society of China, 2007, vol. 17, pp. 276-279.
36. Milan MT and Bowen P, Tensile and Fracture Toughness Properties of SiC Reinforced Al Alloys: Effects of Particle Size, Particle Volume Fraction, and Matrix Strength. JMEPEG, 2004, vol. 13, pp. 775-783.
37. Zhao DG, Liu XF, Pan YC, Liu YX, Bian XF, Microstructure and mechanical behavior of AlSiCuMgNi piston alloys reinforced with TiB2 particles, Journal of Material Science, 2006, vol. 41, pp. 4227-4232.
38. Tong W, Ravichandran G, Christman T, Vreeland T, Processing and properties of SiC-particulate reinforced titanium matrix composites by shock wave consolidation, Journal DE Physique IV Colloque C8, supplkment au Journal de Physique, 1994, vol. 4, pp. 331-336.
39. Aqida SN, Ghazali MI, Hashim J, The effect of the porosity on mechanical properties of the mechanical properties: An Overview, Jurnal Teknologi, 2004, vol. 40, pp. 17-32.
40. Wang QZ, Cui CX, Lu DM, Bu SJ, Fabrication and properties of a novel ZnO/Cu composite, Journal of Materials Processing Technology, 2010, vol. 210, pp. 497-503.

41. Venkateswarlu K, Saurabh S, Rajinikanth V, Sahu RK, Ray AK, Synthesis of tin reinforced aluminium metal matrix composites through microwave sintering, Journal of Materials Engineering and Performance, 2010, vol. 19, pp. 231-236.
42. Singla M, Dwivedi DD, Singh L, Chawla V, Development of Aluminium Based Silicon Carbide Particulate Metal Matrix Composite, Journal of Minerals & Materials Characterization & Engineering, 2009, vol. 8, pp. 455-467.
43. Barekar N, Tzamtzis S, Dhindaw BK, Patel J, Babu NH, Fan Z, Processing of Aluminum-Graphite Particulate Metal Matrix Composites by Advanced Shear Technology, Journal of Materials Engineering and Performance, 2009.
44. Poddar P, Mukherjee S, Sahoo KL, The Microstructure and Mechanical Properties of SiC Reinforced Magnesium Based Composites by Rheocasting Process, Journal of Materials Engineering and Performance, 2009, vol. 18, pp. 849-855.
45. Turk A, Durman EM, Kayali ES, The effect of manganese on the microstructure and mechanical properties of zinc-aluminium based ZA-8 alloy, Journal of Material Science, 2007, vol. 42, pp. 8298-8305.
46. Sharma SC, Girish BM, Somashekar DR, Kamath R, Satish BM, Mechanical properties and fractography of zircon-particle-reinforced ZA-27 alloy composite materials, Composites Science and Technology, 1999, vol. 59, pp. 1805-1812.
47. Ceschini L, Minak G, Morri A, Study on Forging of the AA2618/20 vol.% Al_2O_3p composite: Effects on microstructure and tensile properties, Composites Science and Technology, 2009, vol. 69, pp. 1783-1789.
48. Daoud A, El-Bitar T, El-Azim AA, Tensile and Wear Properties of Rolled Al_5Mg-Al_2O_3 or C Particulate Composites, Journal of Materials Engineering and Performance, 2003, vol. 12, pp. 390-397.
49. Seah KHW, Hemanth J, Sharma SC, Mechanical properties of aluminum/quartz particulate composites cast using metallic and non-metallic chills, Materials and Design, 2003, vol. 24, pp. 87-93.
50. Ren S, He X, Qu X, Humail IS, Li Y, Effect of Mg and Si in the aluminum on the thermo-mechanical properties of pressureless infiltrated SiCp/Al composites, Composites Science and Technology, 2007, vol. 67, pp. 2103-2113.

51. Geng K, Lu W, Zhang D, Sakata T, Mori H, Tensile properties of in situ synthesized titanium matrix composites reinforced by TiB and Nd_2O_3 at elevated temperature, Materials and Design, 2003, vol. 24, pp. 409-414.
52. Mahendra KV, Radhakrishna K, Fabrication of Al-4.5% Cu alloy with fly ash metal matrix composites and its characterization, Materials Science-Poland, 2007, vol. 25, pp. 1-9.
53. Zhang L, Qu X, Duan B, He X, Ren S, Qin M, Microstructure and thermo-mechanical properties of pressureless infiltrated SiCp/Cu composites, Composites Science and Technology, 2008, vol. 68, pp. 2731-2738.
54. Ranganath G, Sharma SC, Krishna M, Muruli MS, A Study of Mechanical Properties and Fractography of ZA-27/Titanium-Dioxide Metal Matrix Composites, Journal of Materials Engineering and Performance, 2002, vol. 11, pp. 408-413.
55. Hyo SL, Yeo JS, Hong SH, Yoon DJ, Kyung HN, The fabrication process and mechanical properties of SiC/Al-Si metal matrix composites for automobile air-condition compressor pistons, Journal of Materials Processing Technology, 2001, vol. 113, pp. 202-208.
56. Chua BW, Lu L, Lai MO, Influence of SiC particles on mechanical properties of Mg based composite, Composite Structures, 1999, vol. 47, pp. 595-601.
57. Lim LG, Dunne FPE, The effect of volume fraction of reinforcement on the elastic-viscoplastic response of metal-matrix composites, International journal of mechanical Science, 1996, vol. 38, pp. 19-39.
58. Breval E, Synthesis routes to metal matrix composites with specific properties: a review, Composites Engineering, 1995, vol. 5, pp. 1127-l133.
59. Tjong SC, Ma ZY, Microstructural and mechanical characteristics of in situ metal matrix composites, Materials Science and Engineering, 2000, vol.29, pp. 49-113.
60. Xiandong S, Chengping L, Zhuoxuan L, Liuzhang O, The fabrication and properties of particle reinforced cast metal matrix composites, Journal of Materials Processing Technology, 1997, vol. 63, pp. 426-431.
61. Kouzeli M, Weber L, Marchi CS, Mortensen A, Influence of damage on the tensile behavior of pure aluminum reinforced with ≥40 vol. pct alumina particles, Acta mater, 2001, vol. 49, pp. 3699-3709.

62. Chawla N, Shen YL, Mechanical behavior of particle reinforced metal matrix composites, Advanced Engineering Materials, 2001, vol. 3, pp. 1438-1656.
63. Shena YL, Chawla N, On the correlation between hardness and tensile strength in particle reinforced metal matrix composites, Materials Science and Engineering A, 2001, vol. 297, pp. 44-47.
64. Kataiah GS, The mechanical properties and fractography of aluminium 6061-TiO_2 composites, International journal of pharmaceutical studies and research, 2010, vol. 1, pp. 17-25.
65. Abdizadeh H, Improvement in physical and mechanical properties of aluminium/zircon composites fabricated by powder metallurgy method, Materials and Design, 2011, Vol. , pp. 4417-4423.
66. Kok M, Production and mechanical properties of Al_2O_3 particle reinforced 2024 aluminium alloy composites, journal of materials processing Technology, 2005, vol. pp. 381-387.
67. Sharma SC, Mechanical properties and fractography of cast lead/quartz particulate composites, materials and design, 1997, vol. 18, pp. 149-153.
68. Ni Z, Sun YS, Xue F, Bai J, Lu YJ, Microstructure and properties of austenitic stainless steel reinforced with in situ TiC particulate, Materials and Design, 2011, vol. 32, pp. 1462-1467.
69. Liu ZD, Tian J, Li B, Zhao LP, Microstructure and mechanical behaviors of in situ TiC particulates reinforced Ni matrix composites, Materials Science and Engineering, 2010, vol. 527, pp. 3898-3903.
70. Hassan SF, Gupta M, Development of a novel magnesium/nickel composite with improved mechanical properties, Journal of Alloys and Compounds, 2002, vol. 335, pp. 10-15.
71. Yi D, Yu P, Hu B, Liu H, Wang B, Jiang Y, Preparation of nickel-coated titanium carbide particulates and their use in the production of reinforced iron matrix composites, Materials and Design, 2013, vol. 52, pp. 572-579.
72. Ramesh CS, Keshavamurthy R, Channabasappa BH, Ahmed A, Microstructure and mechanical properties of Ni-P coated Si_3N_4 reinforced Al6061 composites, Materials Science and Engineering, 2009, vol. 502, pp. 99-106.

73. Velasco F, Gordo E, Isabel R, Navas EMR, Bautista A, Torralba JM, Mechanical and wear behavior of high speed steel reinforced with TiCN particles, International Journal of Refractory Metals & Hard Materials, 2001, vol. 19, pp. 319-323.
74. Li J, Xia C, Zhang Y, Wang M, Wang H, Effects of TiO_2 coating on microstructure and mechanical properties of magnesium matrix composite reinforced with $Mg_2B_2O_5W$, Materials and Design, 2012, vol. 39, pp. 334-337.
75. Gunes I and Kayali Y, Investigation of mechanical properties of borided Nickel 201 alloy, Materials and Design, 2014, vol. 53, pp. 577-580.
76. Fellner P, Cong PK, Ni-B and Ni-Si composite electrolytic coating, Surface and coating technology, 1996, vol. 82, pp. 317-319.
77. Wu Z, Liu L, Shen B, Wu Y, Deng Y, Zhong C, Hu W, Mechanical behavior of a-Al_2O_3-coated SiC particle reinforced nickel matrix composites, Journal of Alloys and Compounds, 2013, vol. 570, pp. 81-85.
78. Wu FB, Li JJ, Duh JG, Evaluation of the mechanical properties and tribological behavior of the CrN coating deposited on mild steel modified with electroless Ni interlayer, Thin Solid Films, 2000, vol. 377, pp. 354-359.
79. Lin S, Zhou K, Dai M, Lan E, Shi Q, Hu F, Kuang T, Zhuang C, Structural, mechanical, and sand erosion properties of TiN/Zr/ZrN multilayer coatings, Vacuum, 2015, vol. 122, pp. 179-186.
80. Wang DZ, Hua QW, Zeng XY,Influences of parameters on microstructures and mechanical properties of $Cr_{13}Ni_5Si_2$ based composite coating by laser-induction hybrid cladding, Surface & Coatings Technology, 2015, vol. 280, pp. 359-369.
81. Xiong Y, Zhuang W, Zhang M, Effect of the thickness of cold sprayed aluminium alloy coating on the adhesive bond strength with an aluminium alloy substrate, Surface & Coatings Technology, 2015, vol. 270, pp. 259-265.
82. Chen C, Duan C, Li Y, Feng X, Shen Y, Effects of Cu content on the microstructures and properties of Cr-Cu composite coatings fabricated via mechanical alloying method, Powder Technology, 2015, vol. 277, pp. 36-46.
83. Xin Y, Huo K, Hu T, Tang G, Chu PK, Mechanical properties of Al_2O_3/Al bi-layer coated AZ91 magnesium alloy, Thin Solid Films, 2009, vol. 517, pp. 5357-5360.

84. Ou YX, Linb J, Che HL, Moore JJ, Sproul WD, Lei MK, Mechanical and tribological properties of CrN/TiNsuperlattice coatings deposited by a combination of arc-free deep oscillation magnetron sputtering with pulsed dc magnetron sputtering, Thin Solid Films, 2015, vol. 594, pp. 147-155.
85. Lima JMC, Souza ACO, Anami LC, Bottino MA, Melo RM, Souza ROA, Effects of thickness, processing technique, and cooling rate protocol on the flexural strength of a bilayer ceramic system, Dental Materials, 2013, vol. 29, pp. 1063-1072.
86. Sharma AK, Gupta D, On microstructure and flexural strength of metal–ceramic composite cladding developed through microwave heating, Applied Surface Science, 2012, vol. 258, pp. 5583-5592.
87. Bouzakis KD, Skordaris G, Bouzakis E, Makrimallakis S, Kombogiannis S, Lemmer O, Fatigue strength of diamond coatings' interface assessed by inclined impact test, Surface & Coatings Technology, 2013, vol. 237, pp. 135-141.
88. Shan YC, Fu QG, Li HJ, Fang Q, Liu XS, Zhao R, Zhang PF, Improvement of the bonding strength and the oxidation resistance of SiC coating on C/C composites by pre-oxidation treatment, Surface & Coatings Technology, 2014, vol. 253, pp. 234-240.
89. Zhang FY, Yan MF, Microstructure and mechanical properties of multiphase coating produced by plasma nitriding Ti coated GB-5083 aluminum alloy, Surface & Coatings Technology, 2014, vol. 253, pp. 268-276.
90. Yang HQ, Yao ZJ, Luo XX, Zhang ZL, Chen Y, Effect of Nb addition on structure and mechanical properties of FeAl coating, Surface & Coatings Technology, 2015, vol. 270, pp. 221-226.
91. Liu X, Kavanagh J, Matthews A, Leyland A, The combined effects of Cu and Ag on the nanostructure and mechanical properties of CrCuAgN PVD coatings, Surface & Coatings Technology, 2015, doi.org/10.1016/j.surfcoat.2015.08.070.
92. Bouzakis KD, Skordaris G, Charalampous P, Dimofte F, Ene NM, Ehinger R, Gardner S, Modrzejewski BS, Fetty JR, Fatigue and adhesion characterization of DLC coatings on steel substrates by perpendicular and inclined impact tests, Surface & Coatings Technology, 2015, vol. 275, pp. 207-213.

93. Ou YX, Lin J, Che HL, Sproul WD, Moore JJ, Lei MK, Mechanical and tribological properties of CrN/TiN multilayer coatings deposited by pulsed dc magnetron sputtering, Surface & Coatings Technology, 2015, vol. 276, pp. 152-159.
94. Cheng J, Liu D, Liang X, Chenb Y, Evolution of microstructure and mechanical properties of in situ synthesized TiC-TiB_2/CoCrCuFeNi high entropy alloy coatings, Surface & Coatings Technology, 2015, vol. 281, pp. 109-116.
95. Banerjee T, Chattopadhyay AK, Structural, mechanical and tribological properties of pulsed DC magnetron sputtered TiN-WSx/TiN bilayer coating, Surface & Coatings Technology, 2015, vol. 282, pp. 24-35.
96. Li NN, Li GL, Wang HD, Kang JJ, Dong TS, Wang HJ, Influence of TiO2 content on the mechanical and tribological properties of Cr_2O_3-based coating, Materials and Design, vol. 88, pp. 906-914.
97. Jina L, Liu G, Li P, Zhoua H, Wang C, Zhoua G, Adhesion strength and thermal shock properties of nanostructured 5La3TiYSZ, 8LaYSZ and 8CeYSZ coatings prepared by atmospheric plasma spraying, Ceramics International, 2015, vol. 41, pp. 12099-12106.
98. Hamzaha E, Bakhsheshi-Rad HR, Ismail AF, Daroonparvara M, Asgaranic MK, Jabbarzare S, Medraj M, Microstructural, mechanical properties and corrosion behavior of plasma sprayed NiCrAlY/nano-YSZ duplex coating on Mg-1.2Ca-3Zn alloy, Ceramics International, 2015, vol. 41, pp. 15272-15277.
99. Aktug SL, Durdua S, Kutbaya I, Usta M, Effect of Na_2SiO_3*$5H_2O$ concentration on microstructure and mechanical properties of plasma electrolytic oxide coatings on AZ31Mg alloy produced by twin roll casting, Ceramics International, 2016, vol. 42, pp. 1246-1253.
100. Hamzaha E, Bakhsheshi-Rad HR, Ismail AF, Daroonparvara M, Yajid MAM, Medraj M, Preparation and characterization of NiCrAlY/nano-YSZ/PCL composite coatings obtained by combination of atmospheric plasma spraying and dip coating on MgeCa alloy, Journal of Alloys and Compounds, 2016, vol. 658, pp. 440-452.
101. Romanova VA, Balokhonov RR, Schmauder S, The influence of the reinforcing particle shape and interface strength on the fracture behavior of a metal matrix composite, Acta Materialia, 2009, vol.57, pp. 97-107.

102. Cuia C, Wu R, Li Y, Shen Y, Fracture toughness of in situ TiCp±AlNp/Al composite, Journal of Materials Processing Technology, 2000, vol. 100, pp. 36-41.
103. Park BG, Crosky AG, Hellier AK, Fracture toughness of microsphere Al2O3–Al particulate metal matrix composites. Composites: Part B, 2008, vol. 39, pp. 1270-1279.
104. Oh KH and Han KS, Short-fiber/particle hybrid reinforcement: Effects on fracture toughness and fatigue crack growth of metal matrix composites, Composites Science and Technology, 2007, vol. 67, pp. 1719-1726.
105. Wang XJ , Wu K, Huang WX, Zhang HF, Zheng MY, Peng DL, Study on fracture behavior of particulate reinforced magnesium matrix composite using in situ SEM, Composites Science and Technology, 2007, vol. 67, pp. 2253-2260.
106. Mochida T, Taya M, Lioyd DJ, Fracture of particles in a particle/metal matrix composite under plastic straining and its effect on the young's modulus of the composite, Materials Transactions JIM, 1999, vol. 32, pp. 931-942.
107. Joel Hemanth, Fracture toughness and wear resistance of aluminum-boron particulate composites cast using metallic and non-metallic chills, Materials and Design, 2002, vol. 23, pp. 41-50.
108. Blatt D, John R, Coker D, Stress intensity factor and compliance solutions for a single edge notched specimen with clamped ends, Engineering Fracture Mechanics, 1996; vol. 41, pp. 521-532.
109. Kruzic JJ, Marks RA, Yoshiya M, Glaeser AM, Cannon RM, Ritchie RO, Fracture and Fatigue Behavior at Ambient and Elevated Temperatures of Alumina Bonded with Copper/Niobium/Copper Interlayers, Journal of American Ceramic Society, 2002, vol. 85, pp. 2531-2541.
110. Agrawal P and Sun CT, Fracture in metal–ceramic composites, Composites Science and Technology, 2004, vol. 64, pp.1167-1178.
111. Srivatsan TS, Hajria MA, Vasudevan VK, Cyclic plastic strain response and fracture behavior of 2009 aluminum alloy metal-matrix composite, International Journal of Fatigue, 2005, vol. 27, pp.357-371.
112. Gupta M, Surappa MK, Qin S, Effect of interfacial characteristics on the failure-mechanism mode of a SiC reinforced A1 based metal-matrix composite, Journal of Materials Processing Technology, 1997, vol 67, pp. 94-99.

113. Wang S.R, Geng H.R, Wang Y.Z and Zhang J.C, (2006). Microstructure and fracture characteristic of Mg-Al-Zn-Si_3N_4 composites, Theoretical and Applied Fracture Mechanics, 46:57–69.
114. Chichili DR and Ramesh KT, Dynamic failure mechanisms in a 6061-T6 $A1/A1_2O_3$ metal-matrix composite, International Journal of Solids Structures, 1995, vol. 32, pp. 2609-2626.
115. Ranjbaran MM, Experimental investigation of fracture toughness in Al356-SiCp aluminium matrix composite, American Journal Society Industrial Research, 2010, vol. 1, pp. 549-557.
116. Velasco F, Dacosta CE, Candela N, Torralba JM, Fracture analysis of aluminium matrix composite materials reinforced with (Ni_3Al)p, Journal of Materials Science, 2003, vol. 38, pp. 521-525.
117. Konopka K, Maj M, Kurzydlowskia KJ, Studies of the effect of metal particles on the fracture toughness of ceramic matrix composites, Materials Characterization, 2003, vol. 51, pp. 335-340.
118. Ergun E, Aslantas K, Tasgetiren S, Effect of crack position on stress intensity factor in particle-reinforced metal-matrix composites, Mechanics Research Communications, 2008, vol. 35, pp. 209-218.
119. Sozhamannan GG, Prabu SB, Paskaramoorthy R, Failures analysis of particle reinforced metal matrix composites by microstructure based models, Materials and Design, 2010, vol. 31, pp. 3785-3790.
120. Heo SP, Yang WH, Kim C, Stress Intensity factors for elliptical arc through cracks in mechanical joints by virtual crack closure technique, KSME International Journal, 2002, vol. 16, pp. 182-191.
121. Guluzade R, Avcı A, Demirci MT, Erkendirci OF, Fracture toughness of recycled AISI 1040 steel chip reinforced AlMg1SiCu aluminum chip composites, Materials and Design, 2013, vol. 52, pp. 345-352.
122. Rittel D, Frage N, Dariel MP, Dynamic mechanical and fracture properties of an infiltrated TiC-1080 steel cermet, International Journal of Solids and Structures, 2005, vol. 42, pp. 697-715.

123. Zhang J, Laird C, Fatigue fracture of tungsten monofilament-reinforced monocrystalline copper matrix composites, Material Science and Engineering, 2012, vol. 283, pp. 126-135.
124. Bacon DH, Edwards L, Moffatt JE, Fitzpatrick ME, Fatigue and fracture of a 316 stainless steel metal matrix composite reinforced with 25% titanium diboride, International Journal of Fatigue, 2013, vol. 48, pp. 39-47.
125. Ye D, Effect of cyclic straining at elevated-temperature on static mechanical properties, microstructures and fracture behavior of nickel-based superalloy GH4145/SQ, International Journal of Fatigue, 2005, vol. 27, pp. 1102-1114.
126. Schlenther E, Ozcoban H, Jelitto H, Faller M, Schneider GA, Graule T, Aneziris CG, Kuebler J, Fracture toughness and corrosion behaviour of infiltrated Al_2O_3-Steel composites, Materials Science & Engineering A, 2014, vol. 590, pp. 132-139.
127. Sabirov I, Kolednik O, Local and global measures of the fracture toughness of metal matrix composites, Materials Science and Engineering, 2010, vol. A527, pp. 3100-3110.
128. Srivatsan TS, Annigeri R, an investigation on cyclic plastic strain response and fracture behavior of steel based metal matrix composites, Engineering Fracture Mechanics, 1997, vol. 4, pp. 451-481.
129. Wang H, Shu X, Liu E, Han Z, Li X, Tang B, Assessments on corrosion, tribological and impact fatigue performance of Ti and TiN-coated stainless steels by plasma surface alloying technique, Surface & Coatings Technology, 2014, vol. 239, pp. 123-131.
130. Puchi-Cabrera ES, Staia MH, Ortiz-Mancilla MJ, La Barbera-Sosa JG, Ochoa-Perez EA, Gutierrez CV, Bellayer S, Traisnel M, Chicot D, Lesage J, Fatigue behavior of a SAE 1045 steel coated with Colmonoy 88 alloy deposited by HVOF thermal spray, Surface & Coatings Technology, 2010, vol. 205, pp. 1119-1126.
131. Al-Fadhli HY, Stokes J, Hashmi MSJ, Yilbas BS, HVOF coating of welded surfaces: Fatigue and corrosion behavior of stainless steel coated with Inconel-625 alloy, Surface & Coatings Technology, 2006, vol. 200, pp. 4904-4908.
132. Natsume MFF Hayashi Y, Akebono H, Kato M, Sugeta A, Fatigue properties and crack propagation behavior of stainless cast steel for turbine runner of hydraulic power generation, Procedia Engineering, 2010, vol. 2, pp. 1273-1281.

133. Xian-ming M, Zhang J, Wei H, Zhao J, Fracture Behavior of Cold Sprayed 304 Stainless Steel Coating During Cold Rolling, Journal of iron and steel research, international, 2012, vol. 19, pp. 57-63.
134. Faisal NH, Ahmed R, Prathuru AK, Spence S, Hossian M, Steel JA, An improved Vickers indentation fracture toughness model to assess the quality of thermally sprayed coatings, Engineering Fracture Mechanics, 2014, vol. 128, pp. 189-204.
135. Li XN, Liang LH, Xie JJ, Chen L, Wei YG, Thickness-dependent fracture characteristics of ceramic coatings bonded on the alloy substrates, Surface & Coatings Technology, 2014, vol. 258, pp. 1039-1047.
136. Podgornik P, Sedlacek M, Cekada M, Jacobson S, Zajec B, Impact of fracture toughness on surface properties of PVD coated cold work tool steel, Surface & Coatings Technology, 2015, vol. 277, pp. 144-150.
137. Huang CA, Yeh YH, Hsu FY, Ding WR, Li CH, Tensile fracture behavior of Ni and CreC/Ni-coated high-carbon tool steel (AISI 1090), Materials Chemistry and Physics, 2015, vol. 166, pp. 57-65.
138. Chen ZB, Wang ZG, Zhu SJ, Tensile fracture behavior of thermal barrier coatings on superalloy, Surface & Coatings Technology, 2011, vol. 205, pp. 3931-3938.
139. Rico A, Munez CJ, Rodriguez J, On the relevance of microstructure in the fracture toughness of nano-structured alumina-3% titania coatings, Surface & Coatings Technology, 2014, vol. 243, pp. 46-50.
140. Movahedi B, Fracture toughness and wear behavior of NiAl-based nanocomposite HVOF coatings, Surface & Coatings Technology, 2013, vol. 235, pp. 212-219.
141. Huang JH, Chen YH, Wang AN, Yu GP, Chen H, Evaluation of fracture toughness of ZrN hard coatings by internal energy induced cracking method, Surface & Coatings Technology, 2014, vol. 258, pp. 211-218.
142. Cho GH, Kim EH, Jung YG, Byeun YK, Improving oxidation resistance and fracture strength of MgO-C refractory material through precursor coating, Surface & Coatings Technology, 2014, vol. 260, pp. 429-432.
143. Chen FL, He X, Munoz PAP, Yin HM, Opening-mode fractures of a brittle coating bonded to an elasto-plastic substrate, International Journal of Plasticity, 2015, vol. 67, pp. 171‑191.

144. Wen M, An T, Hu CQ, Tian HW, Zheng WT, Interfacial fracture for TiN/SiN*x*nano-multilayer coatings on Si(1 1 1) characterized by nano indentation experiments, Materials Science and Engineering A, 2008, vol. 494, pp. 324-328.
145. Schlogl M, Kirchlechner C, Paulitsch J, Keckes J, Mayrhofer PH, Effects of structure and interfaces on fracture toughness of CrN/AlN multilayer coatings, Scripta Materialia, 2013, vol. 68, pp. 917–920.
146. Kumar MS, Pramod R, Kumar MES, Govindaraju HK, Evaluation of Fracture Toughness and Mechanical Properties of Aluminum Alloy 7075, T6 with Nickel Coating, Procedia Engineering, 2014, vol. 97, pp. 178–185.
147. Sastry S, Krishnab M, Uchil J, A study on damping behaviour of aluminite particulate reinforced ZA-27 alloy metal matrix composites, Journal of Alloys and Compounds, 2001, vol. 314, pp. 268–274.
148. Girish BM, Prakash KR, Satish BM, Jain PK, Prabhakar P, An investigation into the effects of graphite particles on the damping behavior of ZA-27 alloy composite material, Materials and Design, 2011, vol. 32, pp. 1050-1056.
149. Lu H, Wang X, Zhang T, Cheng Z, Fang Q, Design, Fabrication, and Properties of High Damping Metal Matrix Composites A Review, Materials, 2009, vol. 2, pp. 958-977.
150. Zhang H, Gu M, Internal friction behavior in SiC particulate reinforced aluminum metal matrix composite in thermal cycling, Journal of Alloys and Compounds, 2006, vol. 426, pp. 247-252.
151. Wu YW, Wu K, Deng KK, Nie KB, Wang XJ, Hu XS, Zheng MY, Damping capacities and tensile properties of magnesium matrix composites reinforced by graphite particles, Materials Science and Engineering A, 2010, vol. 527, pp. 6816–6821.
152. Di-qing W, Bo-lin H, Guang-yao X, Zhao-xia C, Jin-cheng W, Gen-cang Y, High damping capacities of Mg-Cu based alloys, Transaction Nonferrous Material Society of China, 2010, vol. 20, pp. 448-452.
153. Cao W, Zhang C, Fan T, Zhang D, In situ synthesis and damping capacities of TiC reinforced magnesium matrix composites, Materials Science and Engineering A, 2008, vol. 496, pp. 242–246.

154. Zhang J, Perez RJ, Lavernia EJ, Effect of SiC and graphite particulate on damping behaviour of Metal matrix composites, Acta Metallurgy Material, 1994, vol. 42, pp. 395-409.
155. Zhang J, Perez RJ, Lavernia EJ, Gupta M, Damping behaviour of particulate filled 2519 metal matrix composites, Scripta Metallurgical Materillia, 1993, vol 2, pp. 91-96.
156. Wu GH, Dou ZY, Jiang LT, Cao JH, Damping properties of aluminum matrix–fly ash composites, Materials Letters, 2006, vol. 60, pp. 2945-2948.
157. Zhang Y, Ma N, Wang H, Le Y, Li S, Effect of Ti and Mg on the damping behavior of in situ aluminum composites, Materials Letters, 2005, vol. 59, pp. 3775‑3778.
158. Pabst W, Gregorova E, Malangre D, Hostas J, Elastic properties and damping behavior of alumina-zirconia composites at room temperature, Ceramics International, 2012, vol. 38, pp. 5931–5939.
159. Deng KK, Li JC, Nie KB, Wang XJ, Fan JF, High temperature damping behavior of as-deformed Mg matrix influenced by micron and submicron SiCp, Materials Science & Engineering A, 2015, vol. 624, pp. 62–70.
160. Gu J, Zhang X, Gu M, Effect of interphase on the damping capacity of particulate reinforced metal matrix composites, Journal of Alloys and Compounds, 2004, vol. 381, pp. 182-187.
161. Gu J, Zhang X, Gu M, Effect of surface coating of particulate on the overall damping of particulate-reinforced metal matrix composites, Computational Materials Science, 2006, vol. 36, pp. 338-344.
162. Hu J, Liu G, Tang SW, Damping behavior in $Al_{18}B_4O_{33}$w/Al composite containing an interfacial layer with low melting point metal particles, Journal of Alloys and Compounds, 2012, vol. 513, pp. 61-67.
163. Gen-lian F, Zhi-qiang L, Di Z, Damping capacity of $BaTiO_3$/Al composites fabricated by hot extrusion, Transaction Nonferrous Material Society of China, 2012, vol. 22, pp.2512-2516.
164. Prasad DS, Shoba C, Experimental evaluation onto the damping behavior of Al/SiC/RHA hybrid composites, Journal of materials research and technology, 2015, doi.org/10.1016/j.jmrt.2015.08.001.

165. Liu G, Tang S, Ren W, Hua J, Effect of thermal cycling on the damping behavior in alumina borate whisker with and without Bi_2O_3 coating reinforced pure aluminum composites, Materials and Design, 2014, vol. 60, pp. 244–249.

166. Liu G, Tang SW, Hua J, Kong LC, Damping behavior of SnO_2 Bi_2O_3-coated$Al_{18}B_4O_{33}$ whisker-reinforced pure Al composite undergone thermal cycling during internal friction measurement, Materials Science & Engineering A, 2015, vol. 624, pp. 118-123.

167. Montalba C, Eskinb DG, Miranda A, Rojas D, Ramama K, Effect of electroceramic particles on damping behaviour of aluminium hybrid composites produced by ultrasonic cavitation and mechanical stirring, Materials and Design, 2015, vol. 84, pp.110–117.

168. Gu J, Zhang X, Qiu Y, Gu M, Damping behaviors of magnesium matrix composites reinforced with Cu-coated and uncoated SiC particulates, Composites Science and Technology, 2005, vol. 65, pp. 1736–1742.

169. Hu J, Wang XF, Tang SW, A study of damping capacities in pure aluminum matrix composites reinforced with SnO_2-coated and uncoated alumina borate whiskers, Composites Science and Technology, 2008, vol. 68, pp. 2297‑2299.

170. Hu J, Wang XF, Liu G, Effect of SnO_2 coating on the damping capacity and tensile property of alumina borate whisker-reinforced aluminum composite at room temperature, Materials Science and Engineering A, 2010, vol. 527, pp. 657-662.

171. Zhang F, Guo M, Xu K, He G, Wu H, Guo S, Multilayered damping composites with damping layer/constraining layer prepared by a novel method, Composites Science and Technology, 2014, vol. 101, pp. 167-172.

172. Chia CT, Khor KA, Gu YW, Boey F, Viscoelastic properties of plasma sprayed NiCoCrAlY coatings, Thin Solid Films, 2002, vol. 405, pp. 146-152.

173. Wang X, Pei Y, Ma Y, The effect of microstructure at interface between coating and substrate on damping capacity of coating systems, Applied Surface Science, 2013, vol. 282, pp. 60-66.

174. Emadoddin E, Tajally M, Masoumi M, Damping behavior of Al/SiCP multilayer composite manufactured by roll bonding, Materials and Design, 2012, vol. 42, pp. 334‑338.

175. Zhang Q, Cheng L, Wang W, Zhang L, Xu Y, Effect of SiC coating and heat treatment on damping behavior of C/SiC composites, Materials Science and Engineering A, 2008, vol. 473, pp. 254-258.
176. Prasad DS, Shoba C, Prasad BS, Effect of white layer on the damping capacity of metal matrix composites, Materials Science & Engineering A, 2014, vol. 591, pp. 78-81.
177. Prasad DS, Shoba C, Effect of heat treatment on the white layer and its effect on the damping behavior of metal matrix composites, Materials Science & Engineering A, 2014, vol. 599, pp. 25-27.
178. Khor KA, Chia CT, Gu YW, Dynamic mechanical properties of plasma sprayed Ni-based alloys, Materials Science and Engineering A, 2000, vol. 279, pp. 166-171.
179. Khor KA, Chia CT, Gu YW, Dynamic mechanical properties of ZrO_2/NiCoCrAlY composite coatings, Thin Solid Films, 2000, vol. 358, pp. 139-145.
180. Fu S, Ma Y, Gong S, Effect of microstructure of interface between MCrAlY coating and substrate on damping property, Procedia Engineering, 2012, vol. 27, pp. 1024-1032.
181. Patsias S, Tassini N, Lambrinou K, Ceramic coatings: Effect of deposition method on damping and modulus of elasticity for yttria-stabilized zirconia, Materials Science and Engineering A, 2006, vol. 442, pp. 504-508.
182. Wu Q, Li W, Zhong N, Corrosion behavior of TiC particle-reinforced 304 stainless steel, Corrosion Science, 2011, vol. 53, pp. 4258-4264.
183. Xiao Z, Li Z, Zhu A, Zhao Y, Chen J, Zhu Y, Surface characterization and corrosion behavior of a novel gold-imitation copper alloy with high tarnish resistance in salt spray environment, Corrosion Science, 2013, vol. 76, pp. 42-51.
184. Pardo A, Merino S, Merino MC, Barroso I, Mohedano M, Arrabal R, Viejo F, Corrosion behaviour of silicon-carbide-particle reinforced AZ92 magnesium alloy, Corrosion Science, 2009, vol. 51, pp. 841-849.
185. Zhao MC, Schmutz P, Brunner S, Liu M, Song GL, Atrens A, An exploratory study of the corrosion of Mg alloys during interrupted salt spray testing, Corrosion Science, 2009, vol. 51, pp. 127-1292.
186. Martin HJ, Horstemeyer MF, Wang PT, Structure-property quantification of corrosion pitting under immersion and salt-spray environments on an extruded AZ61 magnesium alloy, Corrosion Science, 2011, vol. 53, pp. 1348-1361.

187. Walton CA, Martin HJ, Horstemeyer MF, Wang PT, Quantification of corrosion mechanisms under immersion and salt spray environments on an extruded AZ31 magnesium alloy, Corrosion Science, 2012, vol. 56, pp. 194-208.
188. Song W, Martin HJ, Hicks A, Seely D, Walton CA, Lawrimore WB, Wang PT, Horstemeyer MF, Corrosion behaviour of extruded AM30 magnesium alloy under salt-spray and immersion environments, Corrosion Science, 2014, vol. 78, pp. 353-368.
189. Wang F, Xiong B, Zhang Y, Liu Y, Li Z, Li X, Qu C, Effect of Cu addition on microstructure and corrosion behavior of spray-deposited Zn-30Al alloy, Materials Science and Engineering A, 2012, vol. 532, pp. 100-105.
190. Seetharaman R, Ravisankar V, Balasubramanian V, Corrosion performance of friction stir welded AA2024 aluminium alloy under salt fog conditions, Transactions of Nonferrous Metals Society of China, 2015, vol. 25, pp. 1427-1438.
191. Manivannan S, Gopalakrishnan SK, Babu SPK, Sundarrajan S, Effect of cerium addition on corrosion behavior of AZ61+ XCe alloy under salt spray test, Alexandria Engineering Journal, 2015, doi.org/10.1016/j.aej.2015.10.010.
192. Manivannan S, Dinesh P, Babu SPK, SundarrajanS, Investigation and corrosion performance of cast Mg-6Al-1Zn+XCa alloy under salt spray test, Journal of Magnesium and Alloys, 2015, vol. 3, pp. 86-94.
193. Arrabal R, Pardo A, Merino MC, Mohedano M, Casajus P, Matykina E, Skeldon P, Thompson GE, Corrosion behavior of a magnesium matrix composite with a silicate plasma electrolytic oxidation coating, Corrosion Science, 2010, vol. 52, pp. 3738-3749.
194. Sun GF, Zhang YK, Zhang MK, Zhou R, Wang K, Liu CS, Luo KY, Microstructure and corrosion characteristics of 304 stainless steel laser-alloyed with Cr-CrB_2, Applied Surface Science, 2014, vol. 295, pp. 94-107.
195. Alkhateeb E, Ali R, Virtanen S, Popovska N, Electrochemical evaluation of the corrosion behavior of steel coated with titanium-based ceramic layers, Surface & Coatings Technology, 2011, vol. 205, pp. 3006-3011.
196. Padmavathi C, Upadhyaya A, Agrawal D, Corrosion behavior of microwave-sintered austenitic stainless steel composites, Scripta Materialia, 2007, vol. 57, pp. 651-654.

197. Wang Y, Wang X, Wu K, Wang F, Role of $Al_{18}B_4O_{33}$ Whisker in MAO Process of Mg Matrix Composite and Protective Properties of the Oxidation Coating, Journal of Materials Science & Technology, 2013, vol. 29, pp. 267-272.
198. Hu J, Li YB, Wang HL, Ren WC, Improvement of the corrosion resistance of Cr-N coated aluminum matrix composite by magnetron sputter, Materials Letters, 2008, vol. 62, pp. 1715-1717.
199. Hamdy AS, Alfosail F, Gasem Z, Effect of changing the silica coating pH on the corrosion characteristics of A6092/SiC/17.5p aluminum metal matrix composite in chloride media, Electrochimica Acta, 2013, vol. 107, pp. 518-524.
200. Xuea W, Jin Q, Zhua Q, Huaa M, Ma Y, Anti-corrosion micro-arc oxidation coatings on SiCP/ AZ31 magnesium matrix composite, Journal of Alloys and Compounds, 2009, vol. 482, pp. 208-212.
201. Hu J, Zhao XH, Tang SW, Ren WC, Zhang ZY, Corrosion resistance of cerium-based conversion coatings on alumina borate whisker reinforced AA6061 composite, Applied Surface Science, 2007, vol. 253, pp. 8879-8884.
202. Guo X, Dua K, Guo Q, Wanga Y, Wang R, Wang F, Effect of phytic acid on the corrosion inhibition of composite film coated on Mg-Gd-Y alloy, Corrosion Science, 2007, vol. 76, pp. 129-141.
203. Wang YQ, Zheng MY, Wu K, Micro arc oxidation coating formed on SiCw/AZ91 magnesium matrix composite and its corrosion resistance, Materials Letters, 2005, vol. 59, pp. 1727-1731.
204. Thirumalaikumarasamy D, Shanmugam K, Balasubramanian V, Influence of chloride ion concentration on immersion corrosion behavior of plasma sprayed alumina coatings on AZ31B magnesium alloy, Journal of Magnesium and Alloys, 2014, vol. 2, pp. 325-334.
205. Jegadeeswarana N, Rameshb MR, Bhat KU, Hot Corrosion Studies on As-received and HVOF Sprayed Al_2O_3+CoCrAlTaY on Ti-31 Alloy in Salt Environment, Procedia Engineering, 2013, vol. 64, pp. 1013-1019.
206. Niu L, Chang SH, Su Y, Han D, Li G, A aluminum coating with chromium-free passivating film formed on AZ91D magnesium alloy, Journal of Alloys and Compounds, 2015, vol. 635, pp. 11-15.

207. Richard C, Kowandy C, Landoulsi J, Geetha M, Ramasawmy H, Corrosion and wear behavior of thermally sprayed nano ceramic coatings on commercially pure Titanium and Ti-13Nb-13Zr substrates, International Journal of Refractory Metals & Hard Materials, 2010, vol. 28, pp. 115-123.
208. Gurr M, BauS, Burmeister F, Wirth M, Gonzalez EP, Krebser K, Preubner J, Pfeiffer W, Investigation of the corrosion behavior of NiVAl multilayer coatings in hot salt melts, Surface & Coatings Technology, 2015, vol. 279, pp. 101-111.
209. Hoche H, Grob S, Oechsner M, Development of new PVD coatings for magnesium alloys with improved corrosion properties, Surface & Coatings Technology, 2014, vol. 259, pp. 102-108.
210. Damato C, Betts JC, Buhagiar J, Laser surface alloying of an A356 aluminium alloy using nickel and Ni-Ti-C: A corrosion study, Surface & Coatings Technology, 2014, vol. 244, pp. 194-202.
211. Zhong C, He MF, Liu L, Chen YJ, Shen B, Wu YT, Deng YD, Hu WB, Formation of an aluminum-alloyed coating on AZ91D magnesium alloy in molten salts at lower temperature, Surface & Coatings Technology, 2010, vol. 205, pp. 2412-2418.
212. Magnani M, Suegama PH, Espallargas N, Dosta S, Fugivara CS, Guilemany JM, Benedetti AV, Influence of HVOF parameters on the corrosion and wear resistance of WC-Co coatings sprayed on AA7050 T7, Surface & Coatings Technology, 2008, vol. 202, pp. 4746-4757.
213. Diesselberg M, Stock HR, Mayr P, Corrosion protection of magnetron sputtered TiN coatings deposited on high strength aluminium alloys, Surface and Coatings Technology, 2004, vol. 177-178, pp. 399-403.
214. Dejun K, Jinchun W, Salt spray corrosion and electrochemical corrosion properties of anodic oxide film on 7475 aluminum alloy, Journal of Alloys and Compounds, 2015, vol. 632, pp. 286-290.
215. Chang CH, Jeng MC, Su CY, Chang CL, An investigation of thermal sprayed aluminum/hard anodic composite coating on wear and corrosion resistant performance, Thin Solid Films, 2009, vol. 517, pp. 5265-5269.
216. Natishana PM, Lawrencea SH, Fosterb RL, Lewisb J, Sartwella BD, Salt fog corrosion behavior of high-velocity oxygen-fuel thermal spray coatings compared to

electrodeposited hard chromium, Surface and Coatings Technology, 2000, vol. 130, pp. 218-223.

217. Golru SS, Attar MM, Ramezanzadeh B, Morphological analysis and corrosion performance of zirconium based conversion coating on the aluminum alloy 1050, Journal of Industrial and Engineering Chemistry, 2015, vol. 24, pp. 233-244.
218. Desale GR, Gandhi BK, Jain SC, Particle size effects on the slurry erosion of aluminium alloy (AA 6063), Wear, 2009, vol. 266, pp. 1066-1071.
219. Desale GR, Gandhi BK, Jain SC, Slurry erosion of ductile materials under normal impact condition, Wear, 2008, vol. 264, pp. 322-330.
220. Jha AK, Batham R, Ahmed M, Majumder AK, Modi OP, Chaturvedi S, Gupta AK, Effect of impinging angle and rotating speed on erosion behavior of aluminum, Transaction of Nonferrous Metals Society of China, 2011, vol. 21, pp. 32-38.
221. Prasad BK, Modi OP, Yegneswaran AH, Wear behaviour of zinc-based alloys as influenced by alloy composition, nature of the slurry and traversal distance, Wear, 2008, vol. 264, pp. 990-1001.
222. Prasad BK, Effects of alumina particle dispersion on the erosive-corrosive wear response of a zinc-based alloy under changing slurry conditions and distance, Wear, 2000, vol. 238, pp. 151-159.
223. Lynn RS, On the particle size effect in slurry erosion, Wear, 1991, vol. 149, pp. 55-71.
224. Prasad BK, Slurry Wear Characteristics of a Zinc-Based Alloy, Journal of Materials Engineering and Performance, 2002, vol. 16, pp. 708-714.
225. Prasad BK, Jha AK, Modi OP, Yegneswaran AH, Effect of sand concentration in the medium and travel distance and speed on the slurry wear response of a zinc-based alloy alumina particle composite, Tribology Letters, 2004, Vol. 17, pp. 301-309.
226. Ramesh CS, Keshavamurthy R, Channabasappa BH, Pramod S, Influence of heat treatment on slurry erosive wear resistance of Al6061 alloy, Materials & Design, 2009, vol. 30, pp. 3713-3722.
227. Gupta AK, Prasad BK, Panjoo RK, Das S, Effects of T6 heat treatment on mechanical, abrasive and erosive-corrosive wear properties of eutectic Al-Si alloy, Transactions of Nonferrous Metals Society of China, 2012, vol. 22, pp. 1041-1050.

228. Modi OP, Dasgupta R, Prasad BK, Jha AK, Yegneswaran AH, Dixit G, Erosion of a High-Carbon Steel in Coal and Bottom-Ash Slurries, Journal of Materials Engineering and Performance, 2000, vol. 9, pp. 522-529.
229. Suchanek J, Kuklik V, Zdravecka E, Influence of microstructure on erosion resistance of steels, Wear, 2009, vol. 267, pp. 2092-2099.
230. Zhang T, Li DY, Improvement in the corrosion-erosion resistance of 304 stainless steel with alloyed yttrium, Journal of Materials Science, 2001, vol. 36, pp. 3479-3486.
231. Chung RJ, Tang X, Li DY, Hinckely B, Dolman K, Abnormal erosion-slurry velocity relationship of high chromium cast iron with high carbon concentrations, Wear, 2011, vol. 27, pp. 1454-1461.
232. Wang HW, Stack MM, The erosive wear of mild and stainless steels under controlled corrosion in alkaline slurries containing alumina particles, Journal of materials science, 2000, vol. 35, pp. 5263-5273.
233. Gandhi BK, Singh SN, Seshadri V, Study of the parametric dependence of erosion wear for the parallel flow of solid–liquid mixtures, Tribology International, 1999, vol. 32, pp. 275-282.
234. Gandhi BK, Borse SV, Nominal particle size of multi-sized particulate slurries for evaluation of erosion wear and effect of fine particles, Wear, 2004, vol. 257, pp. 73-79.
235. Neville A, Reza F, Chiovelli S, Revega T, Erosion-corrosion behaviour of WC-based MMCs in liquid-solid slurries, Wear, 2005, vol. 259, pp. 181-195.
236. Mondel DP, Das S, Prasad BK, Study erosive-corrosive wear characteristics of aluminum alloy composites through factorial design of experiments, Wear, 1998, vol. 217, pp. 1-6.
237. Das S, Mondal DP, Dasgupta R, Prasad BK, Mechanisms of material removal during erosion–corrosion of an Al-SiC particle composite, Wear, 1999, vol. 236, pp. 295-302.
238. Wang HW, Stack MM, The slurry erosive wear of physically vapour deposited TiN and CrN coatings under controlled corrosion, Tribology Letters, 1999, vol. 6, pp.23-36.
239. Tu JP, The effect of TiN coating on erosion-corrosion resistance of a-Ti alloy in saline slurry, Corrosion Science, 2000, vol. 42, pp. 147-163.
240. Caicedo JC, Cabrera G, Aperador W, Caicedo HH, Mejia A, Determination of the best behavior among AISI D3 steel, 304 stainless steel and CrN/AlN coatings under erosive-corrosive effect, Vacuum, 2012, vol. 86, pp. 1886-1894.

241. Zhang DW, Lei TC, The microstructure and erosive-corrosive wear performance of laser-clad Ni-Cr_3C_2 composite coating, Wear, 2003, vol. 255, pp. 129-133.
242. Iwai Y, Miyajima T, Honda T, Matsubara T, Kanda K, Hogmark S, Evaluation of erosive wear resistance of TiN coatings by a slurry jet impact test, Wear, 2006, vol. 261, pp. 112-118.
243. Hadad M, Hitzek R, Buergler P, Rohr L, Siegmann S, Wear performance of sandwich structured WC-Co-Cr thermally sprayed coatings using different intermediate layers, Wear, 2007, vol. 263, pp. 691-699.
244. Shivamurthy RC, Kamaraj M, Nagarajan R, Shariff SM, Padmanabham G, Influence of microstructure on slurry erosive wear characteristics of laser surface alloyed 13Cr-4Ni steel, Wear, 2009, vol. 267, pp. 204-212.
245. Singh VP, Sil A, Jayaganthan R, Tribologicalbehavior of plasma sprayed Cr_2O_3-3%TiO_2 coatings, Wear, 2011, vol. 272, pp. 149-158.
246. Knuuttila J, Ahmaniemi S, Mantyl T, Wet abrasion and slurry erosion resistance of thermally sprayed oxide Coatings, Wear, 1999, vol. 232, pp. 207-212.
247. Wang HW, Stack MM, Lyon SB, Hovsepian P, Munz WD, Wear associated with growth defects in combined cathodic Arc unbalanced magnetron sputtered CrNrNbNsuperlattice coatings during erosion in alkaline slurry, Surface and Coatings Technology, 2000, vol. 135, pp. 82-90.
248. Wang HW, Stack MM, Erosion of PVD TiN coatings under simultaneous corrosion in sodium carbonate/bicarbonate buffer slurries containing alumina particles, Surface and Coatings Technology, 1999, vol. 106, pp. 1-7.
249. Zhao HX, Goto H, Matsumura M, Takahashi T, Yamamoto M, Slurry erosion of plasma-sprayed ceramic coatings, Surface and Coatings Technology, 1999, vol. 115, pp. 123-131.
250. Singh VP, Sil A, Jayaganthan R, A study on sliding and erosive wear behavior of atmospheric plasma sprayed conventional and nano-structured alumina coatings, Materials and Design, 2011, vol. 32, pp. 584-591.
251. Taguchi, G, Konishi S (1987).Taguchi Methods: Orthogonal Arrays and Linear Graphs, Tools for Quality Engineering, American Supplier Institute Inc., Dearborn, MI.
252. Taguchi, G (1990). Introduction to Quality Engineering, Asian Productivity Organization, Tokyo.

253. Phadke, MS (1989). Quality Engineering using Robost Design, PrenticeHall, Englewood Cliffs, NJ.
254. Wu Y, Moore WH (1986). Quality Engineering: Product & Process Design Optimization, American Supplier Institute.
255. Siddhartha, Patnaik A, Bhatt AD, Mechanical and dry sliding wear characterization of epoxy–TiO2 particulate filled functionally graded composites materials using Taguchi design of experiment, Materials & Design, 2011, vol. 32, pp. 615-627.
256. Siddhartha, Patnaik A, Bhatt AD, Friction and Wear study of Alumina- Epoxy Homogenous composites and its functionally graded materials, Journal of Tribology, 2011, vol. 133, pp. 11-18.
257. Siddhartha, Patnaik A, Bhatt AD, Functionally graded materials manufacturing techniques: A review, Material Science, 2009, vol. 5, pp. 17-25.
258. Basavarajappa S, Chandramohan G, Wear studies on metal matrix composites: A Taguchi method, Journal of Materials science Technology, 2005, vol. 21, pp.104-114.
259. Patnaik A, Mahapatra SS, Optimization of Wire Electrical Discharge Machining (WEDM) Process Parameters using Taguchi Method, International Journal for ManufacturingScience& Technology, 2008, vol. 9, pp. 129-144.
260. Yoganandh J, Natarajan S, Babu SPK, Erosive Wear Behavior of Nickel-Based High Alloy White Cast Iron Under Mining Conditions Using Orthogonal Array, Journal of Materials Engineering and Performance, 2013, DOI: 10.1007/s11665-013-0539-6.
261. Shannon C, A Mathematical Theory of Communication Bell System Tech, Journal, 1948, vol. 27, pp. 379-423.
262. Zeleny M, (1982). Multiple criteria decision making, McGraw-Hill, New York.
263. Chen S, Wang X, Zhao X, An attribute recognition model based on entropy weight for evaluating the quality of groundwater sources, Journal of China University Mining & Technolgy, 2008, vol. 18, pp. 72–75.
264. Zhi-hong Z, Yi Y, Jing-nan S, Entropy method for determination of weight of evaluating indicators in fuzzy evaluation for water quality assessment, Journal of environmental Science, 2006, vol. 18, pp. 1020-1023.

265. Chowdhury S, Husain T, Evaluation of Drinking Water Treatment Technology: An Entropy- Based Fuzzy Application, Journal of Environment Engineering ASCE, 2006, vol. 132, pp. 1264-1271.
266. Jahan A, M.Y. Ismail, S.M. Sapuan, F. Mustapha. Material screening and choosing methods- A review, 2009, vol. 31, pp. 696-705.
267. Jahan A, M.Y. Ismail, S.M. Sapuan, F.Mustapha. Material selection based on Ordinal data, Materials and Design, 2010, vol. 31, pp. 3180-3187.
268. Ezazi MA, Yusof F, Sarhan AAD, Shukor MHA, Fadzil A. Employment of fiber laser technology to weld austenitic stainless steel 304 l with aluminum alloy 5083 using pre-placed activating flux, Materials & Design, 2015,vol. 87, pp. 105-123.
269. Pai A, Sharma SS, Dsilva RE, Nikhil RG. Effect of graphite and granite dust particulates as micro-fillers on tribological performance of Al6061-T6 hybrid composites, Tribology International, 2015, vol. 92, pp. 462-471.
270. American society for testing and materials (ASTM). Standard E290, Standard test method for Bend testing of material for ductility, West Conshohocken (PA): Annual book of ASTM standards, ASTM, 2011.
271. American society for testing and materials (ASTM). Standard E92, Standard test method for Vickers Hardness of Metallic Materials, West Conshohocken (PA): Annual book of ASTM standards, ASTM, 2011.
272. American society for testing and materials (ASTM). Standard E23, Standard test method for Notched bar impact testing of metallic materials, West Conshohocken (PA): Annual book of ASTM standards, ASTM, 2011.
273. American society for testing and materials (ASTM). Standard E-399, Standard test method for Linear-Elastic Plane-Strain Fracture Toughness KIc of Metallic Materials, West Conshohocken (PA): Annual book of ASTM standards, ASTM, 2011.
274. American society for testing and materials (ASTM). Standard C1624, Standard Test Method for Adhesion Strength and Mechanical Failure Modes of Ceramic Coatings by Quantitative Single Point Scratch Testing, West Conshohocken (PA): Annual book of ASTM standards, ASTM, 2011.

275. American society for testing and materials (ASTM). Standard B117, Standard test method for salt spray (FOG) testing, West Conshohocken (PA): Annual book of ASTM standards, ASTM, 2011.
276. American society for testing and materials (ASTM). Standard G-134, Standard test method Erosion of Solid Materials by a Cavitating Liquid Jet, West Conshohocken (PA): Annual book of ASTM standards, ASTM, 2011.
277. Agarwal G, Patnaik A, Sharma RK, Thermo-Mechanical Properties and Abrasive Wear Behavior of Silicon Carbide Filled Woven Glass Fiber Composites, Silicon, 2014, vol. 6, pp. 155-168.
278. Kaundal R, Role of Process Variables on the Solid Particle Erosion of Polymer Composites: A Critical Review, Silicon, 2014, vol. 6, pp. 5-20.
279. Mummery PM, Derby B.The influence of microstructure on the fracture behaviour of particulate metal matrix composites, Material Science Engineering A, 1991, vol. 135, pp. 221-224.
280. Divecha AP, Fishman SG, Karmakar SD SiC reinforced Aluminium-A Formable Composite, Journal of Metals, 1981, vol. 12, pp. 12-20.
281. Cabrera G, Caicedo JC, Amaya C, Yate L, Saldana JM, Prieto P, Enhancement of mechanical and tribological properties in AISI D3 steel substrates by using a non-isostructuralCrN/AlN multilayer coating, Materials Chemistry and Physics, 2011, vol. 125, pp. 576-586.
282. Lee JW, Duh JG, Wang JH, Mechanical Property Evaluation of Cathodic Arc Plasma-Deposited CrN Thin Films on Fe-Mn-Al-C Alloys, Surface and Coatings Technology, 2003, vol. 168, pp. 223-230.
283. Chu S, Wu R.The structure and bending properties of squeeze-cast composites of A356 aluminium alloy reinforced with alumina particles, Composites Science and Technology, 1999, vol. 59, pp. 157-162.
284. Abdullah Y, Razak Y, Daud RS, Harun M. Flexural strength and fracture studies of Al-Si/SiC_p composites, International Journal of Mechanical and Materials Engineering, 2009, vol. 4, pp. 109-111.

285. Qu Z, He R, Wei K, Pei Y, Fang D, Pre-oxidation temperature optimization of ultra-high temperature ceramic components: Flexural strength testing and residual stress analysis, Ceramics International, 2015, vol. 41, pp. 5085-5092.
286. Bindumadhavan PN, Wah HK, Prabhakaran O, Dual particle size (DPS) composites: effect on wear and mechanical properties of particulate metal matrix composites, Wear, 2001, vol. 248, pp. 112-120.
287. Patnaik A, Mamatha TG, Biswas S, Kumar P.Damage assessment of titania filled Zinc-aluminum metal matrix composites in erosive environment: A comparative study, Materials and Design, 2012, vol. 36, pp. 511-521.
288. Hunt HW, Richmond D, Young RD, Mathews FL. Mechanical Properties of Squeeze Cast Zinc Alloy MMC's, in Proc. of 6th International Conference on Composite Materials, M.L. Mathew, ed., Elsevier Applied Science, London, United Kingdom, 1987: 2209-2218.
289. Seah KHW, Sharma SC, Girish BM, Kamath R, Satish BM. Mechanical properties and fractography of cast lead /quartz particulate composites, Materials and design, 1997, vol. 18, pp. 149-153.
290. Papakyriacou M, Mayer HR, Tschegg-Stanzl SE, Groschl M, Near-threshold fatigue crack growth in $a1_2o_3$ particle reinforced 6061 aluminium alloy, Fatigue Fracture Engineering Material structure, 1995, vol. 18, pp. 477-487.
291. Levin M, Karlsson B, Influence of SiC Particle Distribution and Prestraining on Fatigue Crack Growth Rates in Aluminium AA6061-SiC Composite Material, Material Science and Technology, 1991, vol. 7, pp. 596-607.
292. Kumai S, Yoshida K, Higo Y, Nunomura S, Effects of dendrite cell-size and particle distribution on the near-threshold fatigue-crack growth-behavior, Acta Materials, 1996, vol. 44, pp. 2249-2257.
293. Lee CM, Chu JP, Chang WZ, Lee JW, Jang JSC, Liaw PK, Fatigue property improvements of Ti-6Al-4V by thin film coatings of metallic glass and TiN: a comparison study, Thin Solid Films, 2014, vol. 561, pp. 33-37.
294. Chan RN, Stoner BR, Thompson JY, Scattergood RO, Piascik JR Fracture toughness improvements of dental ceramic through use of yttria-stabilized zirconia (YSZ) thin-film coatings, 2013, Dental Materials vol. 29, pp. 881-887.

295. Singh V, Prasad RC, Tensile and fracture behaviour of 6061 Al-SiCp Metal matrix composites, International Symposium of Research Students on Materials Science and Engineering December 20-22, 2004, Chennai, India.
296. Somekawa H, Kim HS, Singh A, Mukai T, Fracture toughness in direct extruded Mg–Al–Zn alloys, Journal of Materials Research, 2007, vol. 22, pp. 2598-2607.
297. Hemanth J, Fracture toughness and wear resistance of Aluminum-boron particulate composites cast using metallic and non metallic chills. Materials and Design, 2001, vol. 23, pp. 41-50.
298. Zong BY, Zhang F, Wang G, Zuo L, Strengthening mechanism of load sharing of particulate reinforcements in a metal matrix composite, Journal of Material Science, 2007, 42, pp. 4215-4226.
299. Zhang JM, Perez RJ, Wong CR, Lavernia EJ, Effects of secondary phases on the damping behavior of metals, alloys and metal-matrix composites, Material Science Engineering, 1994, vol. 13, pp. 325-389.
300. Gupta MK, Dynamic mechanical analysis of automotive coatings on a metal substrate, Thermo chimica Acta, 1990, vol.166, pp.157-167.
301. Cox J, Luong DD, Shunmugasamy VC, Gupta N, Strbik OM, Cho K, Dynamic and Thermal Properties of Aluminum Alloy A356/Silicon Carbide Hollow Particle Syntactic Foams, Metals, 2014, vol.4, pp.530-548.
302. Licitra L, Luong DD, Strbik OM, Gupta N, Dynamic Properties of alumina Hollow Particle filled Aluminum Alloy A356 matrix Syntactic Foams, Materials and Design, 2015, vol. 66, pp. 504-515.
303. Padhy MK, Saini RP, Effect of size and concentration of silt particles on erosion of Pelton turbine buckets, Energy, 2009, vol. 34, pp. 1477-1483.
304. Jianxin D, Fengfang W, Yunsong L, Youqiang X, Shipeng L, Erosion wear of CrN, TiN, CrAlN, and TiAlN PVD nitride coatings, International Journal of Refractory Metals and Hard Materials, 2012, vol. 35, pp. 10-16.
305. Finnie I, Some observations on the erosion of ductile metals, Wear, 1972, vol. 19, pp. 81-90.
306. Hutchings IM, A model for the erosion of metals by spherical particles at normal incidence, Wear, 1981, vol. 70, pp. 269-281.

307. Rickerby DG, MacMillan NH, The erosion of aluminum by solid particle impingement at normal incidence, Wear, 1980, vol. 60, pp. 369-382.
308. Levy A, Aghazadeh M, Hickey G, The effect of test variables on the platelet mechanism of erosion, Wear, 1986, vol. 108, pp. 23-41.
309. Hutchings IM, Winter RE, Particle erosion of ductile metals: A mechanism of material removal, Wear, 1974, vol. 27, pp. 121-128.
310. Levy AV, Particle erosion of ductile metals: A mechanism of material removal, Wear, 1986, vol. 108, pp. 1-21.
311. Bellman J R, Levy AV, Erosion mechanism in ductile metals, Wear, 1981, vol. 70, pp.1-27.
312. Levy AV, Chik P, The effects of erodent composition and shape on the erosion of steel, Wear, 1983, vol. 89, pp. 151-162.
313. Elzey M., Vancheeswaran R., Myers S., McLellan R. International Conference on Brakes 2000, Automotive Braking-technologies for the 21st Century, Leeds, UK, 2000, 197-205.
314. Satapathy BK, Bijwe J. Performance of friction materials based on variation in nature of organic fibers: Part II. Optimization by balancing and ranking using multiple criteria decision model (MCDM), Wear, 2004, vol. 257, pp. 585-589.
315. Satapathy BK, Bijwe J, Kolluri DK Assessment of fiber contribution to friction material performance using grey relational analysis (GRA). Journal of Composite Materials 2006, vol. 40, pp. 483-501.
316. Kolluri DK, Satapathy BK, Bijwe J, Ghosh A.K. Analysis of load and temperature dependence of tribo-performance of graphite filled phenolic composites. Material Science Engineering A, 2007, vol. 456, pp. 162-169.
317. Satapathy BK, Majumdar A, Tomar BS Optimal design of fly ash filled composite friction materials using combined Analytical Hierarchy Process and Technique for Order Preference by Similarity to Ideal Solutions approach. Materials and Design, 2010, vol. 31, pp. 1937-1944.
318. Zhu Z, Xu L, Chen G, Li Y, Optimization on Tribological properties of aramid fiber and CaSO4 whisker reinforced non-metallic friction material with analytic hierarchy process and preference ranking organization method for enrichment evaluations, Materials and Design, 2010, vol. 31, pp. 551-555.

319. Kim SJ, Kim KS, Jang H, Optimization of manufacturing parameters for a brake lining using Taguchi method. Journal of Material Processing, 2003, vol. 136, pp. 202-208.
320. Hwang CL, Yoon K, Multiple attribute decision making: methods and applications, Lecture Notes in Economics and Mathematical Systems. 1981; 186 (Springer).
321. Opricovic S, Tzeng GH, Compromise solution by MADM methods: A comparative analysis of VIKOR and TOPSIS, European Journal of Operational Research, 2004, vol. 156, pp. 445-455.
322. Opricovic S, Multicriteria optimization of civil engineering systems, Faculty of Civil Engineering, Belgrade, 1998.
323. Tzeng GH, Lin CW, Opricovic S, Multi-criteria analysis of alternative-fuel buses for public transportation, Energy Policy, 2005, vol. 33, pp. 1373-1383.
324. Yu PL, A class of solutions for group decision problems, Management Science, 1973, vol. 19, pp. 936-946.
325. Zeleny M, Multiple criteria decision making, Mc-Graw-Hill, New York, 1982.
326. Bazzazi AA, Osanloo M, Karimi B, Deriving preference order of open pit mines equipment through MADM methods: application of modified VIKOR method, Expert Systems with Applications, 2011, vol. 38, pp. 2550-2556.
327. Jahan A, Mustapha F, Ismail MY, Sapuan SM, Bahraminasab M, A comprehensive VIKOR method for material selection, Material Design, 2011, vol. 32, pp. 1215-1221.
328. Kuo MS, Liang GS, Combining VIKOR with GRA techniques to evaluate service quality of airports under fuzzy environment, Expert Systems with Applications, 2011, vol. 38, pp. 1304-1312.
329. Shemshadi A, Shirazi H, Toreihi M, Tarokh MJ, A fuzzy VIKOR method for supplier selection based on entropy measure for objective weighting, Expert System with Application, 2011, vol. 38, pp. 12160-12167.
330. Yuenur GN, Demirel NC, Group decision making process for insurance company selection problem with extended VIKOR method under fuzzy environment, Expert System with Application, 2012, vol. 39, pp. 3702-3707.
331. Ju YB, Wang A, Extension of VIKOR method for multiple criteria group decision making problem with linguistic information, Applied Mathematical Modeling, 2013, vol. 37, pp. 3112-3125.

332. Wan SP, Wang QY, Dong JY, The extended VIKOR method for multi-attribute group decision making with triangular intuitionistic fuzzy numbers, Knowledge-Based Systems, 2013, vol. 52, pp. 65-77.
333. Chang TH, Fuzzy VIKOR method: A case study of the hospital service evaluation in Taiwan, Information Sciences, 2014, vol. 271, pp. 196-212.
334. Kim Y, Chung ES, Fuzzy VIKOR approach for assessing the vulnerability of the water supply to climate change and variability in South Korea, Applied Mathematical Modeling, 2013, vol. 37, pp. 9419-9430.

List of publications based on the research presented in this thesis

1. **Vikash Gautam,** Amar Patanaik, I. K. Bhat (2015) Thermo-Mechanical and Fracture Characterization of Uncoated, Single and Multilayer (SiN/CrN) Coating on Granite Powder Filled Metal Alloy Composites. Silicon DOI 10.1007/s12633-015-9318-3. **I.F. 1.069**
2. **Vikash Gautam,** Amar Patanaik, I. K. Bhat (2015) Microstructure and Wear Behaviours of Single layer (CrN) and Multilayered (SiN/CrN) Coating on Particulate Filled Aluminum Alloy Composites. Silicon DOI: 10.1007/s12633-015-9357-9. **I.F. 1.069**
3. **Vikash Gautam,** Amar Patanaik, I. K. Bhat (2015) Microstructure and Slurry Erosion Wear Behaviours of Single layer (CrN) and Multilayered (SiN/CrN) Coating aluminum alloy composites. Metallurgical and Material Transaction A **(Communicated)**

Paper published in International/National Conferences

1. **Vikash Gautam,** Amar Patanaik, I. K. Bhat Parametric studies of slurry erosion wear of hydraulic turbine blades using taguchi technique. International conference on emerging paradigms and practices in global technology, management & business wassues. NIT Hamirpur during December 22-24, 2014
2. **Vikash Gautam,** Amar Patanaik, I. K. Bhat (2015) Slurry erosion performance of multilayer coated 1050 aluminum alloy composites. International conference on emerging & futurwastic trends in engineering and technology. Maharaja Agrasen University of technology Solan Baddi during May 8-9, 2015
3. **Vikash Gautam,** Amar Patanaik, I. K. Bhat, Effect of granite dust particulates as micro fillers on mechanical properties of 5083 aluminum alloy composite. National conference on Futuristics in Mechanical Engineering. **M. M. M. University of Technology, Gorakhpur** during November 06-07, 2015

Patent Filled

1. **Vikash Gautam,** Amar Patanaik, I. K. Bhat (2015) Granite powder reinforced hydraulic turbine blades, **1320/DEL/2015**.
2. **Vikash Gautam,** Amar Patanaik, I. K. Bhat (2016) Slurry erosion wear assessment of marble dust powder reinforced aluminium alloy composites hydraulic turbine blade, 201611002651 A

****

Brief Bio-data of the Author

The author, Vikash Gautam born on 29-12-1984 graduated in Mechanical Engineering from B. S. A. College of Engineering & Technology, Mathura, Uttar Pradesh, INDIA in the year 2007. Immediately after the completion of B.Tech he joined PKITM, MAthura as a lecturer in the department of Mechanical Engineering. He finished his Master's in CAD-CAM from National Institute of Technology, Hamirpur, Himachal Pradesh, India in the year 2011. Soon after completion of his M.Tech programme, he joined as Assistant Professor in Mechanical Engineering Department, Govind Ballabh Pant Engineering College, Pauri, Uttarakhand, India.

He has published two research papers in Science Citation Indexed Journals, filed two patents (one is under examination) and presented two research papers in International Conferences or one in National Conferences to his credit. Since 2013, he has been engaged in his Doctoral Research in the area of Development and characterizations of multilayer coated wear materials at M.N.I.T, Jaipur under the Institute Research Fellowship scheme by Ministry of Human Resource Development, Government of India.

****